SO178-KOMEX Cruise Report

July 22 – September 15, 2004
Pusan - Vladivostok – Okhotsk Sea -
Vladivostok - Pusan - Jakarta

Mass exchange processes and balances in the Okhotsk Sea

Edited by

W.-Chr. Dullo, N. Biebow, and K. Georgeleit

Table of contents

INTRODUCTION

Wolf-Christian Dullo and Nicole Biebow

Cruise SO178-KOMEX (<u>K</u>urile <u>O</u>khotsk Sea <u>M</u>arine <u>EX</u>periment) focus sed on detailed structural geological, geochemical, paleoceanographical and petrological investigations in the Okhotsk Sea. The expedition aboard RV SONNE was based on previous cruises conducted in the framework of the KOMEX project and is part of the German-Russian Cooperation funded by the German Federal Ministry of Education and Science and the Ministry for Industry, Science and Technology of the Russian Federation. The major objective of this cruise was the use of technologically sophisticated video-guided instruments, the excellent coring facilities of RV SONNE together with its high-precision navigation system in order to enable detailed hydroacoustic mapping, detailed sampling of vent systems, associated ecosystems, and mineralizations as well as the recovery of long piston cores (25 m) with a high resolution of the stratigraphic column.

The Okhotsk Sea as a semi-enclosed "ocean" provides the unique opportunity to study the distributional patterns of materials, flux rates, and water mass formation, as well as circulation and climate dynamics because of the close spatial relationship and interaction of the geosphere, biosphere, cryosphere, hydrosphere, and atmosphere. Within the global ocean system, the marginal Okhotsk Sea plays a major key role as it provides the highest methane production rate of the northern hemisphere. Due to long-term sea-ice cover, the globally important release of methane into the atmosphere is extremely seasonally regulated. Furthermore, the Okhotsk Sea triggers and controls the water mass formation in the whole Pacific. Hence, these processes influence the climate system and paleoclimate system of the largest ocean of the world and are essential to decipher for an improvement of global climate models. Our investigations provide a twofold essential contribution 1) for a better understanding of the control mechanisms of the oceanographic and climatic evolution of the Pacific Ocean and 2) for the geological evolution of the Okhotsk Sea. In detail, our investigations focussed on five major scientific themes.

Reconstruction of the tectonic framework and the geological evolution of the Okhotsk Sea expressed by their structural morphodynamics as well as the petrology of the seafloor.
The precise position of the Okhotsk Sea within the global pattern of plate tectonics is still not very clear. Especially the opening of the Kurile Basin is one of the central key questions being addressed during our cruise. We mapped in detail the NNW-SSE-trending basement ridge composed of a chain of volcanoes, the newly named "Sonne Chain" which exhibits all features of an extensional rift. This, in turn, underlines a possible opening of the Kurile Basin in NE-SW direction. Furthermore, dredging proved the existence of basaltic andesitic material associated with these volcanoes.

Geochemical, hydrochemical, marine geological and biological characteristics of the different vent systems on the Sakhalin Shelf and in the Derugin Basin.
Methane is released into the Okhotsk Sea and the atmosphere from different sources. Volcanic systems, seeps of hydrocarbon accumulations, as well as gas hydrates and microbially diagenetically produced fluxes are known. We focussed on the near-surface gas hydrates and vent-related mineralization patterns on the northern Sakhalin Slope and in the Derugin Basin. The TV-guided sampling and observation systems provided spectacular views and samples of distinct sites. Detailed sampling of vent biota, for the first time including bacterial mats, pore water analysis, cores through the gas hydrate layer, barites and carbonates as well as a very detailed CTD sampling of methane flares enlarged our knowledge of these systems and provided a dataset for further improved quantification of methane fluxes.

Reconstruction of the paleoceanological and paleoclimatological evolution of the Okhotsk Sea on decadal and centennial time scales.

Holocene and Pleistocene changes and variabilities of the water masses, their circulation pattern, and their productivity in relation to sea-ice cover and sea-level changes can be studied here much more in detail due to high sedimentation rates in contrast to sites in the Pacific Ocean. Our investigation area is characterized by high productivity during warm periods. Therefore, it is an essential key site for the global oceanic carbon production. The formation of the Okhotsk Sea Intermediate Water (deep water) controls the oceanography and the climate of the entire NW Pacific. During our cruise we collected several superlong piston cores along the Sakhalin Slope which provide ideal archives to study the high-resolution climatic and oceanographic variability during the Holocene and the younger Pleistocene as well as the influence of the Amur discharge on the whole system. Moreover, these long cores from the northern part of the Sakhalin Slope will provide information on sporadic large-scale methane expulsions into the water column during the geological past which may have triggered abrupt changes of the climate system.

Establishment of a new method to characterize water mass structures in the geological past by means of silica isotopes.

This newly established proxy of silica isotopes will be studied in the geological record of long sediment cores. However, for calibration, it is essential to study the isotopes from living material caught at different depths and characterizing different water masses. A detailed series of multinet sampling along the Sakhalin Slope was performed in order to cover localities of different production rates. The measurements of silica isotopes will concentrate on diatoms and radiolarians.

Sampling of deep-water bioherms in the Kurile Basin and along the Sakhalin Slope.

Deep-water coral bioherms are presently one of the prime targets in geobiological studies. The detailed hydroacoustic measurement on the Sakhalin Slope and at the margins of the Kurile Basin showed several distinct mound features which all are characterized by an internal bedded structure, thus being no real carbonate build-ups. However, some of these structures are characterized by an intense cover of calcified octocorals represented by *Styleasteridae* and *Isidiidae*. The latter exhibit a growth pattern of mineralized rings, equivalent to tree rings, and, therefore, may serve as a high-resolution archive for intermediate water mass variability. Apart from calcified octocorals, we discovered giant sponge "forests" of non-calcified *Demospongea* associated with non-calcified octocorals. This ecosystem occurs on pronounced slope edges or structural highs.

1. CRUISE NARRATIVE

Wolf-Christian Dullo and Nicole Biebow

After having arrived in Pusan via Frankfurt and Seoul, all German participants of the SO178-KOMEX cruise boarded RV SONNE on July 21 at 9:30 a.m. Pusan is the second largest city of South Korea (population: 4 Mio.) and is located in a beautiful, naturally formed harbor. Our colleagues who had boarded SONNE already in Shanghai had unloaded the containers already during transit to Pusan. Thus, there was no more work left than "only" equipping the labs and storing the coring equipment.

On July 22, 08:36 a.m. ship time, we left for Vladivostok. Weather conditions were fine, the sea was absolutely calm, and air temperature was 26-29°C. We used the transit for getting familiar with shipboard equipment as, for example, Simrad and Parasound. The training for these echosounders was only theoretical, because we were not allowed to run them outside the investigation area. Furthermore, the scientists had access to a new navigation planning system including a global sea chart and some new handling devices.

Full of suspense we awaited to enter Vladivostok harbor. Following the research permission, we crossed 40°04.0 N/ 133°05.1 E on July 23 at 04:00 p.m. ship time (Fig. 1.1). On July 24 at 10:00 a.m., the pilot came on board of SONNE in Ussurysky Bay. He was followed by a stylish pilot boat called "Orient". We went along Askold Island east of Vladivostok and then through a passage between Russian Island in the south and Muravyev-Amursky Peninsula in the north on which Vladivostok is located. At 11:00 a.m., SONNE was tied up at Pier No. 2 directly in front of the famous final station of the Transsibirian railway. Then, custom and immigration procedures began: everything was done very exactly and took quite a long time. While the crew, equipped with seaman passports, went through immigration aboard the vessel, the scientific party had to go to a harbor administration building. The immigration procedure there was similar to that on airports. At 1:30 p.m., everything was finished and we had a walk through the city.

On July 25, the Day of the Russian Navy, the Russian colleagues came on board with their personal belongings which did not have to pass custom. A parade with military vessels was held in Amursky Bay surrounding Vladivostok in the west.

Leaving harbor on July 26 came to be very difficult due to a time-consuming custom and emigration procedure. At 11:00 p.m., all problems were solved somehow and we could leave Vladivostok with a 14 hours delay.

On Wednesday, July 28, at 3 p.m. we passed La Perousa Strait between Sakhalin and Hokkaido Islands. The surface current from the Japan Sea into the Okhotsk Sea accelerated SONNE up to 15.2 kn. Already in the Japan Sea, the weather was becoming worse during the day, and it rained heavily.

On July 29, the first station work began in the Kurile Basin at 46°26`N/ 146°33`E at a water depth of 3,297 m (Fig. 1.2). For successful deployment of the shipboard hydroacoustic devices, Parasound and Simrad, first of all, we needed the density values of the sea water for calibration. Therefore, station work began deploying the CTD. Subsequent to successful calibration, a short hydroacoustic profile was run on this station. Parasound records with a penetration depth of up to 60 m showed an undisturbed sediment sequence on this morphologically monotonous station. Firstly, we deployed the video-controlled multicorer. Due to too much weight, it penetrated so deeply into the soft diatomaceous sediment that the sediment surface got lost. The secondly deployed 10 m long gravity corer went up to the top of the weight into the sediment. Nevertheless, the core recovery was only 4.8 m, because the core catcher already closed after having penetrated a turbidite layer. First analyses of the

water samples yielded a methane anomaly in the western part of the Kurile Basin amounting in the intermediate water layer up to 550 nl/l and in the botton water layer up to 90 nl/l.
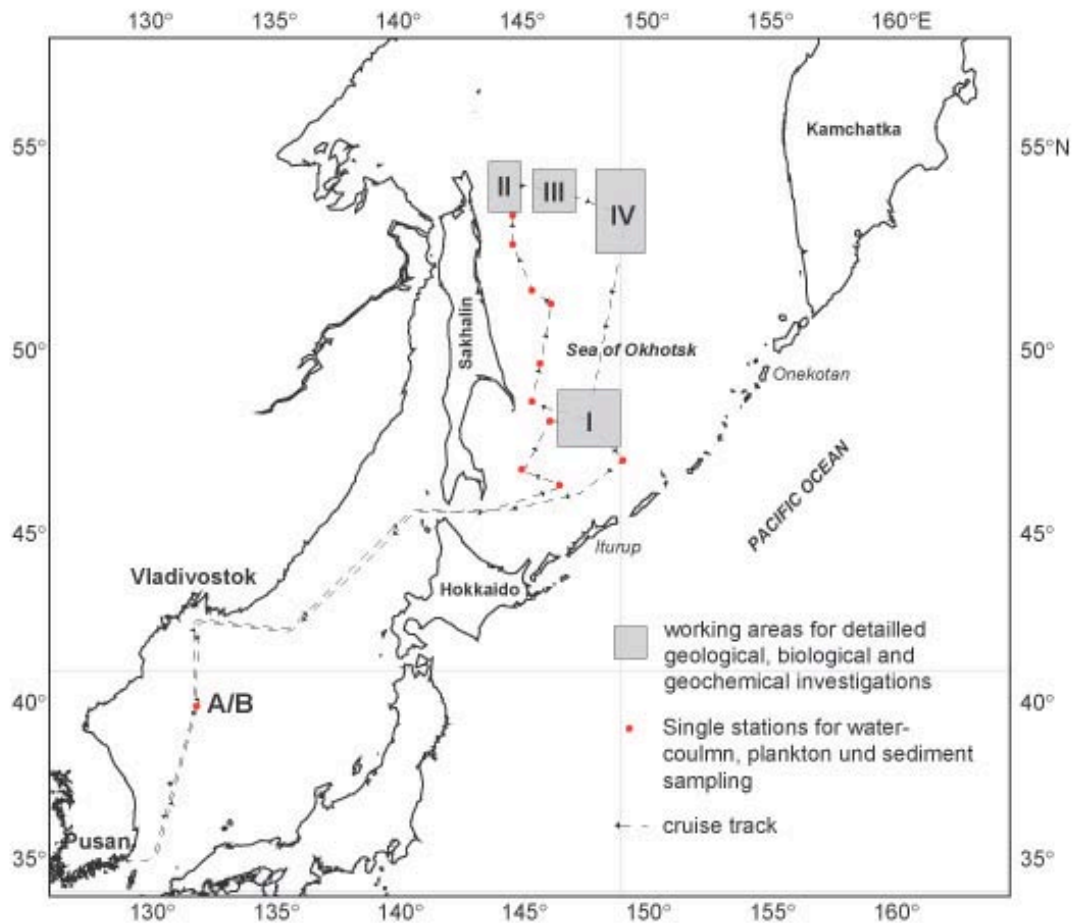
Cruise track of the SO178-KOMEX expedition.
Pusan - Vladivostok - Sea of Okhotsk - Vladivostok - Pusan, July to September 2004

point A/B indicates the point of entrance in exit of the exclusive economic zone of the Russian Federation.

(Mercator-Projection 1:28.000.000 at Latitude 0)

Fig. 1.1: *Cruise track of RV SONNE during SO178-KOMEX cruise.*

The second station in the Kurile Basin at 46°52`N/ 145°03`E at a water depth of 2,995 m was run similar to the first one (Fig. 1.2). Before starting major mapping activities on the northern margin of the basin, we ran a station at the slightly inclined NW slope of the basin at 48°11.8 N/ 146°08.7 E at a water depth of 1,603 m. The long time spent for mapping was used for core sampling and first pore-water analyses. Thanks to weight reduction, the multicorer deployment was this time very successful: in comparison to the deployments in the deeper Kurile Basin, the online TV pictures showed a more moderately churned sediment surface. The H$_2$S smell was much less, too. We recovered sediment cores of about 30 cm length with an undisturbed surface. In only 17 cm sediment depth, the boundary between the soft Holocene and the tough green-gray Glacial sediments was visible indicated also by a layer of pebble dropstones.

On the third station, on the Sakhalin Slope (Fig. 1.2), we deployed a 10 m long kasten corer for the first time. It recovered more than 9.5 m of sediment, thereby even penetrating several dropstone layers at different depths with single dropstones of up to 5 cm in size. Here,

weather became colder with temperatures between 10 and 14°C, but as the rain had stopped after we had passed La Perousa Strait and the sun shined, we decided to sample the kasten corer on the working deck. For the first time, the geochemists took samples for pore water analyses. On all three stations, multinet deployments for mesoplankton determination were run successfully.

The mapping of a supposed spreading axis on the northern slope of the Kurile Basin began in the night of August 1. It revealed a very complex morphological structure with giant slumps and canyons beneath 2,000 m water depth. Above 2,000 m, the northern slope of the basin is characterized by enlongated mounds which are encircled by moats. These mounds form a chain striking in NNW direction. Based on their morphology the mounds might be interpreted as sediment-covered volcanic edifices.

10 dredge tracks were run on three of the volcanic structures. Volcaniclastic rocks like tuffs and lavas (probably basaltic andesites) were recovered which are partly covered by up to 5 cm thick manganese crusts. Detailed lab analyses of these rocks will help to determine the age and origin of the volcanism on the northern slope of the Kurile Basin. During two dredge tracks on sharp edges in shallower waters at about 1,400 m water depth, several bright-red sponges up to 70 cm long and as thick as one`s arm were recovered. Much more interesting, though, was the recovery of calcified octocorals (isidides). In cross-section of the branches of this species, known as bamboo corals, a layered, obviously seasonal growth structure is visible. Therefore, these corals may serve as potential, highly interesting archive for the reconstruction of intermediate-water dynamics.

After having finished investigations in the western Kurile Basin, we worked on several stations along the Sakhalin Slope between 48°43´N/ 146°26´E in the south and 53°25´N/ 144°40´E in the north (Fig. 1.2). On all stations, CTD measurements were carried out. They showed that temperature and salinity decrease in the surface water from south to north. Oxygen content, on the contrary, sharply rises possibly indicating increased productivity.

The first deployment of the piston corer with a length of 15 m resulted in only 5 m of sediment recovery, although the corer superpenetrated. The upper liner was hit by the piston and broke. On the next station, a 20 m long piston corer was deployed yielding as much as 15 m of sediment recovery, but also this time, the upper liner broke due to a too high corer weight. With the aim of closing the gap between the surface and the gained sediment column, we then deployed a gravity corer and recovered a 11 m long sediment core. The reduction of the piston corer`s weight by 50% to 1.5 t solved the problem: on the following station, we recovered 17.38 m of sediments deploying a 20 m long corer. The lower sediments strongly degassed. Due to the degassing, the core expanded by about 20 cm. A high negative chloride anomaly was found in this core within the methanogene sediment layer at about 11 m sediment depth. Methane measurements revealed extremely high values indicating that the chloride anomaly is a result of gas hydrate decomposition. Models show that the in-situ production of methane in microbially and diagenetically very active sediments like the ones here can promote hydrate formation at depths of only ca. 10 to 20 m.

This very good result encouraged us to deploy a 25 m long piston corer, and we were successful: 23.60 m recovery. The stratigraphy of this core covers more than 16 m of Holocene sediment.

The foggy and rainy weather was interrupted from time to time by sunshine. In general, it was dominated by the Eastsiberian Lows crossings the northern Okhotsk Sea. We sometimes had morning air temperatures as low as 6.9°C.

In the fourth week of our working program, we began ventgeological investigations on the northeastern Sakhalin Slope (Fig. 1.2). First of all, the existing bathymetrical maps were supplemented by extended mapping with the Simrad echosounder. The investigations concentrated on active gas venting sites. For the first time during this cruise, bad weather with

wind-forces up to 8 hindered our work so that the last planned piston corer station could not be carried out. This station was successfully repeated with a core recovery of 24.30 m length subsequent to night mapping of the so-called Lavrentyev Fault. The existence of this fault had partly been an assumption so far. Now, its morphology was clearly visible on the Simrad records.
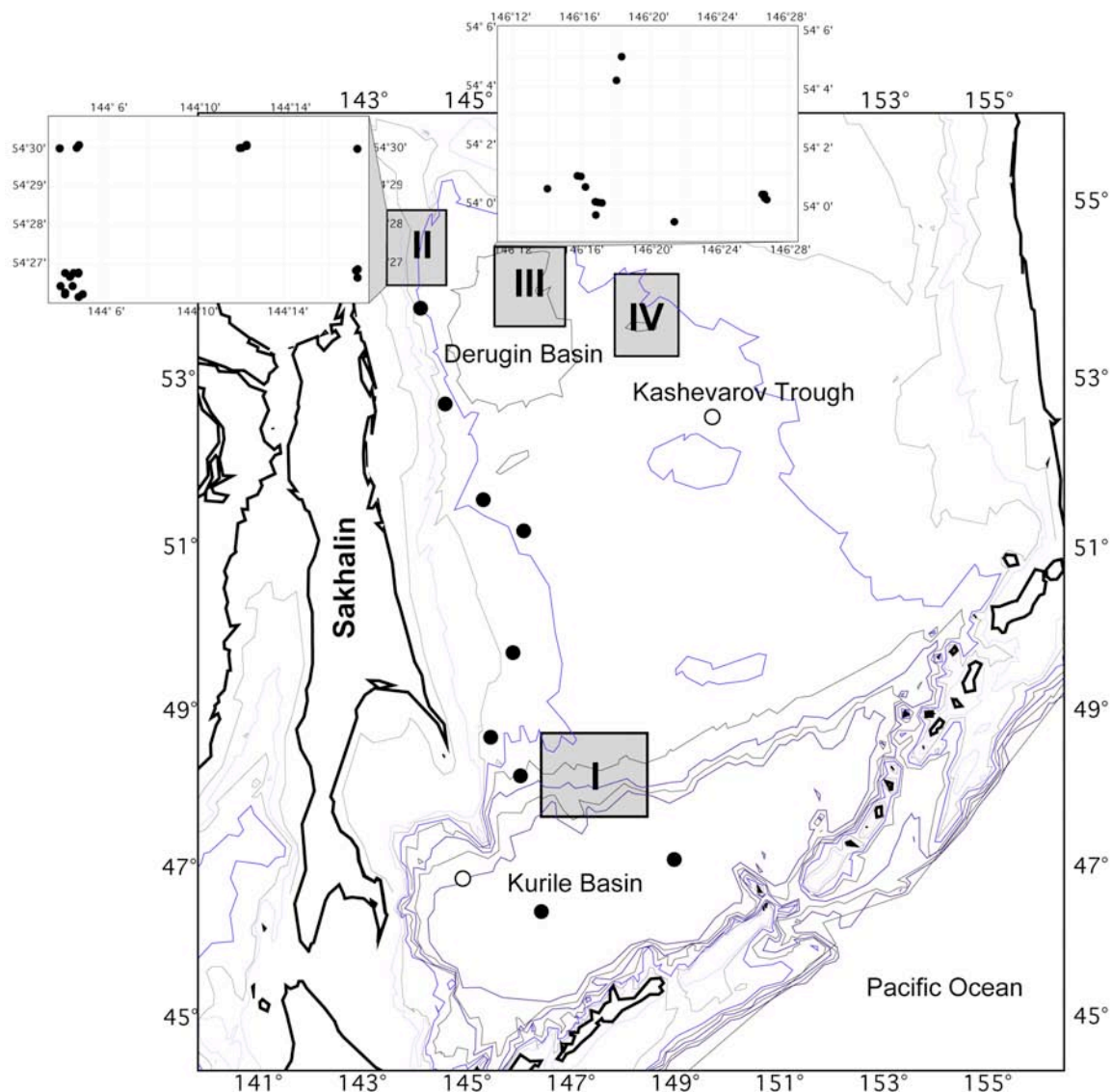
Fig.1.2*: Map of working areas (shaded rectanguars) and stations of SO178-KOMEX cruise. Black dots indicate full sampling stations, open circles indicated stations, where only the CTD and multinet were deployed. For detailled mapping areas, see Fig. 2.1 in Chapter 2.*

In the sediment cores recovered from the Sakhalin Slope, we found numerous carbonate concretions. They occurred not only at fluid venting sites here, but also in areas without gas venting. In one core, there was even glendonite, a pseudomorphose of ikaite. Such mineral precipitates occur in sediments with an increased content of organic material at a temperature around the freezing point.

On the northern slope of Sakhalin we investigated more detailedly three areas in which hydroacoustic records displayed gas bubbles rising in the water column. In all three areas (Obzhirov, Chaos, and Kitami Flare) we recovered sediment cores containing massive gas hydrate layers.

Friday 13th was a black day: our try to penetrate the gas hydrate layer with a 6 m long kasten corer resulted in the recovery of our first and only "banana". Afterwards we deployed the hydrocorer of our colleagues from Vladivostok for the first time. With a weight of only 300 kg the hydrocorer is able to sample coarse sediments. It is equipped with a simple low-pressure chamber at its head which is activated during sediment penetration and pulls the sediments into the liner. The hydrate-containing sediment layers extended over several core meters. With the TV-multicorer, we successfully sampled active fluid vents which are characterized by bacterial mats. Large amounts of carbonate concretions were gained with the TV-grab. The variety of carbonate concretions was strikingly broad here ranging from slice-like, partly layered to grave-like lumpy formations containing numerous *Calyptogena* and gastropodes shells. All these concretions consist of high-magnesium calcite. Apart from that, we found for the first time aragonite concretions. Their structure is very similar to those off Oregon. These samples help us to determine the origin of methane, fluid rising velocities and the microbial methane cycle in the sediment. Analyses of the very diverse mineralisations will help to reconstruct the history of the single vent locations.

At one of the venting sites, the Obzhirov Flare (54°26`N/ 144°04`E), we ran an extensive program for water-column measurements and sampling, the so-called "YoYo-CTD". We thereby did not heave the CTD after each deployment on board, but sampled the deep water layer four times in a row at different stations located about 300 m from one another. With this very effective method we successfully mapped in detail this very heterogeneous methane plume extending over an area of about 1 km^2. Thanks to the Parasound software which the Bremen University kindly put to our disposal we could display the methane plume very well and even detect the sampling CTD on the hydroacoustic image.

The work on the Sakhalin Shelf was successfully finished on Sunday, August 15. After a short transit we started our work in the Derugin Basin with mapping. We ran several profiles across barite mounds with the TV-sled and thereby observed many active barite chimneys which are characterized by white, cauliflower-like structures as large as a ball. Video-controlled multicorer as well as TV-grab deployments were all successful.

During these days the weather was fine, we enjoyed several hours of bright sunshine including impressive sunrises and sunsets. Air temperature did not exceed 12°C, though. For the first time, a low-flying Russian reconnaissance plane "visited" us.

During the fifth week in the Okhostk Sea, we focussed our work on the barite mineralization area in the Derugin Basin using mainly video-controlled equipment. On several TV-sledge profiles we saw an impressive submarine landscape with many barite chimneys. On the Barite Ridge they are up to several meters high. Thanks to a very precise navigation of the vessel as well as a sensitive handling of the winch, the sledge did not crash into one of the chimneys or even got stuck. We observed numerous tracks of snails and mollusks on the extensive, mud-covered seafloor between the chimneys which obviously look for methane vents, thereby using methane sensors.

Subsequent to successful investigations with the sledge, we deployed the TV-grab in order to sample barite chimneys. The recovered material was very porous and extremely soft to crumbly. First analyses revealed an unexpected result: barite is preserved as mineral only on the active, outer parts of the chimneys. A few centimeters beneath the surface barite is recristallized into aragonite. We also gained large amounts of pore water from the porous chimneys which will provide detailed information about the processes going on in the chimneys.

On the top of the Barite Ridge we recovered a sediment core showing very low chloride values in the pore water. Such salt-poor fluids usually form at higher temperatures by transformation of smektite and illite. The isotopical and chemical composition of these fluids will be analyzed at IFM-GEOMAR in order to more precisely determine their origin which probably is responsible for the formation of the barite chimneys.

CTD measurements in the Barite Ridge area yielded increased methane anomalies of about 1,940 nl/l in the bottom water. The methane content in the sediments of the Barite Ridge which we successfully sampled with the Russian hydrocorer is very high, as well, amounting to 100-200 ml/l.

We also ran several TV-sledge profiles on Clam Hill which is characterized by fields closely inhabited by living *Calyptogena* mollusks. Populations are partly so dense that the mollusks sit nearly on one another. The extension of these fields, yet, is seldomly more than 1-2 m^2. At these sites we successfully deployed the TV-grab as well as the TV-multicorer. Methane concentrations in the sediment were here as little as 0.1-0.3 ml/l.

We deployed the piston corer at the deepest place of the Derugin Basin where we expected to recover laminated sediments. The core recovery of 18.30 m was a good result, and the sediments were of promising deeply black-olive color, however they were all bioturbated.

Our station work in the Derugin Basin which also comprised mapping ended on Thursday, August 19. After short transit, reconnaissance mapping works in the Kashevarov Trough began at 54°19.09 N/ 148°00.00 E (Fig. 1.2) in the night of August 20. They did not reveal any evidence for volcanic structures at the surface or in the shallow underground. The basement of the trough consists of tilted blocks striking in W-E direction. The rocks dredged from one of these blocks comprised mainly siliciclastic sediments and conglomerates possibly of terrestrial origin. The orientations of the lineations are similar to those of the Derugin Basin.

Based on satellite images showing a high surface productivity in the southeastern part of the trough we decided to ran a multinet station at 52°35.00 N/ 149°50.00 E (Fig. 1.2).

Due to missing evidence of volcanites in the Kashevarov Trough and bad weather conditions on the Pacific side of the Kurile Islands with a low of 988 mb which made the deployment of heavy equipment impossible, we decided to return to Working area I, the western Kurile Basin (Fig. 1.1). Here, the hydroacoustic mapping was continued and, thus, the map of the submarine volcano chain striking in NNE-SSW direction completed. In the area where we expected volcanites the dredge and TV-sledge were deployed once more. The dredge recovered the expected basaltic to andesitic material and volcanoclastic sediments. On TV-sledge records it was obvious that many of the steep flanks of these submarine volcanic structures consist of volcaniclastic sediments. The submarine plateaus were inhabited by dense populations of crinoids, whereas the hard crusts of the volcaniclastic rocks were settled by styleasterides, non-calicfied octocorals, and sponges. Mapping was continued until the late evening of August 23.

We reached our last station in the Kurile Basin at 47°07.00 N/ 149°06.00 E (Fig. 1.2) with a water depth of 3,340 m in the morning of Tuesday, August 24. We deployed here the CTD, the multinet, and a 20 m long piston corer recovering more than 18 m of sediment.

After our very successful work which was possible only thanks to the excellent cooperation of everyone aboard, we all were looking forward to returning home and bringing in a rich harvest.

On Wednesday, 5:00 p.m., we passed La Perousa Strait enjoying calm sea, blue sky and sunshine. The southernmost edges of the two Peninsulas of Sakhalin were visible. We reached the Japan Sea on August 25 in the late afternoon. Before, we discovered the Russian RV PROFESSOR GAGARINSKY on our radar screen in a distance of only 11.5 nm from SONNE in the strait. Via a short radio contact we got to know that the vessel was on its way to a cruise focussed on mapping around the southern tip of Sakhalin and that none of our colleagues from POI was aboard.

The following Thursday was used to properly clean the labs and to pack the equipment and samples of our Russian colleagues. At the same time, a typhoon called CHABA started to occur in the Pacific east of Japan. It reached an impressive air pressure as low as 910 mb in its center and had a wind velocity of up to 145 kn at the margin of its eye. Nevertheless, the

typhoon should not cause any trouble for us up to Vladivostok.

In the morning of Friday, August 27, we reached the coast off Nakhodka, the international harbor of Russia`s Far Eastern coast. There was quite a lot traffic here. At 1:00 p.m. we met the pilot, and around 2:30 p.m. we tied up at Pier No. 6 in Vladivostok. As usual, we had to wait for the agent and custom. Everything was controlled very thoroughly again. Three hours later, at 6:00 p.m., we were checked in and could leave the vessel. The weather was much cooler than in July, and a slight breeze came up. On Saturday, the samples and equipment of the Russian colleagues were offloaded. We had a brunch with our dear Russian friends, colleagues and their families, before they finally said goodbye and left the vessel.

The weather was great, but the increasing wind indicated that the typhoon was coming nearer. Up to that moment it had kept a stable position off the southeastern coast of Japan. During the evening, the typhoon moved in direction of the Japan mainland, where it lost power and turned westwards. This was the time to leave Vladivostok. On Sunday, August 29, declaration began at 09:30 a.m. and lastet again three hours. This time, all scientists had to pass the emigration procedure in the passengers` terminal. It took us one hour to pass.

We left Vladivostok harbor at 1:20 p.m., and the Japan Sea still was calm. SONNE, although going directly against the current, had a speed of 15 kn.

During the night to Monday, the typhoon changed its direction into NNE. It had already filled up to 945 mb and slightly headed into our direction. We passed the typhoon in a minimum distance of 165 nm. Thanks to this large distance, the wind-force amounted to only 7. On Monday evening, we saw an impressing sulphate-yellow sunset. SONNE was lying calmly, though; she does not even need stabilizers in contrasts to modern research vessels, like METEOR.

On Tuesday we reached Pusan, having calm sea and great weather. The containers were packed, and the reports were finished except for some layout works and smaller corrections and saved on DVD. An excellent cruise with respect to the cooperation between the crew, the German, Italian, and Russian colleagues ended. Thanks to everybody!

2. BATHYMETRY AND PARASOUND INVESTIGATIONS

Boris Baranov, Reinhard Werner, Alexander Chichaev, Anatoly Obzhirov, Anatoly Salyuk, and Igor Tararin

2.1 Introduction

Bathymetric and Parasound investigations conducted during SO178-KOMEX cruise focussed on the follwing targets: 1. mapping of the major morphological features of the areas under investigations for tectonic purposes, 2. search of submarine volcanoes on the northwestern Kurile Basin slope and in the Kashevarov Trough, and 3. mapping of the seeping area on the northeastern Sakhalin Slope and in the barite mineralization area of the Derugin Basin with the aim to obtain an idea about the specific bottom features connected with this phenomenon. In addition, the obtained bathymetric maps and Parasound profiles served as a basis for sediment sampling, OFOS observations, dredging, and hydrocast. The ship-mounted multibeam echosounder SIMRAD EM120 and parametric narrow-beam deep-sea and sediment survey echosounder ATLAS PARASOUND were used for bathymetric surveys and investigations of the uppermost part of the sedimentary cover.

Four areas were investigated: the northwestern slope of the Kurile Basin (Working area I), the northeastern Sakhalin Slope (Working area II), eastern Derugin Basin (Working area III) and Kashevarov Trough (Working area IV). In addition, two orthogonal profiles were run at each station. A total of 2,020 nm of bathymetric profiles was obtained. Depending on water depth, the line spacing varied from 1.2 to 2.7 nm.

2.2 Working area I: Northwestern Kurile Basin slope

Working area I is located in the western part of the northern slope of the Kurile Basin between the southeastern Sakhalin Slope, the Academy of Sciences Rise and the deep Kurile Basin. The central part of Working area I was mapped (Fig. 2.1). The map shows three structural domains with different seafloor morphologies: the upper Kurile Basin slope, lower Kurile Basin slope, and the Kurile Basin seafloor (Fig. 2.2).

The slope break at a depth of about 1,900-2,000 m represents the boundary between the upper and lower slope (Fig. 2.2). The upper slope is very gentle and has a simple relief. Contour lines of its western part strike in NE-SW and of its eastern part in WE directions. The most remarkable feature here is a hill chain which is located between contour lines 1,500-1,700 m and which forms a NNE-SSW-striking line of 20 nm length. The hills have rounded or slightly elongated forms, and their altitude reaches 250 m. Very prominent moats with a depth of up to 100 m exist around each hill. According to Parasound data we suppose that these moats were formed by current activity around the basement outcrops (counturite currents). Outlines of the hills and dredging data suggest that those structures represent volcanic edifices. They probably appeared along a NNE-SSW-striking fault. We named this structure "Sonne Chain" in honour of the research vessel.

Seaward of the slope break, the lower slope becomes steeper and more complicated (Fig. 2.2). As on the upper slope, its western and eastern parts differ from each other with respect to their relief morphology. The western part consists of two NW-SE elongated heights which are separated from the slope break by narrow depressions. The heights have steep slopes of up to 200 m in altitude facing to the NE and SW, respectively. The gentler SW slope, especially of the eastern height, shows evidence of landslide processes. A volcanic edifice was mapped on the eastern side of this height. Its altitude equals 200 m, and its top morphology suggests crater existence.
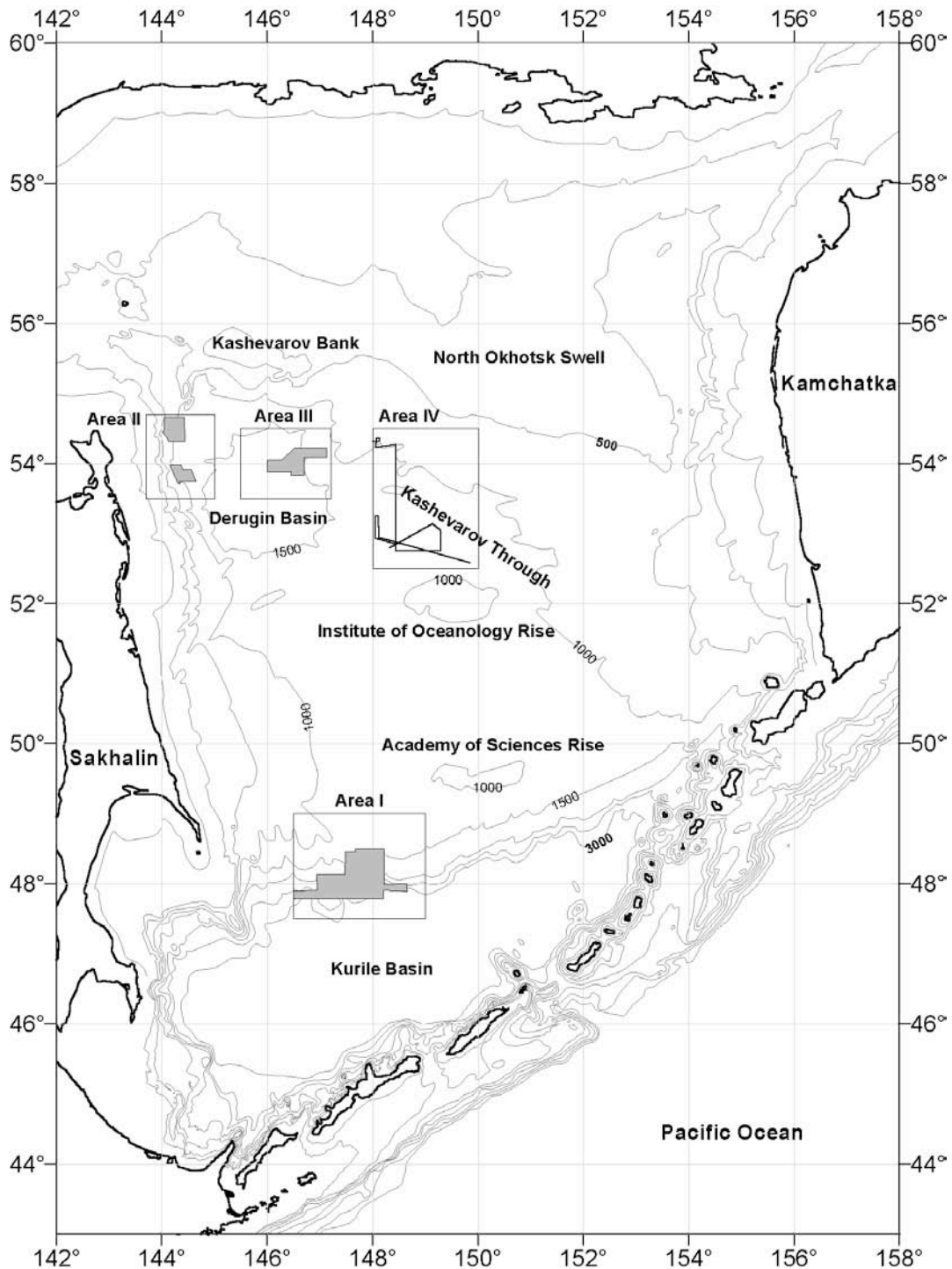
Fig. 2.1: *General morphological features of the Okhotsk Sea and location of the Working areas (rectangulars). Gray polygons indicate the mapped area. Lines show reconnaissance surveys inside Working area IV. Contour interval is 500 m. Additional contour intervals are 200 and 100 m.*

Bedrocks were not dredged here (see Chapter 12). An OFOS track running from the top in SW direction (see Chapter 8) shows outcrops of manganese crust and hard rocks with a visible layering (tuffogenic rocks?). Many canyons striking in NW direction cut the eastern part of the lower slope.

The transition from slope base to basin is located bethween 3,200 and 3,300 m depth. The seafloor is smooth and deepens from the slope base in southern direction towards the basin center.
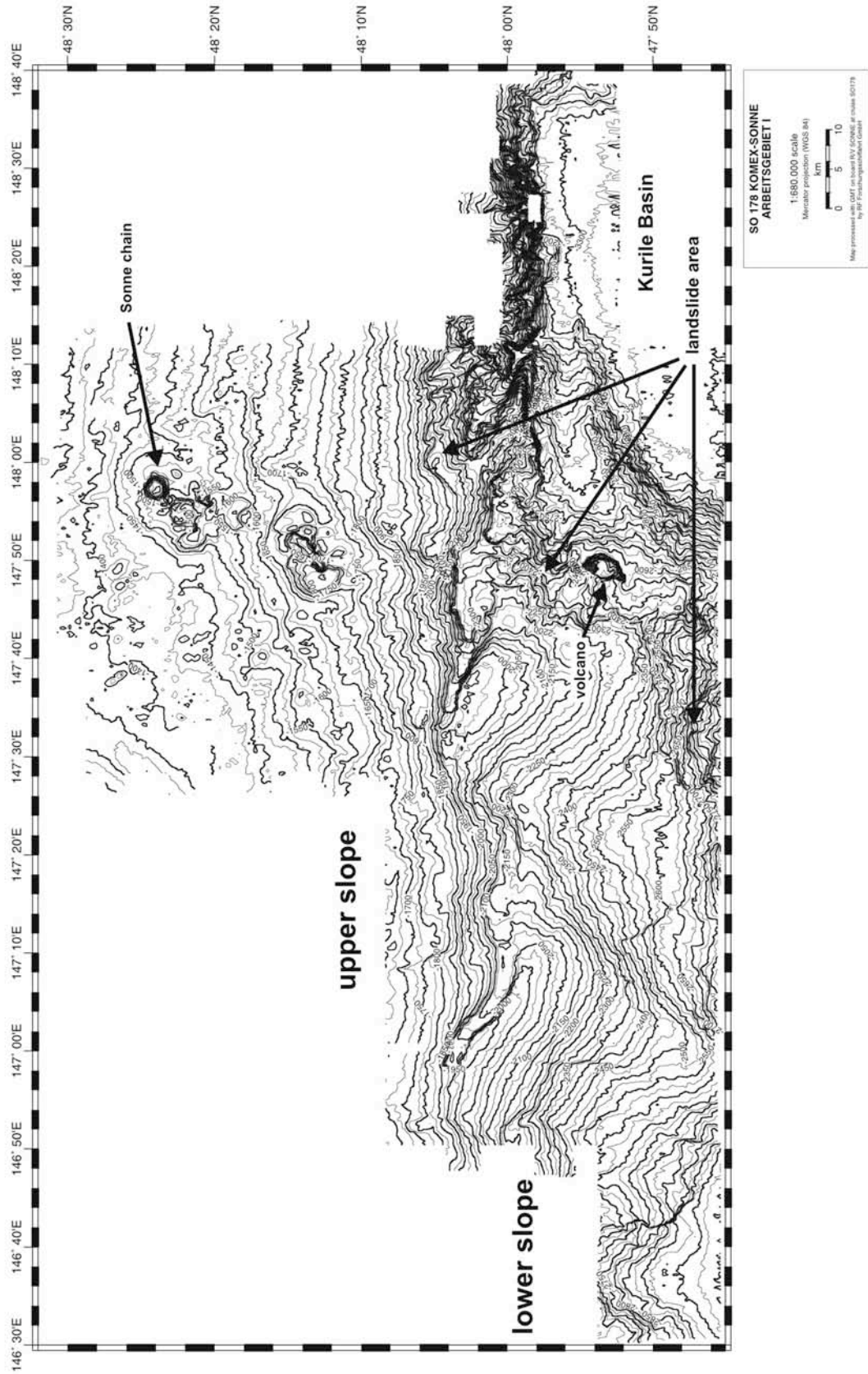
Fig. 2.2: *Bathymetric map of the northwestern Kurile Basin slope (Area I). Contour interval is 25 m. Location of the map is shown in Fig. 2.1.*

2.3 Working area II: Northeastern Sakhalin Slope

In Working area II, two locations were mapped on the northeastern Sakhalin Slope: the Lavrentyev Fault and a seeping area (Fig. 2.1). The Lavrentyev Fault is located in the southern part of Working area II and was discovered during former KOMEX cruises. The relief of this region is characterized by two scarps. The first of them has a NW-SE strike and is expressed in the bottom relief from more than 1,250 m up to the shelf break. The linearity indicates that the scarp represents a fault. Below 1,250 m, the fault is not expressed in the relief, but it can clearly be seen on seismic profiles obtained during the INESSA and SAKURA expeditions of the KOMEX project. It occurs here as a near-vertical boundary dividing the areas wich significantly differ in seismic cross-sections. This shows that the fault is sheared. As single structure, the fault can be traced over a distance of about 50 nm.
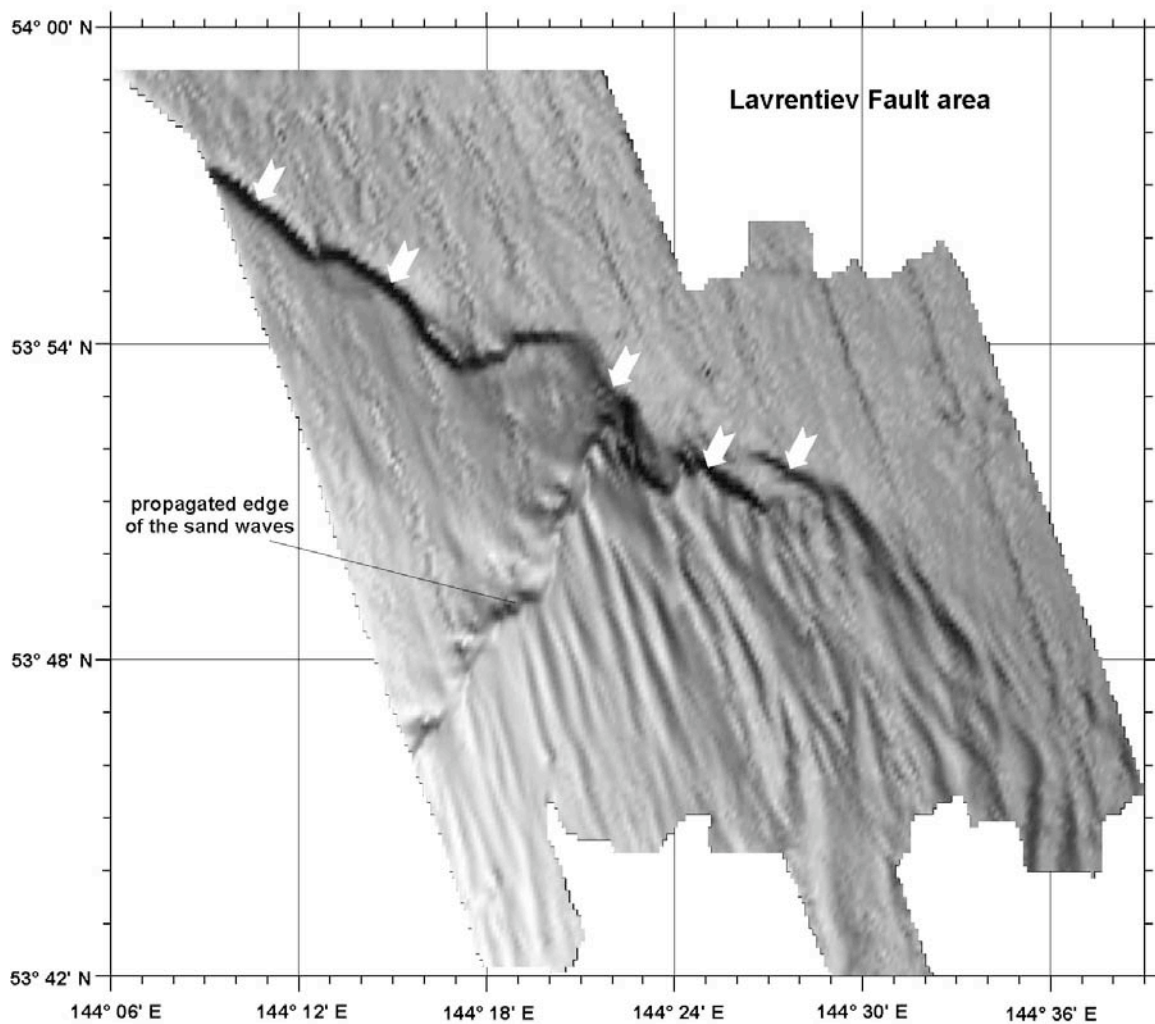
Fig. 2.3: Shaded relief of the southeastern part of the Lavrentyev Fault (southern part of Area II). White arrows indicate the trace of the fault. The fault has an en-echelon structure in its northern part and bifurcates in its southern part. Location of the map is shown in Fig. 2.1.

The second scarp has a NE strike and conjugates with the first at right angle at about 1,200 m depth. The fault characteristics of the first scarp are quite obvious but for the second one these characteristics cannot be ascertained. Its relief shape does not contradict such a supposition, but on several seismic profiles crossing this scarp (KOMEX data) it is not manifested in the sedimentary cover. To obtain more detailed information on the structure of these scarps recent investigations covered their junction.
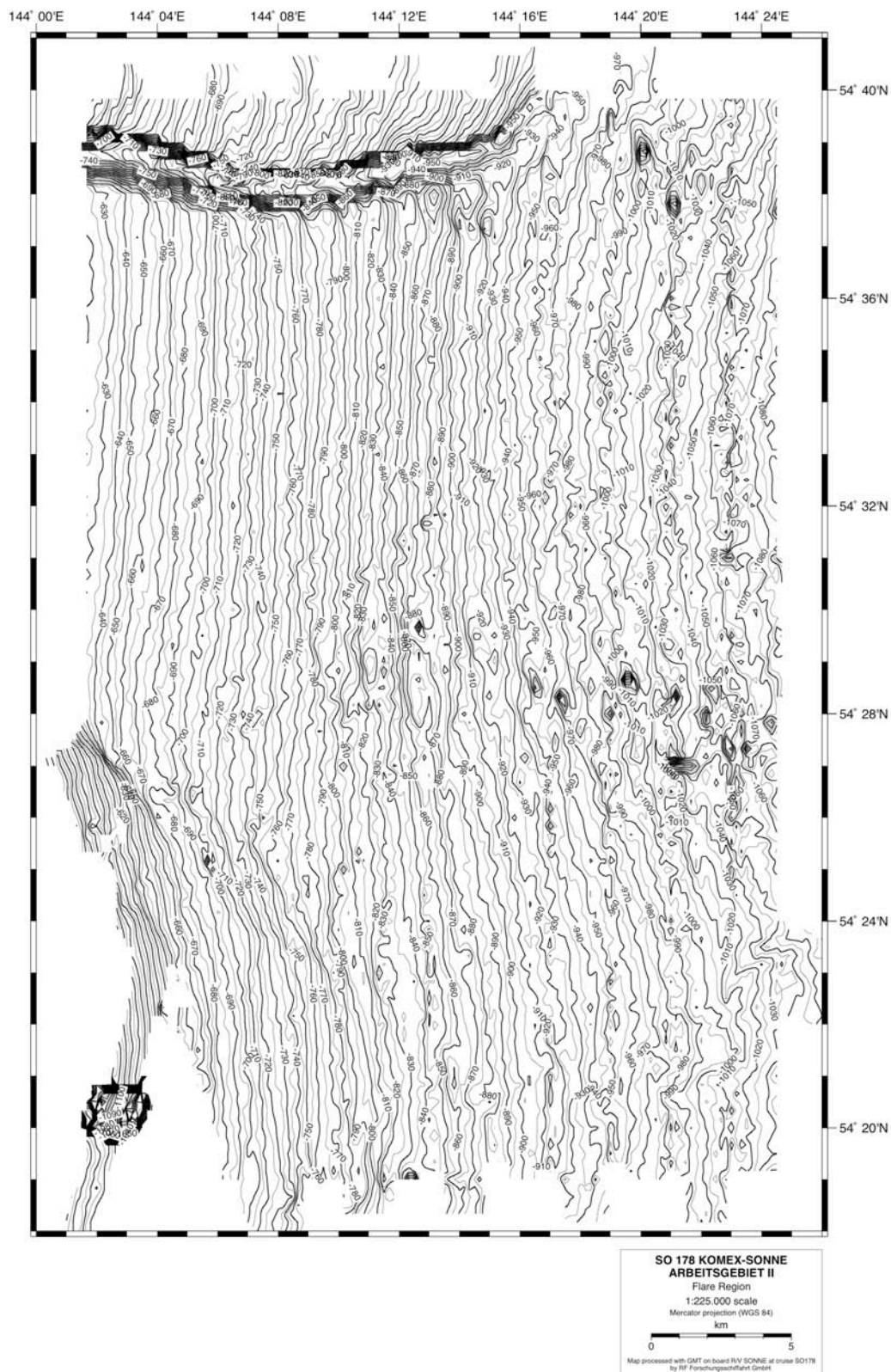
Fig. 2.4: *Bathymetric map of the seeping area (northern part of Area II). Contour interval is 10 m. Location of the map is shown in Fig. 2.1.*

2.3.1 Lavrentyev Fault

The mapped area represents a junction of two scarps and of a sand waves zone (Fig. 2.3). As known from former KOMEX investigations, the sand waves zone ends here and continues further to the south along the lower slope over a distance of about 100 km. The part of the sand waves zone south of the study area was mapped during investigations at station SO178-9 (Appendix 1). The map shows that the separate sand waves have a NS strike and a linear or weakly bended shape. Seismic cross sections (KOMEX data) show that the depth of the sedimentary cover affected by sand waves decreases from south to north. This could indicate propagation of the sand waves to the north. The sand waves become smaller and less continuous upslope.

The first scarp trending in NW-SE directions corresponds to the Lavrentyev Fault itself. Within the study area the fault has a sinistral en-echelon structure (Fig. 2.3). On its southwestern edge the fault starts to bifurcate. Here, it cuts the sand waves which indicates recent activity. The small rounded depression in the central part of the area could be linked to further minor faults. In contrast to the first scarp, the second, SW-NE striking one has bending outlines. This is probably due to the fact that this scarp does not completely cut the sand waves, but follows their outlines. The altitude of the scarp decreases upslope in SW direction, and our former KOMEX investigations show that it disappears in the relief below the 600 m contour line.

2.3.2 Seeping area

In the seeping area located in the northern part of Working area II, mapping was carried out in a depth range of 600-1,080 m to cover the most prominent seepings, namely Obzhirov, Kitami, and Chaos Flare. In general, the slope morphology of this area is extremely simple and the contour lines are very linear and trend in N-S direction (Fig. 2.4). There is one striking feature near to the northern border of the study area: a canyon with a depth of more than 100 m trending in WE direction. The canyon appears at the contour line 920 m and extends up to the western border of the study area. As the altitude of the main seepings equals 5 m and more, the seeping location can be seen best on a map with a contour interval of 5 m. Further processing of the bathymetric, backscattering and Parasound data will give us the opportunity to resolve also small bathymetric features.

2.4 Working area III: Northeastern Derugin Basin

Working area III is located in the northeastern Derugin Basin (Fig. 2.1). Swath bathymetry mapping was carried out in its central part. A small part of this area had been investigated with the towed multibeam echosounder LOLA during KOMEX cruises GE99 in 1999 (Biebow et al., 2000) and LV29 in 2002 (Biebow et al., 2003). That survey focussed on mapping of the barite mineralization area and was restricted to the Barite Mound and adjacent areas. During the SO178-KOMEX cruise, the study area was significantly extended to the west, south and northeast from the Barite Mound.

The bathymetric surveys show that the relief of the eastern Derugin Basin consists of several heights and depressions in between them (Fig. 2.5). In general, the Derugin Basin floor rises in NE direction towards the Kashevarov Bank. The northeastern edge of the study area has a smooth seafloor on which two elongated heights up to 200 m in altitude appear. They have very steep slopes facing to the north and northwest and striking in WE and SW-NE directions, correspondingly. The top of one of the heights has an en-echelon structure suggesting sinistral strike-slip movements. The steep slopes of the other heights, including the Barite Mound, show the same strike.
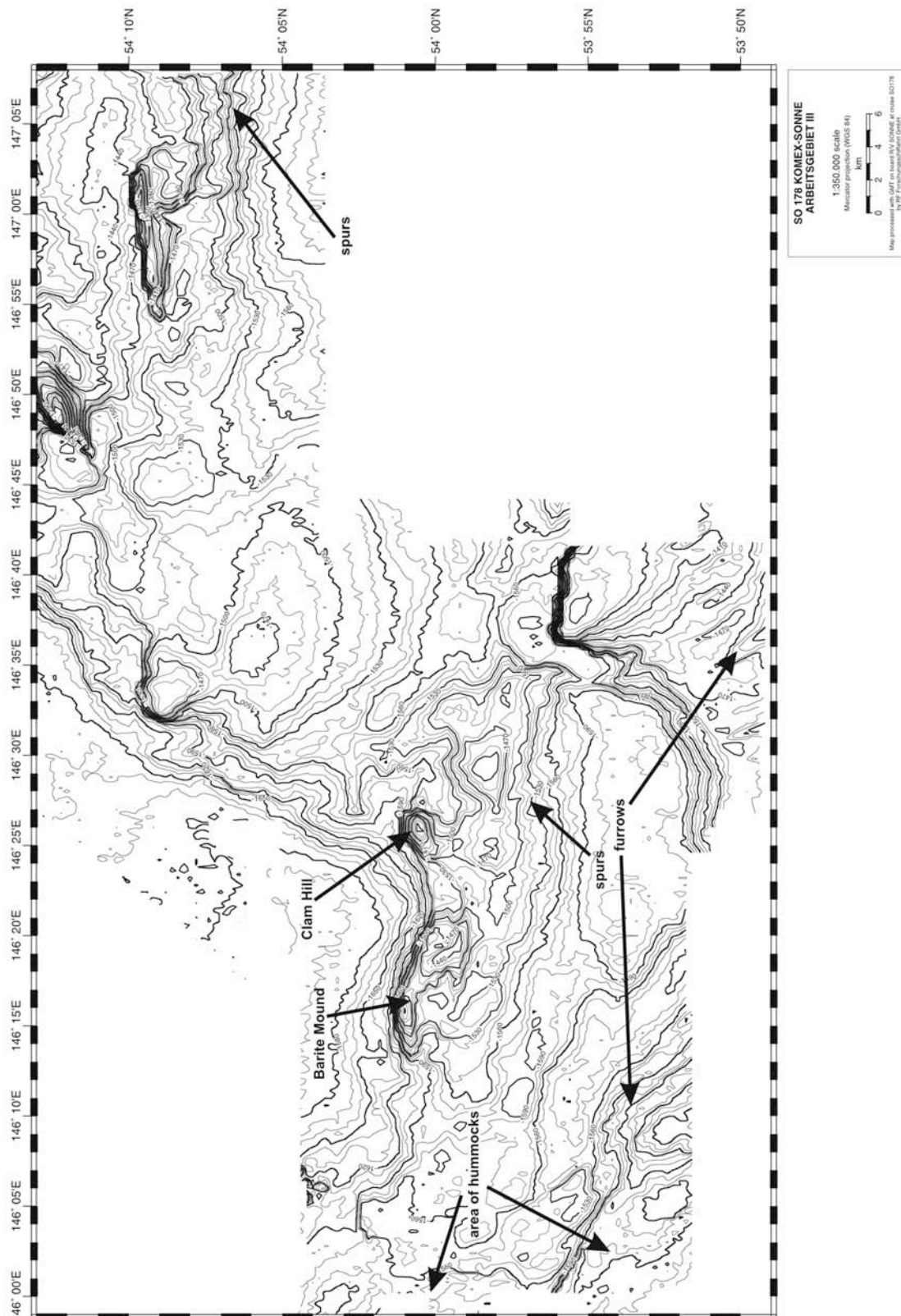
Fig. 2.5: *Bathymetric map of the eastern Derugin Basin (Area III). Contour interval is 10 m. Location of the map is shown in Fig. 2.1.*

There are more small bottom relief features trending in NW-SE direction. They appear as elongated furrows on the top and slope of the southern heights and as small spurs on the southern slopes of the Barite Mound as well as on the southern slope of the E-W-elongated height located in the northeastern edge of the study area.

Parasound profiles show that the faults limit the furrows and spurs. That the faults shift the sedimentary layers and extend up to the seafloor is evidence of their activeness.

The resolution of the swath bathymetry mapping by SIMRAD EM120 is too little to detect single barite edifices on the top of the Barite Mound. However, separate small rounded hummocks that can be linked with isolated barite edifices are visible near the Barite Mound top on the map showing the relief in shaded form. As can be seen on the map with the shaded relief and on Parasound profiles, another, more extended area with a hummocky relief exists in the westernmost part of the study area. Its eastern boundary roughly coincides with the edge of the gentle height trending in NW-SE direction. The hummocks form linear chains that follow the edge contour of the uplift. The origin of these hummocks is unclear.

2.5 Working area IV: Kashevarov Trough

Reconnaissance mapping was carried out in the Kashevarov Trough in order to detect volcanic edifices. The Kashevarov Trough is located between the North Okhotsk Swell and the Institute of Oceanology Rise (Fig. 2.1). This structure has a NW-SE orientation and originates from rifting processes. The existence of volcanoes was suggested here on the basis of seismic profiles obtained during a cruise of RV DMITRY MENDELEEV in 1974 (Belousov & Udintsev, 1981) and the GERDA expedition in 1995 (pilot phase of the KOMEX project).

The newly obtained data does not show any evidence of volcanic structures. The trough basement consists of tilted blocks with an extension from 5 nm to more than 15 nm (Fig. 2.6). The steep slopes limiting the tilted block trend mainly in WE directions. A second lineation trend is visible on the Institute of Oceanology slope where linear, NW-SE-striking furrows occur. So, the orientations of the lineations are similar to those of the Derugin Basin. Our investigations in the Kashevarov Trough show that there is no or only little evidence for volcanism here. The formerly obtained seismic profiles crossed the narrow edges of the tilted blocks. Therefore, those blocks looked like needles-shaped basement outcrops (volcanoes) on the seismic cross sections and were wrongly interpreted as volcanic edifices.

2.6 Preliminary conclusions

Northwestern slope of the Kurile Basin
The morphology of the northwestern Kurile Basin slope supports the idea about the opening of the Kurile Basin along its general strike (Baranov et al., 2002a), because the two heights on the lower slope striking in NW-SE direction could be interpreted - according to their shape - as tilted blocks. The suggested spreading ridge (Sakura Ridge) continues on the slope in the form of a volcanic zone. The volcanic Sonne Chain is a surface manifestation of it. This volcanism may be connected with a rift phase of the Kurile Basin opening.

Northeastern slope of Sakhalin Island (Lavrentyev Fault)
From the fact that the Lavrentyev Fault cuts the sand waves, we may suggest that it is recently active. The second, SW-NE striking scarp probably corresponds to the leading edge of the propagated sand waves.
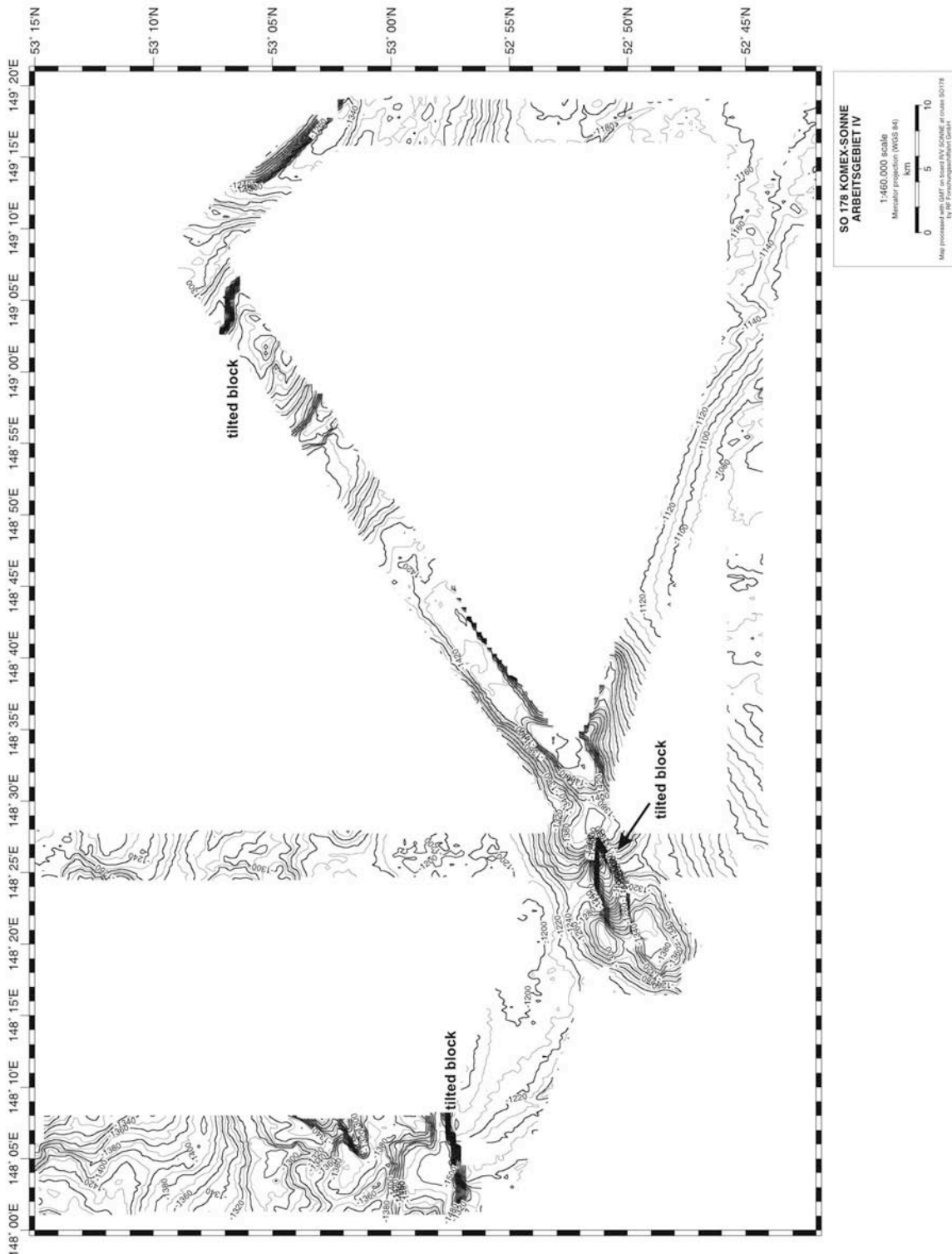
Fig. 2.6: *Bathymetry along the reconnaissance tracks in the Kashevarov Trough. Contour interval is 10 m. Only the southern part of the tracks is shown. Location of the map see in Fig. 2.1.*

Northeastern slope of Sakhalin Island (seeping area)
The morphology of the lower slope is very uniform; therefore the structural pattern of seep distribution may be clarified only subsequent to additional processing of the bathymetric and backscattering data in combination with Parasound and seismic data.

Eastern Derugin Basin

Three lineation directions were distinguished in the eastern Derugin Basin. Two of them, NE-SW and WE, are the steep slopes which correspond to the faults limiting the tilted blocks. The third one appears as elongated furrow and small spurs striking in NW-SE directions. It probably corresponds to the strike-slip faults which shift the tilted block. Parasound data show that these faults are active. This could indicate rejuvenation of the tectonic movements in the Derugin Basin.

Kashevarov Trough

Our investigations in the Kashevarov Trough show that its basement consists of tilted blocks. There is no or only little evidence for volcanism here. Therefore, this structure could be considered as a "dry" rift.

3. FLARE IMAGING

Anatoly Salyuk

3.1 Methods

Flare imaging was done using the shipboard PARASOUND narrow-beam parametric sediment survey echosounder and the PARADIGMA and WINPARADIGMA registration systems modified by Volkhard Spieß from the University of Bremen. To provide simultaneous registration of the Parasound (PS) bottom signal by Paradigma (200 m range) and the water signal by Winparadigma (500 m) at optimal settings, we added the delay box to the registration system (Fig. 3.1).
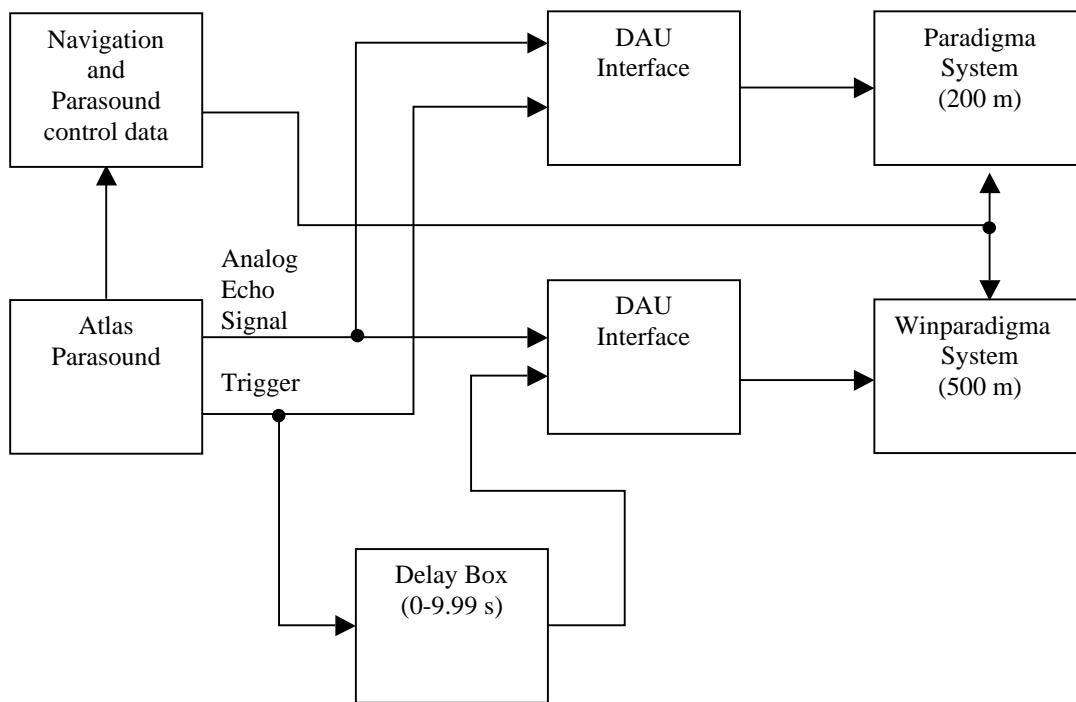
Fig. 3.1: *Flare registration system of the SO178-KOMEX cruise.*

Due to the cyclicity of the rather complex trigger pulse sequences, the delay box allowed to start recording of the reflected water signal by Winparadigma at a certain time interval prior to recording the reflected NBS bottom pulse. This time interval was adjusted to 400-600 ms (300-450 m) for different depths and different modes by manual setting of the delay range of 0.3-0.6 s for the flare imaging (FI) mode and 7.1-7.9 s for the Parasound (PS) mode.
The FI mode operated using the following recommended settings: Parasound (PS) mode, 1 pulse emitted, 20ϒ beam width, 1 ms length of the sounding pulse, 1,000 m depth range, and 500 m depth window range. In the FI mode, the frequency of sounding pulses was 3-5 times higher than in the PS mode.

The PS mode with its long time interval (for our working depth range: 8.3 s) and narrow (4ϒ) beam width is usually not optimal for flare imaging. At high ship speed during Parasound profiling (10 knots or 5 m/s) the distance between 2 consecutive sounding pulses (46 m) not only significantly exceeded the real horizontal scale of single bubble vents (few meters at the seafloor), but also the beam width (40 m at 600 m depth).
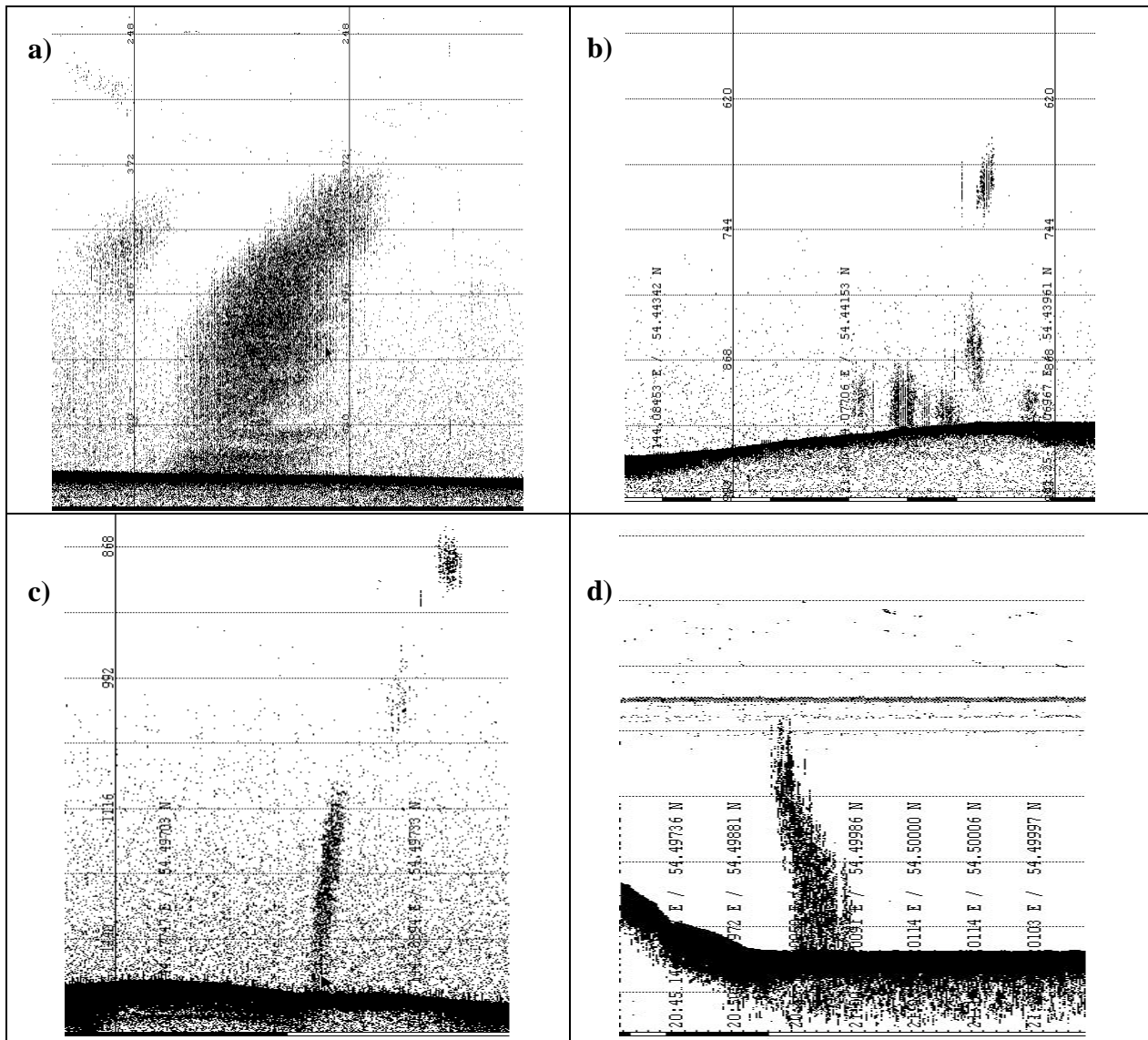
Fig. 3.2: *Examples of flare images from SO178-KOMEX cruise: a – flare a0407, Obzhirov Flare area; b – a2124; c – f0023, Chaos Flare area; d – flare e2057, detected in PS mode, Kitami Flare area.*

A characteristic feature of the used system is a relatively high background level of the reflected acoustic water signal which increases with depth both due to the noise properties of the used acoustic system and an increased amount of scattering objects. Another disadvantage for parallel flare imaging was the appearance of strong artifact lines and bands at some depths related to complex multi-pulse sequences in the pilot sounding mode of the Parasound sediment observations.

3.2 Results

FI surveys were carried out on the northeastern Sakhalin Slope (Working area II) and in the Derugin Basin (Working area III) from August 8 to 18.

Due to time limitations we ran only one special flare imaging survey with reduced speed across the most intensive flares in the main working area which was later densely covered by Simrad and Parasound surveys. Most of the flares were observed during CTD, coring, TV-grab and TV-MUC stations, where Parasound sediment survey was of less priority.
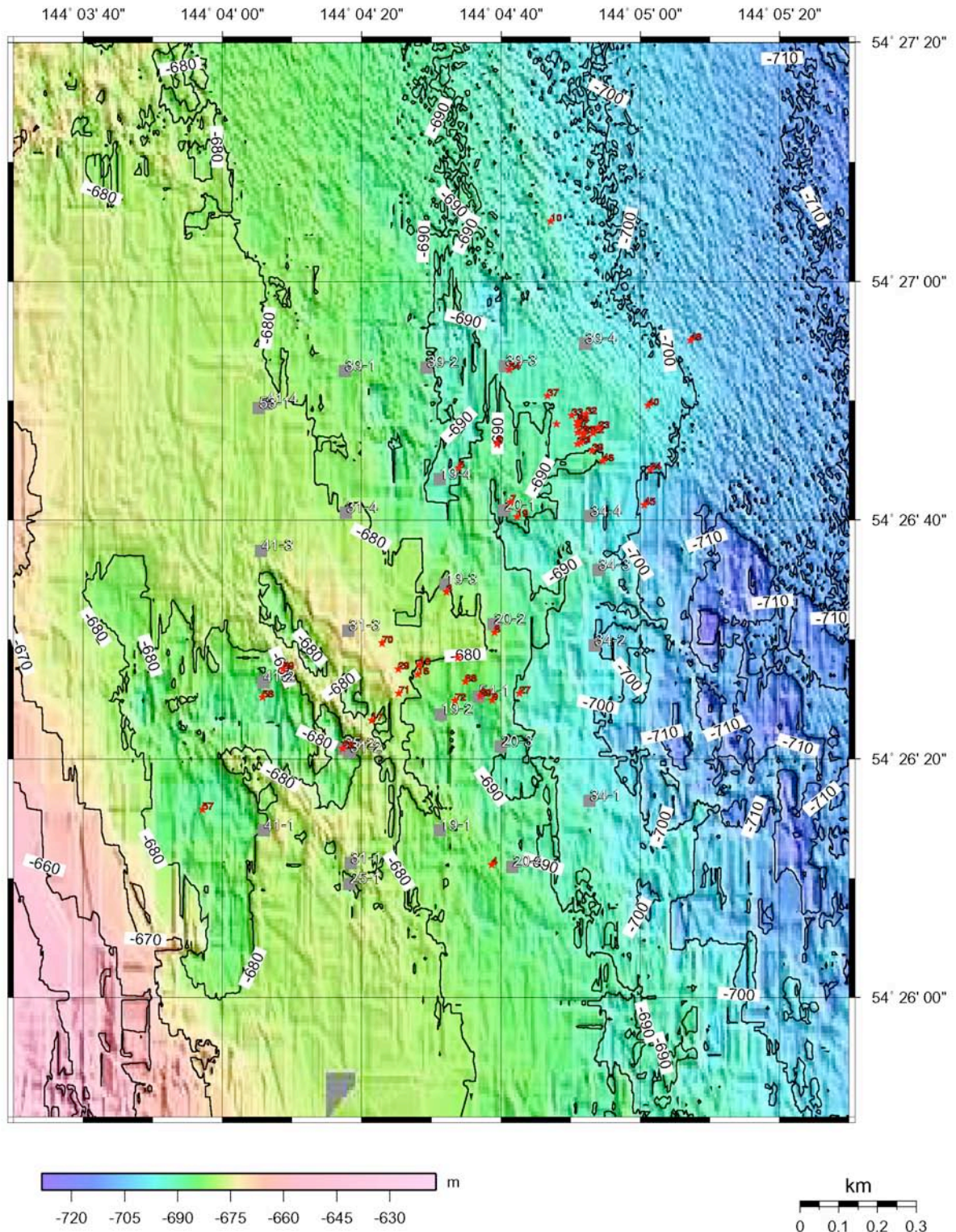
Fig. 3.3: *Map of flares observed at the Obzhirov Flare area including CTD stations.*

About 91 acoustic anomalies were identified as flares, 3 of them in the PS mode parallel to swath bathymetry and Parasound surveys. All these flares were observed only in Working area II from August 10 to 15 (Appendix 2). Some examples of flare images are given in Fig. 3.2. A map of flares observed in the Obzhirov Flare area including "YoYo-CTD" station positions is shown in Fig. 3.3.

Due to the high resolution in the NBS and PS modes, the Parasound system can be used for searching and mapping of active fluid and gas vents at the seafloor using a characteristic decrease in the sediment penetration of the acoustic signal. This decrease occurs as precursor of most flares more than 200-300 m before crossing the vent point and vanishes only 200-300 m after crossing the vent point.

4. WATER COLUMN STUDIES

Anatoly Salyuk, Valery Sosnin, Anatoly Obzhirov, Nicole Biebow, Pavel Tishchenko, Galina Pavlova, Sergey Sagalaev, and Andrea Abelmann

4.1 Introduction

The northeastern Sakhalin Shelf and Slope is one of the study areas for investigation of ventilation of intermediate water depths in the Okhotsk Sea. Fresh-water discharge of the Amur River causes rapid ice formation hindering transport of cold brine water. As a result, the cold brine water sinks to the seafloor north off Sakhalin promoting dense shelf water production. These waters with a temperature near the freezing point are considered to advect east off Sakhalin, thereby ventilating intermediate depths. The main objective for CTD observations during the SO178-KOMEX cruise was to continue monitoring of the oceanographic situation on the northeastern Sakhalin Slope. Additional data will help to improve our understanding of ventilation processes near the slope. Other objectives were to further methane investigations in venting areas and to accompany plankton investigations.

4.2 Water sampling and analysis

We used the Sea-Bird SBE 911Plus CTD with standard conductivity, temperature, pressure, and oxygen sensors and Sea-Bird 24-position Rosette system with 10 l Niskin bottles. CTD data were processed using SBE data processing software for Windows 5.31.
From the total 44 CTD casts carried out during SO178-KOMEX, 2 were done without water sampling due to problems with the closing mechanism of the Niskin bottles. Water samples were collected for oxygen, methane, pH, alkalinity, Ca as well as for δ^{30}Si, δ^{18}O, δ^{15}N, δ^{13}C, and Sr stable isotopes. At some stations, water was sampled for bacteria analyses.

The CTD was lowered and heaved at a speed of 1 m/s. Water samples were taken on upcasts at different depths according to the water structure with an increased coverage near the bottom and surface.
In Working area II, a specific method, the so-called "YoYo-CTD", was applied for small-scale investigations of venting sites: one CTD station comprised here a profile of 4 sites located in about 300-400 m distance from one another. Starting from the seafloor, a bottle was closed every 50 m, in total 6 bottles per site. During transit in between the single sites of one station, the CTD was heaved to 100 m water depth and trailed by the vessel to the position of the next site. We sampled the water column of the Obzhirov Flare, according to our previous investigations the most active flare on the northeastern Sakhalin Slope, on several "YoYo-CTD" stations for CH_4, oxygen and pH analyses.

4.3 Results and discussion
4.3.1 South-north transect

Salinity values of surface waters decreased near the slope northwards from 32.2 to 29.6 in a depth range from 1,350 m to 600 m. The main oceanographic feature of this transect is the typical subarctic summer structure characterized by a warm surface layer with temperatures of 13.3°C in the south and 10°C in the north and a dichothermal layer underneath with a minimum temperature of -1.2°C which is more pronounced in the deep part of the sea (stations SO178-9, SO178-11, SO178-12). At the shallow stations close to the continental

slope, the lower boundary of the dichothermal layer is missing, indicating a high mixing rate and temperature decrease in comparison with offshore stations.

The vertical distribution of dissolved oxygen shows an outstanding subsurface maximum of the summer type of 10.3 ml/l what is an oversaturation by 30%.

The color of surface waters changed from blue in the south to dark-gray in the north, obviously due to Amur River discharge.

All CTD stations on the transect were accompanied by multinet sampling.

The northern part of the transect yielded important features about the vertical thermohaline structure and its temporal variability. An extremely thick dichothermal layer at stations SO178-14 and SO178-16 with negative temperatures up to 200 m depth (-0.77°C at 180 m at station SO178-16) (Fig. 4.1) was observed. Such an unusual vertical extent of the dichothermal layer is a direct evidence of the intrusion of cold dense shelf water into the upper part of intermediate depths.
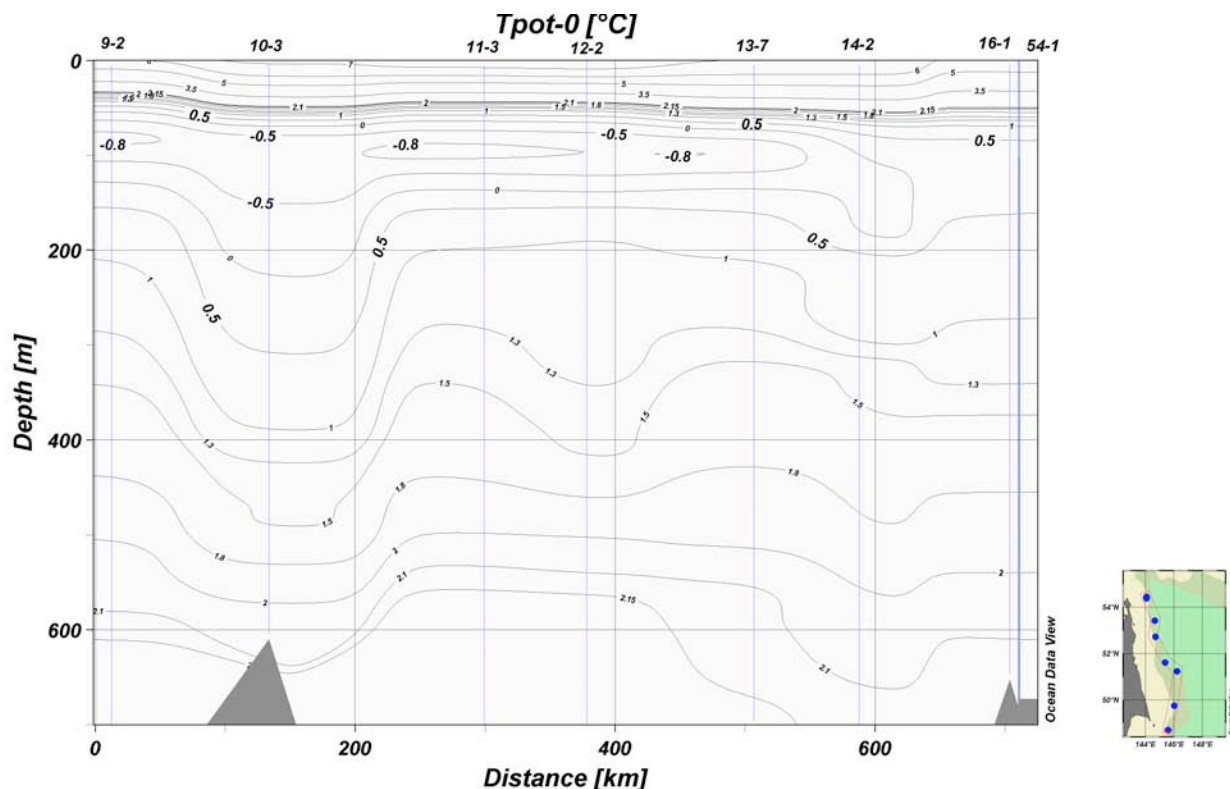
Fig. 4.1: *Potential-temperature section along the Sakhalin Slope.*

Another important feature with respect to ventilation of intermediate depths is the intrusion of cold waters at depths of 270-350 m at the northern edge of the transect of stations SO178-14 - SO178-20. All these heterogeneities were interpreted as one intrusion moving southward and, thus, leaving the investigation area at the Obzhirov Flare.

4.3.2 Venting area

We carried out 11 CTD stations in the Obzhirov Flare area, partly as "YoYo-CTD" (see above).

This area is of special interest not only for geological tasks, but also for oceanographical, because it is a key region for ventilation of intermediate depths in the Okhotsk Sea. Due to lack of temporal observations, there is a gap in understanding the processes going on in this area.

25

Previous KOMEX investigations revealed an outstanding temporal variability of water column properties in this area. Solitary CTD observations allowed us to determine the tidal forcing of intrusion appearance in the water column as diurnal tidal periodicity. During cruise SO178-KOMEX we collected extended temporal data demonstrating a different scale of the temporal variability and more complicated phenomena which take place in the vicinity of the shelf break.

Rapid changes in water column structure occurred abruptly between stations SO178-19 and SO178-20. At station SO178-19 we suddenly, in a time interval of only several minutes, observed a dichothermal layer with a positive temperature and without any intrusions. The usual vertical structure shows a dichothermal layer with a negative temperature and an intrusion at 250-350 m depth. Such different vertical thermohaline structures occurred in a time interval of several minutes and a distance of several meters. This structure with a warm dichothermal layer was well preserved for several days until August 13, 23:19 UTC, when the previous, "normal" thermohaline structure was restored. At "YoYo-CTD" station SO178-41, a small intrusion appeared during downcast at 110-140 m depth, but the temperature value was still positive. Only 3.5 hours later, during upcast, we found a dichothermal layer of -0.49°C in temperature and a new intrusion of cold waters at about 250 m depth. Later, on August 15 at 04:12 UTC, a new intrusion of cold shelf waters appeared in the dichothermal layer and below as well as another one at 170-360 m depth. The minimum temperature was -1.50°C at 250 m. The vertical extent of the dichothermal layer increased significantly in comparison to that observed some days before (Fig. 4.2). We can say we observed the moment of intrusion of cold dense waters into intermediate depths.
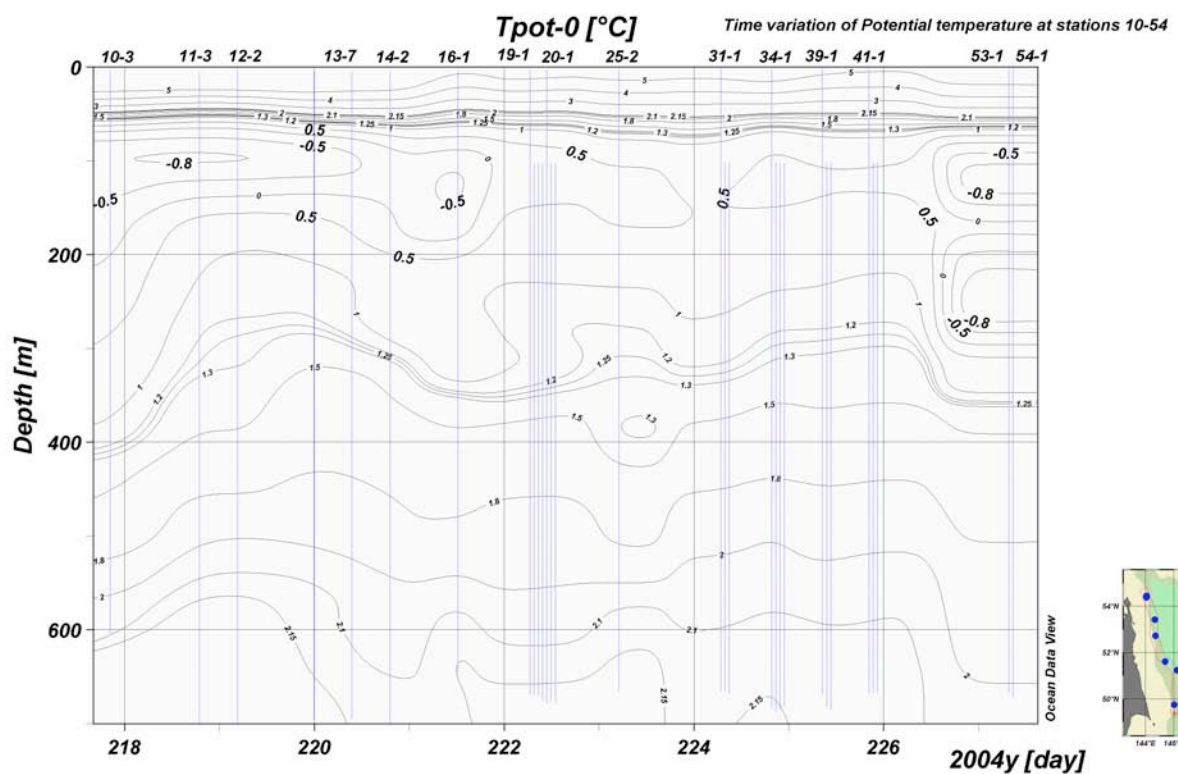
Fig. 4.2: Time variations of potential temperature at the Obzhirov Flare venting area.

The entrainment of dense shelf waters into intermediate depths occurring in the vicinity of the shelf break and on the continental slope shows some regularities. The process starts with the pumping of shelf waters into the water column, which is interrupted by relatively "quite" conditions with a warm dichothermal layer. Within warm conditions, only the upper shelf waters mix with offshore waters causing a temperature increase up to +0.77°C in the dichothermal layer of the slope area.

The "warm dichothermal layer" conditions existed for 3.5 days and then were suddenly disturbed by a new intrusion of cold waters into the subsurface and intermediate water layers. Thereby, the typical subarctic structure of the Okhotsk Sea was restored.

At the moment, we cannnot explain these phenomena. Obviously, they are caused by some kind of periodic forcing, but an overtidal time interval of 3.5 days is beyond our explanation. We need additional oceanographic observations to understand the temporal scales of the variability of water column properties in this area.

4.3.3 Derugin Basin

3 CTD stations were carried out here. SO178-59-1 near a fluid venting site showed a methane anomaly at 50 m above the seafloor. SO178-73-1 was located at the top of the Barite Mound at a place with clear evidence of fluid venting. The water column (Fig. 4.3) is very well mixed at a depth of 40-50 m above the seafloor and characterized by a high methane anomaly accompanied with a negative oxygen anomaly. The mixing is probably due to a lower oxygen and higher methane content and to the buoyancy of the incoming fluids.
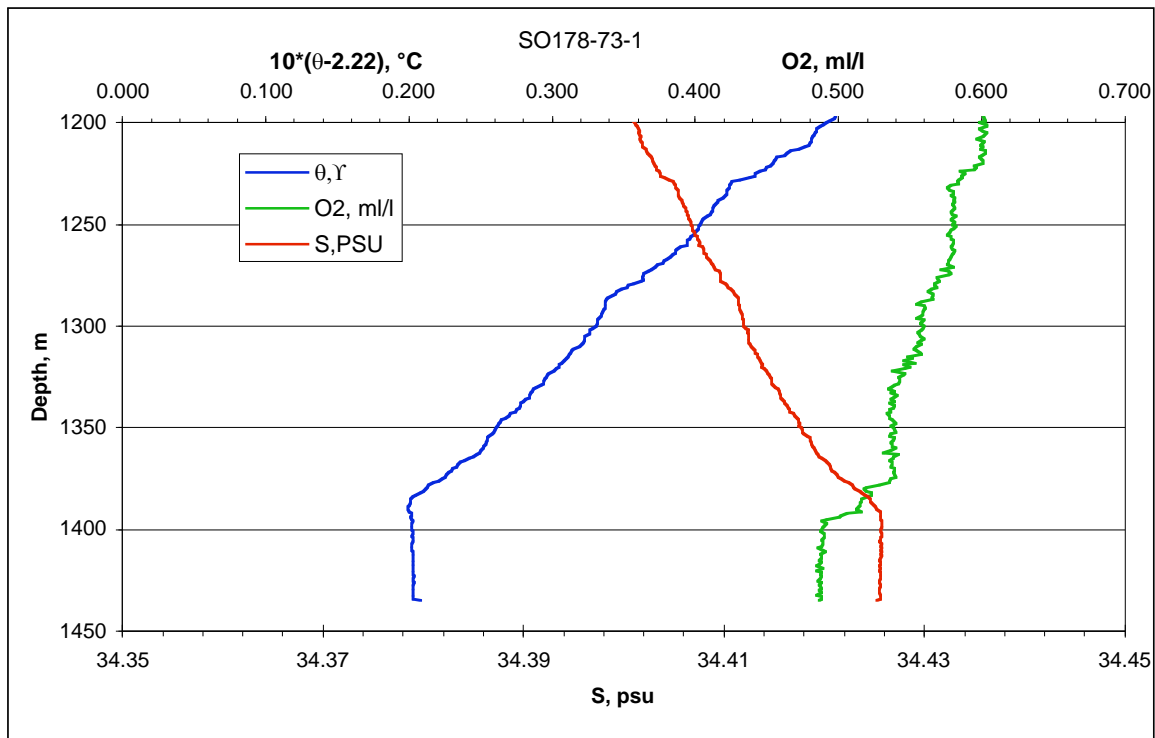
Fig. 4.3: *Strong mixing above the active venting site at the Barite Mound. Vertical water structure - Potential temperature (θ), oxygen (O_2) and salinity (S) above the seafloor at station SO178-73-1.*

Station SO178-78-2 was the deepest and located at about 3 nm north of the Barite Mound area. It shows remnants of methane anomalies at a depth of about 1,500 m, which are probably related to the depth of the venting site of the Barite Mound, and background values for other hydrochemical water properties.

4.3.4 Kurile Basin

3 CTD stations were carried out here: SO178-1-1, SO178-2-1, and SO178-86-1. The most intriguing feature of the water column properties in this area is the outstanding vertical mixing below the dichothermal layer and at intermediate depths up to 1,300 m (SO178-86-1). The lattest station shows furthermore near-bottom negative potential temperatures and positive oxygen anomalies. They are linked to the supply of North Pacific bottom waters in the central part of the Kurile Basin and the area close to Bussol Strait previously revealed during GE99 and LV29 cruises. (Fig. 4.4)
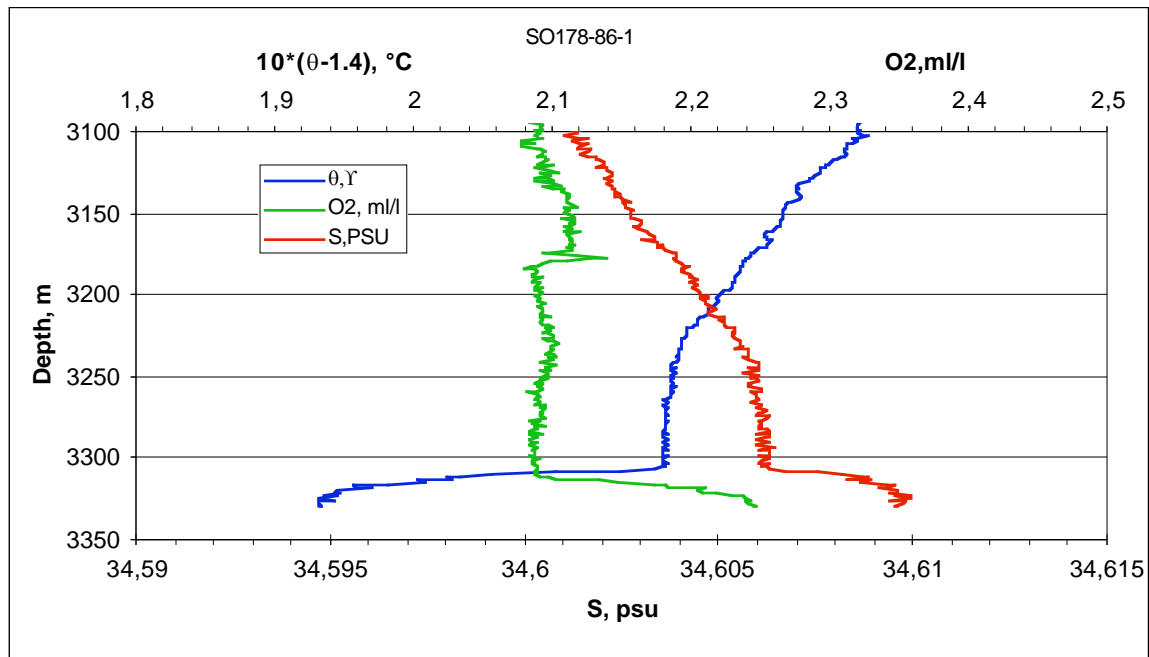
*Fig. 4.4: Bottom water formation in the Kurile Basin: Pacific waters intrude via the Bussol Strait sill (2,320 m) and spread in the near-bottom layer. Vertical water structure: Potential temperature (θ), oxygen (O₂), and salinity (S) above the seafloor at station SO178-86-1.*

5. HYDROCHEMISTRY OF THE WATER COLUMN

Pavel Tishchenko, Galina Pavlova, Sergey Sagalaev, Anatoly Salyuk, Valery Sosnin, Anatoly Obzhirov, and Nicole Biebow

5.1 Introduction

The Okhotsk Sea is one of the most productive areas of the World Ocean. Due to the high primary production, the sediments are in many areas substantially enriched in organic matter. It is commonly accepted that in the sediments of the Okhotsk Sea, early diagenesis of organic matter governs authigenic mineral formation.

Inorganic forms (CO_2, HCO_3^- CO_3^{2-}) of dissolved carbon in seawater are an important factor of the carbon budget in marine environment. These species of carbonic acid dissociation are often considered as carbonate system. Four parameters of the carbonate system are measurable: CO_2 partial pressure (pCO_2), dissolved inorganic carbon

($DIC = CO_2 + HCO_3^- + CO_3^{-2}$), pH, and total alkalinity

($TA = HCO_3^- + 2 \cdot CO_3^{-2} + B(OH)_4^- + PO_4^{-3} + HPO_4^{-2} + HSiO_3^- + HS^- + S^{-2} + org.\ acid - H^+$).

Usually, when two parameters are measured along with T, S, P data (CTD data), other parameters can be calculated using available dissociation constants of the carbonate system (Millero, 1995).

During the SO178-KOMEX cruise we measured two carbonate system parameters: pH (at 15°C), TA and additionally dissolved oxygen content. These data are valuable for estimation of the present status of biogeochemical processes related with carbon in the water column.

5.2 Methods

pH measurements in seawater were carried out by means of a cell without liquid junction (Tishchenko et al., 2001; 2002) as follows:

Glass-electrode-Na$^+$ | test solution | H$^+$-glass-electrode
                            | (standard solution) |
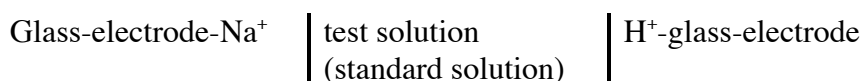
We used glass electrodes responding for hydrogen ions (ESL-43-G) and for sodium ions (ESL-51-G) manufactured by Gomel Plant (Belorussia). For calibration of the cell, a buffer solution of TRIS-TRIS·HCl-NaCl-H$_2$O (m_{TRIS}=$m_{TRISHCl}$=0.04, m_{NaCl}=0.4) was prepared. pH values on "total" scale were calculated as:

$$pH_T = p(a_H / \gamma_{Na})_S + \frac{F \cdot (E_S - E_X)}{RT \ln(10)} + \log\left[\frac{(m_{Na})_S}{(m_{Na})_X}\right] - \log(\gamma_{Na})_X + \log(\gamma_H)_X$$

where E_S, E_X are electromotive forces of the cell in standard and test solution, respectively, and $(m_{Na})_S$ is the molality of sodium ions in standard solutions as determined according to preparation of the standard solution. The molality of sodium in test solutions (seawater) was calculated as:

$$(m_{Na})_X = \frac{13.872 \cdot S}{1000 - 1.00511 \cdot S}$$

Standard values of $p(a_H / \gamma_{Na})_S \equiv -\log(a_H / \gamma_{Na})_S$ in buffer solutions have been tabulated

previously (Tishchenko et al., 2001); activity coefficients of sodium and hydrogen ions are also published (Tishchenko et al., 2001; 2002). During the cruise, the formal standard potential of the cell was constant within ± 0.2 mV. Usually, we calibrated the cell daily. Under these conditions, the error of pH_T measurements was about ±0.003 pH unit.

Total Alkalinity (TA) in seawater samples was analyzed within 3 hours after taking by direct titration in an open cell of 25 ml of seawater with 0.02 N HCl. To remove carbon dioxide during titration, the samples were flushed with a continuous stream of pure nitrogen. A mixture of methylene blue and methyle red was used as indicator, and titration was completed when the green color of the solution turned to light-pink (at the end point pH is equal to 5.4-5.5). The method is well-known as Bruevich's method (Bruevich, 1944) and recommended as standard operating procedure among oceanographers in Russia (Ivanenkov & Bordovsky, 1978). The acid was standardized daily with Na_2CO_3 solution prepared from pre-weighted crystals dried at 280°C. A Brinkman/Dosimat 665 motor-driven piston burette reproducible to ±0.001 ml in the delivered volume was applied for analysis. Based on analysis of seawater replicates, an analytical precision of ±1.6 µM/kg (n=10) for total alkalinity was achieved.

Dissolved oxygen was determined by the modified Winkler method (Carpenter, 1965). In this version of the method, the end point was detected photometrically at a wave length of 350 nm. Automatic titration was carried out using Dosimate burette, photometer and PC. Estimated from replicates, precision of oxygen analysis generally amounted to ±1 μM.

Samples for *dissolved calcium* (Ca) in seawater were given into 140 ml plastic flasks and preserved with hydrochloric acid to create pH=2. These samples will be analyzed by complexometric titration of 10 g of seawater (Tsunogai, 1968) in the shore-based laboratory at POI. EGTA is used as titrant and GHA [glyoxal-bic (2hydroxyanil)], a sensitive reagent for calcium, is used as metal indicator at pH 11.7. Calcium is extracted into a small volume (4 ml) of organic solvent (n-Butanol) as its GHA-complex and titrated with EGTA (9.580 mM). The end point is sharp and occurs when the red color of the organic layer vanishes. The EGTA is standardized daily with standard calcium solution prepared from highly pure calcium carbonate. A correction factor of 0.9946 is applied to account for Sr and Mg during titration. The Brinkman/Dosimat 665 motor-driven piston burette reproducible to ±0.001 ml in the delivered volume is applied for analysis. This method provides precision less than 0.1%.

Samples from Niskin bottles were analyzed for pH, alkalinity and dissolved oxygen. Dissolved inorganic carbon (DIC), CO_2 partial pressure (pCO_2), pH in situ and saturation degree of water columns with respect to aragonite (L_a) and calcite (L_c) were calculated using general accepted procedures (Millero, 1995) and carbonic acid constants suggested by Lucker et al. (2000).

5.3 Results and discussion

Hydrochemical data were obtained from 24 stations along with CTD hydrographic data for different areas in the Okhotsk Sea (Fig. 5.1). The complete water column dataset is shown in Appendix 3.1, the used abbreviations are listed in Tab. 5.1. Additionally, MUC data are presented in Appendix 3.2.

Tab. 5.1: *Used symbols, units, and abbreviations*

TA	Total alkalinity, mM/kg
$pH_t(15)$	PH_t measured at 15 °C in "total" scale
$PH_{in\ situ}$	pH at in situ temperature and pressure in "total" scale
DIC	Dissolved inorganic carbon, mM/kg
pCO_2	Partial pressure of carbon dioxide, µatm
La	Aragonite saturation degree
Lc	Calcite saturation degree
O_2	Oxygen concentration, mM/kg

One part of the data is presented in sections of stations SO178-1-1, SO178-3-2, SO178-10-3, SO178-12-2, SO178-13-7, SO178-14-2, and SO178-16-1 (Fig. 5.2 - 5.8). We also compared data profiles for different study areas (Fig. 5.9 and 5.10). Additionally, the biological term of apparent oxygen utilization (AOUb) was calculated according to the scheme published by Tishchenko et al. (1999). These results are presented in Fig. 5.11.

From the obtained data we can draw the following preliminary conclusions:
1.   Seawater is undersaturated below 100-150 m and 250-500 m in aragonite and calcite, respectively (Fig. 5.7, 5.8, and 5.10).
2.   Negative values of AOU in the upper layer (Fig. 5.11) indicate that production of organic matter exceeds destruction and respiration processes.
3.   Due to photosynthetic activity, the upper water layer of the Okhotsk Sea is undersaturated in atmospheric CO_2 ($pCO_{2atmospheric} \cong 365$ µatm) (Fig. 5.6). Therefore, the Okhotsk Sea is a sink for atmospheric CO_2 during the studied season.
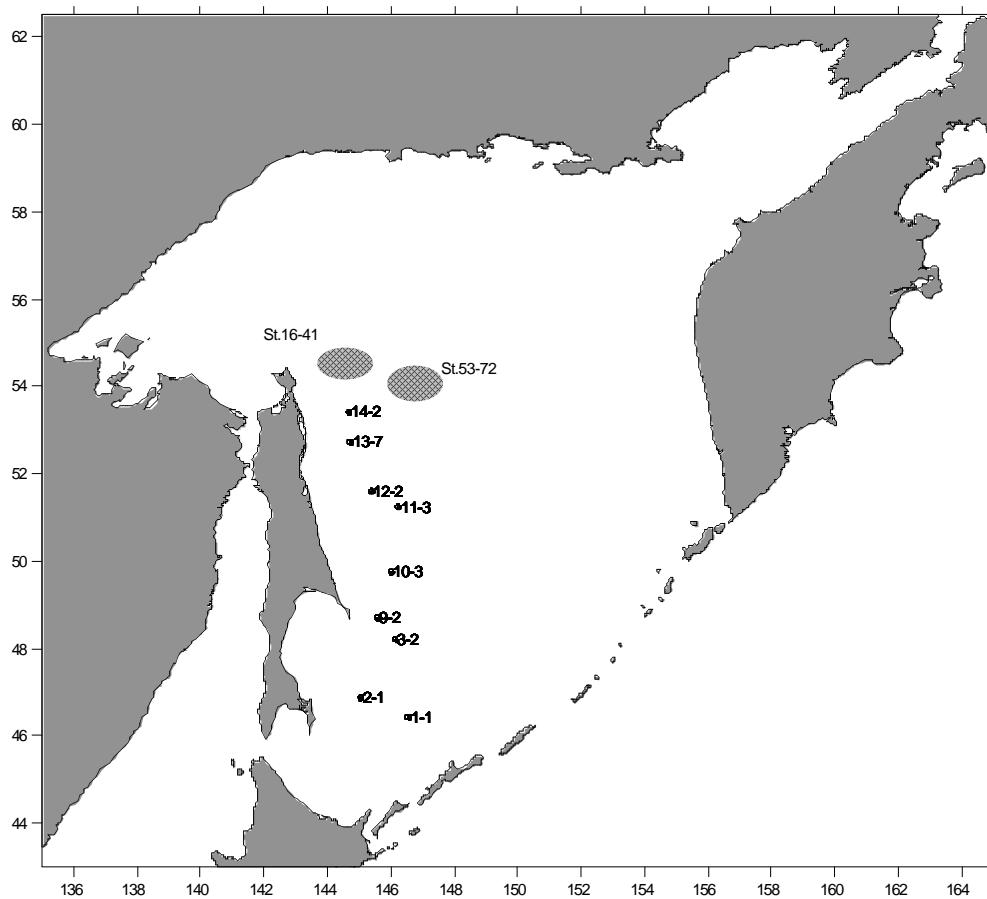
***F*ig.5.1:** *CTD stations of cruise SO178-KOMEX.*
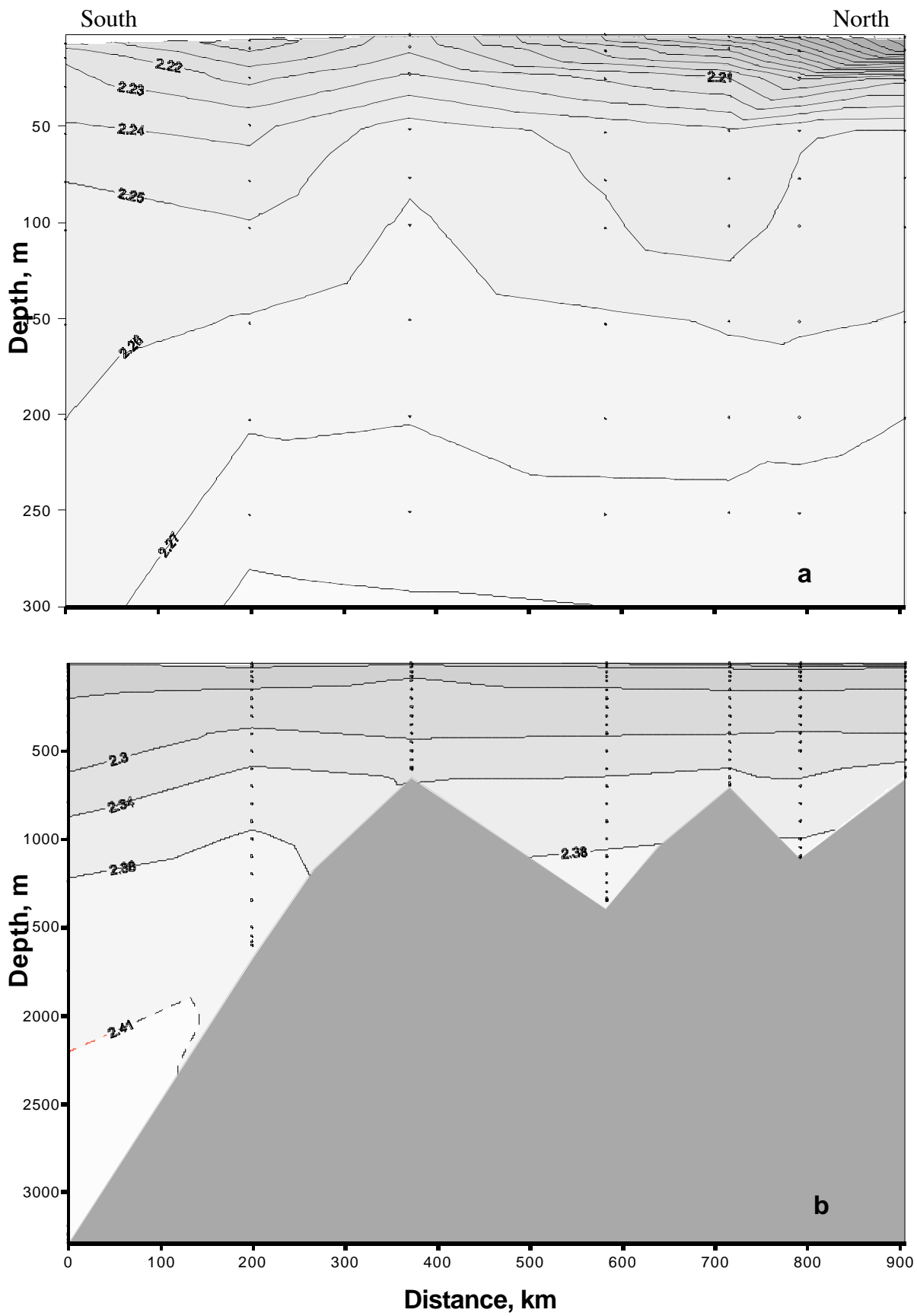
Fig. 5.2: TA (mmol/kg) at stations SO178-1-1, -3-2, -10-3, -12-2, -13-7, -14-2, -16-1.

South   North
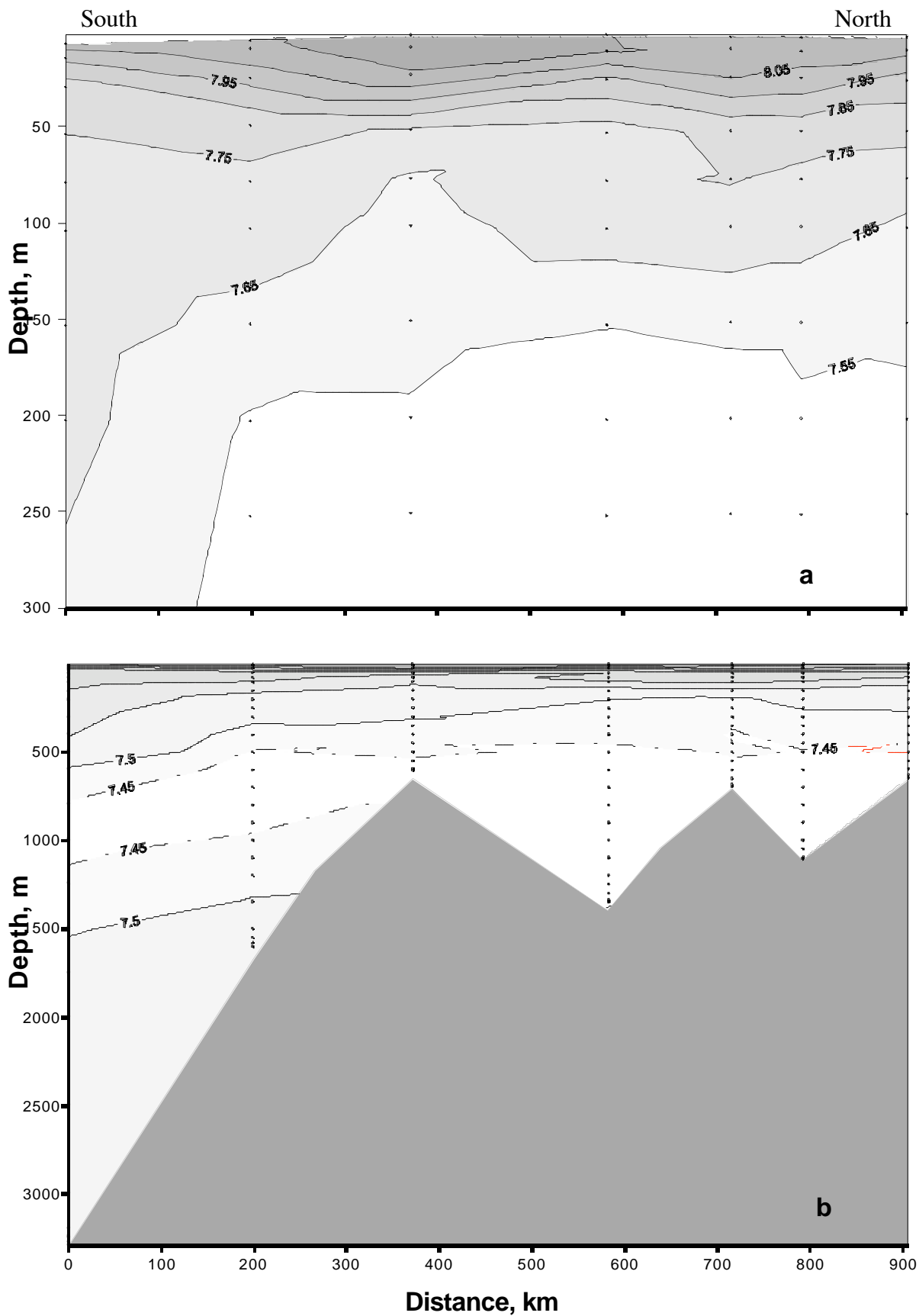
Fig. 5.3: *pH_{in situ} at stations SO178-1-1, -3-2, -10-3, -12-2, -13-7, -14-2, -16-1.*

South   North
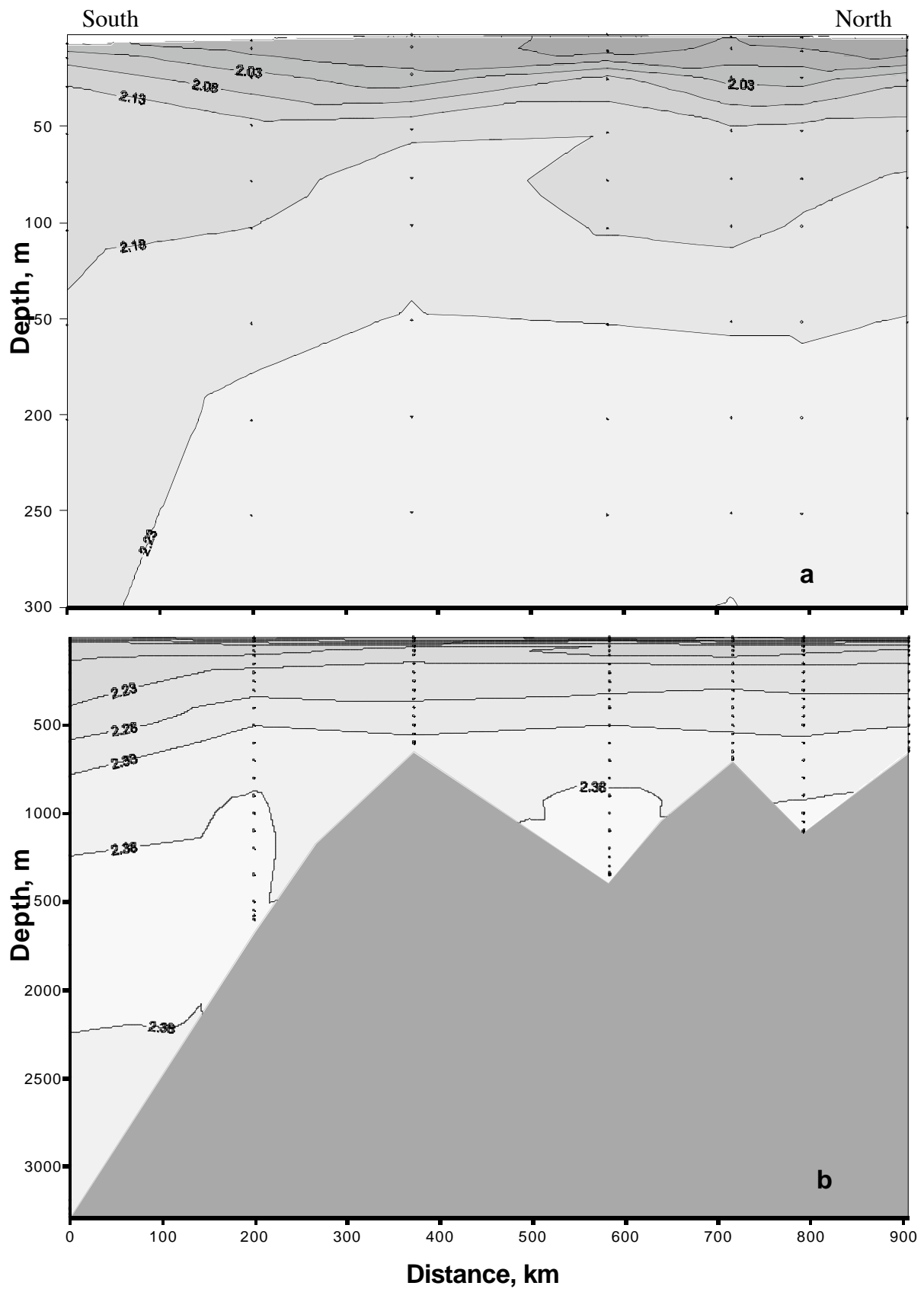
Fig. 5.4: *DIC (mmol/kg) at stations SO178-1-1, -3-2, -10-3, -12-2, -13-7, -14-2, -16-1.*
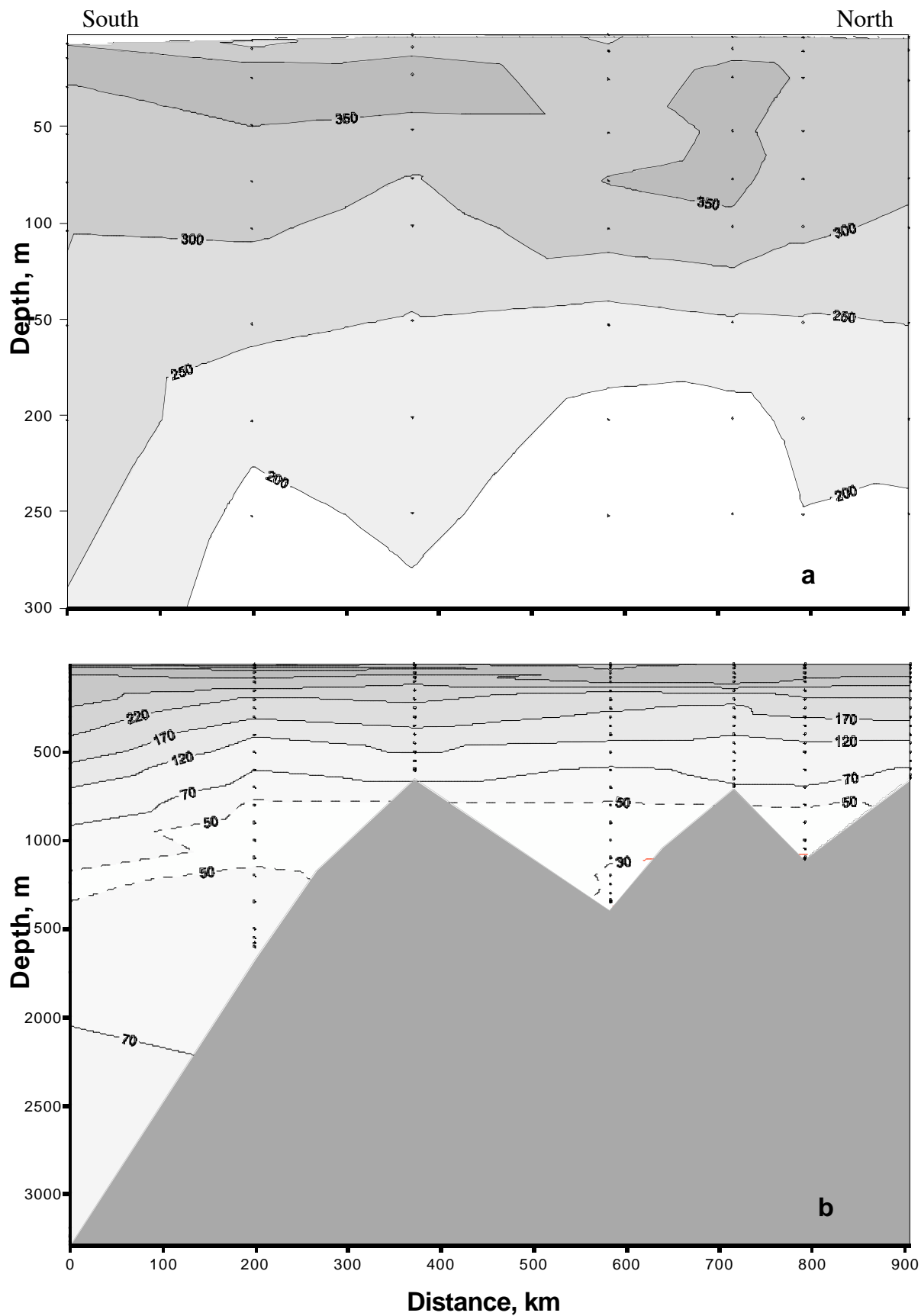
Fig. 5.5: Dissolved oxygen (mol/kg) at stations SO178-1-1, -3-2, -10-3, -12-2, -13-7, -14-2, -16-1.

South   North
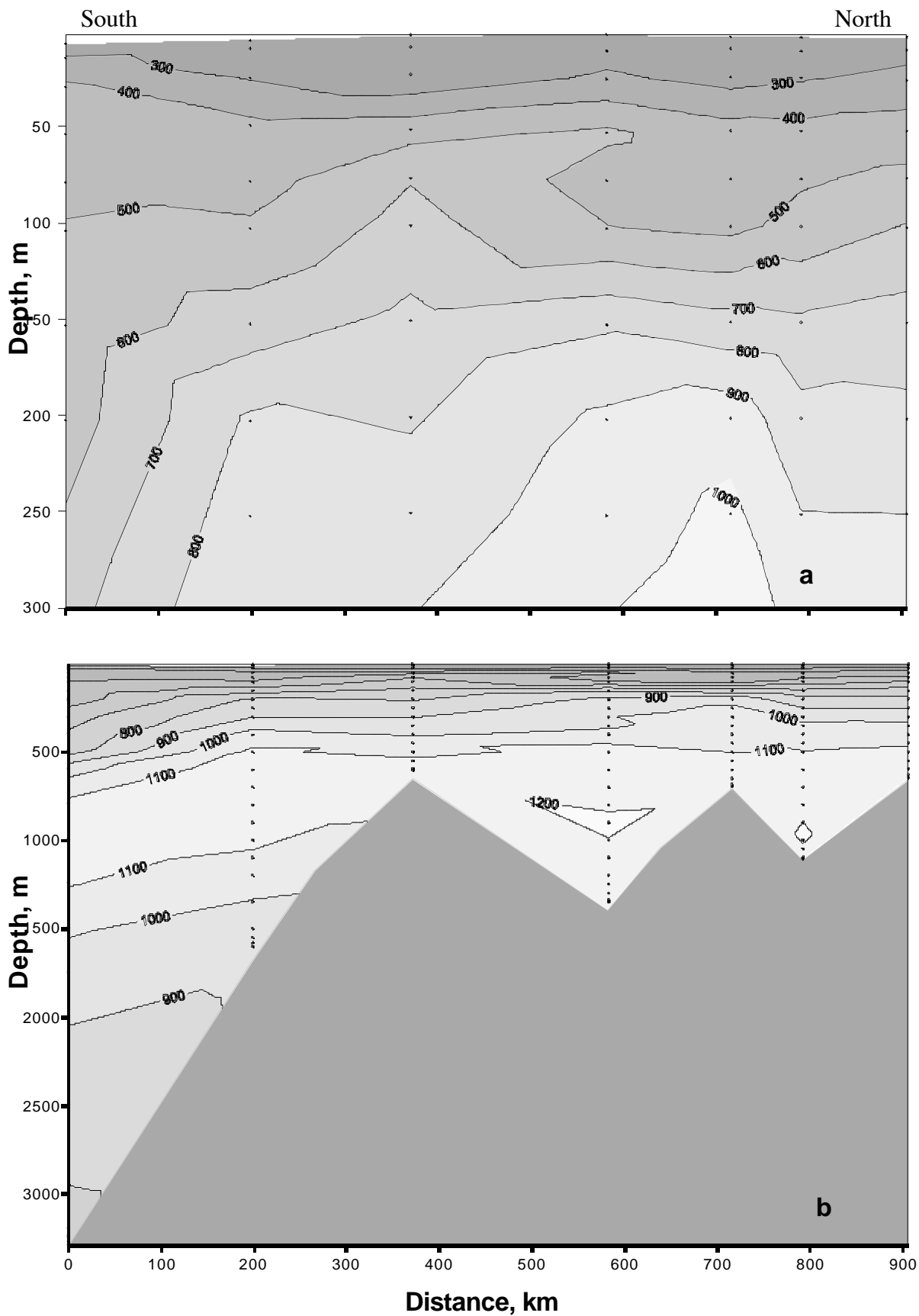
Fig. 5.6: *CO$_2$ partial pressure (µatm.) at stations 1-1, 3-2, 10-3, 12-2, 13-7, 14-2, 16-1.*
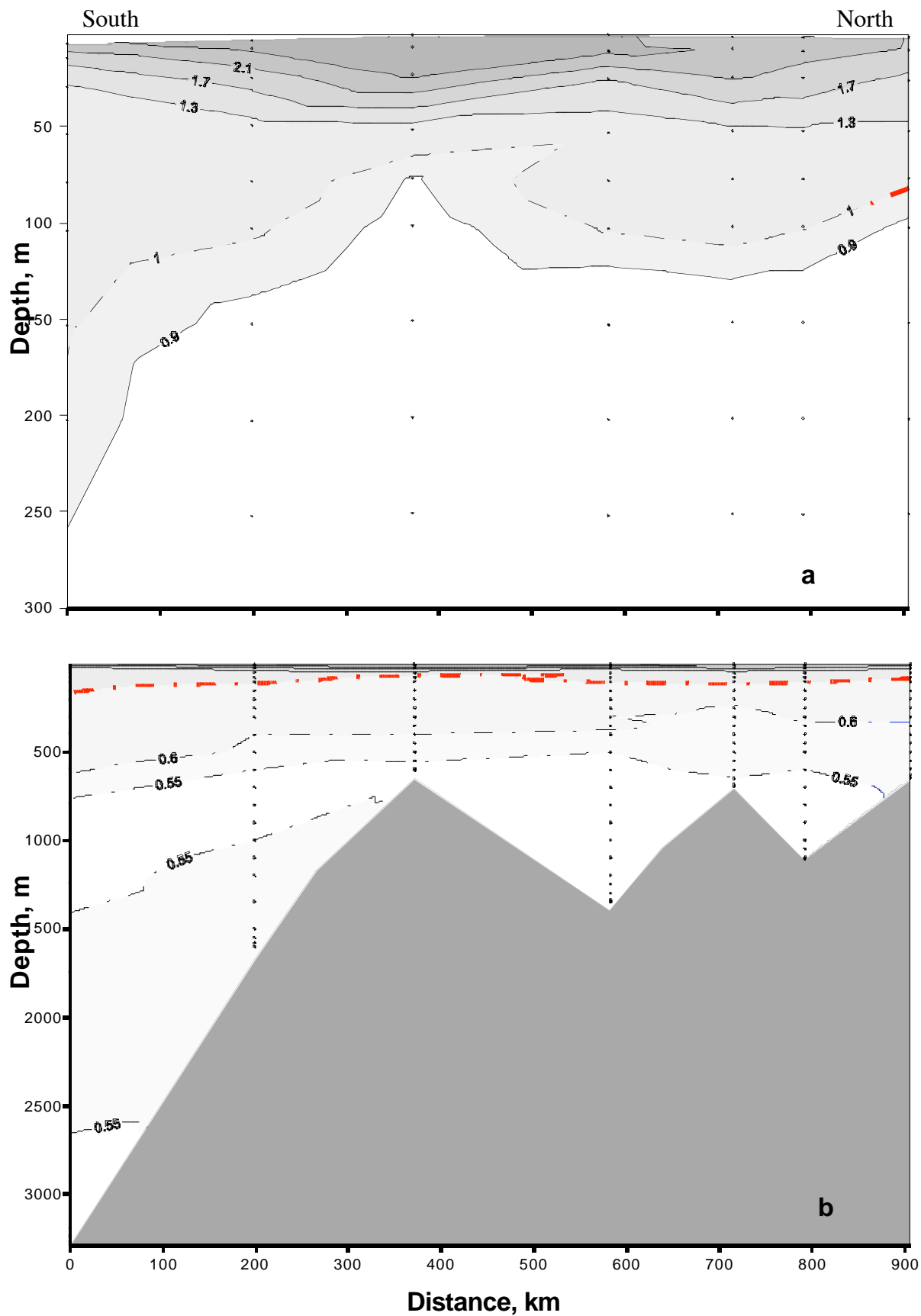
Fig. 5.7: *Aragonite saturation degree of seawater at stations SO178-1-1, - 3-2, -10-3, -12-2, -13-7, -14-2, -16-1.*
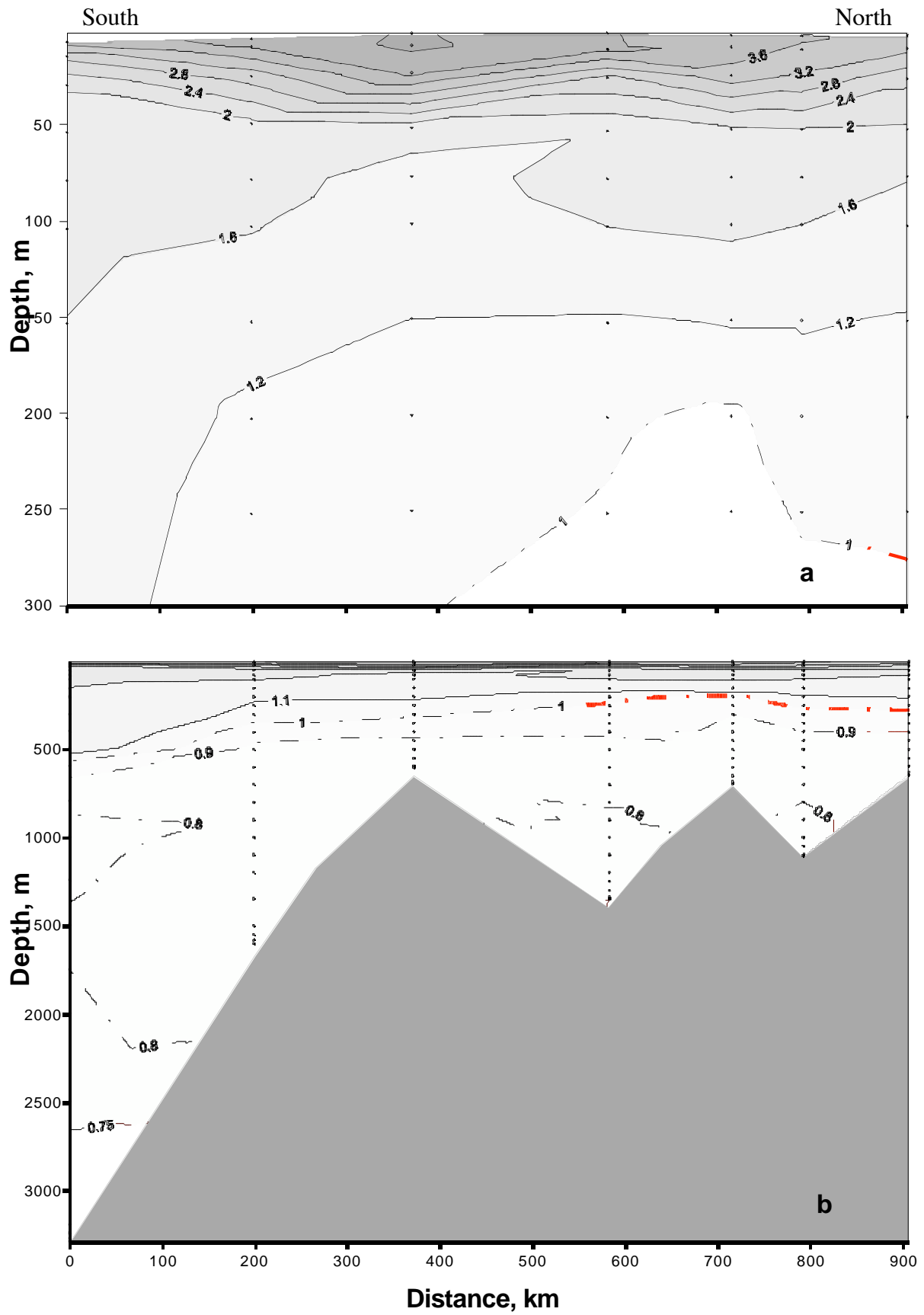
Fig. 5.8: *Calcite saturation degree of seawater at stations SO178-1-1, - 3-2, -10-3, -12-2, -13-7, -14-2, -16-1.*
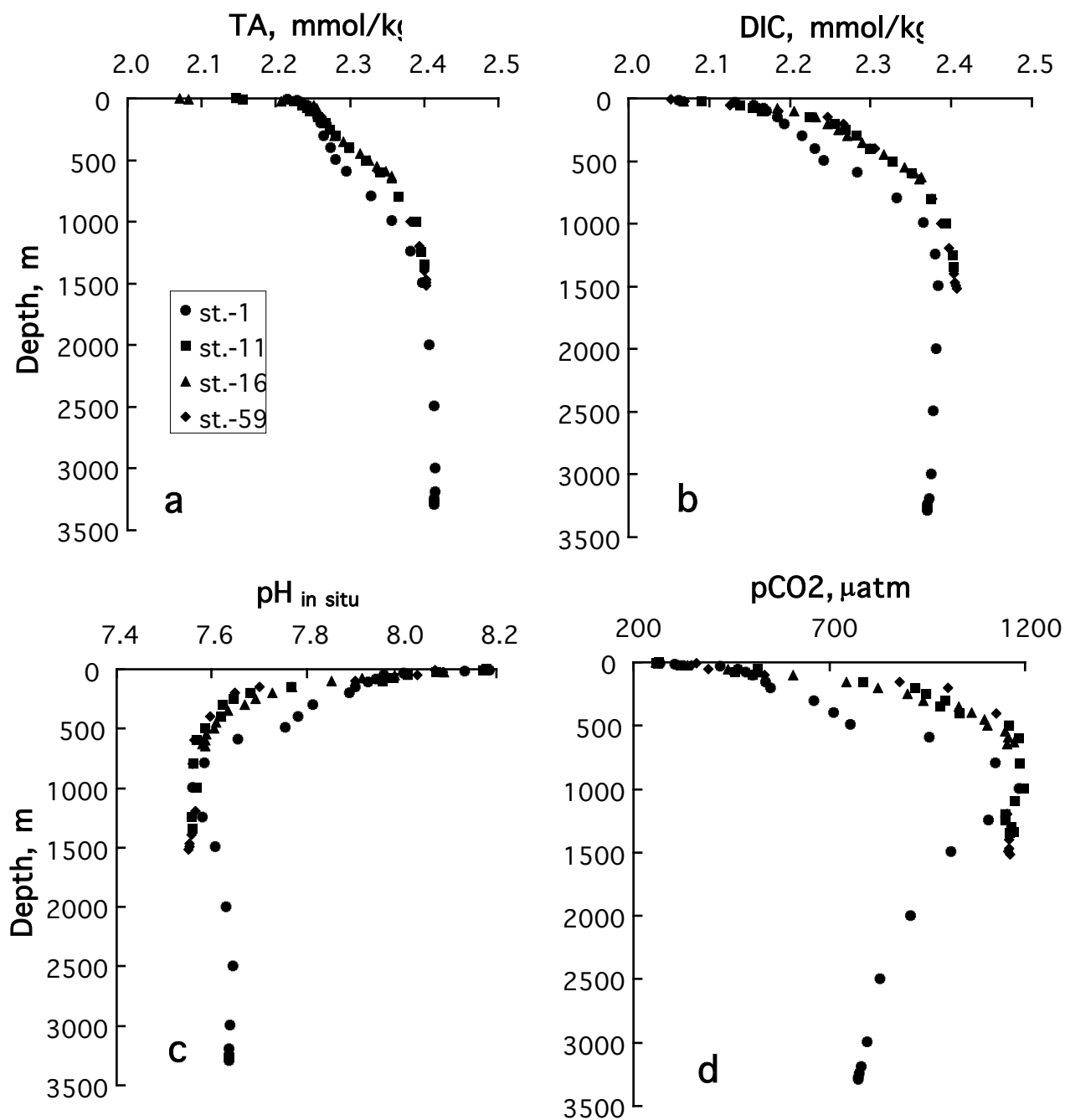
Fig. 5.9: *Profiles of TA (a), DIC (b), and pH$_{in\ situ}$ (c) pCO$_2$ (d) for different studied areas (Stations SO178-1-1, -11-3, -16-1, -59-1).*
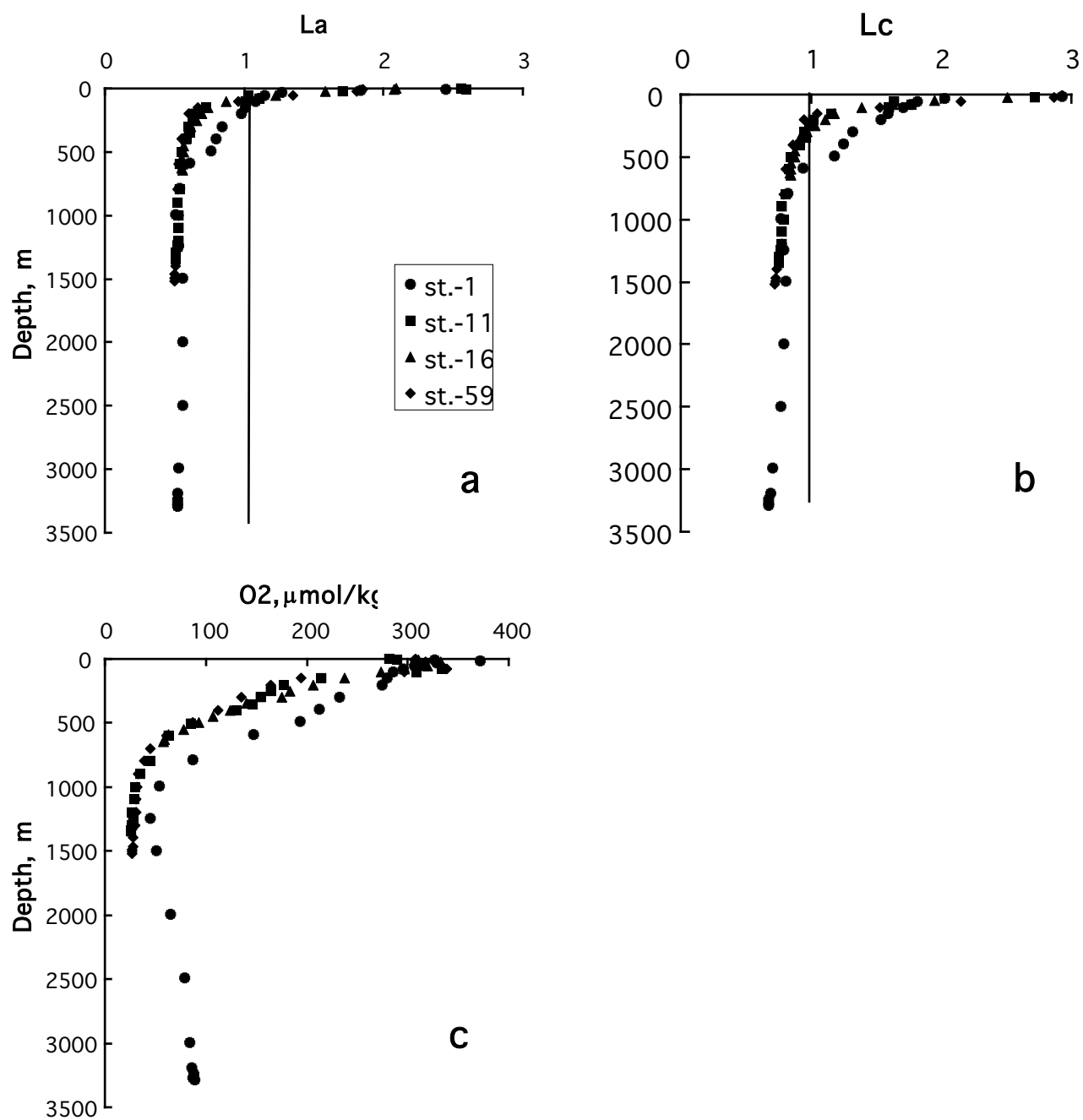
Fig. 5.10: *Profiles of saturation degree of seawater for aragonite (a), saturation degree of seawater for calcite (b), and dissolved oxygen (c) for different studied areas (Stations SO178-1-1, -11-3, -16-1, -59-1).*
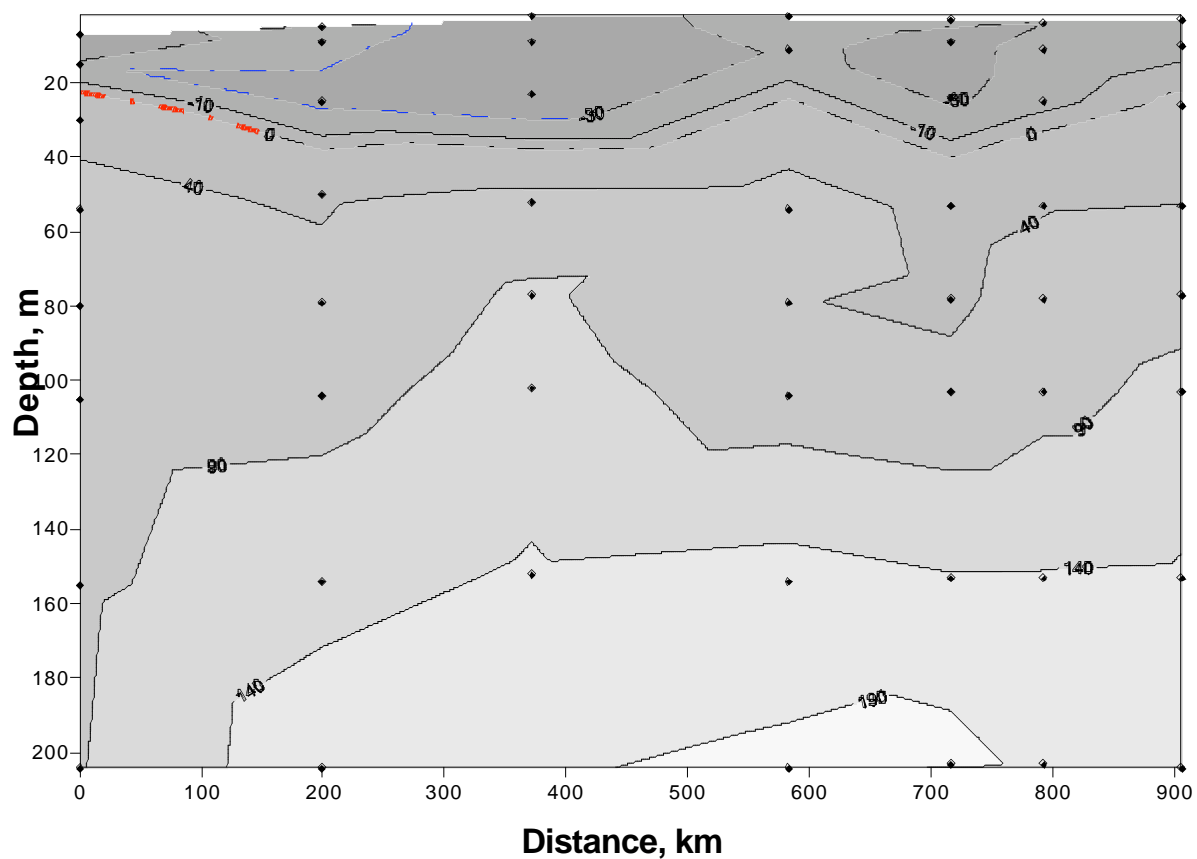
Fig. 5.11. *Section of the biological term of apparent oxygen utilization (µmol/kg) at stations SO178-1-1, -3-2, -10-3, -12-2, -13-7, -14-2, -16-1.*

6. METHANE DISTRIBUTION IN THE WATER COLUMN AND SEDIMENT

Anatoly Obzhirov, Olga Vereschagina, Anatoly Salyuk, and Sergey Sagalaev

6.1 Introduction

Methane investigations in the water column and sediment of the western part of the Okhotsk Sea started in 1984 (Obzhirov, 1993). They were extensively carried out in the framework of the KOMEX project from 1998 to 2002 (Obzhirov et al., 2002).
Previous methane investigations revealed the following regularities in the methane distribution in the water column and sediment.

<u>6.1.1 Methane distribution in the water column</u>

1. The background methane concentration usually is 50-70 nl/l in the surface water. In the subsurface layer (depth 75-100 m), the maximum methane concentration amounts to 100-120 nl/l. It decreases to 15-20 nl/l in the bottom layer of the deeper part of the Okhotsk Sea (>1,000 m).
2. The methane concentration in the water column exceeds background values when there are methane sources in the sediment as oil and gas deposits and/ or gas hydrates. In this case, methane rises into the water column and creates an anomaly from the bottom water up to the surface water with maximum values of 20,000-200,000 nl/l and 500-1,000 nl/l, respectively.
3. Many methane flares were detected on the northeastern Sakhalin Shelf and Slope. Monitoring of these flares revealed a quantative growth from 2 flares in 1988 to about 100 in 2002. This growth was caused by an increase of the seismo-tectonic activity in this area. As a result of the increased activity, a fault zone opened via which methane rises from oil-gas-bearing deposits and gas hydrates as well as from beneath the gas hydrate layer into the water column.

<u>6.1.2 Methane distribution in the sediment</u>

1. The background methane concentration is usually 1-5 μl/l in the horizon from the surface sediments to 200 cm sediment depth. This is connected with sulphate-reduction processes. Downcore concentration increases to10-50 μl/l at 10 m sediment depth.
2. The methane concentration sharply increases up to 100-1,000 μl/l even in surface sediments if much organic matter is present in the sediments.
3. Gas hydrates occur in the upper sediment layer in 5 areas of the northern Sakhalin Slope usually located within gas flare areas. It is possible that a second (young) gas hydrate layer formed from a methane flux rising from below the gas hydrates.

<u>6.1.3 Purposes of methane investigations during cruise SO178-KOMEX</u>

To study the methane distribution in longer sediment cores than those recovered during previous cruises.
To observe gas hydrate and gas flare areas with video-controlled devices as the TV-MUC, TV-grab and TV-sled OFOS.
To examine the methane distribution in the water column of the Obzhirov Flare area more detailedly using the the so-called "YoYo-CTD" (see Chapter 4).
To study the methane distribution in other, formerly not investigated areas.

6.2 Methods

Water was taken from Niskin bottles of the CTD Rosette. Gas was extracted from the water sample via a vacuum line. The vacuum method allows to extract 70-80% of methane. Methane was analyzed with the gas chromatograph SRI. In the sediments, methane was measured with the Head Space method. To control the measurements, gas standards were used for calibration.

6.3 Results

6.3.1 Methane distribution in the water column

Methane was measured in the water column at 16 "full" stations (from bottom to surface) and 5 "YoYo-CTD" stations (from bottom to 250 m above the seafloor) as well as in the bottom water of TV-MUC cores at 15 stations (Appendix 4). On the eastern Sakhalin Slope from 46°25`N to 48°41`N (stations SO178-1-1, SO178-2-1, SO178-3-1, and SO178-9-2) the methane concentration in the water column is almost at background level amounting to 50-60 nl/l in the surface layer, 100-130 nl/l at about 50 m depth (subsurface maximum) and decreasing to 15-20 nl/l in the bottom layer. At station SO178-2-1, small methane anomalies (90 nl/l) were found in the bottom water (depth 2,976 m) as well as an anomaly (120-500 nl/l) in the intermediate water layers from 100 to 500 m. Methane is possibly advected into this area with water intrusions from the Sakhalin Shelf. Here, oil-gas deposits and great methane anomalies in the water column are present. The anomaly in the bottom water of station SO178-2-1 may be created by methane either from the sediment or the intrusions from the shelf.

The methane distribution at stations SO178-11-3 (51°14`N) and SO178-12-2 (51°36`N) is the same as on the profile between 46°25`N - 48°41`N. It represents an extension of the methane anomaly in the subsurface and intermediate layers of station SO178-2-1. At station SO178-10-3 (49°44`N), the methane concentration sharply changes showing anomalously high values (200-500 nl/) from surface to bottom and an anomaly (1100-1500 nl/l) at the horizon 50-100 m. Whether these concentrations are caused by oil-gas deposits and/ or gas hydrates is not yet clear.

The regularity which was observed in the methane concentrations of the southern investigation area changed at station SO178-13-7 (52°43`N). Here, an anomaly (203 nl/l) occurs at 500 m depth and increases towards the bottom (695 m) to 864 nl/l. The source of methane in this area are gas hydrates and/ or oil-gas-bearing sediments.

The water column at station SO178-14-2 (53°24`N) is characterized by a methane anomaly (200-1073 nl/l) in intermediate water layers from 150 to 800 m depth. The methane distribution is here similar to that in the southern area (49°44`N, station SO178-10-3): a methane-containing water layer is advected from the shelf into this area.

At stations SO178-16-1 (54°22`N) and SO178-54-1 (54°26`N, Obzhirov Flare area), methane anomalies were measured in the bottom water (800-1,200 nl/l) and intermediate water layer (800-900 nl/l). Oil-gas deposits, gas hydrates, and a water layer intrusion from the shelf are the sources for these anomalies. A more detailed study of the methane distribution in the lower part of the water column was here carried out with the "YoYo-CTD" (Appendix 4).

The water columns in the Barite Mound area (eastern Derugin Basin, stations SO178-59-1 and SO178-73-1), in the Clam Hill area (station SO178-78-2), and near the central part of the Okhotsk Sea (station SO178-82-1) show a stable methane distribution pattern. In the surface
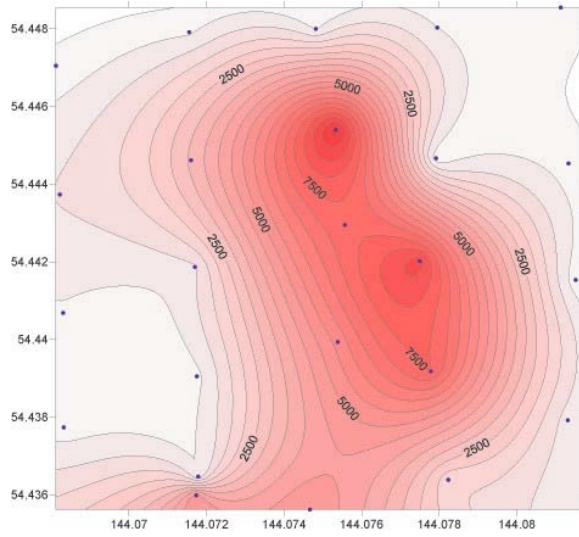
Fig. 6.1: *Distribution of CH₄ (nl/l) in the bottom water layer (675 m).*
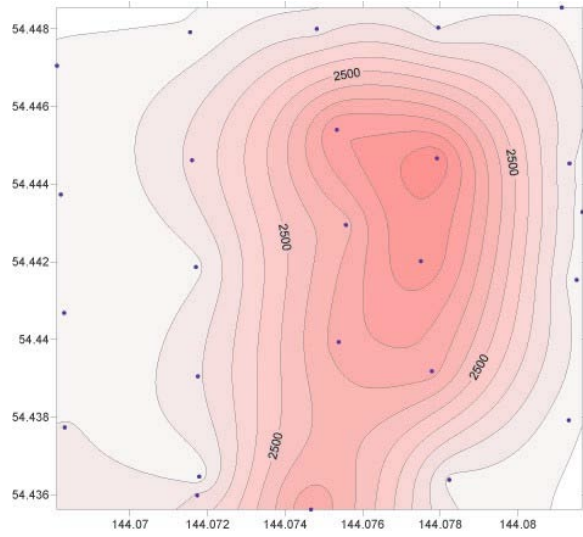
Fig. 6.2: *Distribution of CH₄ (nl/l) 50 m above the seafloor (625 m).*
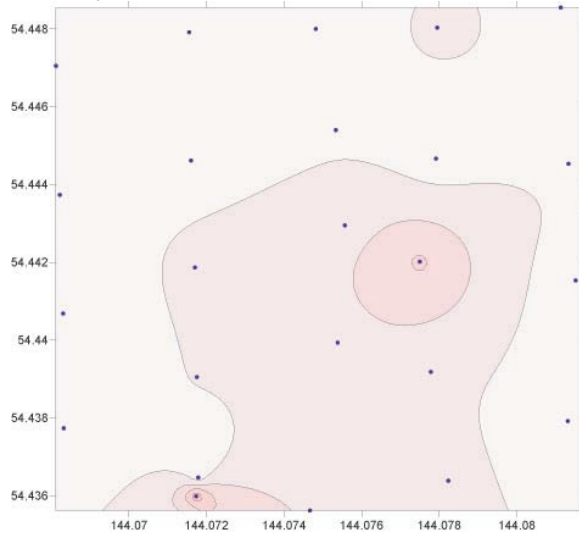
Fig. 6.3: *Distribution of CH₄ (nl/l) 100 m above the seafloor (575 m).*
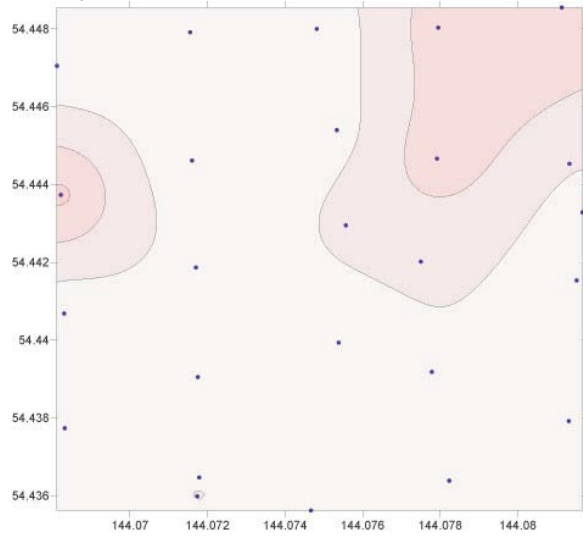
Fig. 6.4: *Distribution of CH₄ (nl/l) 150 m above the seafloor (525 m).*
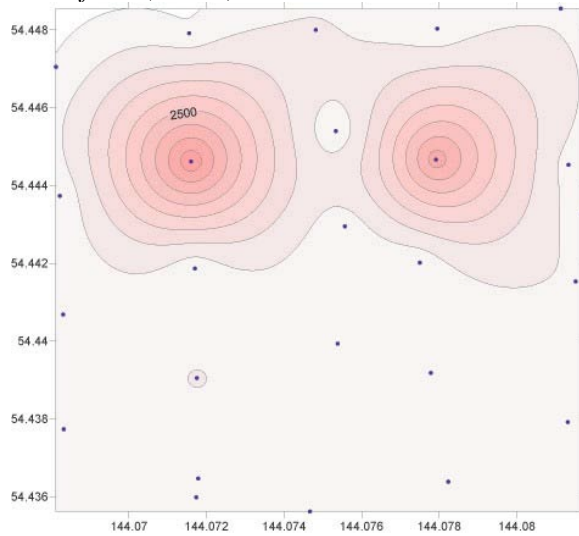

**Fig. 6.5:** *Distribution of CH₄ (nl/l) 200 m above the seafloor (475 m).*
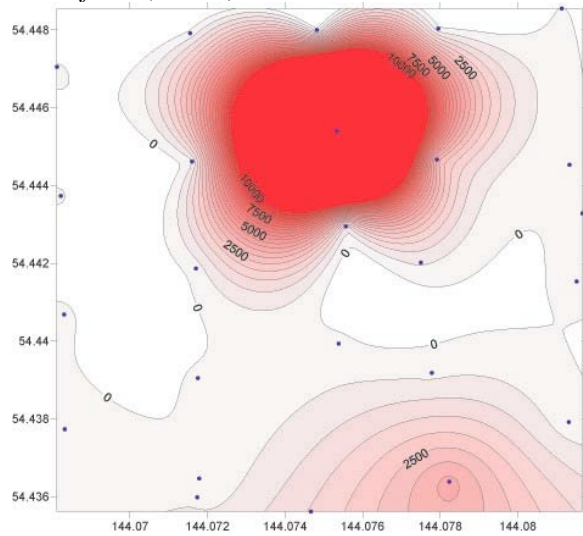
Fig. 6.6: *Distribution of CH₄ (nl/l) 250 m above the seafloor (425 m).*

and subsurface layers (75-100 m), the methane concentration is at background level (60-70 nl/l) or sightly increased (100-120 nl/l), respectively. At greater depths, the methane concentration usually decreases to 30-20 nl/l. When there is no other methane source in the sediments, the methane concentration in the bottom water is at background level (26 nl/l at station SO178-82-1). In the Barite Mound area (station SO178-73-1), the methane concentration reaches 1,943 nl/l. This anomaly was observed during all former cruises (Biebow & Hütten, 1999; Biebow et al., 2000). It occurs in a very thin layer (70-100 m), and its source is still unknown. At station SO178-86-1 (Kurile Basin), the methane concentration does not exceed background values: 80 nl/l at the surface, 140-160 nl/l at the subsurface maximum (depth 50-100 m), and as little as 25 nl/l in the bottom water (depth 3,328 m). A methane anomaly (155 nl/l) was measured at 236 m above the seafloor. Its origin is still unknown, it could be an intermediate water intrusion from the slope.

In the Obzhirov Flare area (54°26.775 N), a gas distribution survey in the lower water column (from the bottom at 666 m up to a depth of 426 m) was carried out at 5 stations covering an area of 1 km^2 (Appendix 4). Water samples were taken every 50 m at 6 horizons. Obzhirov Flare was the center of the surveyed area. Three regular methane distribution patterns were established as a result of the survey:

1. a decrease of the methane concentration in the bottom water layer in direction from the center (2,000-6,000 nl/l) to the edge of the flare (200-600 nl/l);

2. a marked layer at about 500-550 m water depth with a low methane concentration (70-150 nl/l);

3. unstability of the water column in the Obzhirov Flare area.

The methane concentration sharply changes in adjacent water layers as well as in vertical as in horizontal direction (Fig. 6.1 - 6.8). This unstability may be caused by different activity intensities of the individual flares (methane bubbles flux) and by water currents at different depths.

Water samples taken from the TV-MUC cores (Appendix 4) in general contain similar methane concentrations like the bottom water samples taken from the Niskin bottles (CTD stations). Great methane anomalies were found in the Kitami Flare (36,125 nl/l) and Obzhirov Flare areas (22,305 nl/l), where the bottom water was in contact with bacteria mats.

6.3.2 Methane distribution in the sediment

Methane was measured in 11 sediment cores (Appendix 4).

The methane concentration in the sediment core recovered from the Sakhalin Slope at 48°11`N (station SO178-3-4) is at background level ranging from 2 $\mu$l/l in the surface sediment to 10 $\mu$l/l at the core base (10 m). At 49°44`N (station SO178-10-5) the sediment core contains a background methane concentration (3-93 μl/l) up to 500 cm sediment depth. From 600 cm to 1,000 cm sediment depth, the methane concentration increases to 210-4,776 μl/l. A second sharp increase to 34,378 μl/l was measured in the core base (1,100-1,200 cm). Thus, 3 sediment horizons with different methane concentrations occur: layer 0-500 cm with a background concentration, layer 600-1,000 cm with a 10 times higher value, and layer 1,100-1,200 cm with a 10 times higher value in comparison to the layer above.

This methane distribution pattern was also observed at station SO178-11-5 (51°14`N). Horizon 0-500 cm contains a background methane concentration (8-56 μl/l). The methane concentration increases by 10 times in horizon 600-800 cm and by 100 times (67,188 μl/l) in horizon 1,000-1,100 cm. Further downcore from 1,200 cm to the base at 1,700 cm, the methane concentration decreases by 2 times. An almost similar pattern was found at station SO178-12-3 (51°36`N). Here, the concentration is at background level in horizon 0-400 cm. In horizon 500-900 cm it rises by 5-10 times, and from 1,000 cm to the base (1,700 cm), the methane concentration sharply increases by 100 times (45,000-65,000 μl/l).
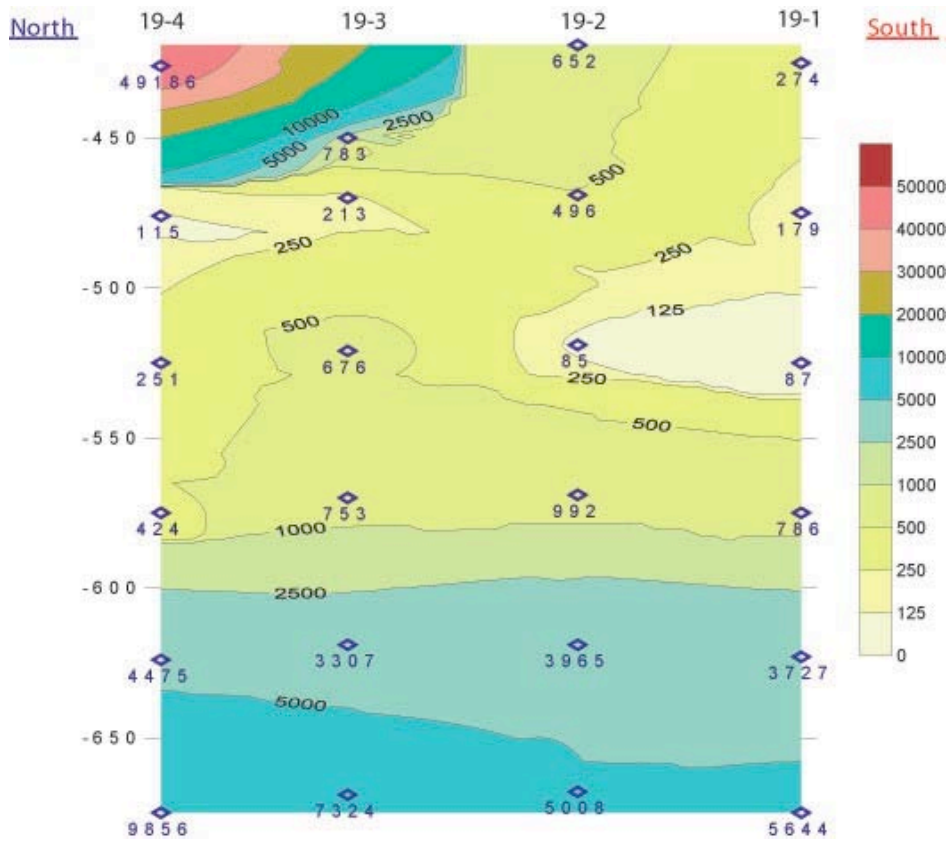
Fig. 6.7: *Methane distribution in the profile of station SO178-19 ("YoYo-CTD").*
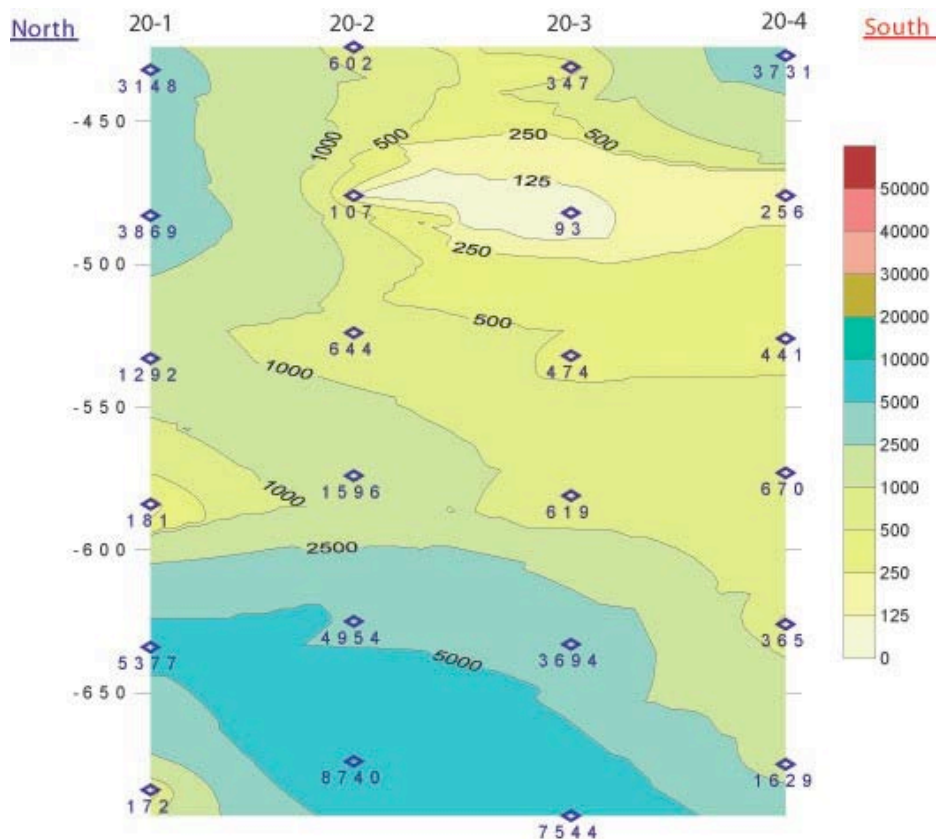

Fig. 6.8: *Methane distribution in the profile of station SO178-20 ("YoYo-CTD").*

Another example for this regularity is station SO178-78-1 in the Derugin Basin (54°04`N, 146°18`E). A background concentration (40-70 μl/l) was measured in horizon 0-400 cm. From 500 cm to the core base (1,800 cm), the methane concentration increases by 500-1,000 times (30,000-50,000 μl/l). At 1,100 cm sediment depth, there is another sharp increase to 80,000 μl/l. In the Barite Mound area (stations SO178-62-1 and SO178-69-1) a huge methane anomaly (70,000-200,000 μl/l) was measured from core top to base (0-500 cm). This methane concentration in the sediment may be linked with gas hydrate occurrences in this area.

On the Sakhalin Slope at 52°43`N, a whole sediment core (station SO178-13-6) from top (54 cm) to base (2,324 cm) shows anomalously high methane values (30,000-60,000 μl/l, at the top – 896 μl/l). In the gas hydrate-bearing Obzhirov Flare area (station SO178-26), the methane concentration in the upper sediment layer (100 cm) which contained small pieces of gas hydrates reached 1,112,196 μl/l.

6.4 Summary
6.4.1 Methane distribution in the water column

1. Methane anomalies occur in the intermediate water layer (100-559 nl/l, depth 100-500 m) and bottom water (19-90 nl/l) of the Kurile Basin. They are possibly caused by water layers with high methane concentrations moving from the Sakhalin Shelf down the slope. In the deep western Kurile Basin methane additionally rises from the sediments into the bottom water.

2. At almost all stations on the Sakhalin Slope (except for station SO178-11-3) the same methane distribution pattern was observed: a high concentration (200-400 nl/l) at about 500 m depth. Additionally, another great anomaly (1,100-1,500 nl/l) occurred in the upper water layer (50-100 m) of station SO178-10-3.

3. A high methane value (864 nl/l) was measured close to the bottom water layer at station SO178-13-7. Methane comes here from the sediment into the water column, possibly from oil-gas-bearing layers and/ or gas hydrates. The great methane anomaly in the sediment at station SO178-12-3 supports this supposition. At station SO178-10-3, in contrast, methane is mostly intruded by a water layer from the Sakhalin Shelf, and only a part rises from the sediment.

4. Anomalous concentrations (100-400 nl/l and 900-1200 nl/l, respectively) occur in the bottom water (depth 600-1,100 m) and two intermediate layers (550 m and 350 m) on the Sakhalin Slope south of Obzhirov Flare (from 53°24.977N to 54°22.625N). These concentrations are caused by methane flux from the sediments and an intrusion from the shelf with a high methane concentration.

5. The lower part of the water column in the Obzhirov Flare area is characterized by layered methane concentrations. The bottom layer has a high methane concentration (4,000-6,000 nl/l). The methane content decreases by 10-20 times at about 500 m water depth (about 100-150 m above the seafloor), whereas it increases at 200-250 m above the seafloor. This layering is due to changes in the activity of methane bubbles flux and the mobility of the water layers.

6. The methane anomaly (1,000-2,000 nl/l) in the Barite Mound area is stable. It affects a 70 - 100 m thick water layer from the top of the mound upwards.

7. The measurements of TV-MUC and CTD samples show similar methane concentrations in the bottom water. Methane concentrations of 20,000-30,000 nl/l were found in TV-MUC samples from the gas hydrate-bearing Obzhirov and Kitami Flare areas.

6.4.2 Methane distribution in the sediment

1. For sediment cores from 3 stations on the Sakhalin Slope and 1 station near the Barite Mound a typical methane distribution pattern can be established: the upper horizon (0-500 cm) contains background methane concentrations (2-20 mkl/l). The methane concentration rises by 10 times in horizon 500-900 cm, and a great methane anomaly of 60,000-80,000 μl/l occurs at 11-12 m sediment depth. This layer possibly contains about 3-5% of gas hydrates. Below this layer the methane concentration decreases by about 2 times, although still being very high (20,000-40,000 mkl/l).
2. Gas hydrate-bearing sediments show very high methane concentrations of 1,100 ml/l. The methane concentrations depend on the quantity of gas hydrate in the sediment.
3. The sediment in the Barite Mound area show a 100 times higher methane concentration (100-200 ml/l) than the sediment in the Clam Hill area (0.1-0.3 ml/l). It is possible that gas hydrates in the Barite Mound sediments occur at greater depths.
4. The methane distribution in sediments of the central part of the Okhotsk Sea is similar to that on the Sakhalin Slope: a low concentration in the surface sediment (0.04 ml/l) and a sharp increase from 200 cm downcore (to 50 ml/l at 1,700 cm sediment depth).

7. PORE WATER GEOCHEMISTRY

Klaus Wallmann, Pavel Tishchenko, Galina Pavlova, Matthias Haeckel, Giovanni Aloisi, and Thomas Mosch

7.1 Pore water sampling and analysis

Sediment samples were squeezed in a cold room at 4°C temperature and 2-4 bar using a polypropylene apparatus pressurized by argon and equipped with 0.45 μm cellulose acetate membrane filters to separate the pore water from the sediment matrix.

Pore water samples were stored in the refrigerator at 4°C and sub-samples for sulfide determination, metal analysis (ICP), $\delta^{18}O$ and $\delta^{13}C$ measurements were taken and conserved within two hours after squeezing. Sulfide samples were conserved with 47.6 mM zinc-acetate solution, supra-pure HCl (50 μl of 30% HCl solution) was added to dissolved metal sub-samples (4 ml), and $\delta^{13}C$ samples (1 ml) were given into gas-tight vials previously purged with nitrogen gas. All vials used for pore water storage were previously washed with acid and Milli-Q water to prevent sample contamination.

As pore water samples rapidly lose alkalinity and Ca during storage, these parameters were determined within some hours after sampling. The other nutrients and dissolved ions (phosphate, ammonia, silica, magnesium, and chloride) proved to be more stable and were thus analyzed during the following days.

7.1.1 Dissolved calcium

Samples for dissolved calcium (Ca) in pore water were analyzed during 2-6 hours after squeezing by complexometric titration of 1 ml of pore water dispensed in 10 ml deionized water using the same procedure as with seawater analyses. Correction factor concerning strontium (Sr) will be calculated after analysis of pore water for Sr at the shore-based laboratory of IFM-GEOMAR. The Brinkman/Dosimat 665 motor-driven piston burette reproducible to ±0.001 ml in the delivered volume was applied for analysis. Based on analysis in pore water replicates, analytical precision of ±7 μmol/kg (n=8) for calcium in pore water was achieved in this study.

7.1.2 Dissolved alkaline earth metals (AEM)

The seawater of 35 psu salinity is approximately 0.055M in magnesium, 0.01M in calcium and 0.0001M in strontium, other divalent metals being present at the p.p.b. level. The concentration of magnesium can be derived from total concentration of alkaline earth metals (AEM) and determined calcium concentration. The total concentration of alkaline earth metals were determined by photometric method with EDTA, with eriochrome black T as indicator. The procedure is the following: 1 ml of pore water, 5 ml of ammonium buffer, 0.1 ml indicator and 10 ml of pure water were added into a titration vessel, then a fiber optic cell was immersed into the titration vessel, and the titration curve was recording on a Brinkmann PC-2000 photometer at wave length 540 nm. The end point was calculated using least square method for treatment of titration curve. IAPSO water with a known concentration of magnesium and calcium of 54 mM and 10.55 mM, respectively, is used as primary standard. Standard deviation of this method was found to be 0.15%.

7.1.3 Total alkalinity

Samples for total alkalinity (TA) in pore water were analyzed within 2-3 hours after squeezing by direct titration in an open cell of 1 ml of pore water dispensed in 10 ml deionized water with 0.02 N HCl using the same procedure as with seawater titration (Bruevich's method). Bruevich's method is convenient to work with small sample volumes and allows to avoid the errors caused by H_2S oxidation during titration. The Brinkman/Dosimat 665 motor-driven piston burette reproducible to ±0.001 ml in the delivered volume was applied for analysis. Replicate measurements (n=8) indicated stable values and an analytical precision of ±10 µmol/kg for total alkalinity in pore water was achieved in this study.

7.1.4 Total dissolved sulfide

Sulfide samples were conserved with zinc acetate gelatine solution (23.8 mM in Zn acetate) adding 4 ml solution to 1 ml pore water. The Zn-bearing solution was added to fix sulfide as colloidal zinc sulfide whereas the gelatine was used to inhibit ZnS precipitation. The resulting ZnS colloidal solution was mixed with 40 µl phenylen-diamin and 40 µl $FeCl_3*6H_2O$ and the absorbance was measured after 10 min to 1 hour at 670 nm using a Hitachi UV/VIS Spectrometer. A linear calibration curve was obtained in the concentration range of 0-57 μM ΣH_2S. The sufide standard solution was titrated with sodium thiosulfate to determine the true concentration of the standard. Samples were diluted into the calibration range before reagent addition.

7.1.5 Dissolved nutrients

Dissolved silicate, phosphate, nitrate, and ammonia were measured applying standard photometric procedures on a HitachiUV/VIS Spectrometer. The analysis of nutrient concentrations was disturbed in anoxic samples with high ΣH_2S concentrations. Thus, sulfide-bearing samples were acidified with HCl (20 μl conc. HCl per 3 ml sample) and bubbled with nitrogen gas prior to analysis. By this procedure, sulfide was converted into hyrogen sulfide and transferred into the atmosphere.

Dissolved silica was determined diluting a volume of 0.5 ml sample (pore water and seawater) or standard to 5.0 ml with deionized Milli-Q water and 0.2 ml heptamolybdate solution. After 30 minutes, 0.2 ml oxalic acid solution and ascorbic acid were added. The blue-colored silicomolybdic complex took another 60 minutes to develop before the absorbance could finally be measured at 810 nm.

For the analyses of phosphate, 2 ml of pore water sample or standard were diluted with 4 ml pure water; subsequently 0.1 ml ascorbic acid and 0.1 ml heptamolybdate reagent were added, and the absorbance was measured after 10 minutes at 880 nm.

For the ammonia determination, 1 ml water sample or standard was diluted with 4 ml Milli-Q water and 0.2 ml phenol solution was added. After 2 minutes 0.1 ml citrate buffer and 0.2 ml DTT reagent were added and the samples were kept at room temperature protected from sunlight for about 24 hours before the absorbance was measured at 630 nm.

Nitrate was reduced to nitrite by percolating the solution through a column filled with Cd granulate. Reagents were added and the sum of nitrate and nitrite was measured photometrically.

3-4 KAL
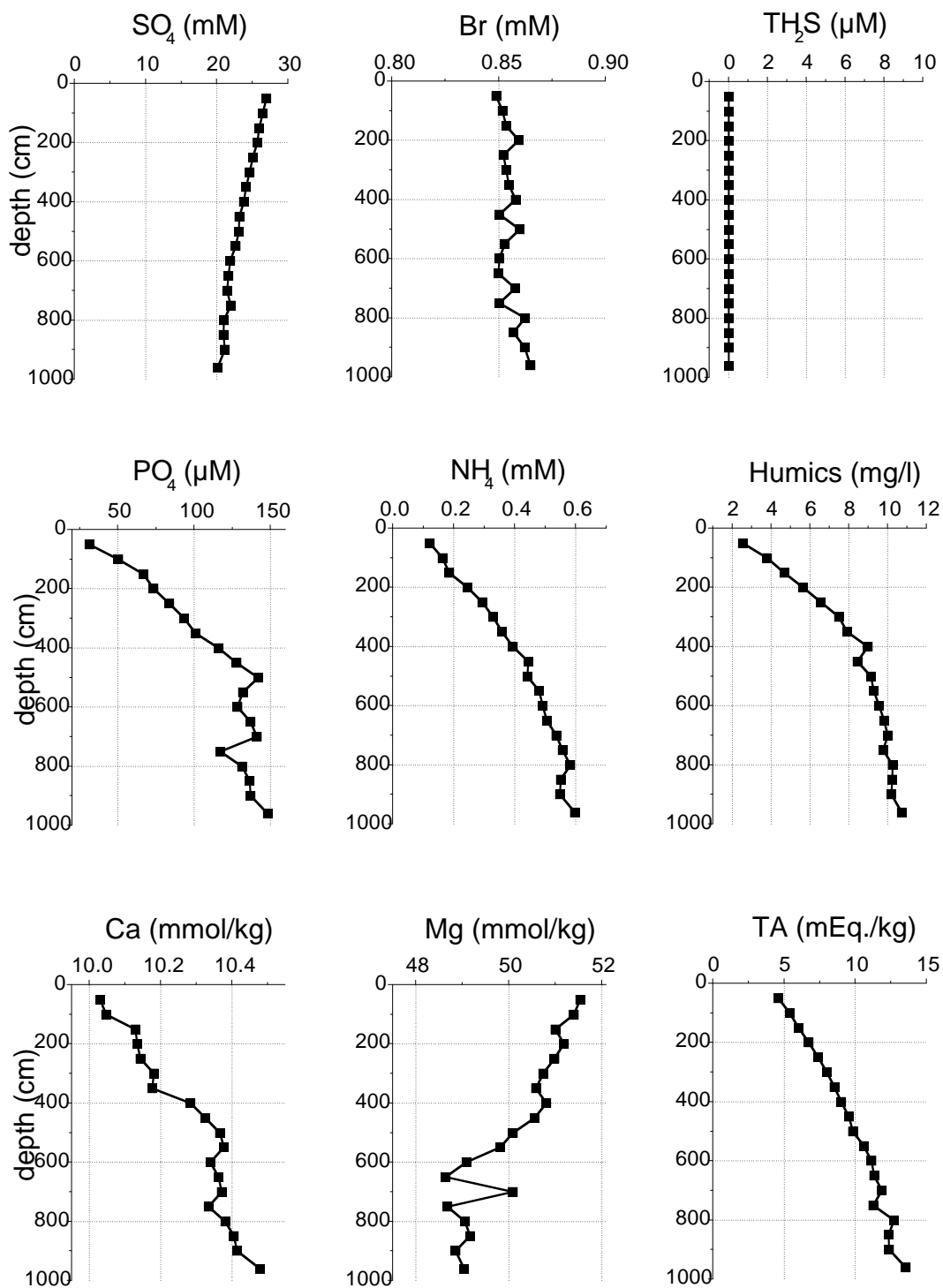
Fig. 7.1: *Pore water composition at station SO178-2-4 KAL (southern Sakhalin Slope).*
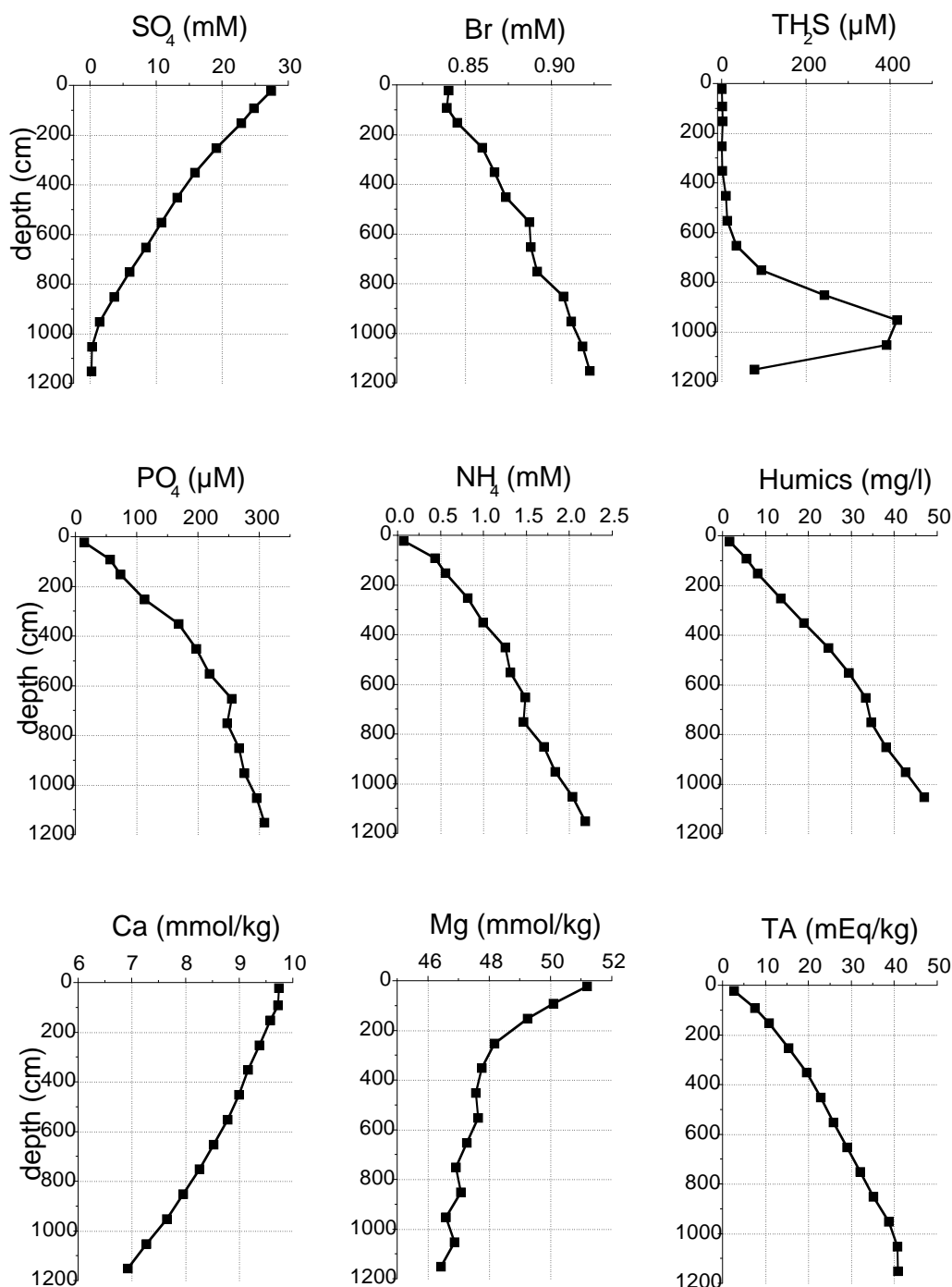
10-6 SL

Fig. 7.2: *Pore water composition at station SO178-10-6 SL (Sakhalin Slope).*

7.1.6 Anion concentrations

Dissolved chloride, bromide, and sulfate were determined using ion-chromatography. We used a Methrom ion-chromatograph equipped with a conventional anion-exchange column and carbonate-bicarbonate solution as an eluent. Standard deviations were found to be 1% for chloride, 2% for sulfate, and 5% for bromide.

7.1.7 Humic substances

The concentration of dissolved humics was measured by UV-adsorption spectroscopy at a wavelength of 254 nm using humic acid as a standard solution which was extracted from shallow marine sediments taken at Armur Bay, Vladivostok. Linear and well reproducible calibration curves were obtained in the concentration range of 0-50 mg/l. The standard deviation of this method was found to be 2%. High concentrations of dissolved sulfide disturb the measurement of humic substances because poly-sulfides, elemental sulfur and other UV-absorbing products are formed upon sulfide oxidation. Hence, samples have to be degassed to remove dissolved sulfide. Alternatively, samples can be aged for several weeks until the intermediate products of sulfide oxidation are further reacted into more stable species (thio-sulfate, sulfate) which do not absorb light at 254 nm. During the cruise, we were able to yield good results for most pore water samples with sulfide concentrations below 5 mM. However, humic substance concentrations determined in extremely sulfide-rich samples (> 5 mM) are probably erroneous and too high because poly-sulfides and other sulfur-bearing substances contributed substantially to the observed UV absorption.

7.2 Results and discussion

Pore waters were separated from surface sediments recovered in 6 hydrocorer (HYC) deployments, 2 kasten corer (KAL), 5 piston corer (KL), 10 multicorer (TV-MUC), 3 gravity corer (SL), and 3 TV-grab (TVG) deployments (Tab. 7.1). They were analyzed for dissolved nutrients (ammonia, phosphate, silica, nitrate), anions (chloride, sulfate, bromide), alkalinity, sulfide, calcium, total alkaline earth metals (AEM), and dissolved humic substances as described in the methods section. A complete list of measured concentrations is given in Appendix 5.
Cores SO178-26-1 KL and SO178-44-1 SL were only sampled for gas hydrates. Pore water samples were not taken because the sediment consisted almost entirely of gas hydrates. Core SO178-44-1 SL was only 40 cm long because the gravity corer could not penetrate into the hydrate layer. At station SO178-51-1 a TVG deployment recovered large amounts of carbonate concretions but no sediments. Hence, pore waters could not be taken. The other TVG samples were sub-sampled with a push-corer to obtain sediment and pore water depth profiles.

7.2.1 Early diagenetic processes and silicate weathering in Sakhalin Slope sediments

A series of up to 25 m long sediment cores were taken in a south-north transect along the Sakhalin Slope and in the Derugin Basin (SO178-3-4 KAL, SO178-10-6 SL, SO178-11-5 KL, SO178-12-3 KL, SO178-13-6 KL, SO178-29-2 KL, SO178-78-1 KL). In the following, we show the results obtained from 4 of these deployments (SO178-3-4 KAL, SO178-10-6 SL, SO178-13-6 KL, SO178-29-2 KL). The sulfate penetration depth decreased from more than 10 m in the southernmost station (SO178-3-4 KAL, Fig. 7.1) to less than 3-5 m at the northern slope stations (Figs. 7.3 and 7.4) reflecting the general increase in marine productivity and terrigeneous sedimentation towards the north which had also been observed in previous expeditions of the KOMEX project (GE99, LV29). Dissolved bromide is released into the pore water via degradation of marine particulate organic matter (POM). It shows an increase in concentration with sediment depth and reaches high concentrations in the northern cores due to more intense POM degradation processes (Figs. 7.1 - 7.4). Dissolved sulfide is produced via microbial sulfate reduction and is removed from pore waters by the precipitation of pyrite and other iron sulfide minerals. In the southern core (Fig. 7.1), sulfide concentrations remained below the detection limit (1 μM) whereas strong maxima of up to 4 mM were

observed in the other cores marking the sediment horizon of most intense sulfate reduction and sulfide production. Sulfide concentrations were always much lower than the observed sulfate depletion indicating that most of the sulfide produced via sulfate reduction is fixed in iron sulfide minerals. Iron oxides for sulfide fixation are probably supplied by the Amur River as coatings on clay minerals and other riverine particles.

Tab. 7.1: Pore water sampling sites during cruise SO178-KOMEX.

Station SO178-	Location (N, E)	Depth (m)	Working Area	Remarks
3-4 KAL	48°11.833 146°08.743	1602	Southern Sakhalin Slope	10 m
9-3 MUC	48°41.516 145°34.565	839	Southern Sakhalin Slope	
10-6 SL	49°44.878 146°00.476	613	Sakhalin Slope	
11-4 MUC	51°13.997 146°12.998	1186	Northern Sakhalin Slope	
11-5 KL	51°14.000 146°12.999	1182	Northern Sakhalin Slope	17.4 m
12-3 KL	51°36.322 145°26.142	1211	Northern Sakhalin Slope	16.99 m
13-3 MUC	52°43.880 144°42.648	702	Northern Sakhalin Slope	
13-6 KL	52°43.881 144°42.647	713	Northern Sakhalin Slope	23.68 m
22-1 MUC	54°26.778 144°04.847	688	Obzhirov Flare	Clam shells
23-1 SL	54°26.760 144°04.889	689	Obzhirov Flare	Gas hydrates
24-1 MUC	54°26.785 144°04.902	689	Obzhirov Flare	Clam shells
26-1 KL	54°26.779 144°04.857	690	Obzhirov Flare	Gas hydrates
29-2 KL	53°50.000 144°14.232	771	Northern Sakhalin Slope	24.3 m
36-1 KAL	54°26.764 144°04.917	688	Obzhirov Flare	1.65 m
37-1 MUC	54°30.071 144°12.337	871	Kitami Flare	Bacterial mats
38-1 MUC	54°30.076 144°17.261	962	Chaos Flare	Bacterial mats
42-1 SL	54°29.985 144°12.335	873	Kitami Flare	1.87 m
44-1 SL	54°30.050 144°17.253	961	Chaos Flare	Gas hydrates
46-1 MUC	54°26.660 144°04.812	689	Obzhirov Flare	Bacterial mats
48-1 HYC	54°30.000 144°12.043	855	Kitami Flare	Gas hydrates
49-1 TVG	54°29.996 144°12.121	859	Kitami Flare	Concretions
51-1 TVG	54°29.998 144°17.244	954	Chaos Flare	Concretions
52-1 HYC	54°29.973 144°17.188	950	Chaos Flare	Gas hydrates
58-1 MUC	54°00.056 146°17.784	1529	Barite Area	Near chimney
62-1 HYC	54°00.937 146°15.745	1441	Barite Area	Top of ridge
65-1 TVG	54°00.014 146°17.170	1497	Barite Area	Chimney
66-1 HYC	54°00.182 146°26.618	1489	Clam Hill	Background
69-1 HYC	54°00.501 146°14.002	1563	Barite Area	Concretions
71-1 TVG	54°00.307 146°26.466	1460	Clam Hill	Barite crusts
72-1 MUC	54°00.560 146°16.212	1563	Barite Area	Near clams
74-1 HYC	54°00.305 146°26.565	1476	Clam Hill	Barite crusts
78-1 KL	54°04.188 146°18.012	1690	Derugin Basin	18.40 m

Phosphate and ammonia are produced by POM degradation. Hence, the concentrations of these nutrients increase downcore and towards the north. Phosphate is removed from pore waters by adsorption on particles and by the formation of authigenic minerals (mostly francolite and other Ca-PO$_4$-CO$_3$-F mineral phases). The decrease in dissolved phosphate observed at about 17 m in core SO178-13-6 KL probably marks a horizon of intense

phosphate precipitation and mineral formation. In the northernmost core SO178-29-2 KL, phosphate decreases towards the base indicating a precipitation process occurring in deeper

13-6 KI
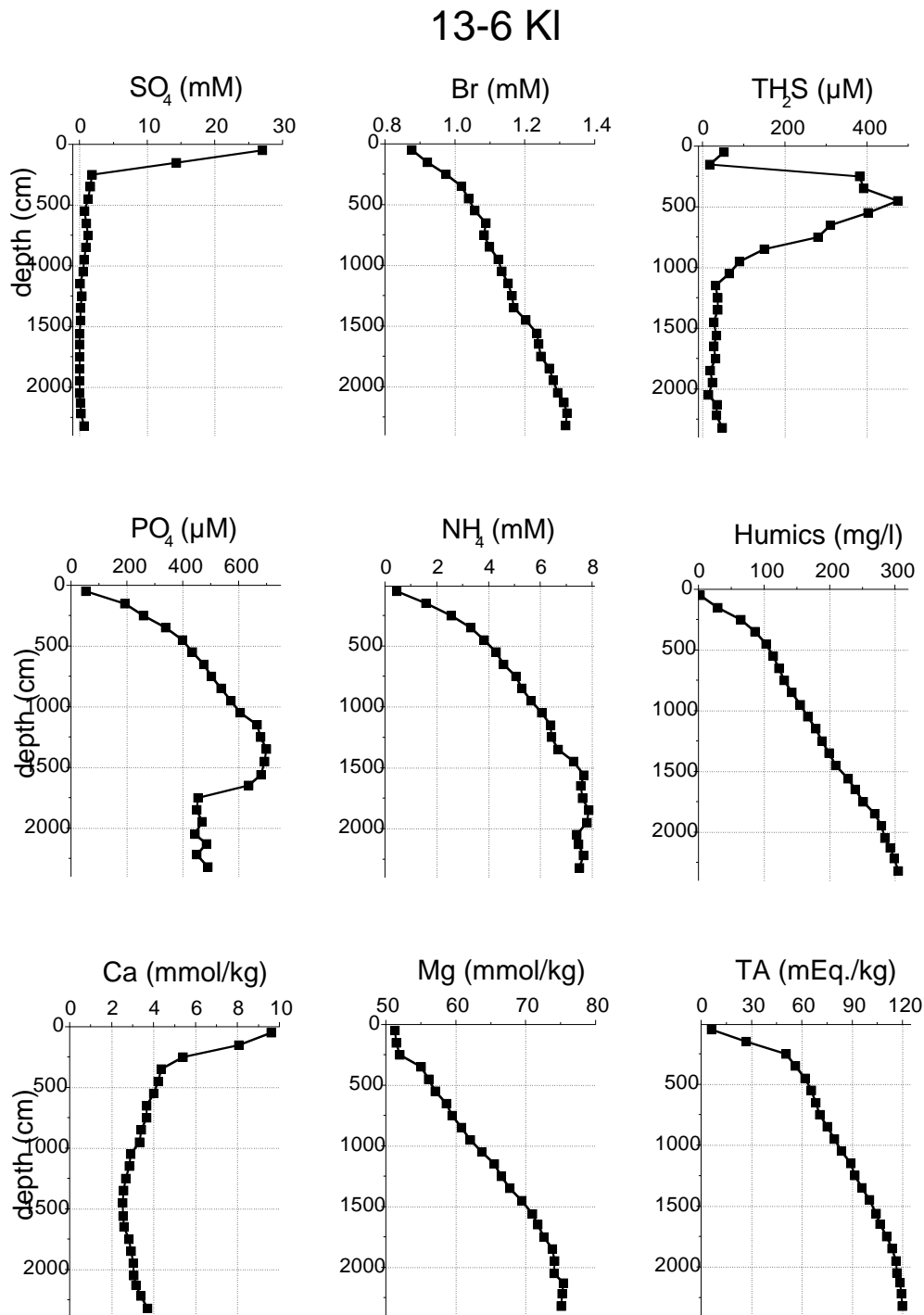
Fig. 7.3: *Pore water composition at station SO178-13-6 KL (northern Sakhalin Slope).*

sediment horizons. Ca concentrations increase over the same depth interval suggesting that phosphate may be removed by the precipitation of a Ca-P-mineral phase at depth. The precipitation kinetics of these minerals are known to be sluggish so that high rates of POM degradation and phosphate release may result in strong oversaturations. Hence, the high phosphate concentrations observed at large sediment depths (up to 800 μM) surpass the solubility of common P-bearing minerals by several orders of magnitude. Ammonia is taken

up by clay minerals and other reactive solids via adsorption. Thus, only about 50% of the produced ammonia appears in the pore waters while the remaining half is fixed in particles.

29-2 KL
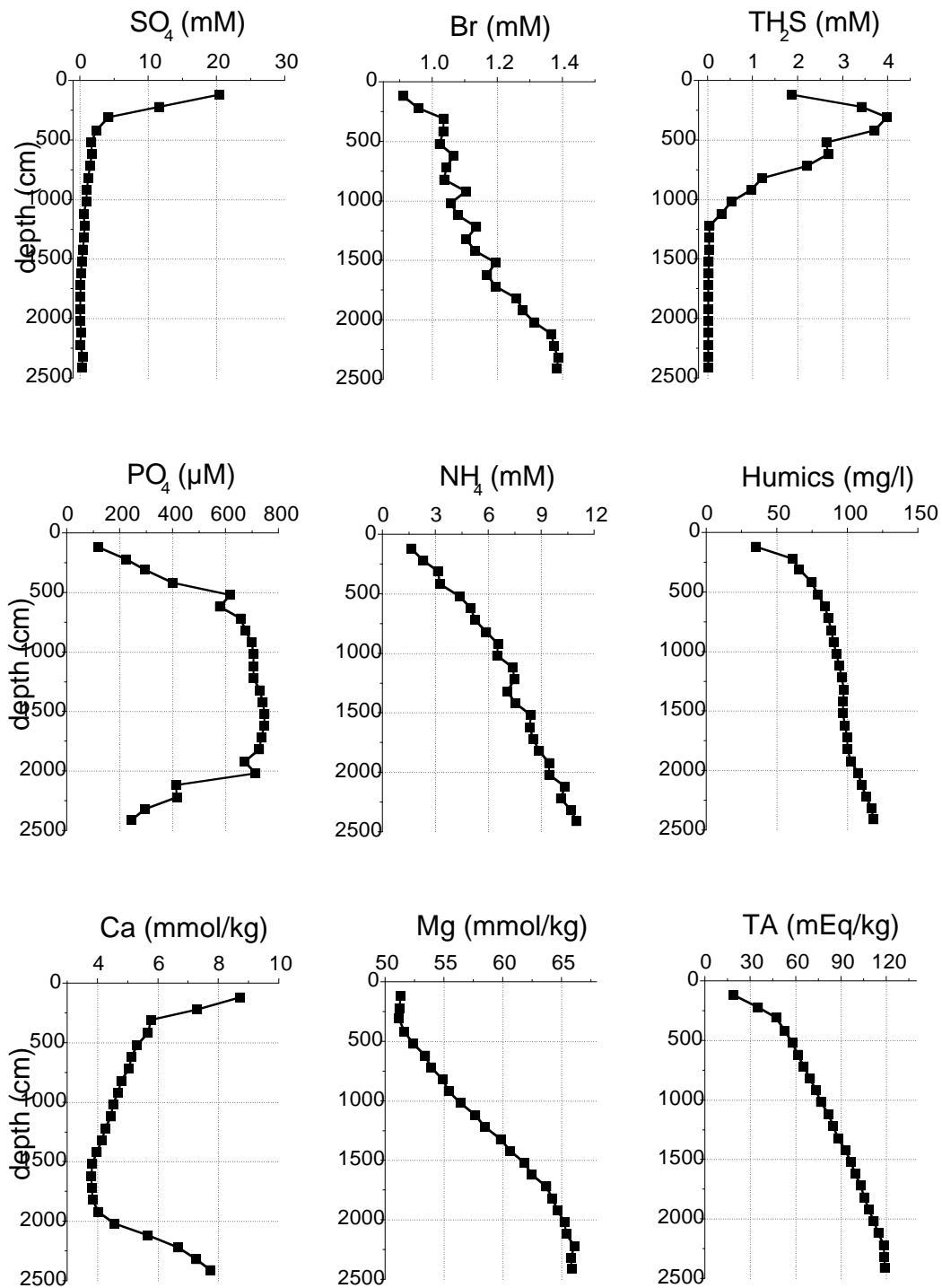
Fig. 7.4: Pore water composition at station SO178-29-2 KL (northern Sakhalin Slope).

Humic substances show a nutrient-type behavior. The concentration of dissolved humics increases downcore and towards the north (Figs. 7.1 - 7.4). Humic substances are formed both in terrestrial and marine environment. It seems to be likely that a large fraction of the humics at the northern stations originates from riverine particles delivered by the Amur River and

deposited mostly in northern mid-slope areas. The release into the dissolved phase may be caused by microbial activity. Fermenting bacteria which are very abundant in anoxic marine sediments produce enzymes hydrolysing biogenic macromolecules such as proteins, carbohydrates, and lipids. It seems to be possible that some chemical bounds in the complex mixture of macromolecules, operationally defined as humic substances, are cleaved by these enzymes so that smaller and better soluble entities are produced and released into the pore water. At station SO178-13-6 KL, extremely high concentrations of up to 300 mg/l were determined at the core base (Fig. 7.3). Strong concentration gradients were observed in all cores implying a significant diffusive transport of humics into the overlying bottom waters. Our preliminary results suggest that a considerable fraction of POM delivered into the sediments may be returned as dissolved humics into the ocean.

Dissolved calcium concentrations increase with depth at the southernmost station (Fig. 7.1) while a strong decrease is observed at the other stations. At the base of the cores from the northernmost stations, Ca concentrations increase again to higher values (Figs. 7.3 and 7.4). Sulfate reduction releases both CO_2 and HCO_3 into the pore water. Pending on the rate of sulfate reduction and pyrite formation, the overall result may either be carbonate dissolution or precipitation. The anaerobic oxidation of methane (AOM) within the methane-sulfate transition zone underlying the sulfate-bearing horizons releases large amounts of HCO_3 inducing further $CaCO_3$ precipitation. Within the methanogenic zone, carbonates tend to be dissolved due to CO_2 production. Our results imply that low rates of sulfate reduction favor carbonate dissolution while carbonate is precipitated mostly at the base of the sulfate-bearing layer where AOM prevails. In the deeper methanogenic layers Ca concentrations start to increase again suggesting carbonate dissolution or silicate weathering at depth.

Dissolved magnesium shows a significant decrease with depth in sulfate-bearing surface sediments (Figs. 7.1 and 7.2) and a strong increase in the underlying methanogenic zone (Figs. 7.3 and 7.4). Magnesium may be removed from pore waters by diagenetic processes. Calcite and aragonite may recrystallize into high-Mg calcite and dolomite so that Mg is taken up in newly formed authigenic carbonate phases. Moreover, Mg-bearing silicate phase may form from biogenic opal and terrigenous metal oxides (inverse weathering). Considering the high abundance of biogenic opal and terrigenous matter and the low carbonate contents of the slope sediments it seems to be more likely that Mg is taken up in newly formed silicate phases. The strong release of Mg in the underlying methanogenic zone may be due to various processes. Mg adsorbed to clay mineral surfaces may be replaced by ammonia or other cations and released into solution. Moreover, dissolved humic substances are know to form rather stable complexes with Mg so that the adsorption equilibria of Mg may be shifted further towards the dissolved form. Finally, silicate weathering may occur and release metal ions into solution. Climatic conditions in the Armur drainage area severely favor physical erosion rather than chemical weathering processes on land. Thus, large amounts of feldspars and other reactive silicates may be transported by the river and delivered to the slope areas under investigation. Methanogenic sediments provide a favorable environment for chemical weathering processes. They are rich in dissolved CO_2 and organic acids which are both known to significantly accelerate silicate weathering in soils. Moreover, pH is rather low (~6) due to ongoing CO_2 production and humic acids are abundant which may complex released metal ions and may thus further favor the dissolution of silicate phases. It is possible that authigenic silicate phases formed in the overlying sediments via reverse weathering are re-dissolved in the deeper methanogenic layers (reverse weathering). However, the uptake of Mg in surface sediments seems to be too weak to support the strong increase in Mg observed at stations SO178-13-6 KL and SO178-29-2 KL. Hence, we believe that the weathering and dissolution of reactive terrigenous silicate phases may be the ultimate source of dissolved Mg in the investigated methanogenic sediment layers (Figs. 7.3 and 7.4).

Total alkalinity increases downcore and towards the north due to POM degradation processes. The increase in alkalinity within the zones of sulfate reduction and AOM is easy to understand because both processes release alkalinity according to their overall stoichiometry:

*Sulfate reduction with pyrite and $FeCO_3$ formation*
$$C(H_2O)(NH_3)_x + 1/2\ SO_4^{2-} + 1/2\ FeOOH + (1/4 + x)\ H^+ \Rightarrow$$

$$3/4\ HCO_3^- + x\ NH_4^+ + 1/4\ FeS_2 + 1/4\ FeCO_3 + H_2O$$
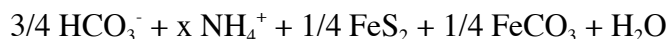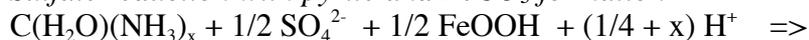
Anaerobic oxidation of methane (AOM)
$$CH_4 + SO_4^{2-} \Rightarrow \quad HS^- + HCO_3^- + H_2O$$
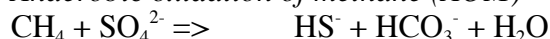
However, POM degradation via methanogenesis produces only small amounts of alkalinity because organic carbon is converted into CO_2 and CH_4 rather than HCO_3:

POM degradation via methanogenesis
$$C(H_2O)(NH_3)_x + x\ H^+ \Rightarrow \quad 1/2\ CO_2 + 1/2\ CH_4 + x\ NH_4^+$$
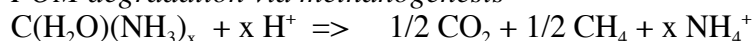
Methanogenesis is a complex microbial process involving many intermediates such as molecular hydrogen, acetate and other organic acids. Moreover, some methane is produced by CO_2 reduction rather than organic matter degradation. However, the reducing agents used in CO_2 conversion (mainly H_2) are generated from the break-down of organic matter so that it is difficult to escape the constraints of the overall stoichiometry shown above. The role of intermediates is shown in the following example:

POM degradation via fermentation followed by CO_2 reduction

$$C(H_2O)(NH_3)_x + x\ H^+ + H_2O \quad \Rightarrow CO_2 + 2\ H_2 + x\ NH_4^+$$
$$1/2\ CO_2 + 2\ H_2 \quad \Rightarrow\ 1/2\ CH_4 + H_2O$$
$$\overline{C(H_2O)(NH_3)_x + x\ H^+ \Rightarrow \quad 1/2\ CO_2 + 1/2\ CH_4 + x\ NH_4^+}$$
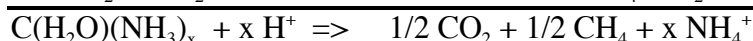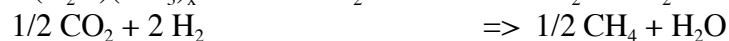
where the sum of both reactions has the same stoichiometry as the reaction above.

The stoichiometry and the rate of alkalinity generation may change if the composition of organic matter differs from that of the Redfield sugar used in the reactions above ($C(H_2O)(NH_3)_x$ where $x = 16/106$). Thus, the decomposition of organic acid anions such as acetate produces HCO_3 rather than CO_2:

Degradation of organic acid anions in methanogenic sediments
$$CH_3\text{-}COO^- + H_2O \quad \Rightarrow \quad HCO_3^- + CH_4$$
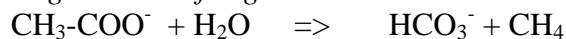
It might be possible that organic acid anions adsorbed to the surface of terrigenous particles are degraded preferentially within the studied sediment section resulting in alkalinity production. Little is known about the reactivity of humics and other acids bound to clay particles but it seems to be unlikely that these acid anions are so abundant and labile that most of the alkalinity increase is caused by their degradation. It could also be possible that some of the alkalinity increase in the methanogenic sediment layer of cores SO178-13-6 KL and SO178-29-2 KL (Figs. 7.3 and 7.4) is caused by the upward diffusion of organic acid anions (including also humic acids) produced in deeper sediment layers followed by decomposition into methane and bicarbonate. Because of charge balance constraints the diffusion of anions would be accompanied by a corresponding flux of cations. Thus, Mg^{2+} cations might be transported to the surface complexed by organic acid anions to produce both the increase in

Mg and alkalinity observed in our data. However, the concentration gradients of Mg, humic acids and also alkalinity at the base of cores SO178-13-6 KL and SO178-29-2 KL are very small so that upward diffusion seems to be of only minor importance.

37-1 MUC
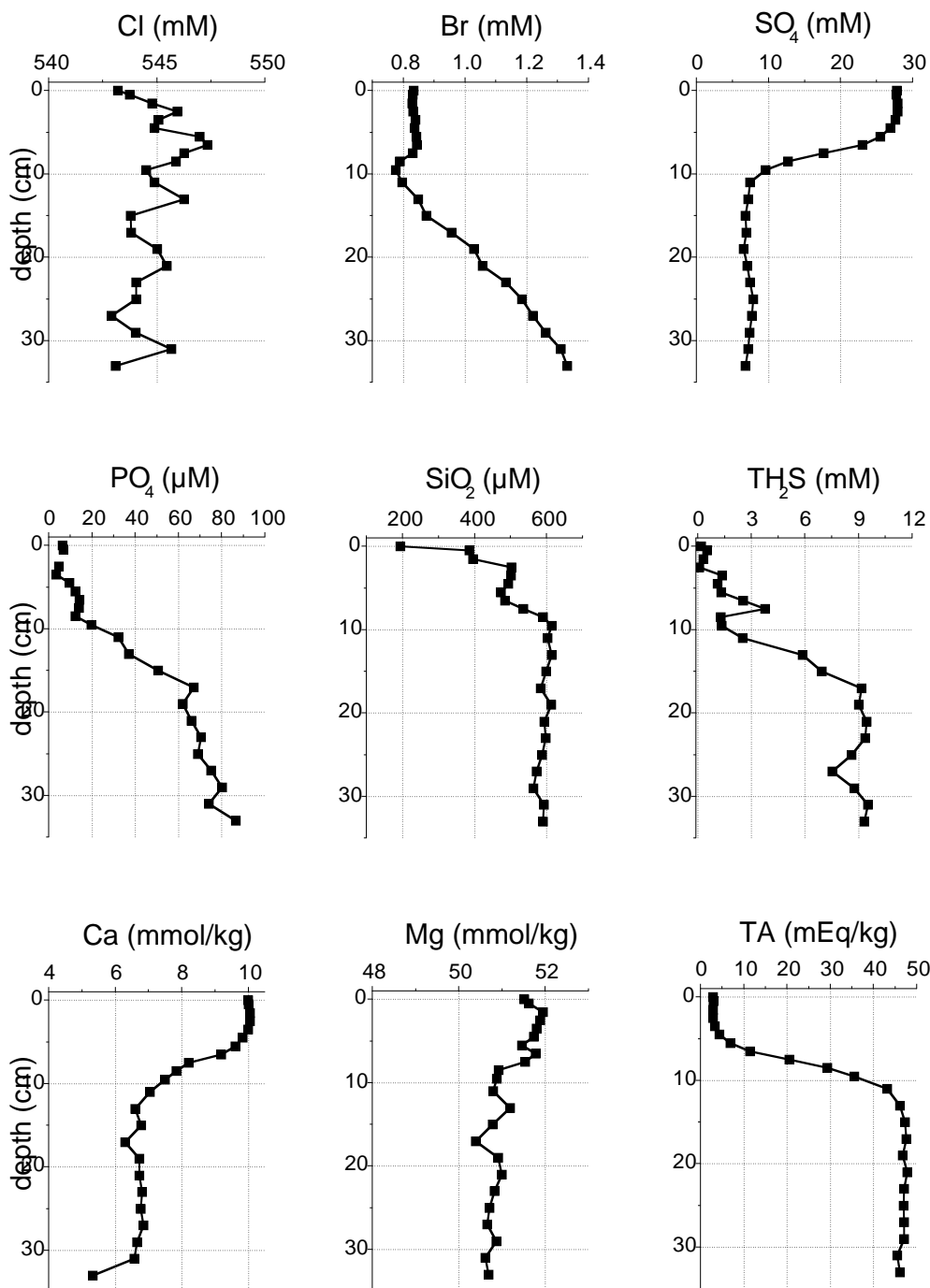
Fig. 7.5: Pore water composition in surface sediments covered by bacterial mats (SO178-37-1 MUC, Kitami Flare).

Humic substances contain carboxylic acid groups which take up protons upon acid addition and thus contribute to the measured total alkalinity value. Humic and fulvic acids typically have carboxylic acid contents in the order of 10 mEq. per g C and a C-content of about 50%.

Taking these numbers, the maximum humic acid content measured at the base of core 13-6 (300 mg/l) may contribute about 1.5 mEq. per kg solution corresponding to 1-2% of the measured total alkalinity (120 mEq./kg). This contribution is quite substantial and will be investigated in more detail in our shore-based laboratories. However, it is clear that the bulk of the observed alkalinity is not caused by organic acids but rather by dissolved inorganic carbon species.
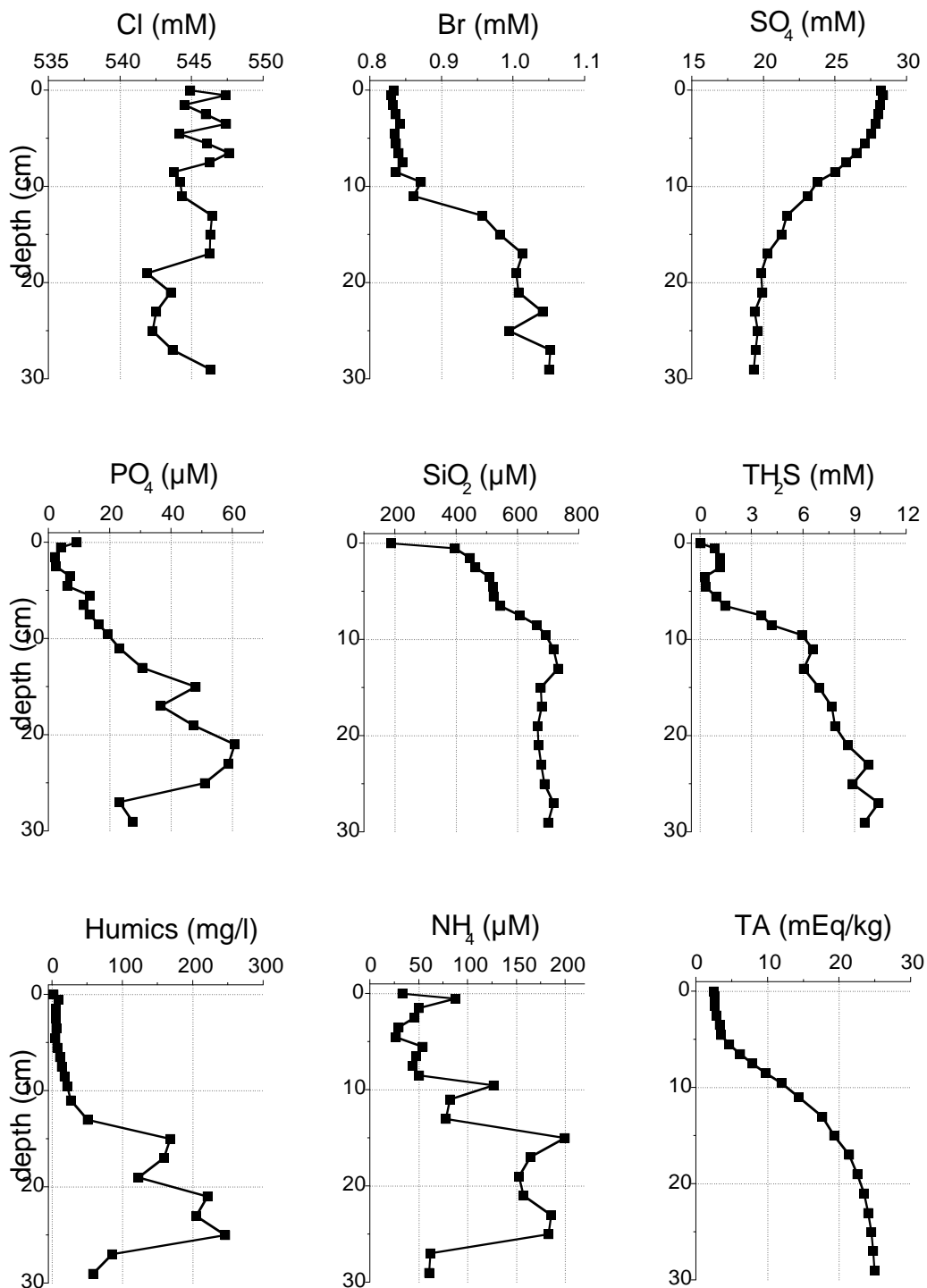

Fig. 7.6: *Pore water composition in surface sediments covered by bacterial mats (SO178-38-1 MUC, Chaos Flare).*

Considering all other alternatives, we believe that most of the alkalinity increase in the methanogenic layer of cores SO178-13-6 KL and SO178-29-2 KL is caused by silicate weathering. CO_2 acts as an acid in the chemical weathering of silicates being converted into bicarbonate. On long geological time scales, silicate weathering is the most important sink for atmospheric CO_2. Our new data suggest that silicate weathering is not limited to the terrestrial realm but may also proceed in methanogenic marine sediments, especially in areas where reactive silicate minerals are delivered by large river systems and where the climatic conditions preclude intense weathering on land. If true, this result would have major implications for the understanding of the geological carbon cycle.

7.2.2 Gas venting, gas hydrate formation and fluid convection at the northern Sakhalin Slope

Three methane venting areas were sampled during our cruise. These include the Obzhirov Flare which was intensely studied in previous expeditions of the KOMEX cruise (LV28, GE99, LV29) and the Kitami and Chaos Flares which were discovered during the CHAOS expedition in 2003.

Using the TV-guided multicorer, we were able to locate and sample surface sediments covered with bacterial mats at all three vent locations. The mats were several centimeters thick and covered extensive areas of the seafloor. They are known to mark areas of rapid methane ascent where sulphide is produced by AOM and consumed by the overlying bacterial mat. Consistent with our expectations, surface sediments were gas-rich containing high concentrations of methane and H_2S. Gas bubbles could be observed to ascend through the sediments while the cores were handled on deck.

The pore water data (Figs. 7.5 - 7.7) give evidence for rapid anaerobic methane oxidation and complex mixing processes. Dissolved sulphate remained close to seawater values in the upper 5 cm and was rapidly consumed below that depth due to AOM. However, sulphate was not completely depleted and at one site sulphate concentrations increased again in the lower portion of the core (Fig. 7.7). Total alkalinity and dissolved sulphide showed similar trends confirming that AOM was focussed to a narrow sediment horizon at about 10-20 cm depth. In the over- and underlying sediment horizons transport processes overprinted any sign of sulphate reduction, sulphide production and alkalinity generation. Ca and Mg concentrations measured at station SO178-37-1 MUC indicated carbonate precipitation within the AOM zone. Nutrient concentrations were generally low confirming that sulphate was not reduced via POM degradation but rather by AOM.

The high sulphate and sulphide concentrations at the base of the cores clearly show that methane is not delivered by rapidly ascending fluids because pore waters in the northern Sakhalin Slope area are essentially sulphate-free and sulphide-depleted at sediment depths of several meters (compare Figs. 7.3, 7.4, and 7.5 - 7.7). Hence methane is not supplied by deep fluids but rather by rising gas bubbles. The ascent of gas bubbles was directly observed at the seafloor during one TV-MUC dive and is documented through numerous hydroacoustic measurements. Rising gas bubbles may induce eddy diffusive mixing so that seawater is mixed into the surface sediment. Moreover, small-scale convection cells may be established by rising bubbles and by hydrate formation in underlying sediment layers adding further complexity to the transport processes prevailing in the studied surface sediments (see discussion in the following paragraph). Interestingly, dissolved silica concentrations remained at a rather high level (Figs. 7.5 - 7.7) suggesting that the mixing is slow compared to the rate of biogenic opal dissolution. This may give some constraints on mixing and convection rates which will be exploited in future model studies.

46-1 MUC
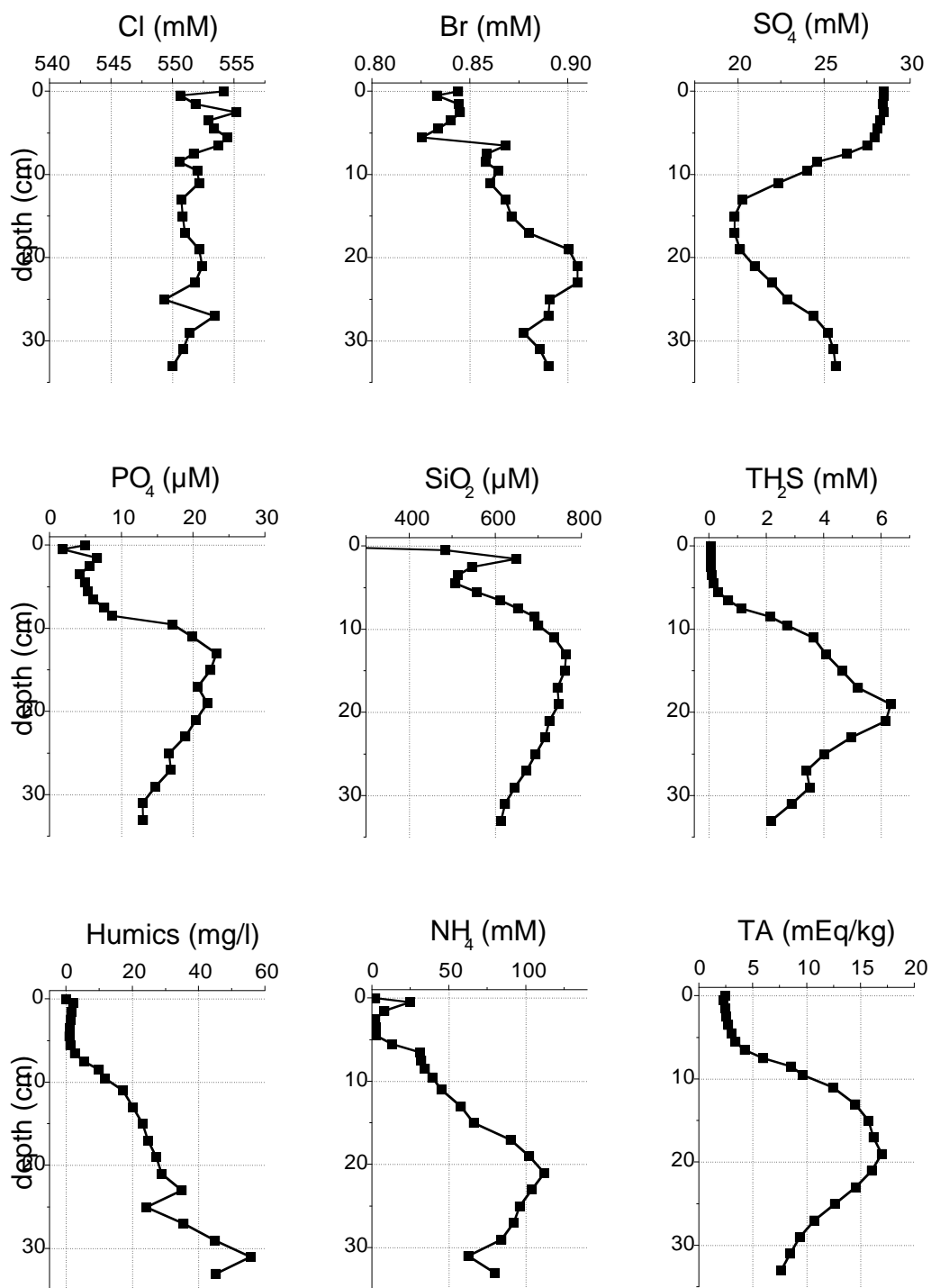
Fig. 7.7: *Pore water composition in surface sediments covered by bacterial mats (SO178-46-1 MUC, Obzhirov Flare).*

23-1 SL
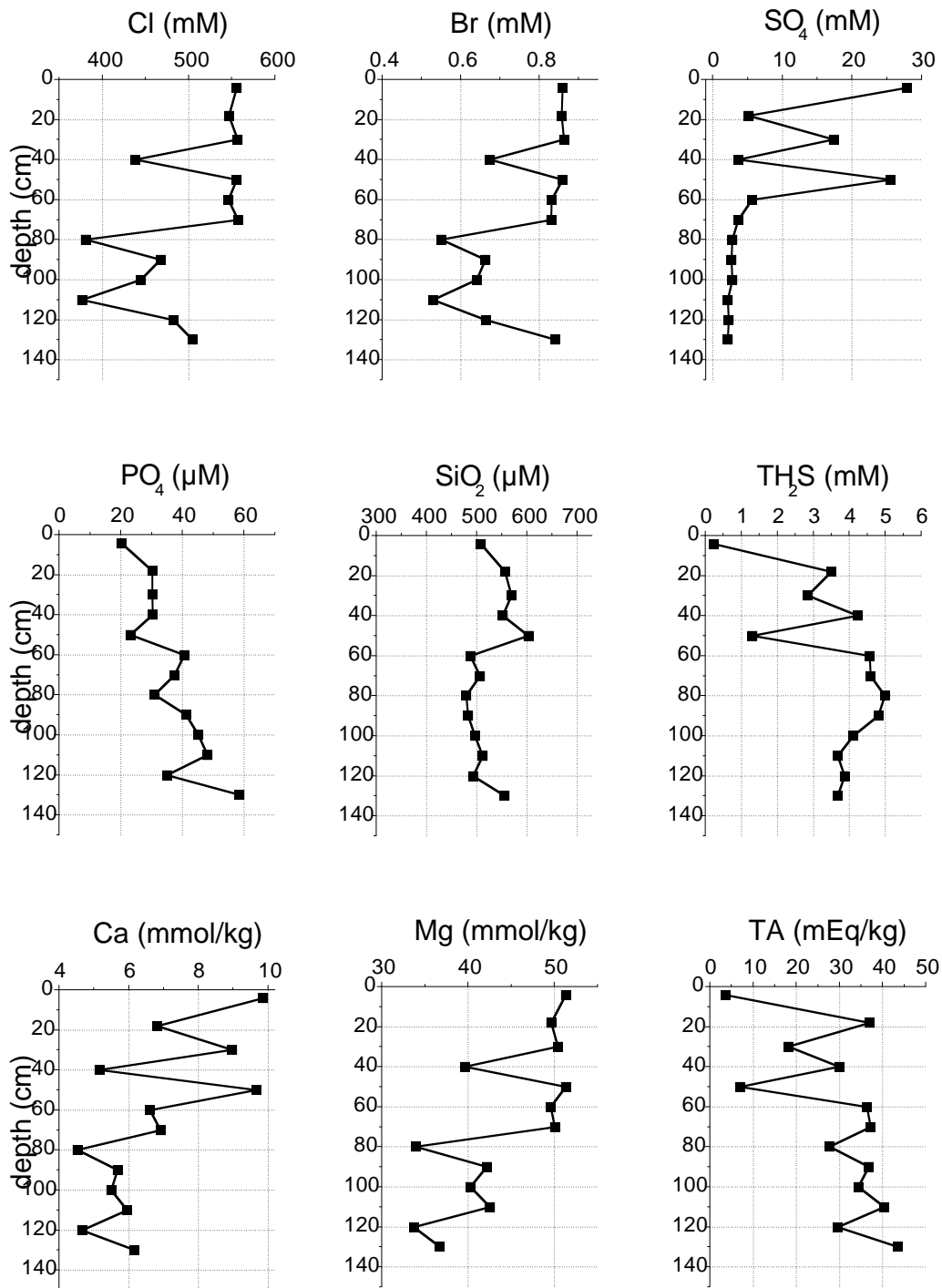
Fig. 7.8: *Pore water composition in hydrate-bearing sediments (SO178-23-1 SL, Obzhirov Flare).*

48-1 HYC
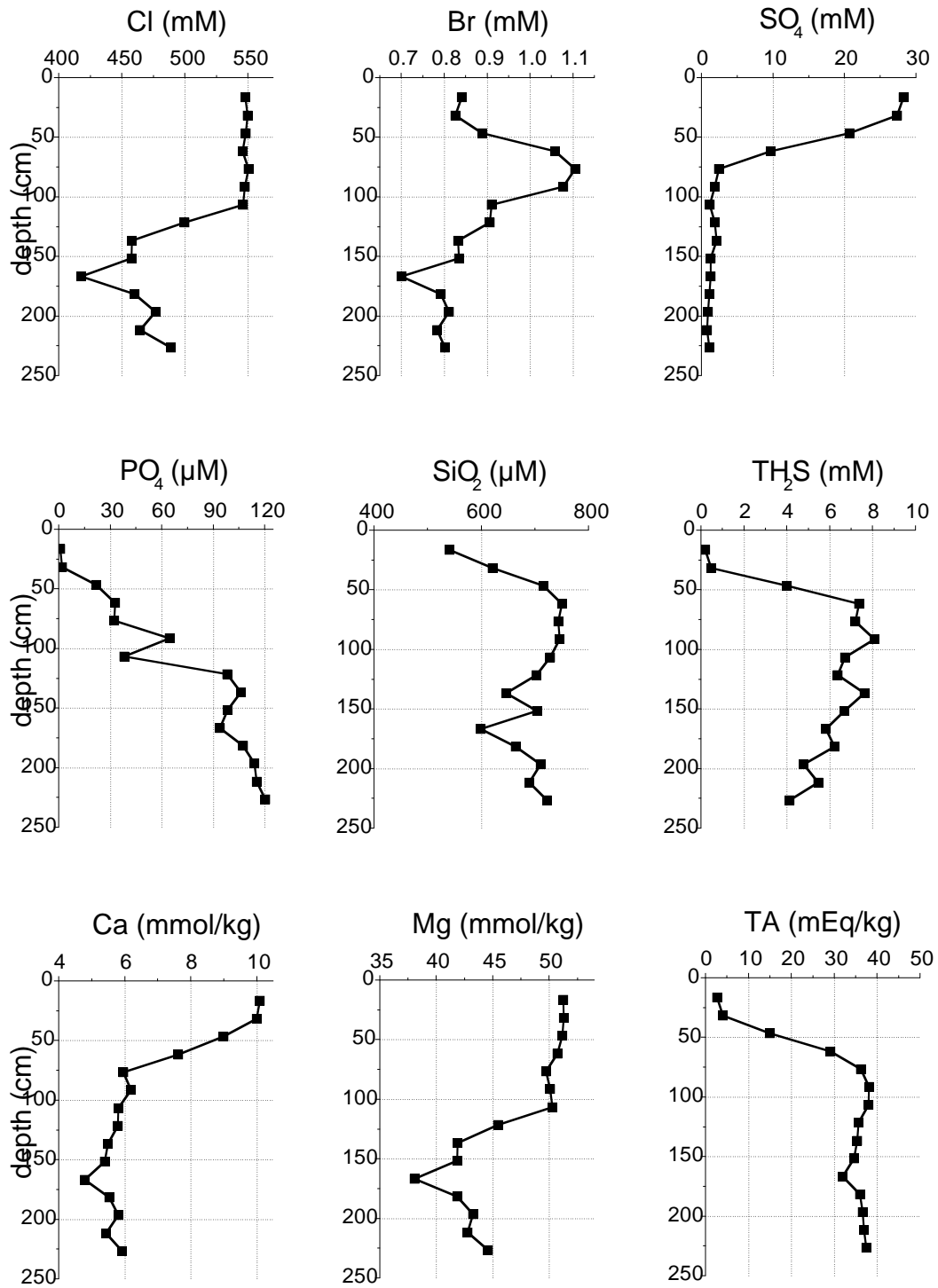
Fig. 7.9: *Pore water composition in hydrate-bearing sediments (SO178-48-1 HYC, Kitami Flare).*

52-1 HYC
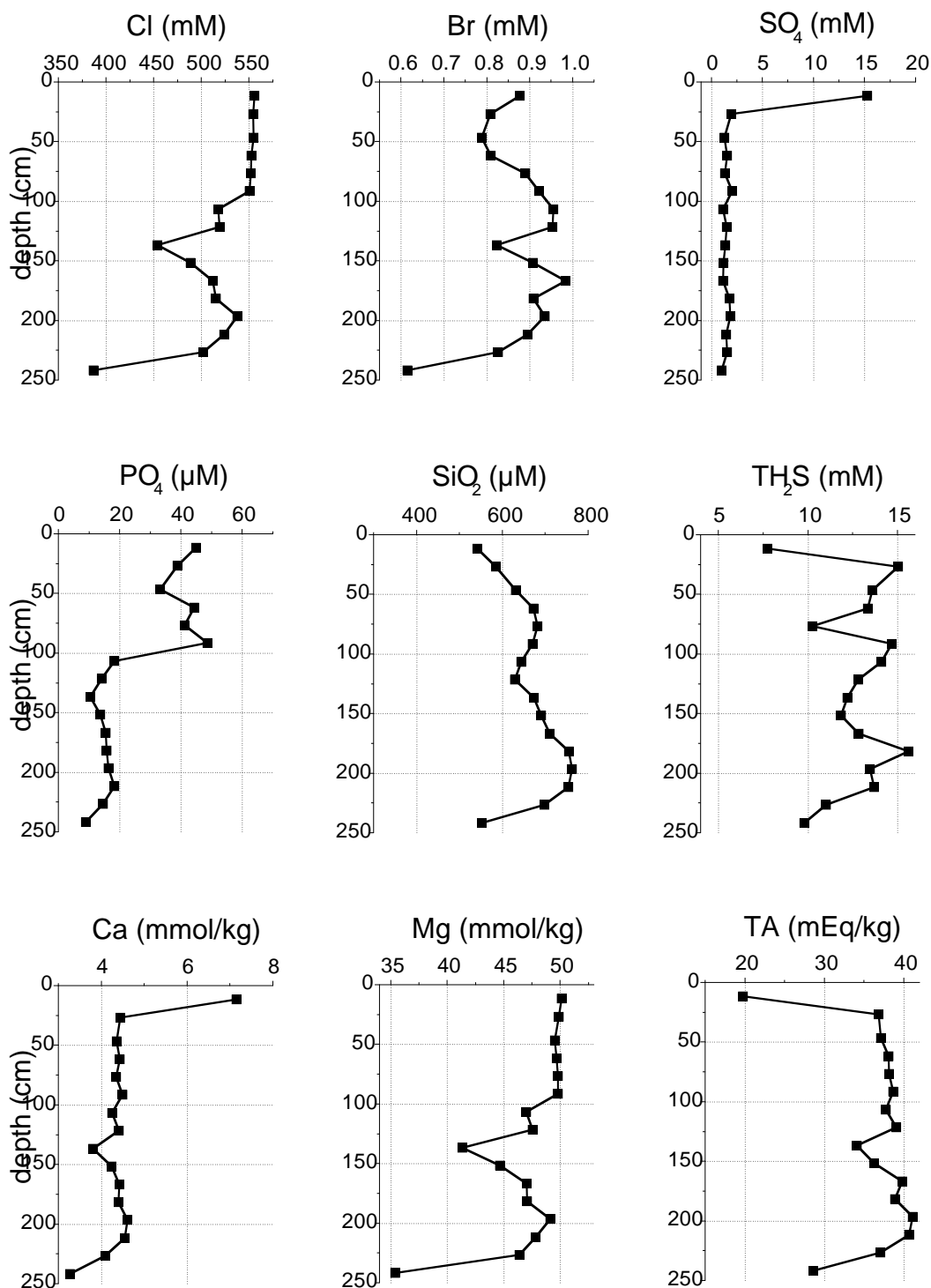
Fig. 7.10: *Pore water composition in hydrate-bearing sediments (SO178-52-1 HYC, Chaos Flare).*

At all three vent sites, we were able to recover hydrate-bearing surface sediments using the gravity corer and hydrocorer. Samples were taken every 10 cm and gas hydrates were allowed to dissociate and melt completely prior to pore water separation so that freshening of pore fluids reflects the total content of gas hydrates in the sampled sediment intervals. At the

Obzhirov Flare, gas hydrates extended over the entire length of the sediment core (SO178-23-1 SL, 140 cm, Fig. 7.8). At the Kitami Flare the hydrate-bearing sediment horizon extended from a depth of 120 cm to the base of core SO178-48-1 HYC (240 cm, Fig. 7.9). Sediments retrieved from the Chaos Flare (SO178-52-1 HYC) contained hydrates from 100 cm depth to the base at 240 cm (Fig. 7.10). We were not able to penetrate through the hydrate-bearing zone into underlying hydrate-free sediment horizons. At the Obzhirov Flare area we recovered discrete and thin layers of gas hydrates during previous KOMEX cruises (GE99, LV29) but never retrieved such a massive layer of hydrate-bearing sediment as at station SO178-23-1 SL. The higher abundance of gas hydrates observed during SO178 may indicate more rapid gas ascent than during previous years.

Core SO178-23-1 SL showed strong chloride, bromide, and magnesium depletions at a sediment depth of 40 cm and from 80 to 130 cm depth marking major layers of gas hydrate occurrence (Fig. 7.8). Sulphate concentrations decreased with depth due to AOM but showed enhanced values at 30 cm and 50 cm depth. Interestingly, these sulphate maxima were accompanied by maxima in dissolved calcium and minima in total alkalinity and dissolved sulphide. The layers at 30 cm and 50 cm depth are obviously affected by the inflow of seawater washing away the products of AOM. It seems possible that a convection system is established either by the ascent of gas bubbles or by other processes. A massive gas hydrate layer is situated at 40 cm depth in between the two seawater-affected layers. Gas hydrate formation is an exothermic process. It may thus be imagined that convection is induced by the warming of pore waters via hydrate formation. Models of hydrothermal convection have to be adapted and applied to test this hypothesis. If the modelling would confirm this idea, yet another mechanism would be established possibly explaining the complex flow patterns observed in hydrate-bearing sediments. The upper three samples of core SO178-23-1 SL nicely match the high-resolution pore water profile obtained under a bacterial mat at the Obzhirov Flare (Fig. 7.7). It is thus likely that the increase in dissolved sulphate at the base of the multicorer sediments is caused by a hydrate-driven convection cell.

At the Kitami and Chaos Flares, sulfate concentrations decrease rapidly and regularly with depth due to AOM (Figs. 7.9 and 7.10). The profiles show no obvious signs of convection but carry the signature of AOM and carbonate precipitation. Samples are strongly diluted by fresh water released from dissociated gas hydrates below a sediment depth of 100 cm indicating that a large fraction of the sediment volume was occupied by gas hydrates under in-situ conditions.

7.2.3 Fluid ascent and barite chimney formation in the Derugin Basin

We recovered two sediment cores from the Barite Area carrying the signature of deep fluids. One of the cores was taken at the top of the Barite Ridge (SO178-62-1 HYC, Fig. 7.11). It contains no dissolved sulfate and is strongly depleted in magnesium (22 mmol/kg) and chloride (520 mM) from the top to the base of the core while dissolved silica is very high (1,000 μM). The strong gradients between the fluid at the core top and the overlying seawater imply very high rates of fluid ascent. The chemical composition of the pore fluids indicates that they come from a source area located at several km depth where freshwater is released by smectite-illite transformation and magnesium is taken up during sediment-water interactions at elevated temperatures.

The second core was taken at the northwestern flank of the Barite Ridge (SO178-66-1 HYC, Fig. 7.12). It contains the same deep fluid as core SO178-62-1 HYC below 100 cm depth but ambient seawater in the top 100 cm. The two pore water bodies are separated by an extremely sharp boundary producing very steep concentration gradients. It is interesting to note that the

62-1 HYC
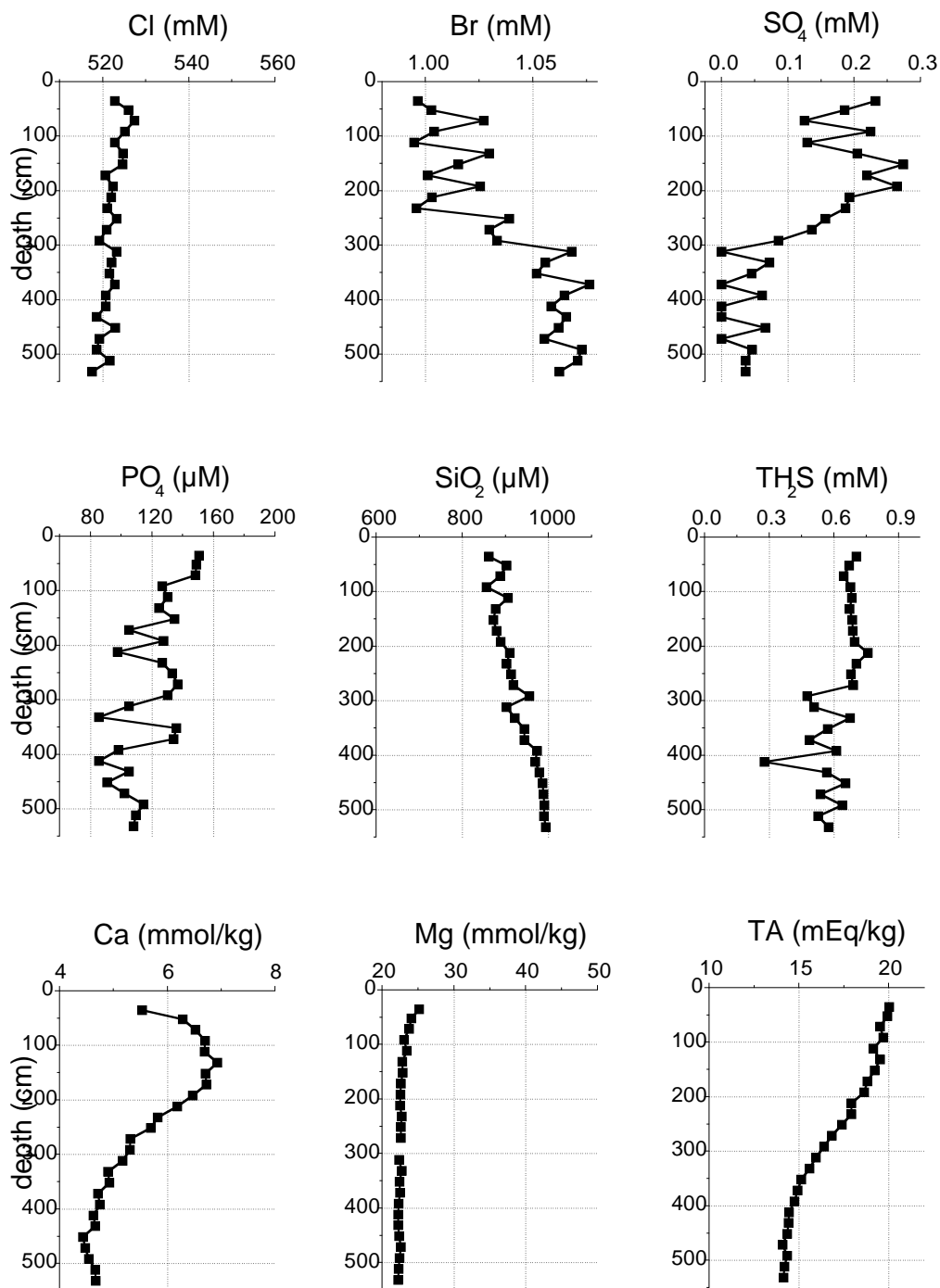
Fig. 7.11: *Pore water composition in sediments retrieved from the top of Barite Ridge (SO178-62-1 HYC).*

69-1 HYC
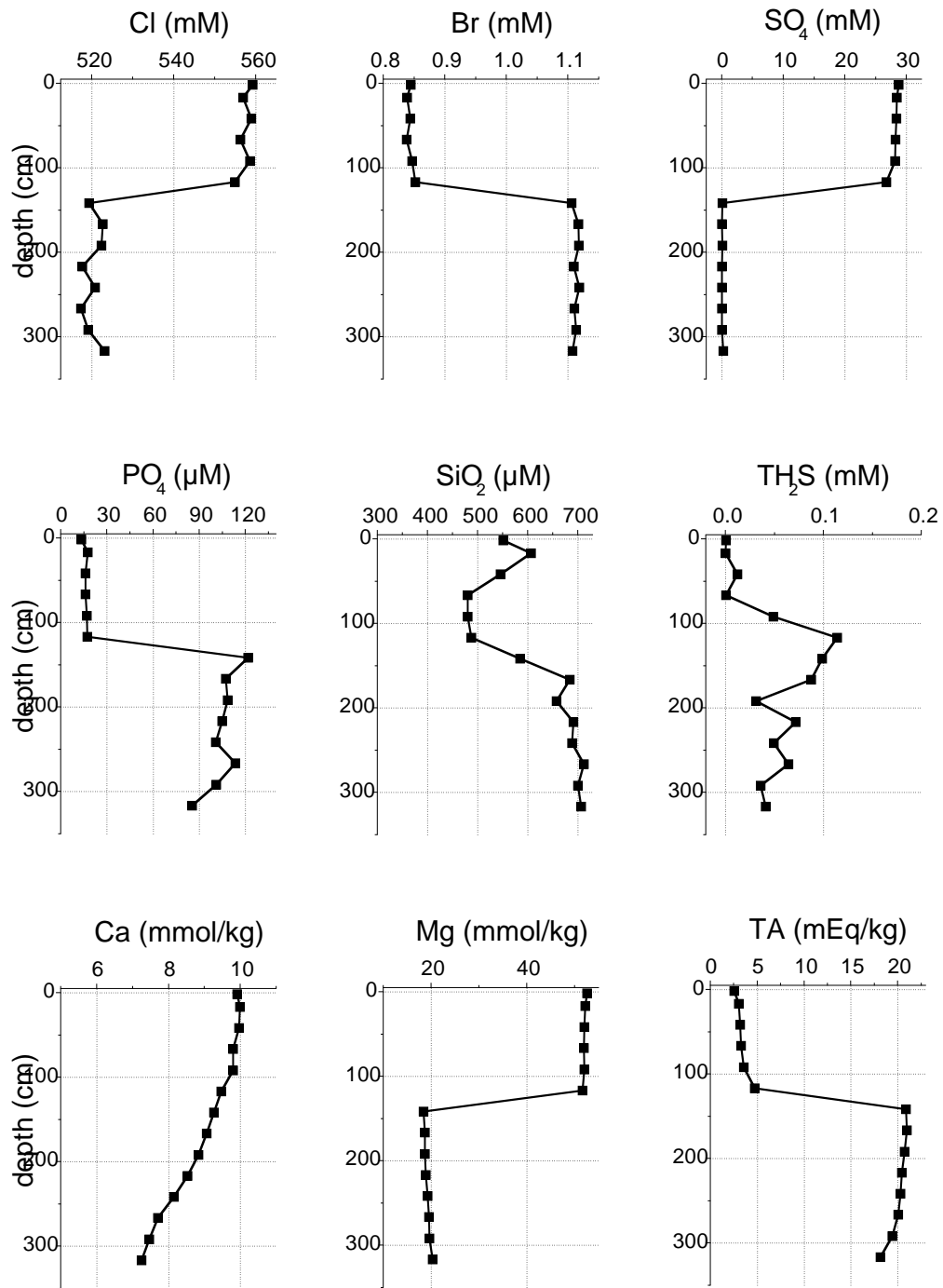
Fig. 7.12: *Pore water composition in sediments retrieved from the northwestern flank of Barite Ridge (SO178-66-1 HYC).*

strong decrease in dissolved sulfate over this boundary is not accompanied by a sulfide maximum. Thus, the boundary does not mark a layer of high microbial turnover but rather the boundary between two different transport regimes. It seems possible that warm and freshened fluids rapidly ascending to the seafloor induce a shallow thermohaline convection cell in surface sediments flushing the top meter of the surface sediments with ambient bottom waters.

The deep fluids from these two cores will be analyzed for their chemical and isotopic composition in our home laboratories to further constrain the source depth and origin of these fluids which are probably responsible for the formation of the large barite chimneys occupying extended areas of the Derugin Basin. Pending on the results of these analysis, we will obtain important constraints on the fluid flow system leading to the built-up of giant barite chimneys in this unique area of active fluid flow.

8. OFOS OBSERVATIONS

Giovanni Aloisi, Matthias Haeckel, Klaus Wallmann, Boris Baranov, and Reinhard Werner

8.1 Summary

12 OFOS (Ocean Floor Observation System) lines were run on the Sakhalin Slope, in the Derugin Basin and the Kurile Basin during cruise SO178-KOMEX (Tab. 8.1). Eleven lines in the first two areas (Figs. 8.1 and 8.2) were aimed at studying seafloor methane and fluid venting areas; one line in the Kurile Basin was aimed at exploring a bathymetric high (Volcano No. 1) which is possibly a submarine volcanic structure (Fig. 8.3). On the Sakhalin Slope and in the Derugin Basin the positions of the OFOS lines were chosen based on the location of acoustic flares, the distribution of patches of high backscatter recorded in side-scan sonar surveys (Fig. 8.4), and the position of promising geological structures identified during bathymetric and seismic surveys during the CHAOS and SO178-KOMEX cruises. The high backscatter recorded from the three flare areas is possibly due to the presence of gas in the sediment and hard substrates such as carbonate crusts, concretions, and chemoherms at the seafloor. On the Sakhalin Slope, two new gas venting areas, the Chaos and Kitami Flare areas, were explored and one previously known gas venting area, the Obzhirov Flare area, was revisited. In the Derugin Basin area, one line was run on Barite Ridge, two on Clam Hill and two on previously unexplored bathymetric features, one mound (Derkachev Mound) and one ridge (Reference Ridge), possibly the locus of fluid seepage/ gas venting. During all OFOS deployments, conductivity, temperature and depth were recorded with the OFOS-mounted CTD. OFOS observations were completed by shorter video surveys carried out during TV-multicorer (TV-MUC) and TV-grab deployments.

The dynamic positioning system of RV SONNE was used extensively to follow planned OFOS tracks with high precision. In addition, the position of the OFOS on the seafloor was monitored. These features of the OFOS deployments were useful both to precisely map the distribution of venting-related features (clam fields, carbonates crusts, barite chimneys) and to choose the locations for seafloor sampling to be carried out with other instruments (coring, TV-MUC, TV-grab).

New results include the observation of gas bubble streams at the Obzhirov Flare area, of pockmarks at the Kitami and Chaos Flare areas and of carbonate constructions ("chemoherms") at all explored flare areas. In addition, cold seep fluids were possibly recognized by the OFOS-mounted CTD both on the Sakhalin Slope and in the Derugin Basin. Furthermore, gas and fluid expulsion-related features observed in OFOS deployments during previous cruises (clam fields, bacterial mats and barite chimneys) were observed during cruise SO178-KOMEX. Of the two newly explored areas (Derkachev Mound and Reference Ridge), only the Derkachev Mound showed evidence of fluid seepage in the form of chemosynthesis-based benthic communities.

8.2 Sakhalin Slope
8.2.1 Types of seafloor terrains observed

The occurrence of the different types of seepage-related terrains in the surveyed flare areas is summarized in Tab. 8.2. The spatial distribution of these features is shown in Figs. 8.5, 8.6, and 8.7. Detailed backscatter maps of the three flare areas obtained during cruise SO178-KOMEX are shown in Figs. 8.8, 8.9, and 8.10. The distribution of vent-related features observed on the OFOS surveys correlates well with the extent of the high backscatter patches.

Tab. 8.1: OFOS stations carried out during cruise SO178-KOMEX

Date	Station	Location	at s.f.	off s.f.	Duration	Latitude N	Longitude E	Depth (m)
10.08.2004	SO178 -18-1	Obzhirov Flare	01:19	05:29	04:42	54°26.409/ 54°26.803	144°02.466/ 144°04.79	606/ 689
12.08.2004	SO178 -32-1	Kitami Flare	11:03	13:16	02:53	54°29.636/ 54°29.976	144°12.077/ 144°12.433	
12./ 13.08.2004	SO178 -35-1	Chaos Flare	00:12	01:49	02:22	54°29.614/ 54°30.244	144°17.130/ 144°17.198	959/ 964
14.08.2004	SO178 -43-1	Kitami Flare	01:22	03:02	02:19	54°30.066/ 54°29.995	144°12.002/ 144°11.846	854/ 850
14.08.2004	SO178 -45-1	Chaos Flare	05:29	06:50	02:02	54°29.810/ 54°30.000	144°16.605/ 144°17.609	948/ 985
15.08.2004	SO178 -50-1	Chaos Flare	00:52	02:16	02:07	54°29.934/ 54°29.933	144°17.453/ 144°16.777	970/ 957
15./ 16.08.2004	SO178 -57-1	Barite Ridge	21:35	01:32	04:59	54°01.653/ 53°59.935	146°15.654/ 146°16.467	1628/ 1529
16./ 17.08.2004	SO178 -63-1	Clam Hill	23:45	02:01	03:11	54°00.100/ 54°00.777	146°26.749/ 146°25.448	1531/ 1471
17.08.2004	SO178 -67-1	Reference Ridge	11:59	15:00	03:51	54°08.289/ 54°08.829	146°58.988/ 146°59.090	1474/ 1468
18.08.2004	SO178 -70-1	Clam Hill	00:32	01:34	02:01	54°00.303/ 54°00.322	146°26.751/ 146°25.823	1487/ 1423
18./ 19.08.2004	SO178 -76-1	Derkachev Mound	22:33	23:57	02:22	53°58.190/ 53°58.990	146°29.396/ 146°29.544	1435/ 1460
22.08.2004	SO178 -84-1	Volcano No. 1	20:39	21:46	01:07	47°54.241/ 47°54.006	147°49.274/ 147°48.627	2185/ 2342

The different types of terrains encountered at the flare areas of the Sakhalin Slope are briefly described below:

The *background seafloor* is composed of fine-grained sediments (silt-mud); rare debris, mainly cobbles, most of which are probably ice-rafted, are also present. Fish, holothurians and crabs are the most common benthic macrofauna unrelated to fluid seepage. Infauna is thought to be present too, and may be abundant, as suggested by the many centimeter-sized holes in the sediment. The amount of benthic macrofauna unrelated to fluid seepage decreases with water depth from the Obzhirov Flare area (water depth ~ 600-690 m) to the Kitami and Chaos Flare areas (water depth ~ 850 m and 960 m, respectively).

Tab. 8.2: Occurrence of the different types of seep and vent-related features in the Sakhalin Slope flare areas

Flare area	Clam fields	Shell fields	Bacterial Mats	Chemoherms	Bubble streams	Pockmarks	Carbonate concretions and crusts
Obzhirov	X	X	X	X	X	-	X
Kitami	X	X	X	X?	-	X	X
Chaos	X	X	X	X	-	X	X

Clam fields (Fig. 8.11a) are present in the central part of the flare areas. These consist of chemosynthesis-based species (*Calyptogena* and/or *Conchocele*?) which have been previously reported from the flare areas of the Sakhalin Slope (Sahling et al., 2003), and are indicative of active methane emission. Clam fields are up to 10 m across and can be very densely packed with clams which are mostly partly buried in the sediment. Clam fields proved to be hard to

penetrate with the TV-MUC. Clams occur also singularly, at the end of tortuous trails which suggest migration in search for H_2S-rich sediments. *Shell fields* which contain mostly clam shells are also present and can be extremely dense so that the underlying sediment is not visible. These shell fields mark the location of past methane emission.

Bacterial mat fields (Fig. 8.11b) occur in the central part of the flare areas. These are areas of seafloor up to 10-15 m across covered by white bacterial mat patches surrounded by patches of black, reduced sediment. Successful deployment of the TV-MUC on these fields confirmed the presence of bacterial mats and the emission of methane-rich fluids.

In the areas most densely populated by clam colonies, a hard, irregular substrate is visible, covered by a few centimeters of soft sediment. TV-grab deployment from this terrain recovered abundant irregularly shaped *carbonate concretions* very likely formed by carbonate mineral precipitation associated to anaerobic methane oxidation. Carbonates also appear to form continuous *crust pavements* (Fig. 8.11c) which, however, were not sampled. In addition, *chemoherm-like constructions* (Fig. 8.11d) were observed which have a relief of up to 50 cm and are densely packed with clam shells. Gas venting in the form of two *bubble streams* (Fig. 8.11e) was observed from one chemoherm structure.

Depressions several meters wide and a few decimeters to one meter deep were observed in the Kitami Flare area. These may be analogous to small-scale *pockmarks* (Fig. 8.11f) described from other areas of seafloor venting such as the North Sea. The walls of the observed pockmarks show how the top few decimeters of sediments are very rich in clam shells and concretions which stick out from the sediment. Bacterial mats are present at the center of some pockmarks.

8.3 Derugin Basin

OFOS observations in the Derugin Basin were aimed at looking for sites to deploy the TV-grab and the TV-MUC in known areas of fluid seepage (Barite Ridge and Clam Hill) and to explore bathymetric features looking for new areas of fluid seepage (Derkachev Mound and Reference Ridge).

Tab. 8.3: Occurrence of the different types of seep and vent-related features in the Derugin Basin area

Area	Clam fields	Shell fields	Bacterial Mats	Barite chimneys	Barite crusts
Barite Ridge	X	X	-	X	-
Clam Hill	X	X	X	-	X
Derkachev Mound	X	X	-	-	-
Reference Ridge	-	-	-	-	-

8.3.1 Types of seafloor terrains observed

OFOS observations during the SO178-KOMEX cruise confirmed the distribution of the seafloor terrains described during cruises LV28 and LV29 in the Derugin Basin (Biebow & Hütten, 1999; Biebow et al., 2003). The occurrence of seepage-related terrains in the Derugin Basin during cruise SO178-KOMEX is summarized in Tab. 8.3. Their spatial distrubution in

the Barite Ridge, Clam Hill, Derkachev Mound and Reference Ridge areas is shown in Figs. 8.13, 8.14, and 8.15.

The different types of seafloor terrains encountered in the Derugin Basin during cruise SO178-KOMEX had already been described during the LV28 and LV29 cruises. They are briefly introduced below:

The *background seafloor* is mostly light-gray with red-brown patches. TV-MUC deployments showed that the light-gray color is due to the presence of a layer of organic detritus at the sediment surface. The brownish-red color occurs when the underlying layer of manganese oxides is uncovered by bioturbating organisms. 2-5 cm wide burrows, often with a 10-15 cm rim of accumulated sediment particles surrounding them are very frequent. Sediment under the manganese oxides is light-gray so that if burrowing organisms dig holes deeper than the depth of the manganese oxide layer, they produce a ring of light-gray sediment around the burrow. Sparse debris is also present on the seafloor and consists of particles of variable size, from centimeters to several decimeters across. These particles are probably of ice-rafted origin. Occasionally, straight trails several centimeters wide are seen. These are traced by large (10 cm) gastropods which were observed at the end of some of these trails. Benthic macrofauna (crabs, starfish) are rare compared to the shelf and slope areas.

The fringe area of fluid seepage is similar to the background seafloor area, except for the occurrence of seepage-related clams (*Calyptogena*?) that occur singularly and in *clam colonies* which at Clam Hill are associated to *bacterial mats* (Figs. 8.12 a, b). The seafloor is often crossed by clam trails which lead to clusters of clams; these trails are narrower (2-3 cm) than those left by the passage of gastropods and are winding. In the fringe area, barite debris is present on the seafloor. Debris increases considerably in abundance and size towards the barite build-ups in the Barite Ridge area (boulders of more than 1 m across are common) suggesting that considerable amounts originate from the break-down of authigenic barite constructions.

In the Barite Ridge area, massive *barite build-ups* 7 to 10 m high (Figs 8.11c, d) dominate the landscape. They are separated by stretches of "fringe-type" seafloor a few to 40 m across. Often, authigenic barite build-ups are as wide at the base as they are high, giving the impression of a truncated pyramid construction (massive barites). Less often, they build vertically elongated, slim columnar structures (chimneys), a few meters in diameter and up to 7-10 m high. Commonly, the surface of the authigenic barite is dark due to an authigenic manganese oxide layer deposited on the barite. White patches of authigenic barite occur in decimetric to metric barite protrusions in the upper part of the barite chimneys (Fig. 8.12c) and in cracks and fissures in the massive barites, marking the locations of current fluid seepage and authigenic barite precipitation.

Most of the authigenic precipitate on Clam Hill occurs as decimeter-thick *barite crusts* (Fig. 8.12e).

8.4 Kurile Basin

OFOS track SO178-84-1 was carried out on the southern flank of the northern top of Volcano No. 1 (Fig. 8.16) because several dredge tracks at this volcano edifice did not provide clear information on its nature and composition. OFOS revealed a rough morphology (Fig. 8.12f) and large outcrops of lithified, possibly volcaniclastic sediments which are partly covered with manganese crusts. Lavas were not visible along the OFOS track. At some places the

sediments show a clear layering. Small canyons cut the sediments at the lower slope. Both layers and canyons strike in NW direction. Large sediment blocks (m-scale) occur at the base of the northern top. Taken together, the northern top of Volcano No. 1 appears to consist completely of disturbed volcaniclastic sediments (see also Chapter 12).

8.5 Bottom water salinity and temperature anomalies in methane seep/ vent areas

The depth, salinity and potential temperature profiles obtained with the OFOS-mounted CTD during the 12 OFOS dives of the SO178-KOMEX cruise are shown in Figs. 8.17 to 8.29. The general trends in salinity and potential temperature with depth in the various investigated areas are discussed in Chapter 4. Here, we concentrate on an anomaly in salinity and potential temperature that was recorded at the Kitami and Chaos Flare areas and in the Derugin Basin. In these three instances, the potential temperature increases by roughly 0.8°C while the salinity decreases by roughly 0.02‰ (Figs. 8.20, 8.21, and 8.23). The maximum deviation from the background temperature and salinity conditions is attained in approximately two minutes while background salinity and temperature conditions are attained with an exponential decay only after 20 minutes from the time of maximum anomaly. Both the magnitude of these anomalies and the time needed for the anomaly to fade away are very similar in the three cases. The origin of such anomalies is not clear. Obstruction of the measuring cell by organic particles could produce the salinity anomaly, although the effect on the temperature is not easily predictable. Alternatively, these anomalies could be produced by the presence of fluids near the seafloor being less saline and warmer than ambient bottom waters. Two of these anomalies occurred in the close vicinity of seep-related features (a barite chimney in the Derugin Basin and a bacterial mat site in the Kitami Flare area) and it is possible that they record the expulsion of fluids there. This is supported by the observation that fluids expelled from the Barite Mound area are less saline than ambient bottom waters (see Chapter 7). The anomaly recorded at the Chaos Flare area, however, occurs on background seafloor. Should it be produced by fluid expulsion, it would indicate that the expelled fluids are carried laterally by bottom currents for hundreds of meters while remaining very close to the seafloor.
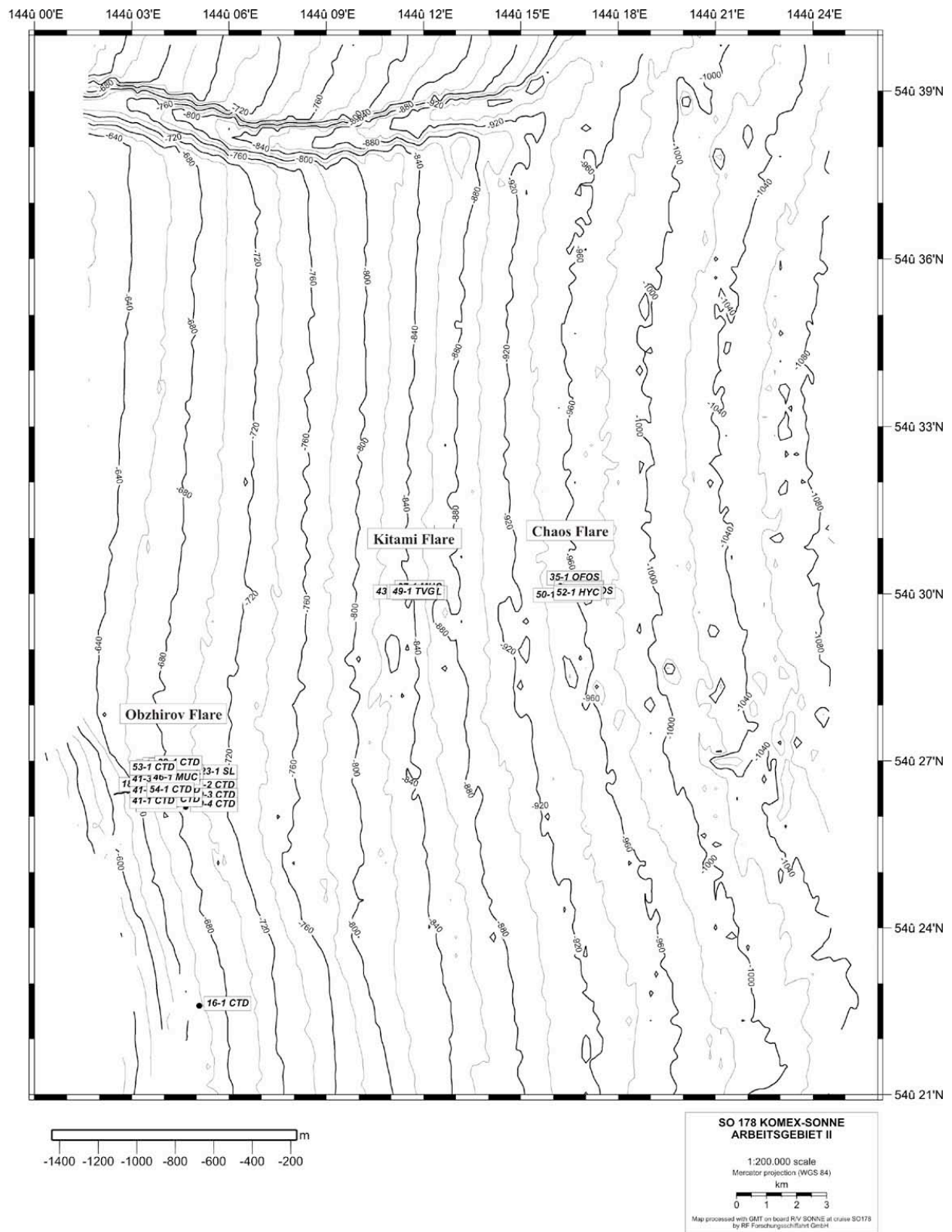
Fig. 8.1: *General bathymetric map of the Sakhalin Slope sector investigated during cruise SO178-KOMEX showing the position of the Obzhirov, Kitami and Chaos Flare areas.*
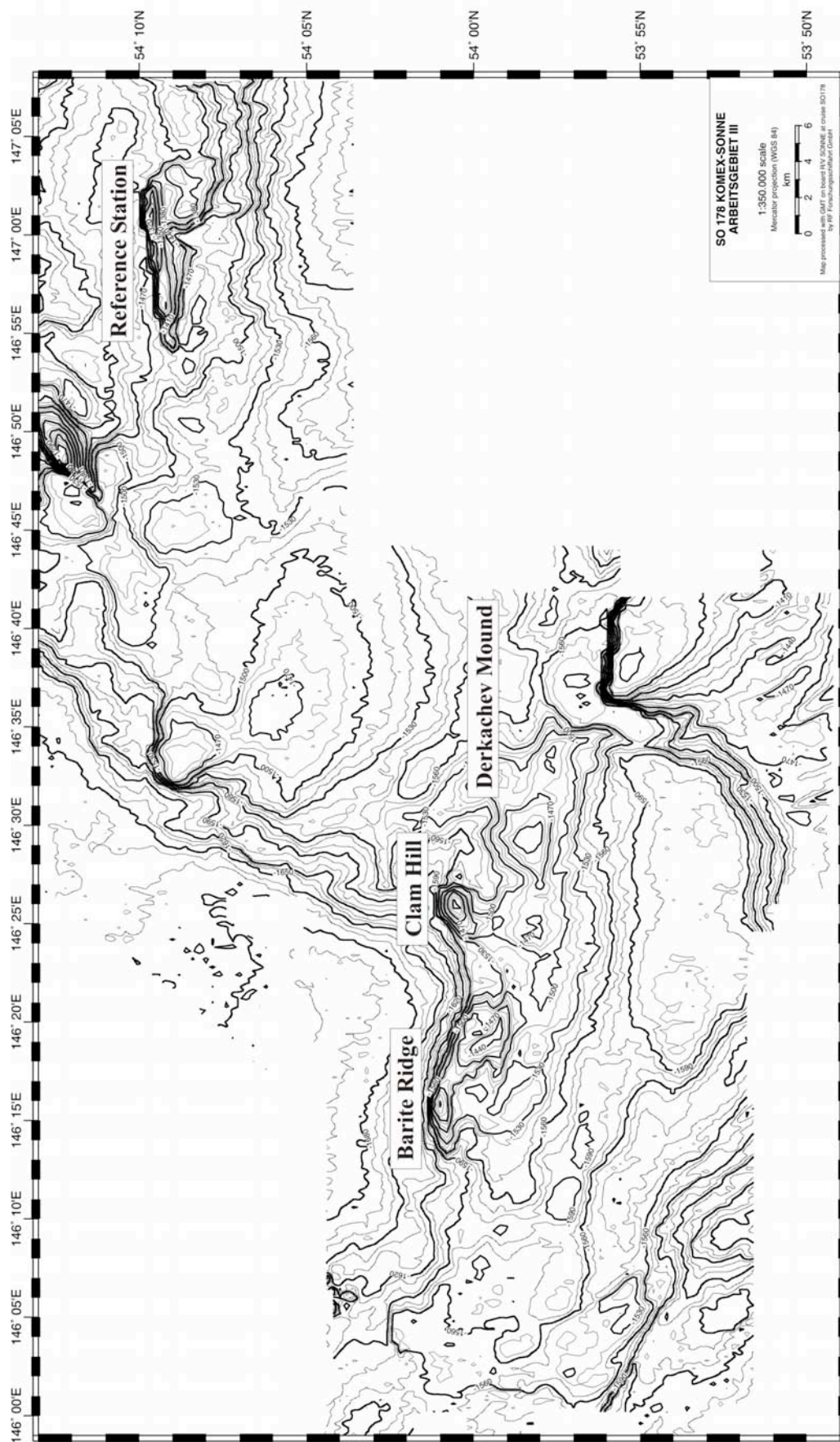
Fig. 8.2: *General bathymetric map of the Derugin Basin area investigated during cruise SO178-KOMEX showing the position of Barite Mound, Clam Hill, Derkachev Mound and Reference Ridge.*
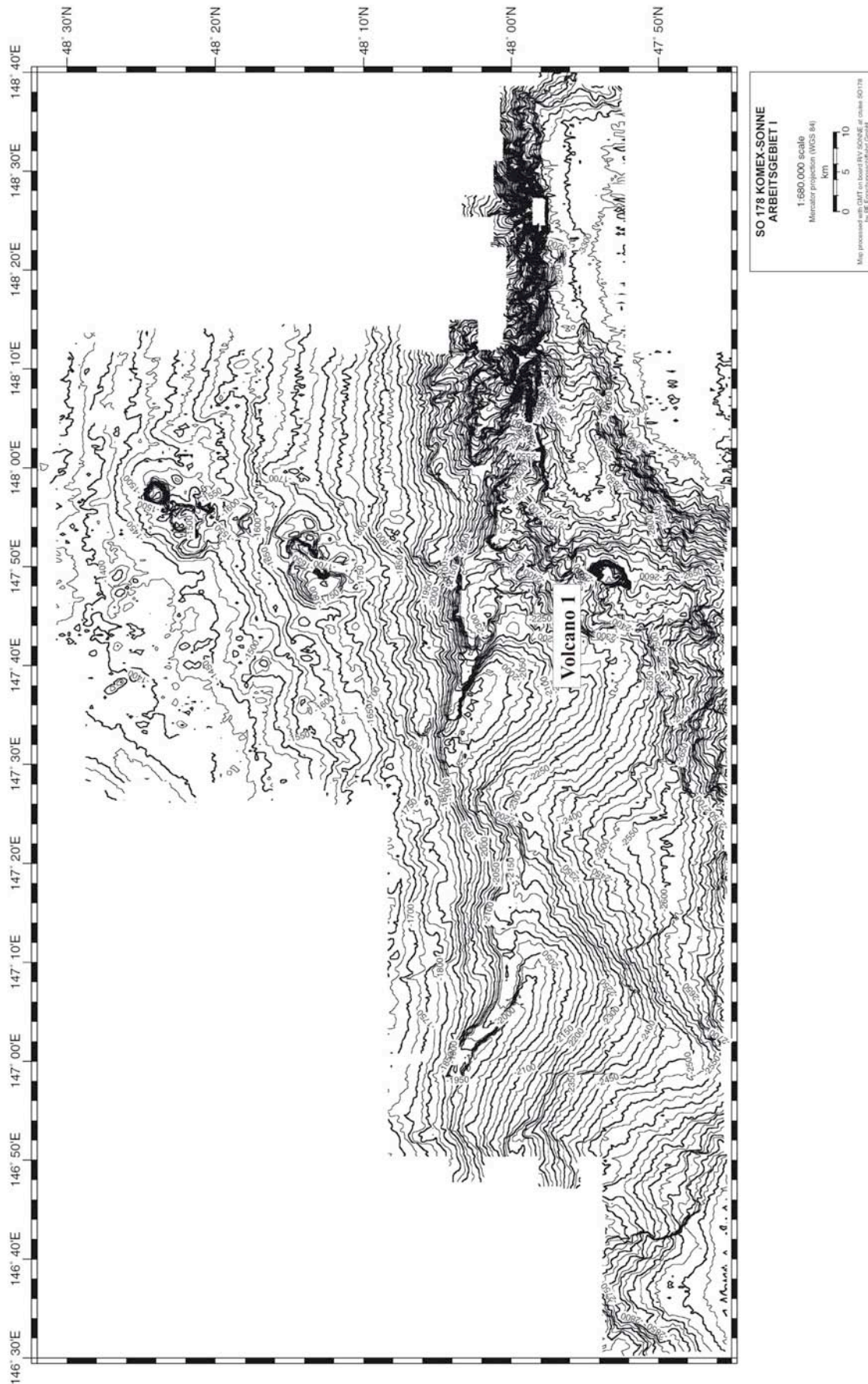
Fig. 8.3: *General bathymetric map of the Kurile Basin area investigated during cruise SO178-KOMEX showing the position of Volcano No. 1.*
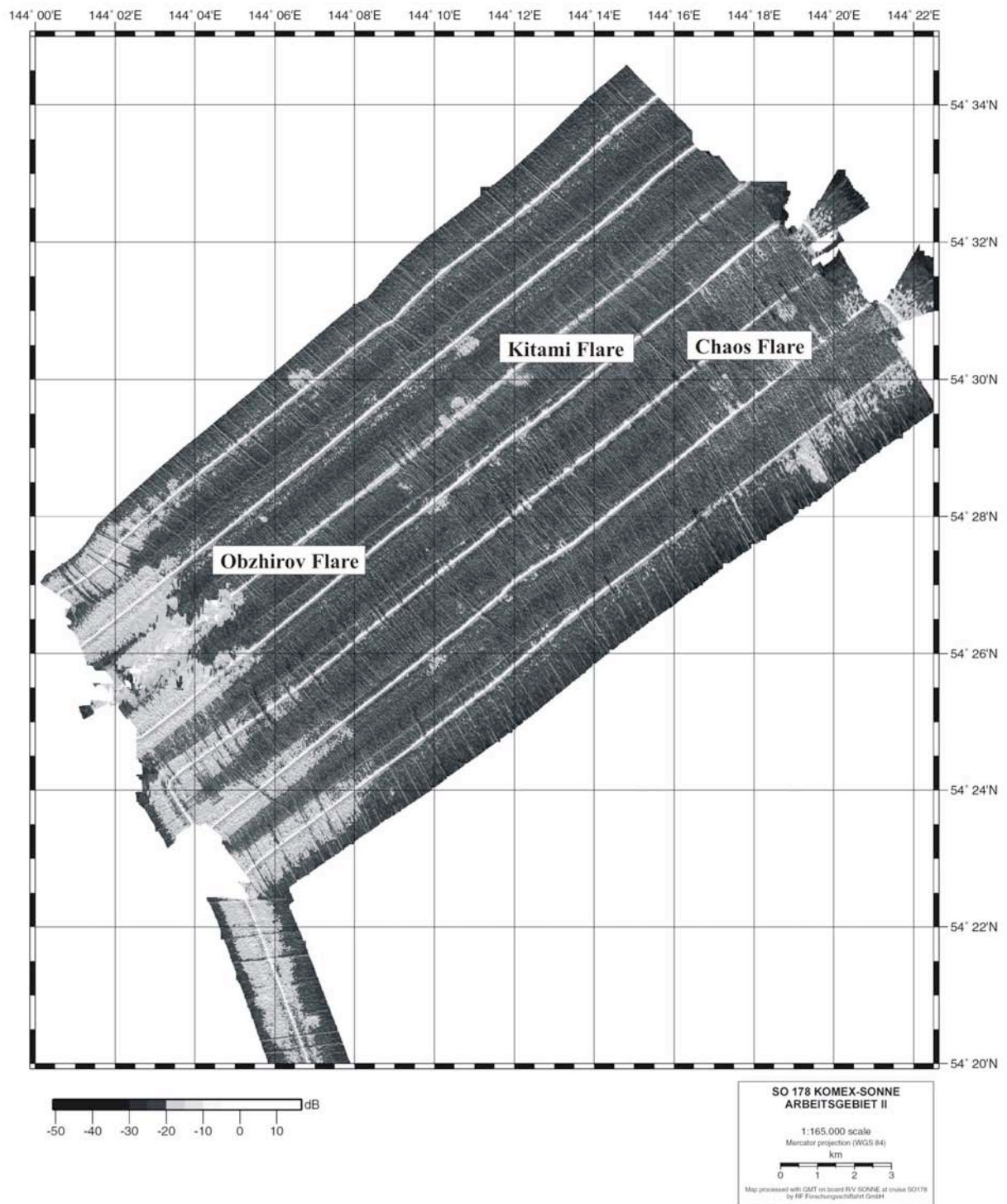
Fig. 8.4: *General backscatter map of the Sakhalin Slope sector investigated during cruise SO178-KOMEX. The Obzhirov, Kitami and Chaos Flare areas are characterized by high backscatter.*
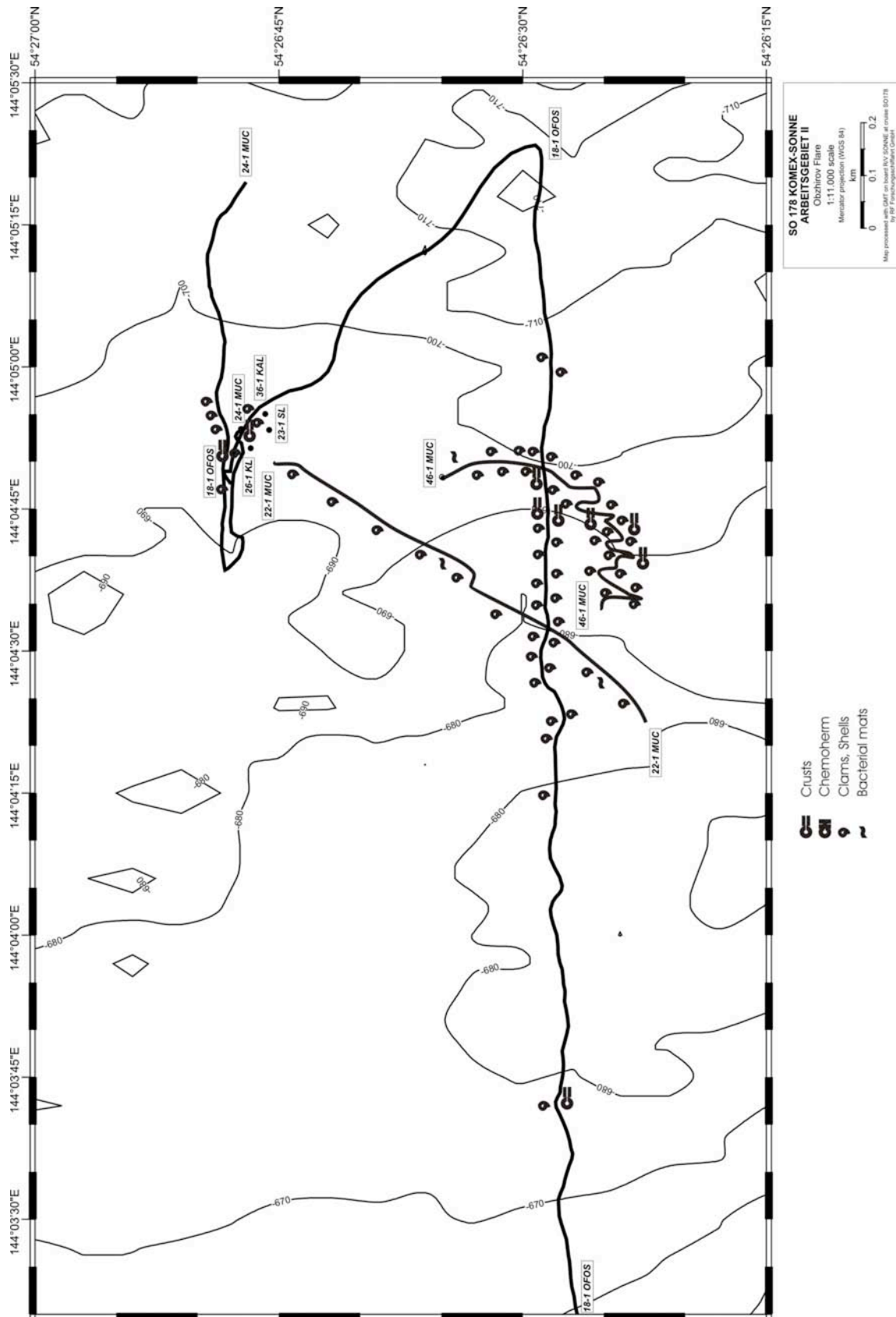
Fig. 8.5: *Detailed bathymetric map of the Obzhirov Flare area showing the tracks followed during video surveys and the distribution of seep- and vent-related features observed during surveys.*

80
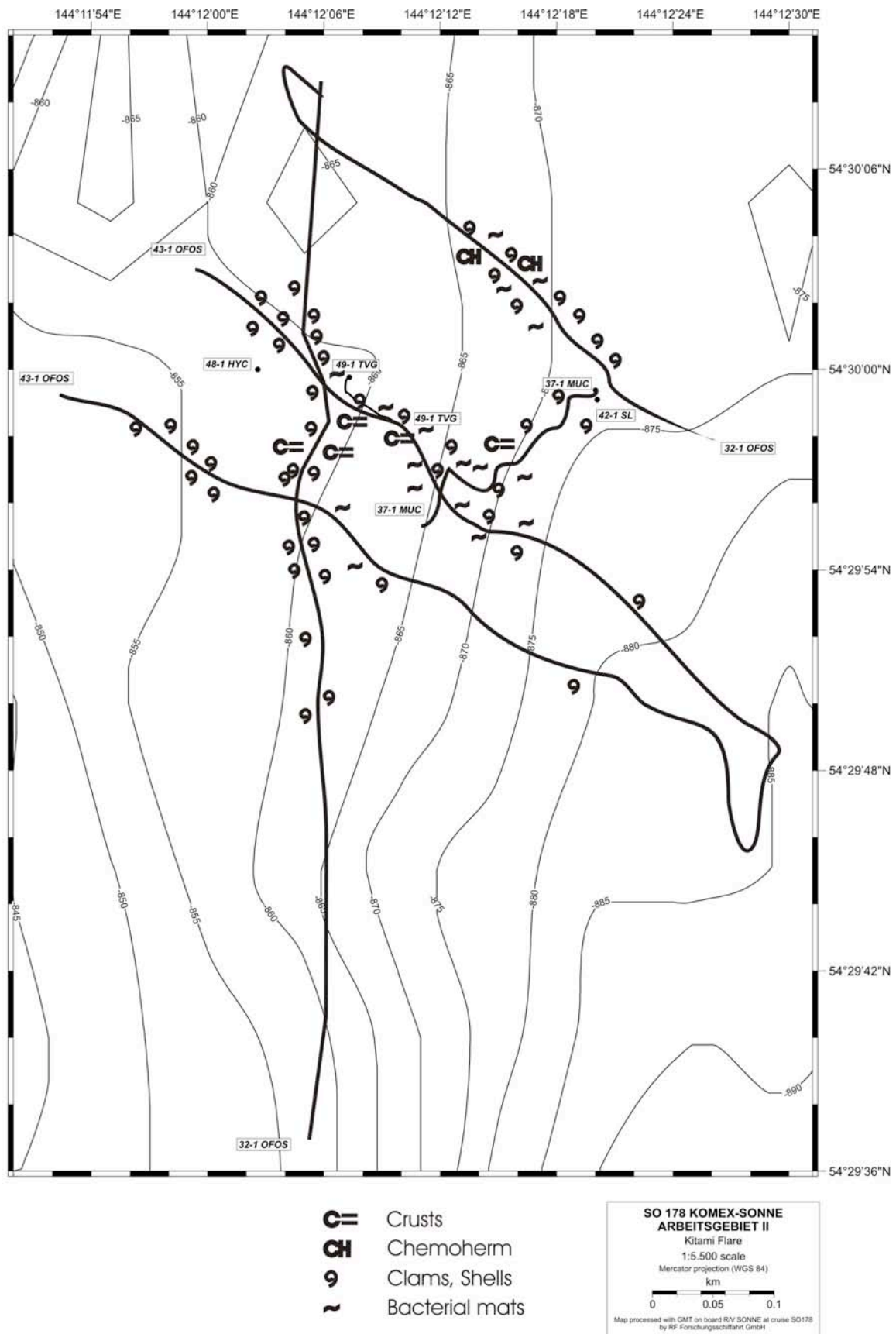
Fig. 8.6: *Detailed bathymetric map of the Kitami Flare area showing the tracks followed during video surveys and the distribution of seep- and vent-related features observed during surveys.*
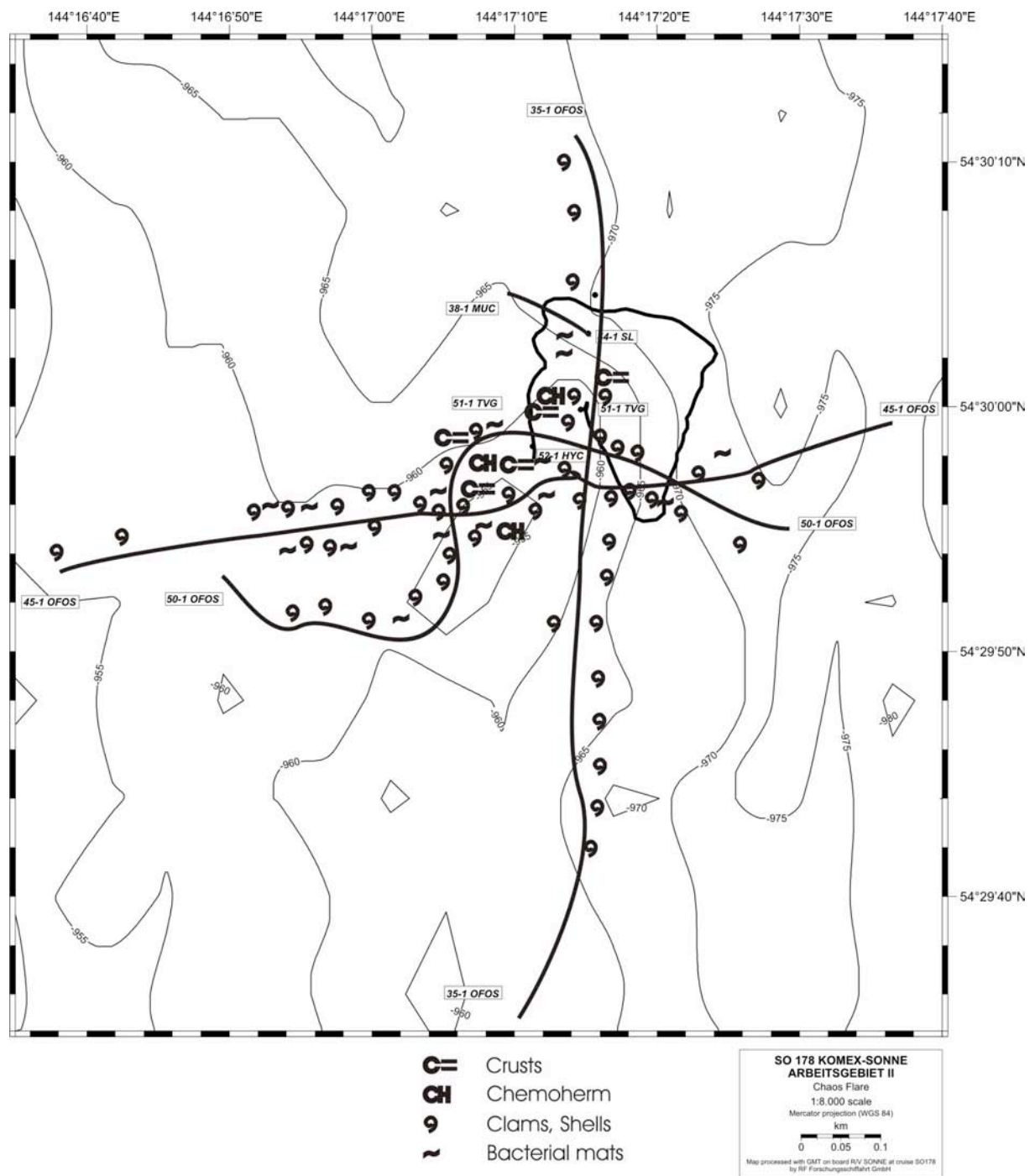
**Fig. 8.7:** *Detailed bathymetric map of the Chaos Flare area showing the tracks followed during video surveys and the distribution of seep- and vent-related features observed during surveys.*
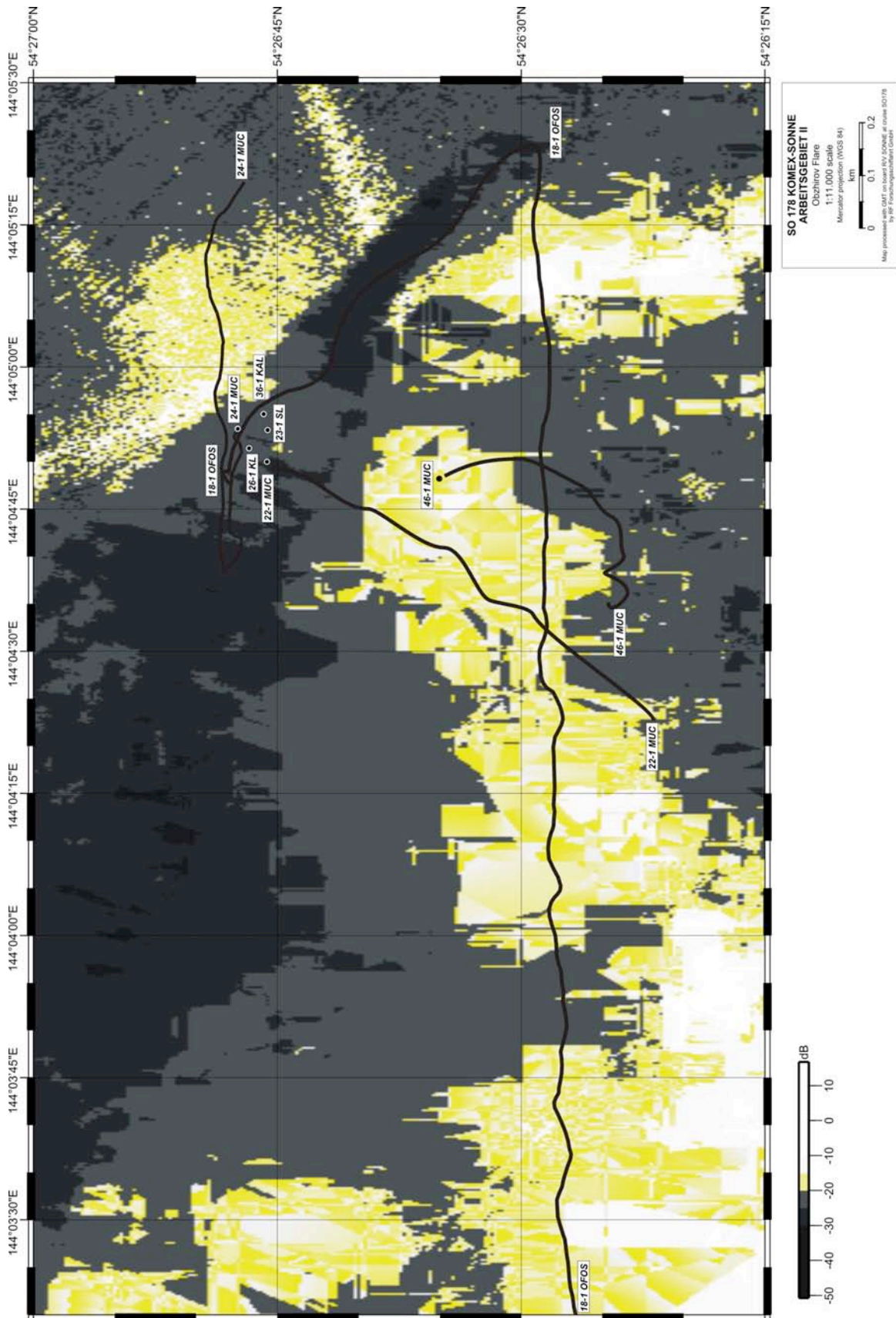
Fig. 8.8: *Detailed backskatter map of the Obzhirov Flare area.*
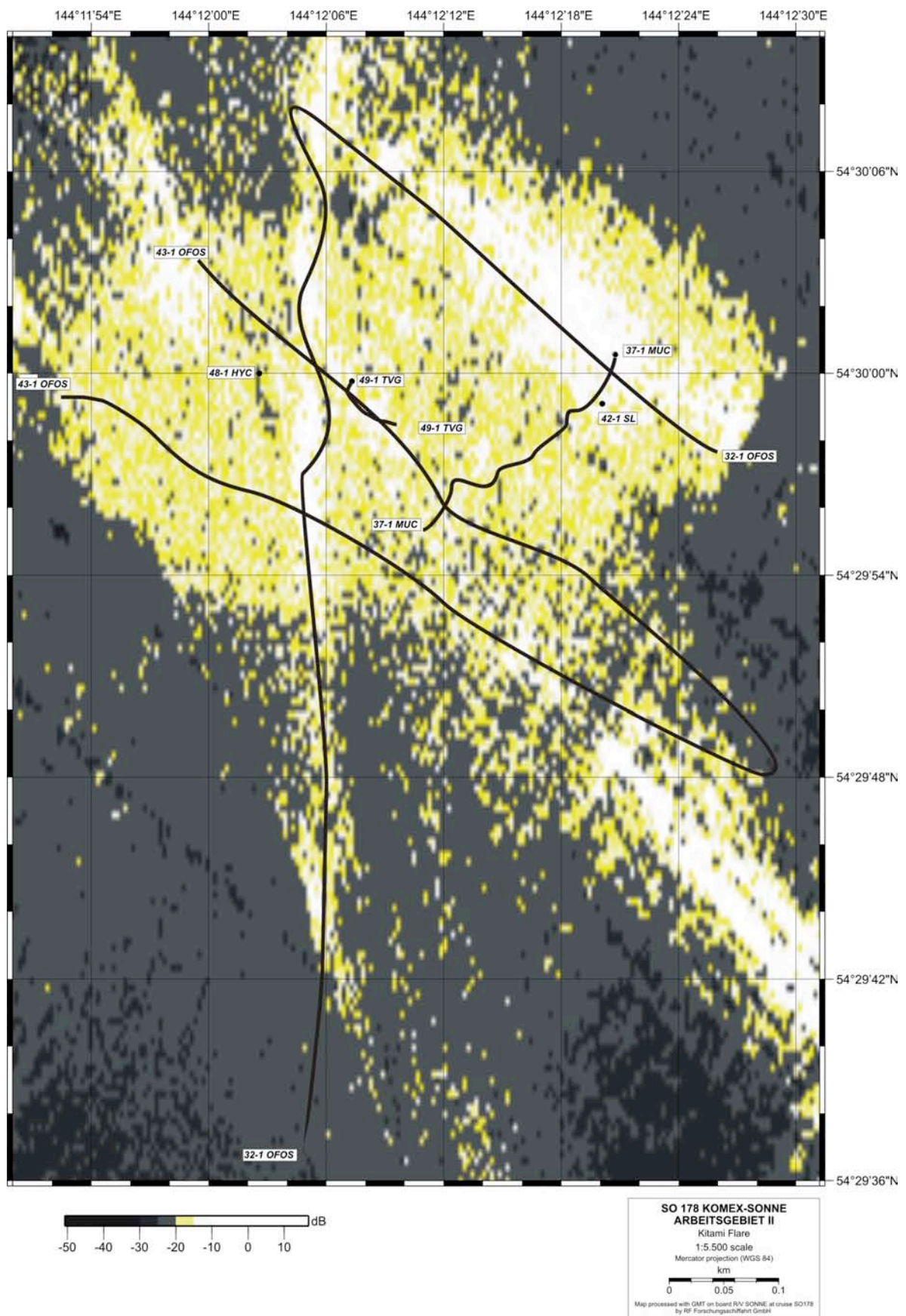
Fig. 8.9: *Detailed backskatter map of the Kitami Flare area.*
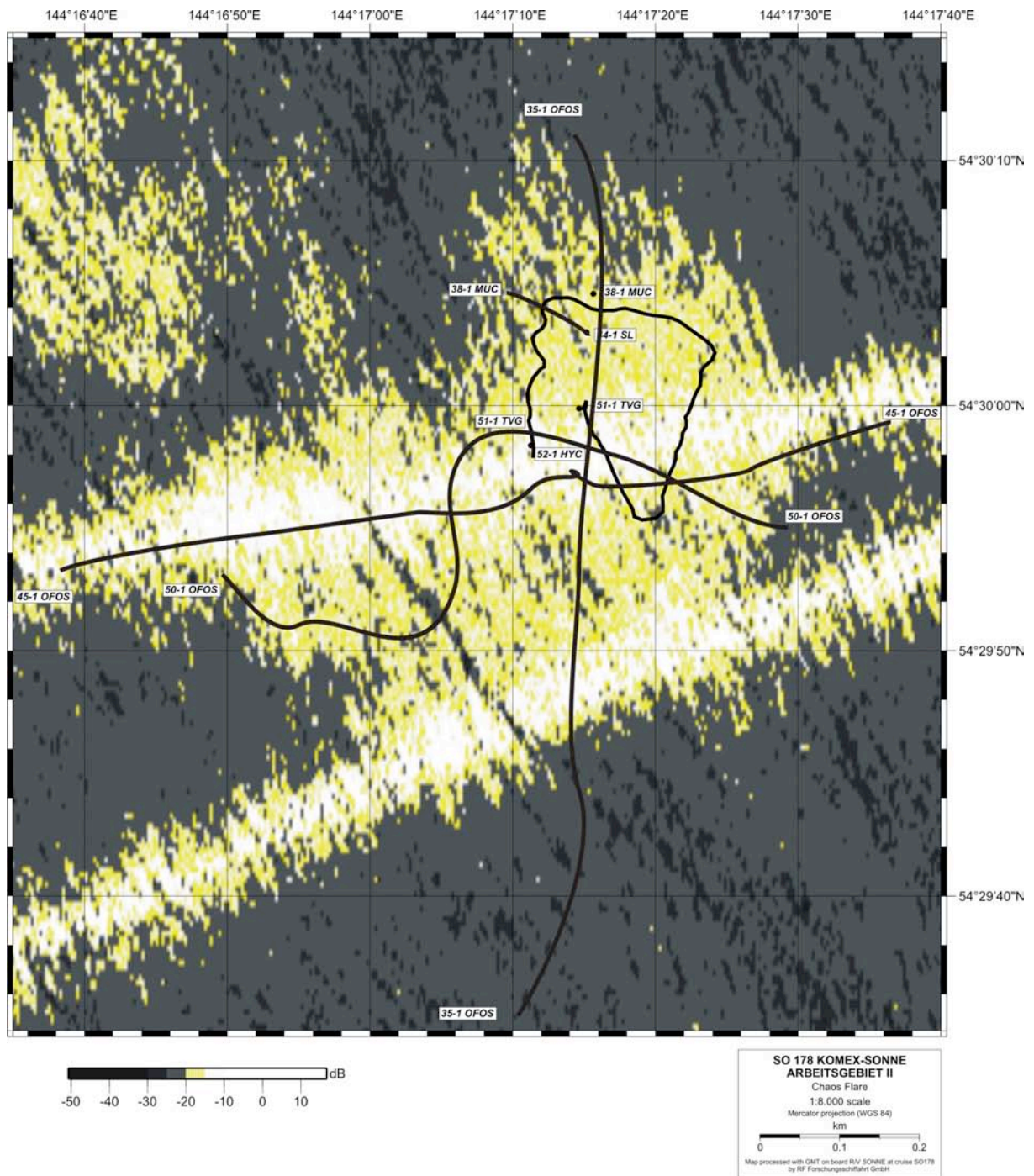
Fig. 8.10: *Detailed backskatter map of the Chaos Flare area.*
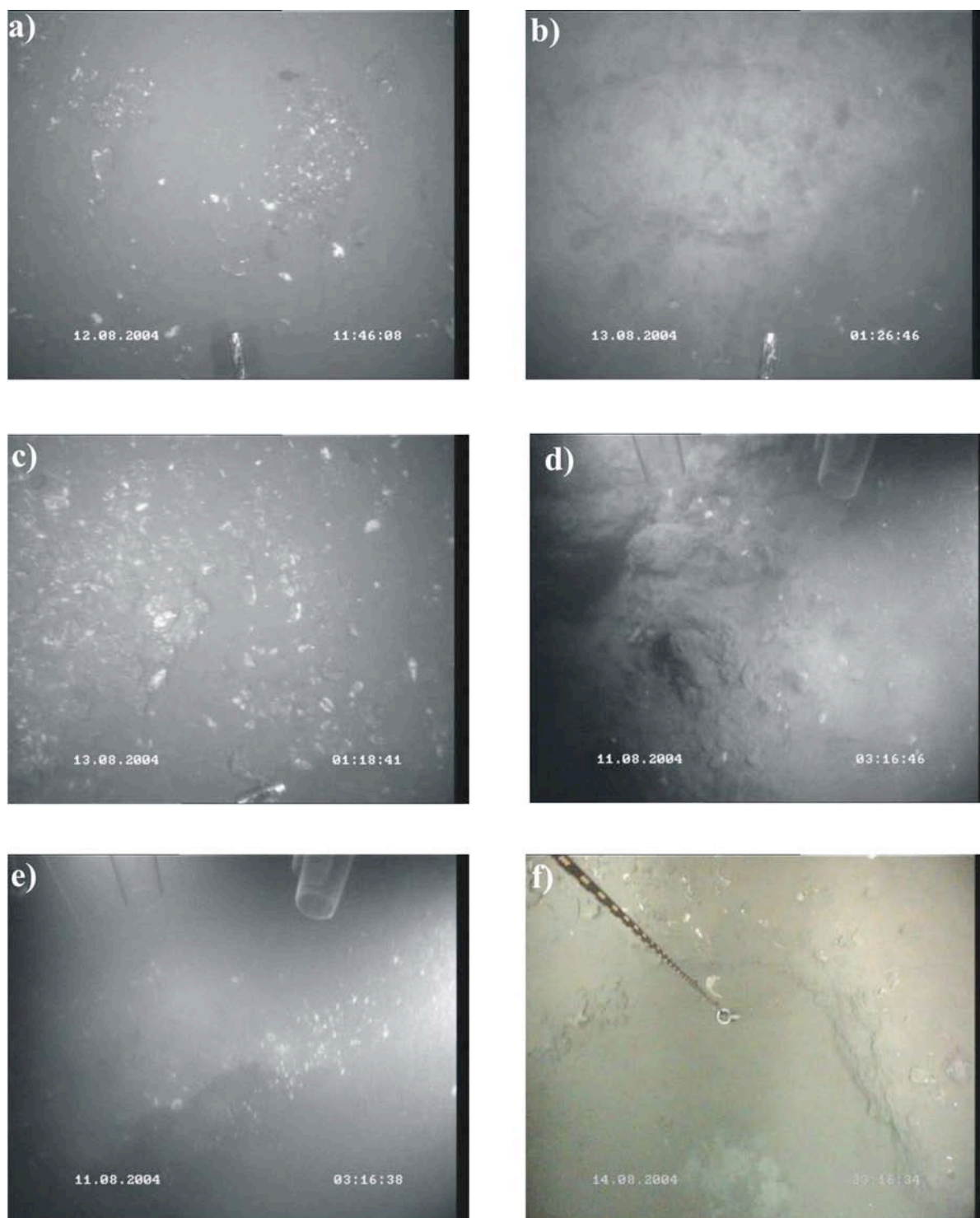
Fig. 8.11: *Seafloor terrains observed at the flare areas on the Sakhalin Slope. a) Clam fields, Kitami Flare area; b) Bacterial mats, Chaos Flare area; c) Carbonate pavement with clams, Chaos Flare area; d) chemoherm; e) bubble streams, Obzhirov Flare area; f) Pockmark, Chaos Flare area.*
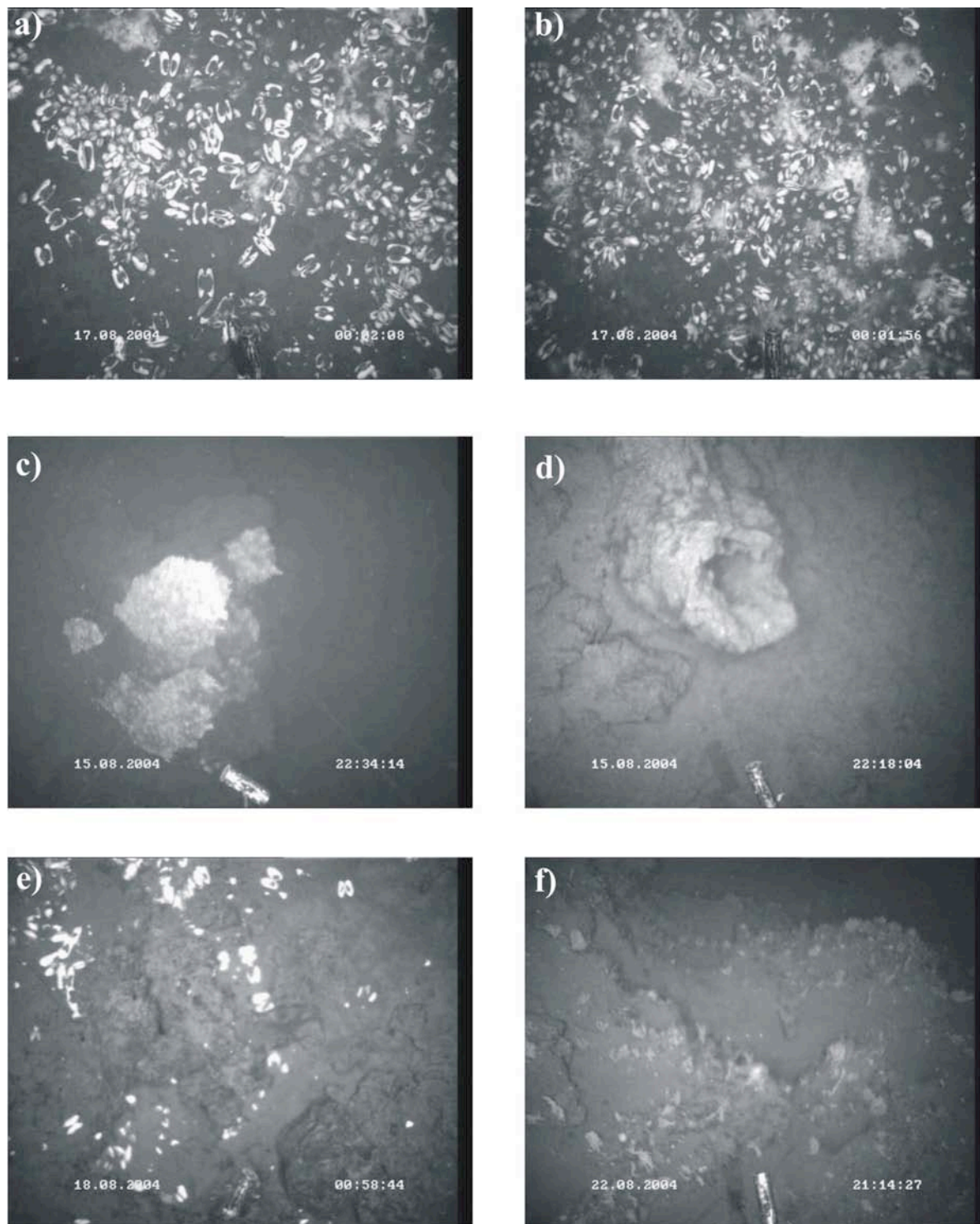
Fig. 8.12: *Seafloor terrains observed in the Derugin Basin area and in the Kurile Basin. a) und b) Clams and bacterial mats, Clam Hill; c) Recent barite chimney, Barite Mound; d) Old, truncated and hollow barite chimney, Barite Mound; e) Barite crusts, Clam Hill; f) Volcanoclastic deposits?, Kurile Basin.*
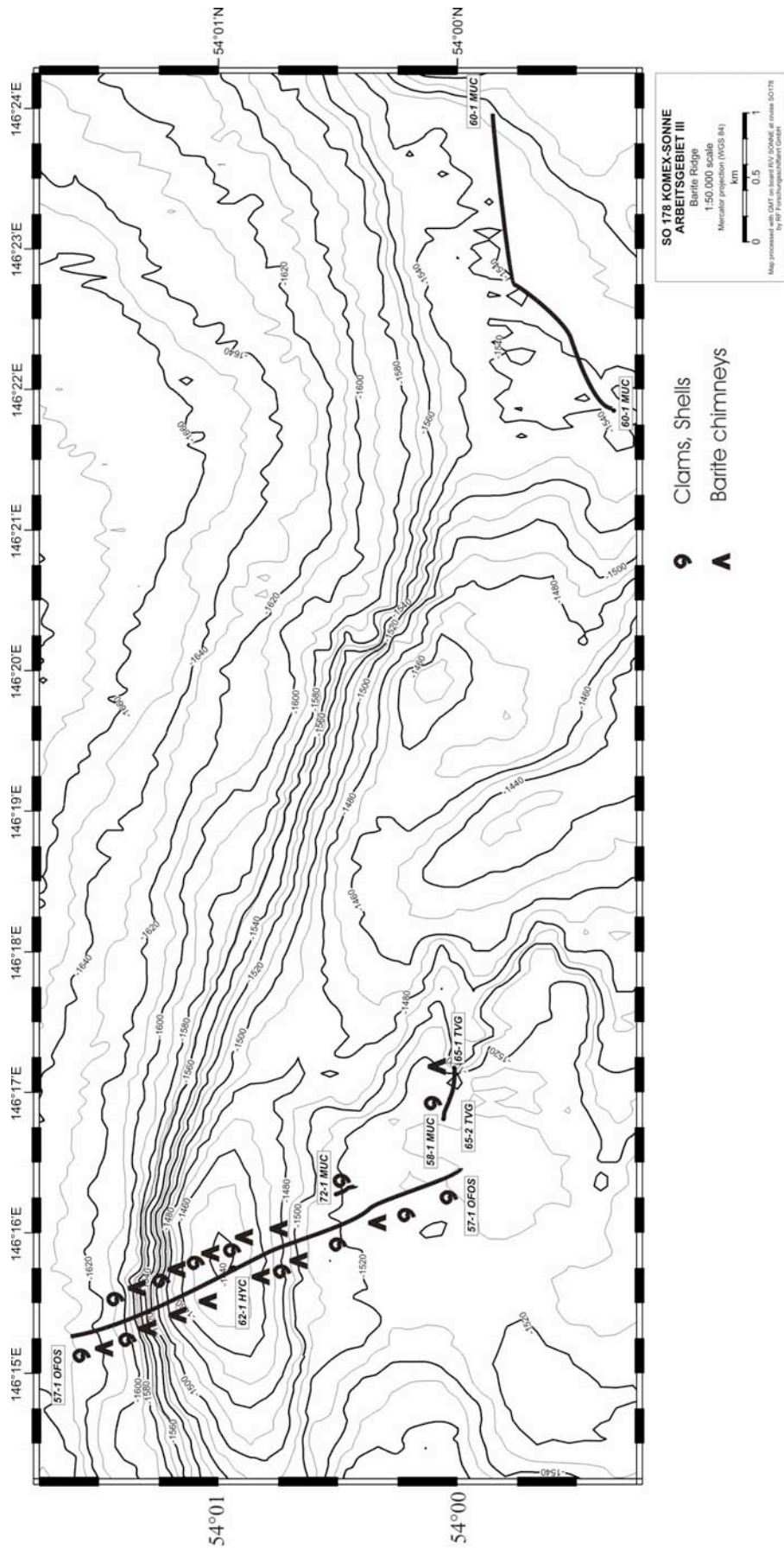
Fig. 8.13: *Detailed bathymetric map of Barite Mound and Clam Hill showing the tracks during video surveys and the distribution of seep- and vent-related features observed during surveys.*
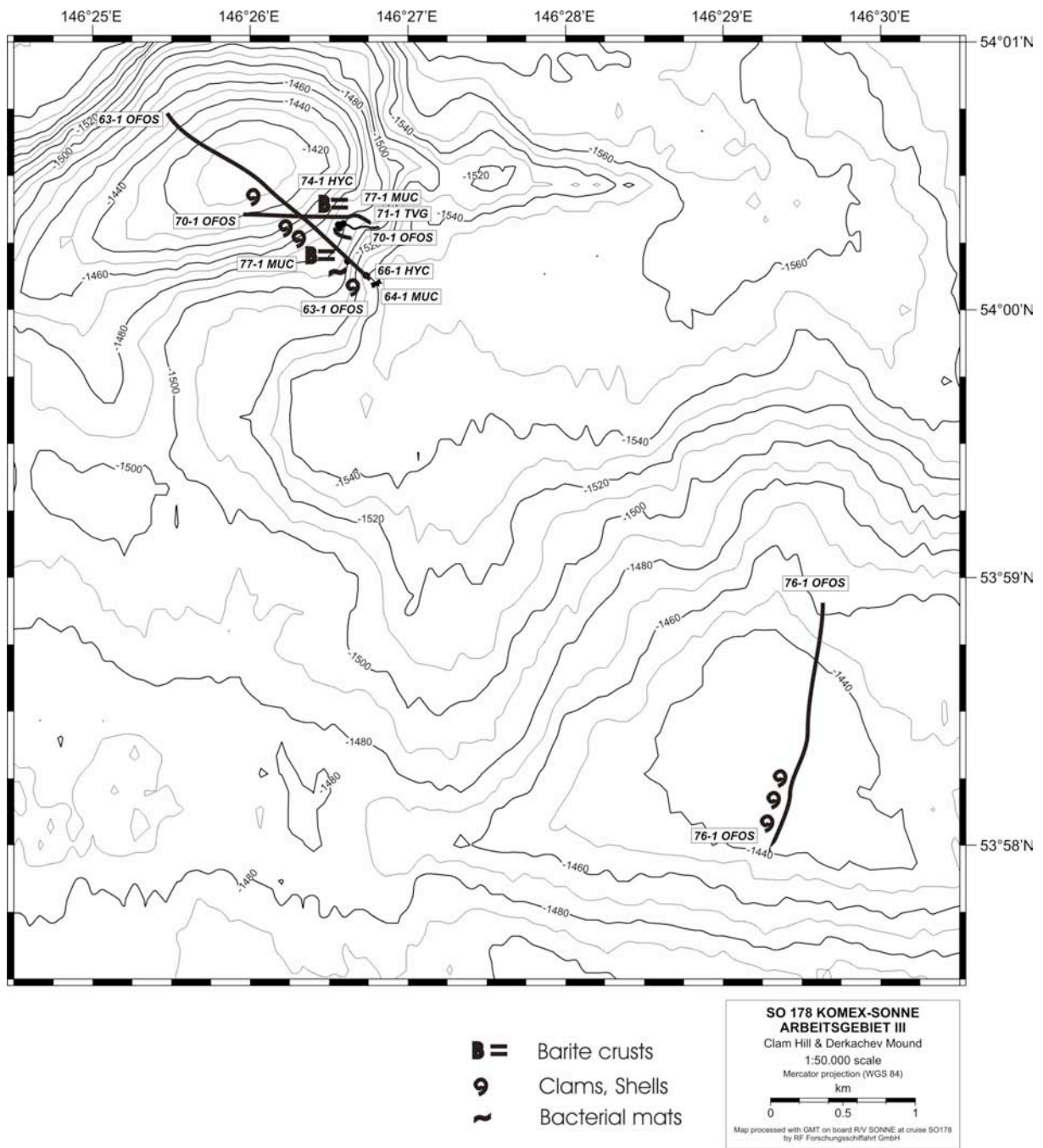
***Fig. 8.14:*** *Detailed bathymetric map of Clam Hill and Derkachev Mound showing the tracks during video surveys and the distribution of seep- and vent-related features observed during surveys.*
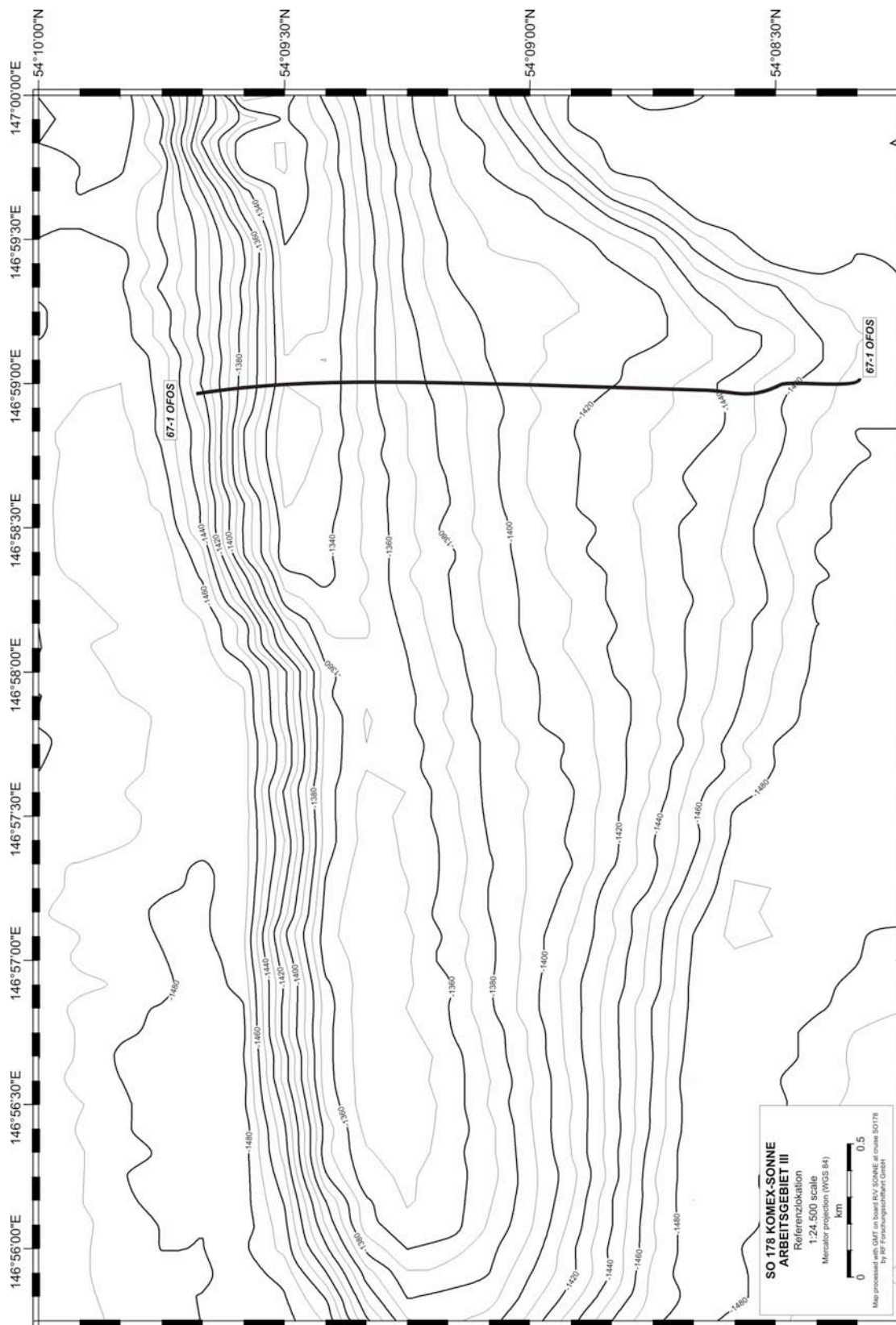
Fig. 8.15: *Detailed bathymetric map of Reference Ridge showing the tracks followed during the OFOS survey.*
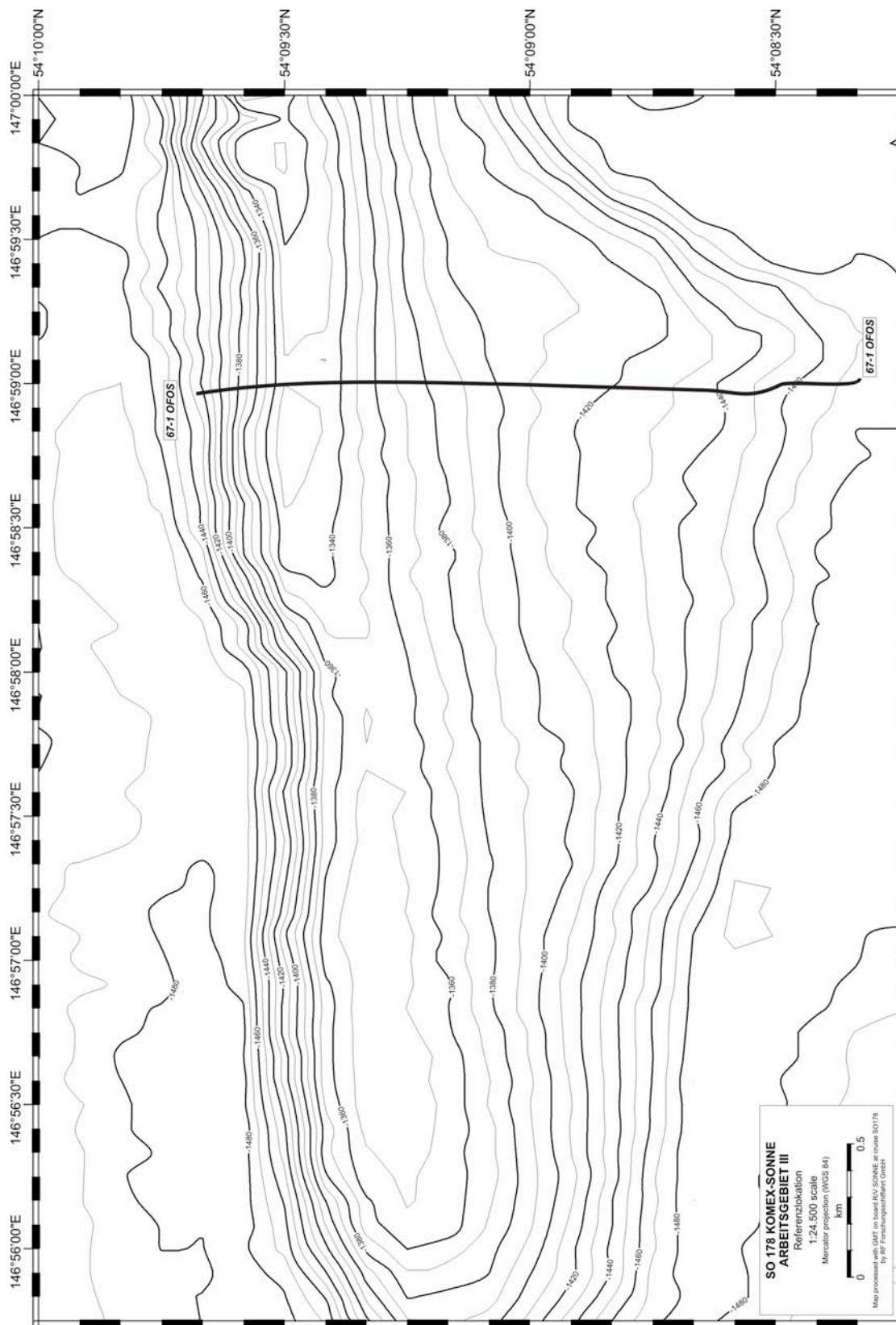
Fig. 8.16: *Detailed bathymetric map of Volcano No. 1 showing the tracks followed during the OFOS survey.*
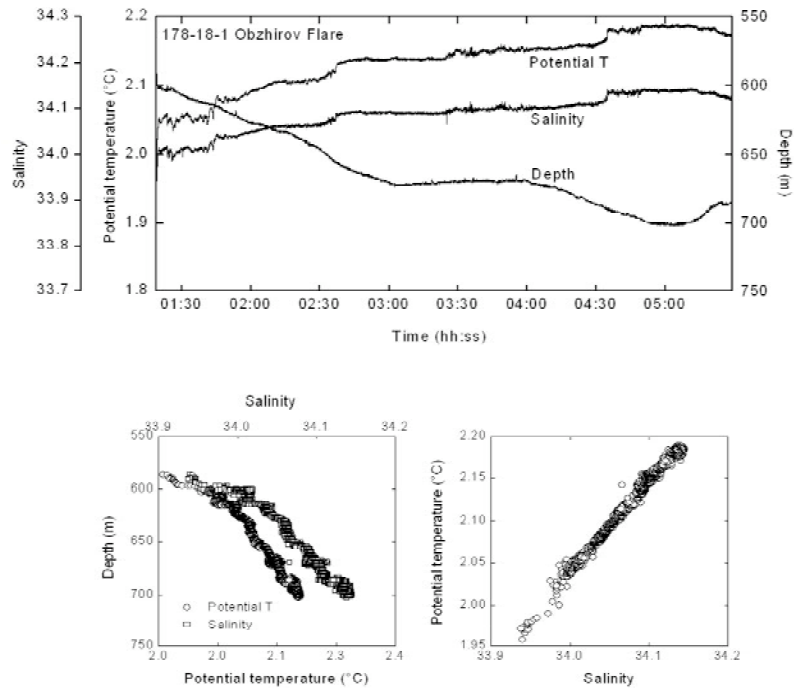
Fig. 8.17: *Depth, salinity and potential temperature profiles obtained with the OFOS-mounted CTD during OFOS station SO178-18-1 at the Obzhirov Flare.*
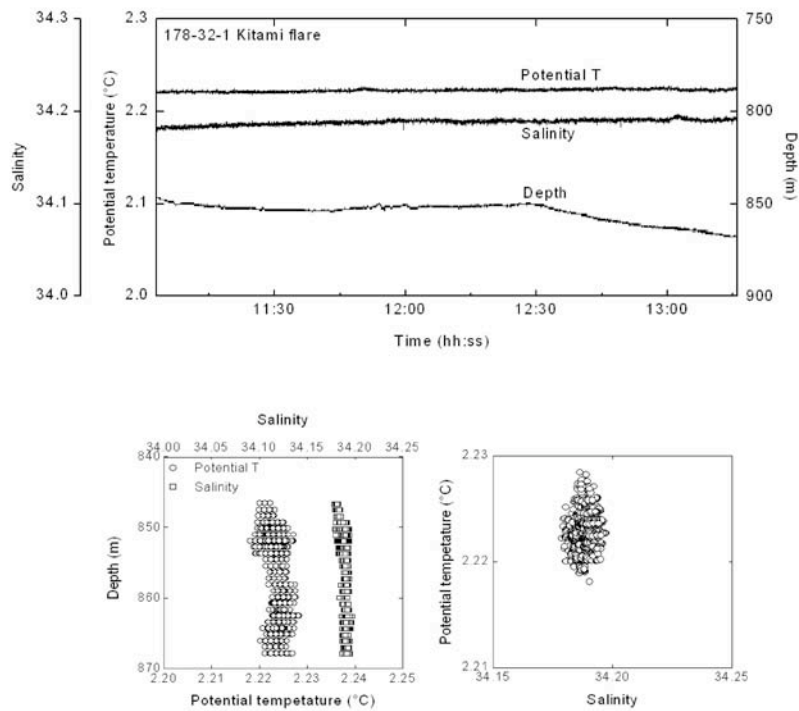
Fig. 8.18: *Depth, salinity and potential temperature profiles obtained with the OFOS-mounted CTD during OFOS station SO178-32-1 at the Kitami Flare.*
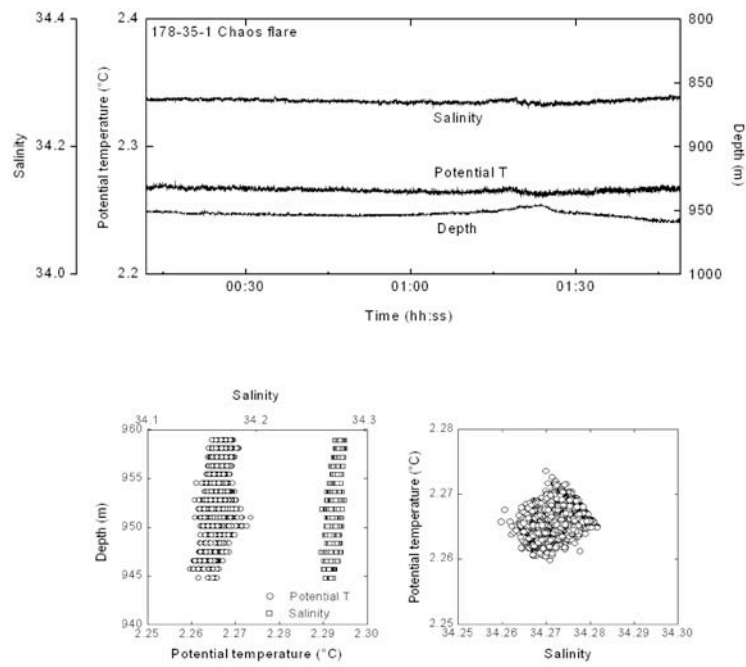
Fig. 8.19: *Depth, salinity and potential temperature profiles obtained with the OFOS-mounted CTD during OFOS station SO178-35-1 at the Chaos Flare.*
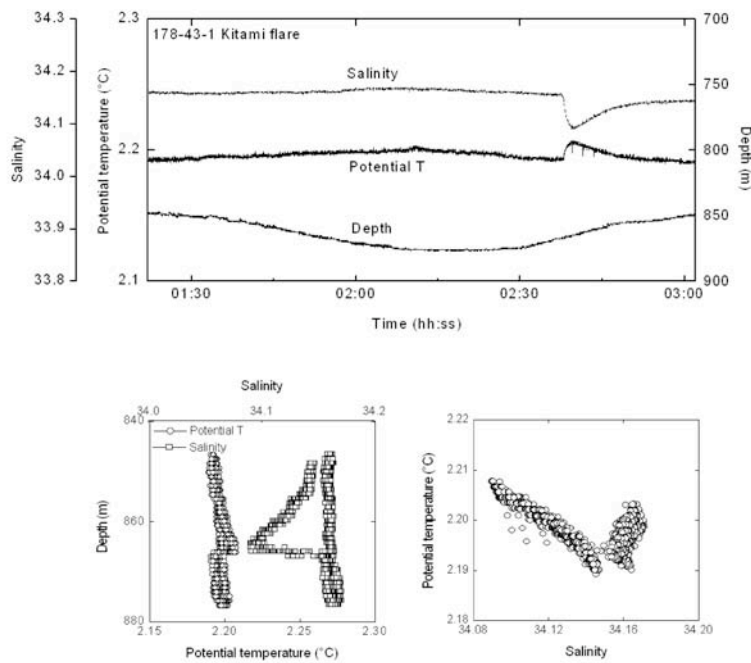
Fig. 8.20: *Depth, salinity and potential temperature profiles obtained with the OFOS-mounted CTD during OFOS station SO178-43-1 at theKitami Flare. An anomaly in salinity and potential temperature can be seen at 02:40.*
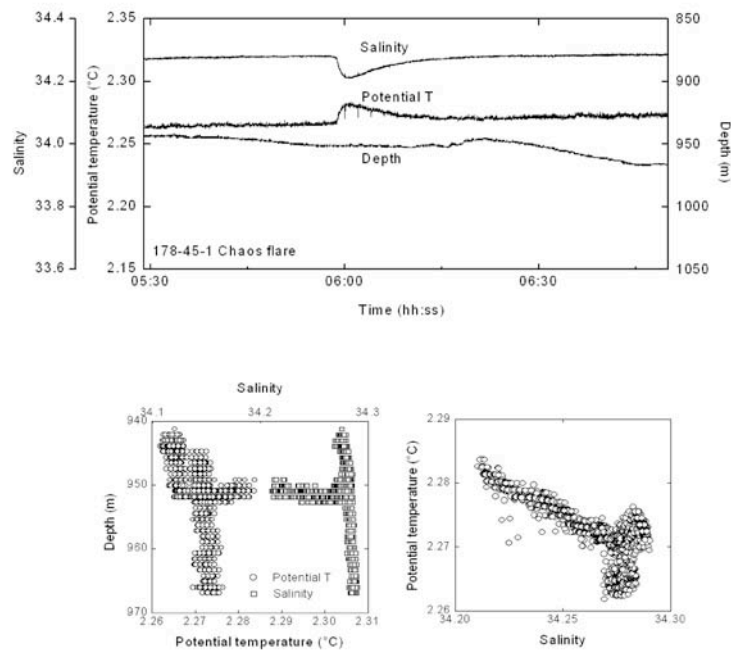
Fig. 8.21: *Depth, salinity and potential temperature profiles obtained with the OFOS-mounted CTD during OFOS station SO178-45-1 at the Chaos Flare. An anomaly in salinity and potential temperature can be seen at 06:00.*
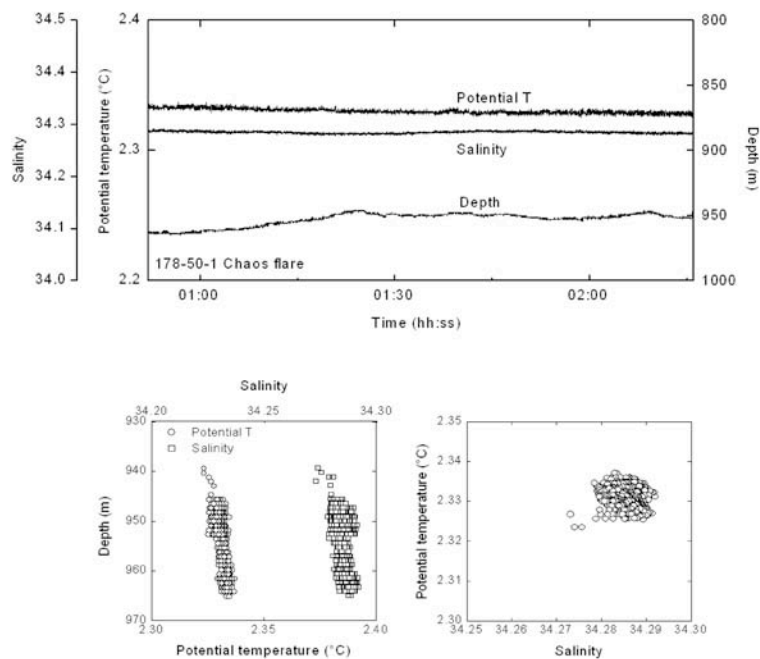
Fig. 8.22: *Depth, salinity and potential temperature profiles obtained with the OFOS-mounted CTD during OFOS station SO178-50-1 at the Chaos Flare.*
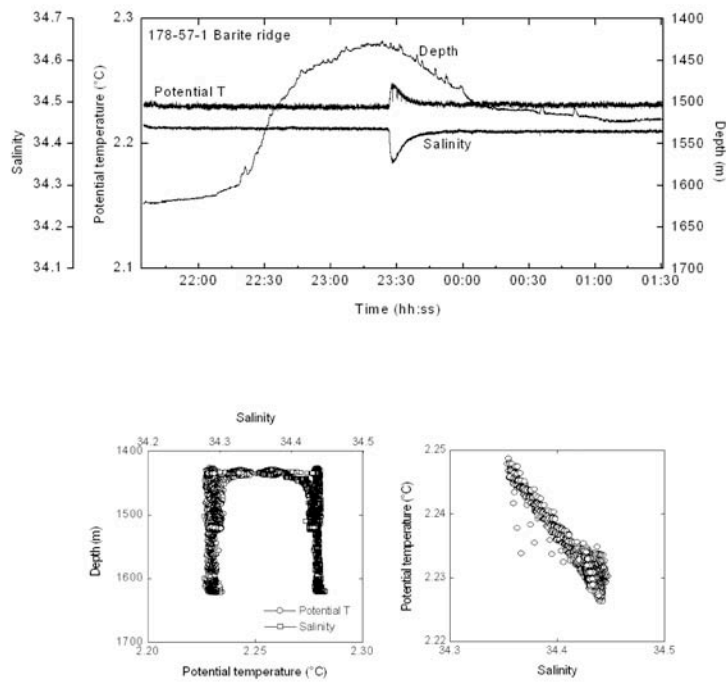
Fig. 8.23: *Depth, salinity and potential temperature profiles obtained with the OFOS-mounted CTD during OFOS station SO178-57-1 at Barite Ridge. An anomaly in salinity and potential temperature can be seen at 23:25.*
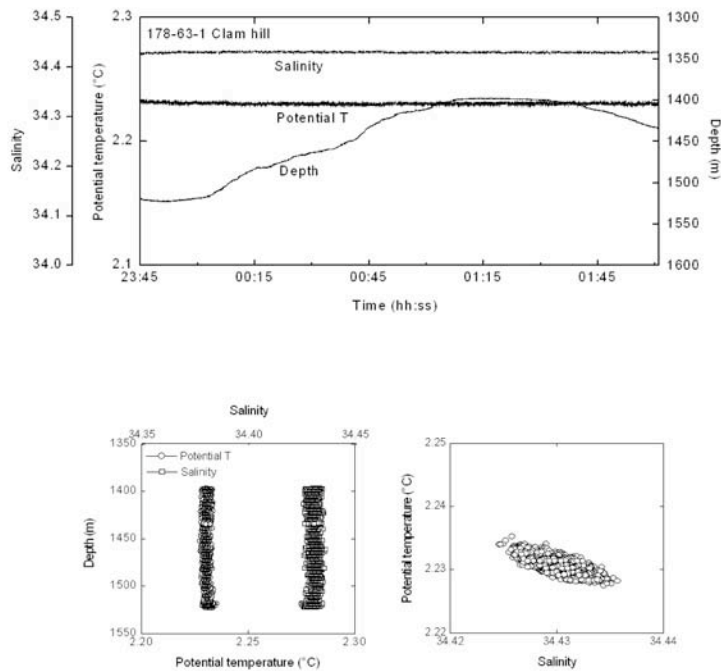
Fig. 8.24: *Depth, salinity and potential temperature profiles obtained with the OFOS-mounted CTD during OFOS station SO178-50-1 at Clam Hill.*
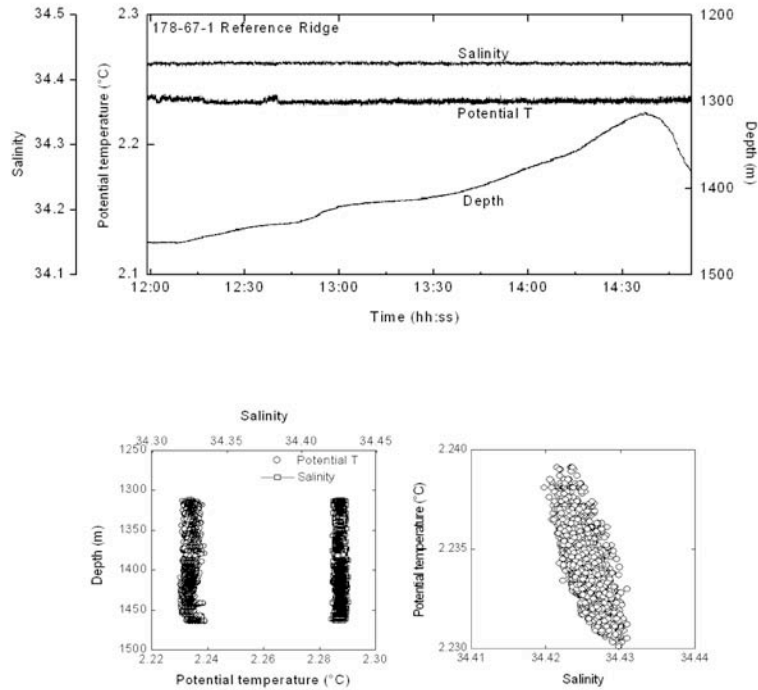
Fig. 8.25: *Depth, salinity and potential temperature profiles obtained with the OFOS-mounted CTD during OFOS station SO178-67-1 at the Reference Ridge.*
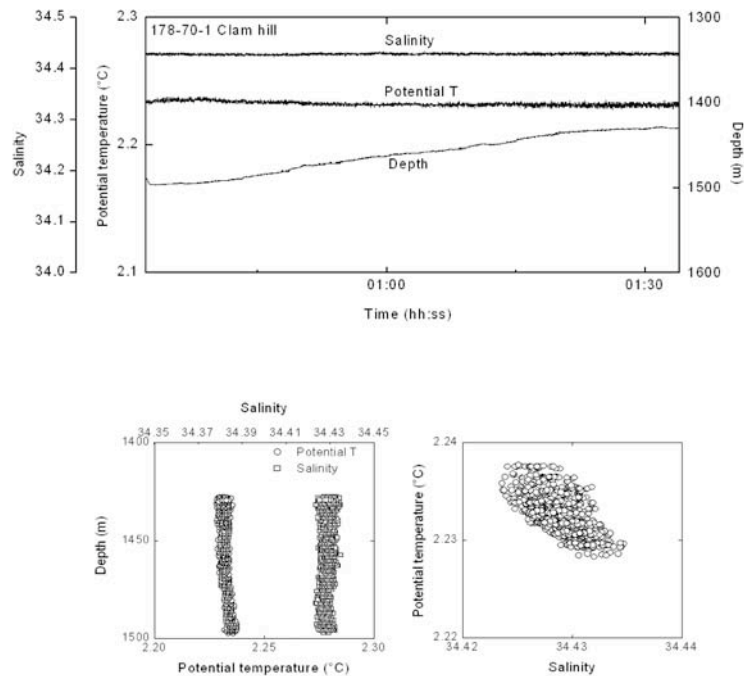
Fig. 8.26: *Depth, salinity and potential temperature profiles obtained with the OFOS-mounted CTD during OFOS station SO178-70-1 at Clam Hill.*
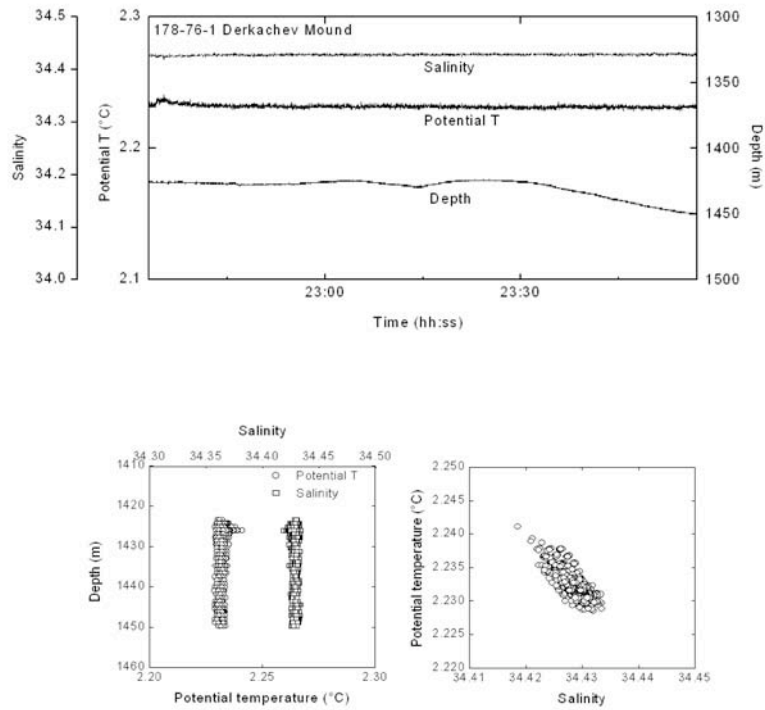
Fig. 8.27: *Depth, salinity and potential temperature profiles obtained with the OFOS-mounted CTD during OFOS station SO178-76-1 at the Derkachev Mound.*
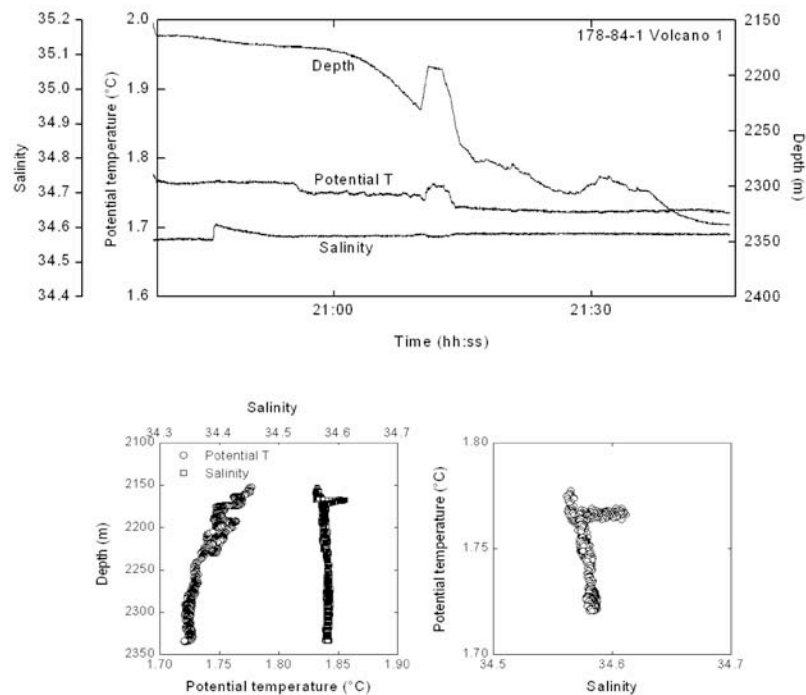
***Fig. 8.28:*** *Depth, salinity and potential temperature profiles obtained with the OFOS-mounted CTD during OFOS station SO178-84-1 at Volcano No. 1. The anomaly between 21:10 and 21:14 was produced by hauling the OFOS due to technical problems with the video equipment.*

9. SEDIMENTS AND AUTHIGENIC PRECIPITATES OF COLD-SEEP AREAS

Alexander Derkachev, Natalya Nikolaeva, Giovanni Aloisi, Klaus Wallmann, Alexander Bosin, and Lester Lembke

9.1 Slope of Sakhalin Island

7 sediment cores of 40 to 197 cm length were taken on the Sakhalin Slope in the Obzhirov (SO178-23-1, SO178-26-1, SO178-36-1), Kitami (SO178-42-1, SO178-48-1) and Chaos (SO178-44-1, SO178-52-1) Flares.

The structural and material composition of these sediments are rather close as the stations are located near to each other. The sediments are mainly of silty clay (less often of clay and clayey silt), and they consist of siliceous fragments (diatoms, less often radiolaria). Terrigenous clayey–silty and sandy material is present as admixture. An olive-green sediment color is dominant. Lenses and interlayers of darker gray color (SO178-36-1) as well as lenses and spots of black color (admixture of hydrotroilite) occur at single horizons.

All cores taken in gas flare areas show a characteristic sediment structure. A similar structure was observed earlier at other gas venting sites of the Sakhalin Slope (Ginsburg & Soloviev, 1994; Biebow & Hütten, 1999; Biebow et al., 2000; 2003; Derkachev et al., 2002). Hydrotroilite, carbonate concretions, and a strong H_2S odor are typical sediment features. Specific water- and gas-saturated horizons with a characteristic lumpy texture as well as numerous chemosynthetic mollusk fauna (mainly *Calyptogena*) and its fragments occur. The amount of such fauna is increased near centers of methane flux; sometimes shelly horizons formed there (Appendix 6). Numerous lenses and interlayers of gas hydrates were found in the lower part of most cores (SO178-23-1, SO178-26-1, SO178-44-1, SO178-48-1, and SO178-52-1) from 17 up to 152 cm sediment depth. The thickness of the hydrate-saturated sediments reaches 1.5 m (see Appendix 6). Gas hydrates occur as thin interlayers and lenses within the sediments. The sediments are strongly influenced by frost at horizons containing large amounts of gas hydrates. Clear signs of gas hydrates (water- and gas-saturated horizons, pseudobrecciated texture) were found in cores where gas hydrates could not be discovered.

Carbonate concretions were sampled in variable amounts (from single concretions up to concretionary horizons) in the upper part of all cores above the hydrate-bearing sediment layers whereas within the hydrate-bearing horizons, they occur very seldomly (SO178-23-1, SO178-48-1). The carbonate precipitates differ in morphology and size; weakly consolidated, homogeneously colored (light-green) precipitates (from some mm up to 5 cm in size), however, dominate which contrasts well with the surrounding sediments. At some horizons (SO178-36-1, 46-60 cm), they are soft and lumpy. Concretions and crusts cementing *Calyptogena* shells occur in some cores.

During TV-grab deployments (SO178-49-1, SO178-51-1), numerous carbonate concretions and crusts with different morphology and composition as well as mollusk fauna were recovered. Soft, flat concretions of greenish-gray color with a large amount of swells (up to 15 cm in size) dominate at station SO178-49-1 whereas flat crusts of greenish-gray color (up to 12 cm in size and 0.3-0.8 cm in thickness) occur less often. A laminated structure (up to 8-10 laminas) is well visible on some of these crusts. All types of concretions recovered here are similar in mineral composition. Preliminary microscope study showed that they consist of Mg-calcite.

A significant amount of concretions and crusts (more than 10 kg), mainly precipitates of irregular shape (up to 20 cm in size) with numerous smoothed swells, was recovered in the Chaos Flare at station SO178-51-1 (Fig. 9.1). Their density ranges from soft, moderate dense to dense. Greenish-gray and light-gray varieties dominate (Fig. 9.1a). They have a calcite-aragonite composition with a variable quantitative proportion of these mineral phases. Branchy carbonate crusts (up to 45 cm in size) are widely distributed among these carbonate

precipitates. Their outer surface is smooth with small subparallel swells and consists of a calcite-aragonite mixture. Their inner aragonite surface is branchy with numerous cavities and holes (Fig. 9.1b). Frequent inclusions of mollusk shells appear. Crusts often consist of strongly bioturbated sediments mixed with numerous shell fragments (Fig. 9.1c). Interestingly, the crusts with aragonite cement described above were recovered in the Sakhalin gas and fluid venting area for the first time. With respect to morphology and mineral composition these crusts are close to carbonate precipitates of Hydrate Ridge, Cascadia convergent margin (Greinert et al., 2001; Bohrmann et al., 2002). The formation of these carbonates is linked with near-seafloor gas hydrate deposits and their destabilization.
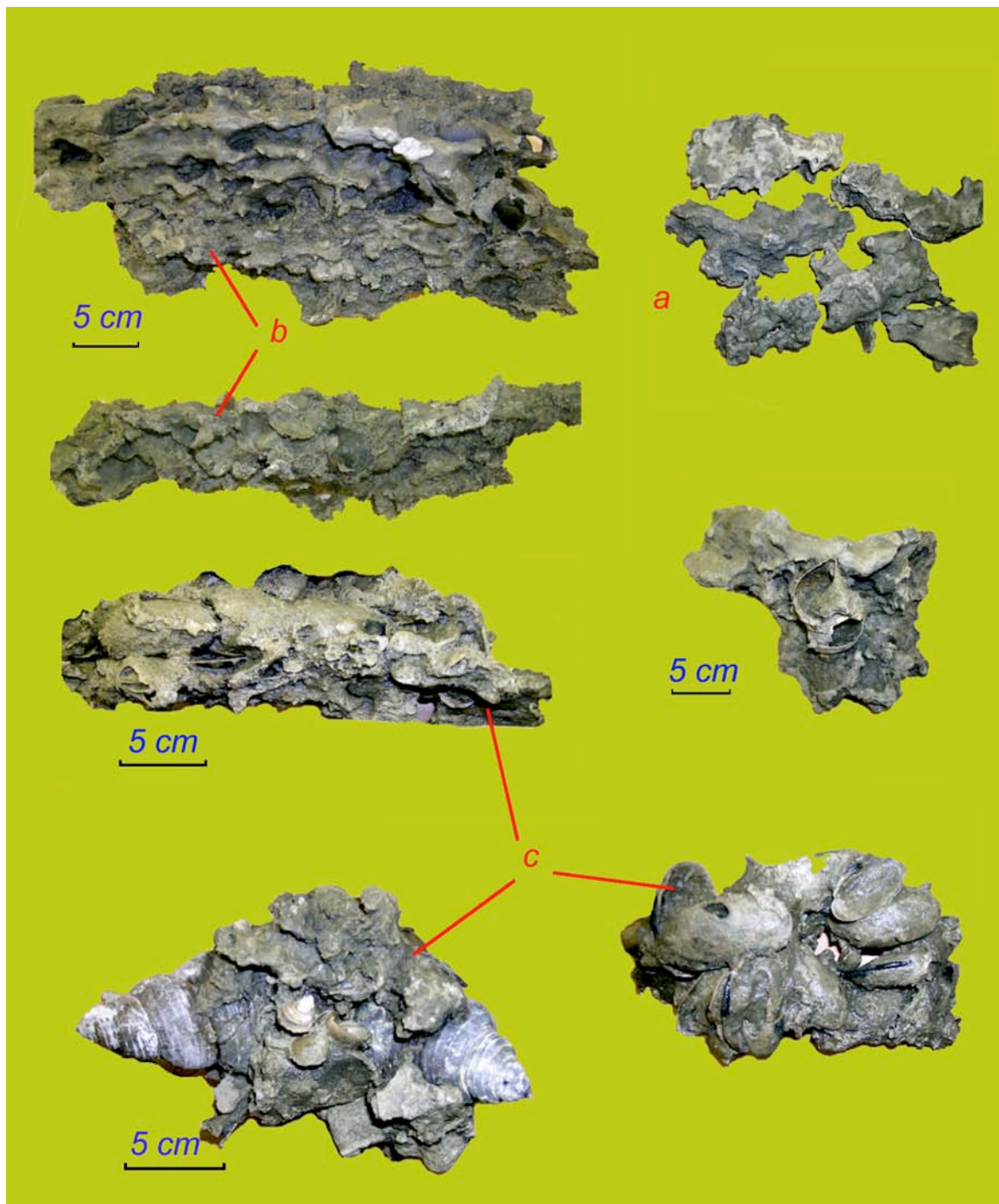

Fig. 9.1: *Carbonate crusts from station SO178-51-1. See explanations in the text.*

9.2 Derugin Basin

Two cores were taken in the Barite Mound area revealing a section of Late Pleistocene deposits typical for this area which contain both gas-saturated sediments and numerous authigenic carbonate-barite precipitates. The sediments mainly consist of terrigenous clayey silt with a significant admixture of sandy particles. Dropstones were found, too.

At station SO178-62-1, gas-saturated sediments occur from 20 cm sediment depth downcore. Authigenic mineral formation probably starts above this horizon at 10-22 cm depth. A congestion of carbonate and carbonate-barite precipitates is significant for this horizon. Besides, the content of cryptocrystalline calcite is increased here in silty-clayey sediments. A significant amount of authigenic carbonate-barite precipitates was found at 110-122 and 258-266 cm sediment depth. Thin lentiform interlayers of yellowish-white color (up to 1-2 mm in thickness) are visible at 283 cm near to consolidated carbonate lenses.

Station SO178-69-1 is located in the western part of the Barite Mound area which had not been investigated earlier. A sediment section typical for gas-fluid emanations areas was recovered here. Gas-saturated sediments occur below 118 cm. The first carbonate and carbonate-barite precipitates (including carbonate crusts up to 8 x 0.5 cm in size) appear at 67-72 cm. Below this depth, they are seldom except for horizon 130-144 cm in which the sediments are enriched in precipitates.

Investigations including submarine video-surveys (OFOS, TV-MUC, TVG) were also carried out on Clam Hill, another active center of gas-fluid emanations and barite mineralization which is located 5 km east of the Barite Mound and which was discovered during cruise LV29 (Biebow et al., 2003). They confirmed wide distribution of chemosymbiotnic fauna forming large congestions. Both barite crusts enclosing mollusk congestions and small barite hillocks were clearly visible on the seafloor. TV-grab observations showed that one of these hillocks is a barite build-up in the form of a chimney. Sampling with the TV-grab recovered lots of fragments of this chimney (more than 100 kg) consisting of pure, strongly water-saturated, porous barite fragments (up to 0.5-0.6 m in size). Similar barites were taken earlier in large amounts in the Barite Mound area where they form numerous chimneys of up to 20 m height (Biebow & Hütten, 1999; Biebow et al., 2000; 2003). More detailed investigations of the barite chimneys from the Barite Mound revealed, however, essential differences. Many fragments contain carbonate mineralization unusual for barite chimneys. This mineralization developped in the pore space of travertine-like barites and mainly consists of aggregates of Mg-calcite and aragonite. It occurs only in the middle part and in the lower root part (transition to underlying sediments) of the barite chimneys. The strong H_2S odor characteristic for these fragments is evidence of sulphate-reduction processes taking place within the body of the barite chimneys. The samples representing the transitional part from barite chimneys to underlying sediments are cemented by microcrystalline diagenetic barite and contain a small amount of aragonite. They are strongly bioturbated and contain fragments of *Calyptogena* shells. Unfortunately, it was not possible to obtain representative samples of underlying sediments from the barite chimney area.

At station SO178-65-2, only barite crusts (up to 40 cm in size) were recovered with the TV-grab. Numerous tubular and spherical authigenic-diagenetic barite precipitates were observed in the underlying sediments (Fig. 9.2). All crusts are covered by a thin, dark-brown coat of iron and manganese hydroxides. Many crusts have such a coat on both sides, the outer and inner. This is evidence of long-time exposition of these crusts above the water-sediment boundary. With respect to morphology and mineral composition, these crusts are similar to crusts taken earlier in this area at station LV29-99 (Biebow et al., 2003). Core SO178-74-1 from this area is characterized by silty sand at the top and fine sand at the base. Barite crust similar to that of station SO178-65-2 occurs on the seafloor and overlaps the sediments. Diagenetic barites as spherolites, their aggregates, and tubular and branchy bodies are distributed beneath the barite crust in the upper part of the sediment sequence (0-40 cm).
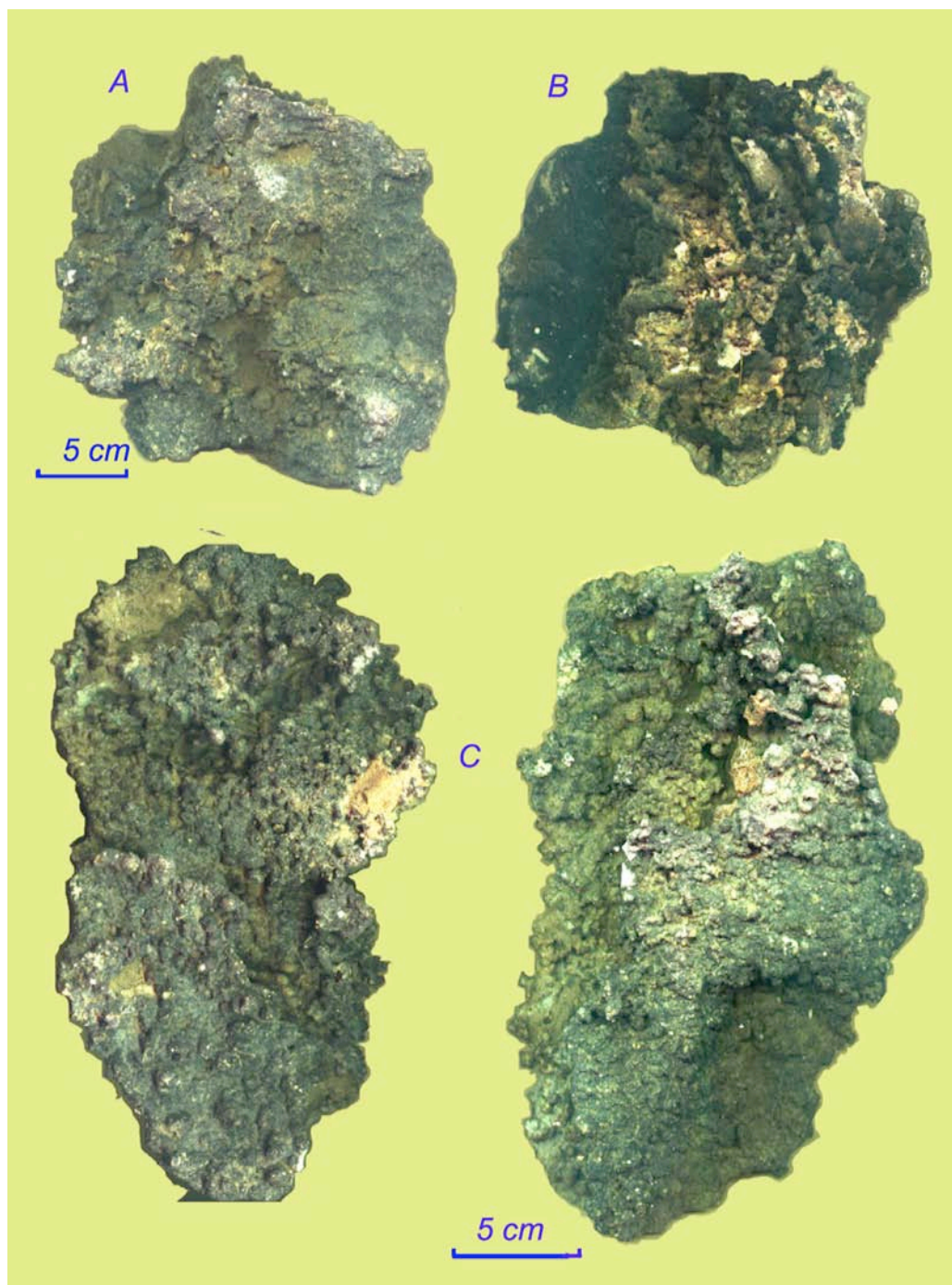
Fig. 9.2: *Barite crusts from station SO178-65-2, a – flat barite crust up to 1 cm thick, upper part, b – the same, lower part, c – flat barite crusts (up to 1.5 cm thick) with numerous tubercular swells consisting of ball-shaped aggregates of barite crystals.*

Buried fragments of barite crusts occur, too. No signs of carbonate mineralization and barite chimneys were observed in this area.

From morphology and internal structure we can conclude that the barite crusts formed at near-bottom sediment horizons close to the water-sediment boundary. They probably formed at sites of slow flux of fluid flow enriched in barium. Reconnaissance investigations with the OFOS were carried out on an isometric rise located in some kilometers distance south of the study area. This investigation showed signs of active cold seeps in the near-top part of this rise (colonies of alive and dead chemosymbiontic mollusk fauna). This allows to suggest with a high probability that carbonate and barite mineralization takes place within this area, as well.

101

10. PALEOCEANOLOGY AND SEDIMENTATION

Alexander Derkachev, Lester Lembke, Natalya Nikolaeva, Alexander Bosin, Martin Ziegler, Katharina Georgeleit and Nicole Biebow

10.1 Introduction

Based on previous results of the RV *Akademik Lavrentyev* and MV *Marshal Gelovany* expeditions LV27, LV28, LV29, and GE99, several important and still unsolved paleoceanographic problems in the Okhotsk Sea during the Late Quaternary should be clarified on the SO178-KOMEX cruise.

> Are short-term Holocene climatic variations as observed in several KOMEX gravity cores in or out of phase with the rapid climatic variations recorded in Greenland ice cores and in records from low-latitude monsoon reference sites (Cariaco Basin, Hulu and Dongge Cave, Oman)? What are the characteristic timescales on which changes and cycles in Holocene climate variability occur and what implication may be drawn from those for possible forcing factors? How do high- and low-latitude forcings interact on interdecadal to millennial-scale timescales (atmospheric vs. oceanic, PDO vs. ENSO), and how has the sedimentation area of the Amur River changed with changing sea level?
>
> Are the rapid climate changes during the last glacial in phase with the Dansgaard-Oeschger Events observed in the North Atlantic and on Greenland? Do the Okhotsk Sea sediments also show a warming during stadials as proposed in the North Pacific by Kiefer et al. (2001) and currently under controversal discussion (e.g. Rohling et al. 2003; Hendy et al., 2002; Hendy & Kennett, 2003)?
>
> How far does the methane degassing event observed in core GE99-24-2 reach laterally? What is the reason for such degassing events? What is the possible impact on atmospheric greenhouse gas variability and ocean carbonate chemistry? Do paleo-dissociation events also occur during the glacial Terminations and MIS3-4? How does methane degassing effect the geochemistry of stable isotopes and trace metals in formanifera?
>
> How strong is the intermediate water ventilation during the Glacial and what is its vertical distribution?
>
> How does the coupling between the North Pacific and the Okhotsk Sea intermediate water oceanography look like? How big has been the exchange between inflowing Pacific waters and outflowing Okhotsk Sea waters in the geological past? When do similar boundary conditions in the Okhotsk Sea and North Pacific exist, when different? How does this effect the faunal composition of the water masses?

These questions were objected to be solved during the SO178-KOMEX cruise by deploying long piston or kasten corers (up to 25 m) at distinct stations on the northern Kurile Basin slope, the Sakhalin Slope, and in the Derugin Basin.

10.2 Material and methods

During cruise SO178-KOMEX the following steps of sediment sampling and processing were performed:

10.2.1 Sampling approach

A TV-guided multicorer (TV-MUC) was used for sampling of surface sediments. The system is equipped with 7 plastic tubes (each 10 cm diameter) and an underwater telemetry unit (Aditec), 2 flood lights (Deep-Sea Power & Light) or Xenon-lamps (Oktopus) and 1 or 2 cameras (Deep-Sea Power & Light). The TV-MUC was successfully deployed on 22 stations with a total recovery of 115 liners with sediment.

An Ocean Instruments piston corer was used for sediment sampling. The system consists of steel tubes (575 cm length each, 144 mm diameter), a trigger weight, a releasing mechanism and is equipped with a coretop penetration weight of 2 tons. The system is used with rigid PVC-liner tubes for sediment recovery allowing permanent assessment of original sediment in the liner. During SO178-KOMEX cruise, core recovery with the piston corer added up to 153 m.

On the Northern Kurile Basin slope a 10 m long kasten corer was used, as well, in order to sample a big amount of sediment to get enough benthic foraminifera for isotope analyses. The kasten corer consists of steel boxes of 30*30 cm in diameter and 5 m length each. The coretop weight is 3 tons.

A Hydrostatic Corer (hydrocorer, HYC) 126 mm in diameter and 6 m in length was used in vent areas with authigenic minerals and for gas hydrate sampling. During SO178-KOMEX cruise the total core recovery with the Hydrostatic Corer added up to ca. 19 m. Aboard, a total of appr. 110 m of sediment cores was opened, described, measured, and sampled as described below.

1. Cores were cut into segments of 1m length and labeled following recommendations of Holler (1995).

2. Measurement of magnetic susceptibility: We used a Bartington loop sensor (MS2C) with a control unit (MS2) directly connected to a PC-laptop for data storage. The ring-shaped sensor generates a low-intensity magnetic field (f = 565 Hz), which is altered in its frequency by the sediment put into the loop depending on the amount of ferromagnetic minerals in the core section measured. Measurement interval was 1 cm.

3. Cores were split vertically and divided into work (W) and archive (A) halves. Sediment in the liner segments was leveled and covered with cling film.

4. The archive half was color-scanned with a handheld Minolta CM 507d Spectralphotometer in 1 cm spacing according to methods outlined in Biebow & Hütten (1999).

5. Measurements of humidity were carried out by a microwave meter (MWM-8) in direct contact with the sediment which is covered by cling wrap.

6. 5cc syringe samples were taken at 5 cm (10 cm) intervals for subsequent land-based analysis of physical properties (pp-samples). Syringes were closed with caps and sealed with Temflex tape. Sealed syringes were welded airtight in evacuated PE foil bags to minimize loss of pore water content. During the cruise, samples were stored refrigerated at 4-6°C.

7. Visual core descriptions were carried out on the archive halves of core segments. Classification of sedimentary texture and lithology generally follows modified recommendations of the ODP program (Sachs et al., 2000). Classification of randomly occurring dropstones is described by Powers (1982), grain sizes of the terrigenous fraction are classified as recommended by Shepard (1954).

8. Smear slides were taken from the cores in order to corroborate the onboard visual core descriptions. Initial analysis (estimates of grain size distribution and components) was carried out using the shipown Leitz polarization microscope with a 100 x - 500 x magnification according to grain size composition.

9. The working half of selected cores was sampled completely by 1 cm (2 cm for mineralogy) slices for direct processing in the home laboratories.

10.2.2 Sediment stratigraphy and age model

In order to get an initial sediment stratigraphy and preliminary age models of the cores, we used the following proxies: visual sediment description, semi-quantitative analysis of smear slides, color spectra, magnetic susceptibility, water content, and tephrochronology. For stratigraphic interpretation of these datasets we followed the multiproxy stratigraphy developed for Okhotsk Sea sediments based on oxygen isotope stratigraphy, AMS radiocarbon datings, sediment color and magnetic-susceptibility records, calcium carbonate/ opal content and tephrochronology (Gorbarenko et al., 1998; Biebow & Hütten, 1999; Biebow et al., 2000; Gorbarenko et al., 2002).

10.3 The sediments of the Kurile Basin and the Sakhalin Slope

In total, nine cores were raised from the western part of the Okhotsk Sea, most of them along a S-N transect at the Sakhalin continental margin. Due to our objectives outlined above, most core stations were set within intermediate water depths between 600 m and 1,300 m.

In the following, we try to establish preliminary age models for most of the cores that were object to onboard analyses. Details about the oceanographic settings, the general lithological features of sediments and tephra layers as well as a comprehensive overview of the different sedimentological and stratigraphic features in the Okhotsk Sea are given in preceding cruise reports of KOMEX expeditions (Biebow & Hütten, 1999; Biebow et al., 2000; Biebow et al., 2003) and a number of articles (e.g. Gorbarenko et al., 2002; Nürnberg & Tiedemann, in press)

In our setting, especially along the Sakhalin margin, where sedimentary settings with high accumulation rates during the Holocene and MIS 2-4 are to be expected, reliable lithostratigraphic markers are rather scarce; specifically we use the following tie points and characteristics for a preliminary age assessment:

> The very soft diatomaceous ooze sequence in the upper parts of the cores, known to build up around 8 ka and reaching its characteristic first maximum around 6 ka. Evidence is derived by smear slides and a significant change in the color b* and, to a lesser extent, lightness values. However, we are aware of the fact that this onset may be diachronous in some areas.

> Two horizons with pronounced maxima in carbonaceous microfossil content (foraminifera and coccoliths) occur at the glacial Terminations Ia and Ib. These productivity spikes last into the onset of the warming periods and are observed globally in a number of locations (NE Pacific, Japan Sea, Southern Ocean). Identification is accomplished by smear-slide analysis and, in some cases, by changes in the lightness values of the color series.

> A number of tephra layers may give independent age control points, specifically key layers like *K0* (8500 cal. yrs BP), *K2* (26 ka) or *Spfa-1* (ca. 35 ka). Provisional identification was achieved by microscopic analysis onboard. Details concerning identificaton and chemistry of the tephras are given in Kaiser (2001) and Gorbarenko et al. (2002).

> The onset of the Holocene with termination Ia and Ib usually causes a significant decrease in the magnetic susceptibility (MS) values due to decreased contents of ice-rafted debris (IRD), and cocomitant increases in fluvial (clay) terrigenous supply and primary producitivity.

> We use the regional stratigraphic terms known from Northern European locations as "Younger Dryas" and "Bølling-Allerød" sensu lato for convenience. This short cooling interval between the first Holocene warming period and the Termination Ib, causes

significant changes in MS values in the Okhotsk Sea, often matching other Northern Hemisphere oxygen isotope reference records.

MIS 2-4 usually displays considerably higher MS values than the Holocene, as well, a shift in color b* values is to be expected.
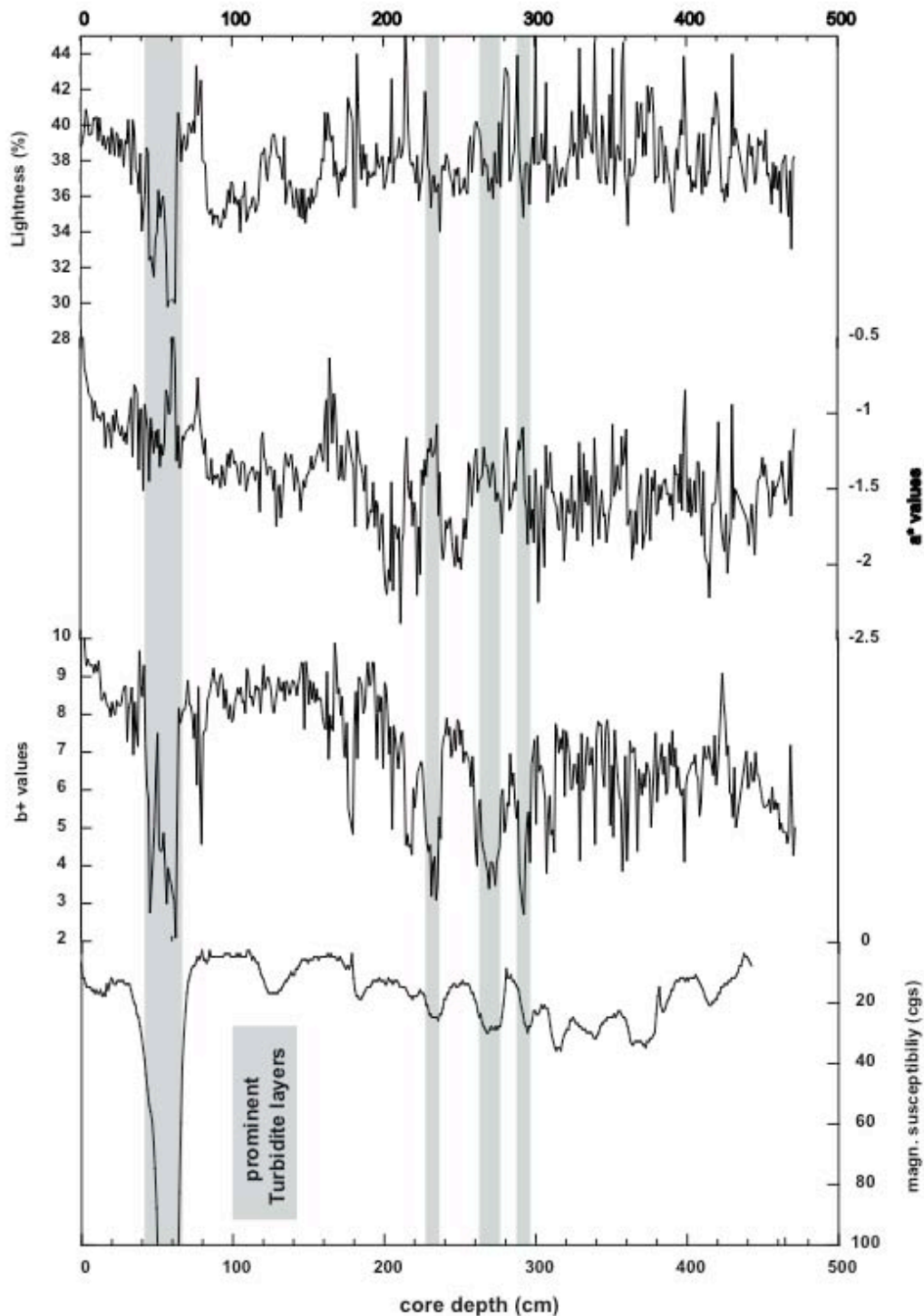
Fig. 10.1: *Piston core SO178-1-4 KL; color scanning and magnetic-susceptibility series. Panels from top to bottom: lightness reflectance (%), color a* (red-green) values, color b* (blue-yellow) values, magnetic-susceptibility record (cgs units, inverted). The gray-shaded areas indicate the presence of prominent turbidites.*
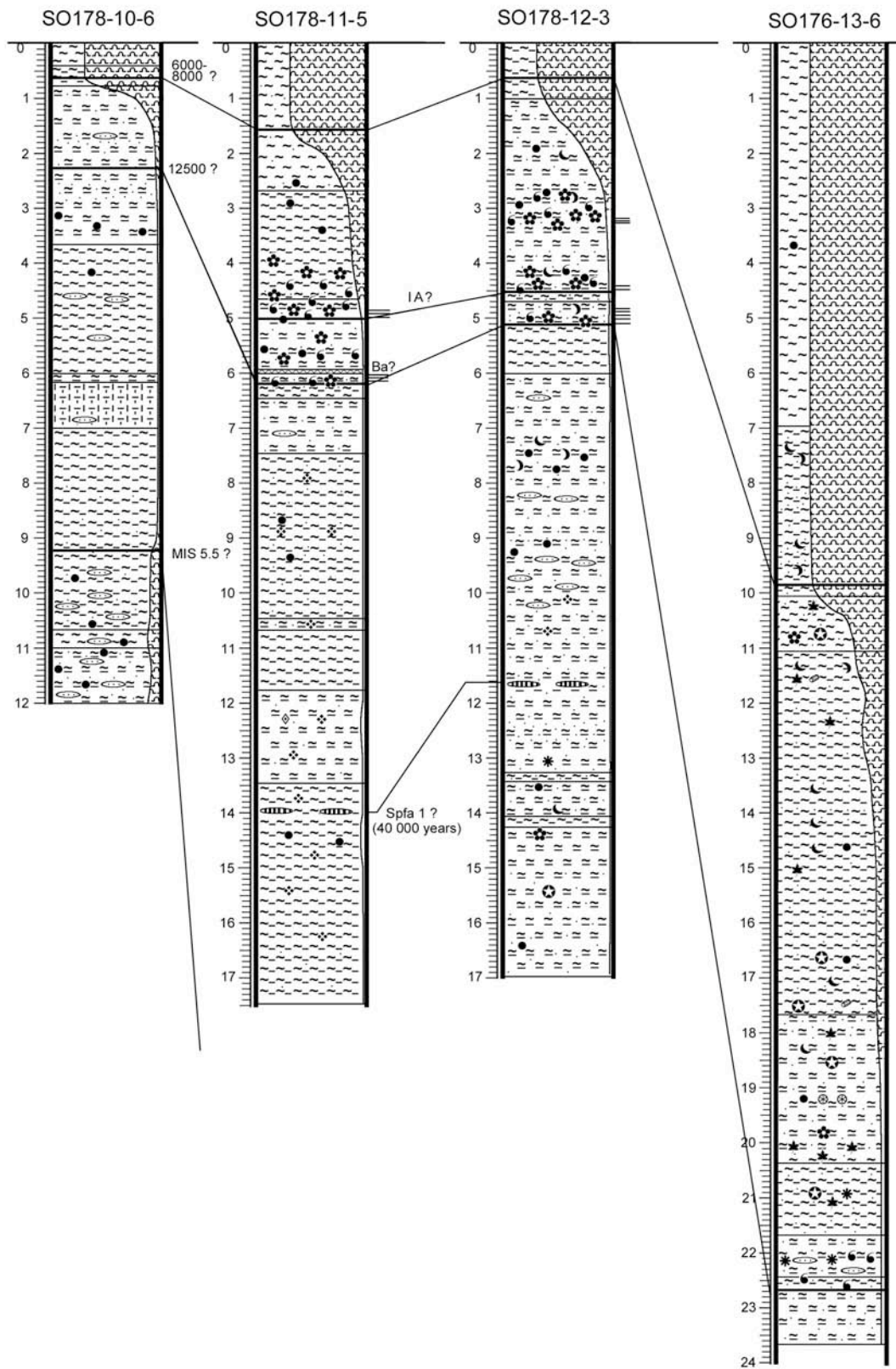
Fig. 10.2: *Lithostratigraphic comparison of piston cores SO178-10-6 SL, SO178-11-5 KL, SO178-12-3, and SO178-13-5 KL, lines between the series indicate correlation patterns as indicated by smear slide analysis and core descriptions. See legend of core descriptions (Appendix 6).*

10.3.1 SO178-1-4 SL (3,316 m water depth, 46°26.005' N, 146°32.994' E)

Core SO178-1-4 SL was taken in the western part of the deep Kurile Basin. The sediment section we recovered mainly consists of alternating homogeneous terrigenous clay and numerous turbidity layers with variable thickness. The more prominent turbidites leave distinct marks in the susceptibility and color records of this core. They are indicated by gray bars in Fig. 10.1. Smaller layers also leave their imprint in our scanning series, a fact that makes establishing a reliable preliminary age model almost impossible. By semi-quantitative relation of biosiliceous to terrigenous material, we conclude the thickness of the Holocene not to exceed 1 m. Significant amounts of cryptocrystalline calcite occur at 119 and 183 cm. In the Okhotsk Sea, these calcitic mineralizations are connected to the onset of the last deglaciaction.

10.3.2 SO178-3-4 KAL (1,602 m water depth, 48°11.833` N, 146°08.743` E)

Core SO178-3-4 KAL was taken at the upper northwestern slope of the Kurile Basin. The sediment section at this site consists of greenish-gray sediments with abundant sandy particles and dropstones. Units displaying these lithological features belong to Pleistocene deposits of the Okhotsk Sea. The increase in the relative amount of carbonate fragments and coccoliths in the upper part of the core indicates that the thickness of the Holocene does not exceed 30 cm. Tephra layer *K2* as a regional tephrochronological marker horizon (age: 26 ka according to Gorbarenko et al., 2002) was identified at 153 cm core depth and supports our lithostratigraphic results. Besides, further tephra lenses were discovered at 190 cm and at 678 cm. Based on our preliminary stratigraphy, it is reasonable to assume that the horizon at 190 cm core depth consists of tephra *Spfa-1* (age about 40,000 years, Gorbarenko et al., 2002). The increased content of diatom fragments with foraminiferal fragments and rare coccolithes at 710-750 cm core depth lets us attribute the sediments of this lower part of the core to MIS 5. Due to the nature of the kasten corer, no scanning was applied to the core to further support our notions.

10.3.3 SO178-10-5 KL/10-6 SL (613 m water depth, 49°44.878 N, 146°00.476 E),
          SO178-11-5 KL (1182 m water depth, 51°14.000 N, 146°12.999 E),
          SO178-12-3 KL (1211 m water depth, 51°36.322 N, 145°26.142 E)

The following suite of piston cores falls along the S-N transect at the continental margin of E Sakhalin. Thus, rather similar sections of Holocene-Late Pleistocene age were recovered in these cores, especially at stations SO178-11-5 KL and SO178-12-3 KL. Features repeat each other in remarkable detail in the whole core section. According to the onset of diatom oozes and carbonate layers, the thicknesses of Holocene sections generally increase to the north. They vary between 200-220 cm (SO178-10-6 KL), and up to 500 cm (SO178-12-3 KL) and 620 cm (SO178-11-5 KL) (see Fig. 10.2 for comparison).

In core SO179-10-5 KL, lithological evidence points to an onset of the Holocene around 250 cm core depth. Taking the logged MS values, however, we could also well establish the Termination I at approximately 100-120 cm core depth in accordance with a significant increase of MS downcore and an observed increase in sand/silt content (Fig. 10.3). The last 6-8 ka diatom-rich sequence would then be comprised in the upper 40-60 cm only which would be also in accordance with the color b* value curve. This shows a significant shift around 120 cm towards Holocene values (which is matched also in the other color records) and a second, marked increase around 60 cm core depth. However, with the currently available datasets, this offset remains unsolved and has to be cleared by further onshore studies (see light-gray and also hatched area in Fig. 10.3). In any case, the sediments of the lower part of the core (1,000-1,500 cm) are enriched in diatomic fragments, and they may thus belong to MIS 5.
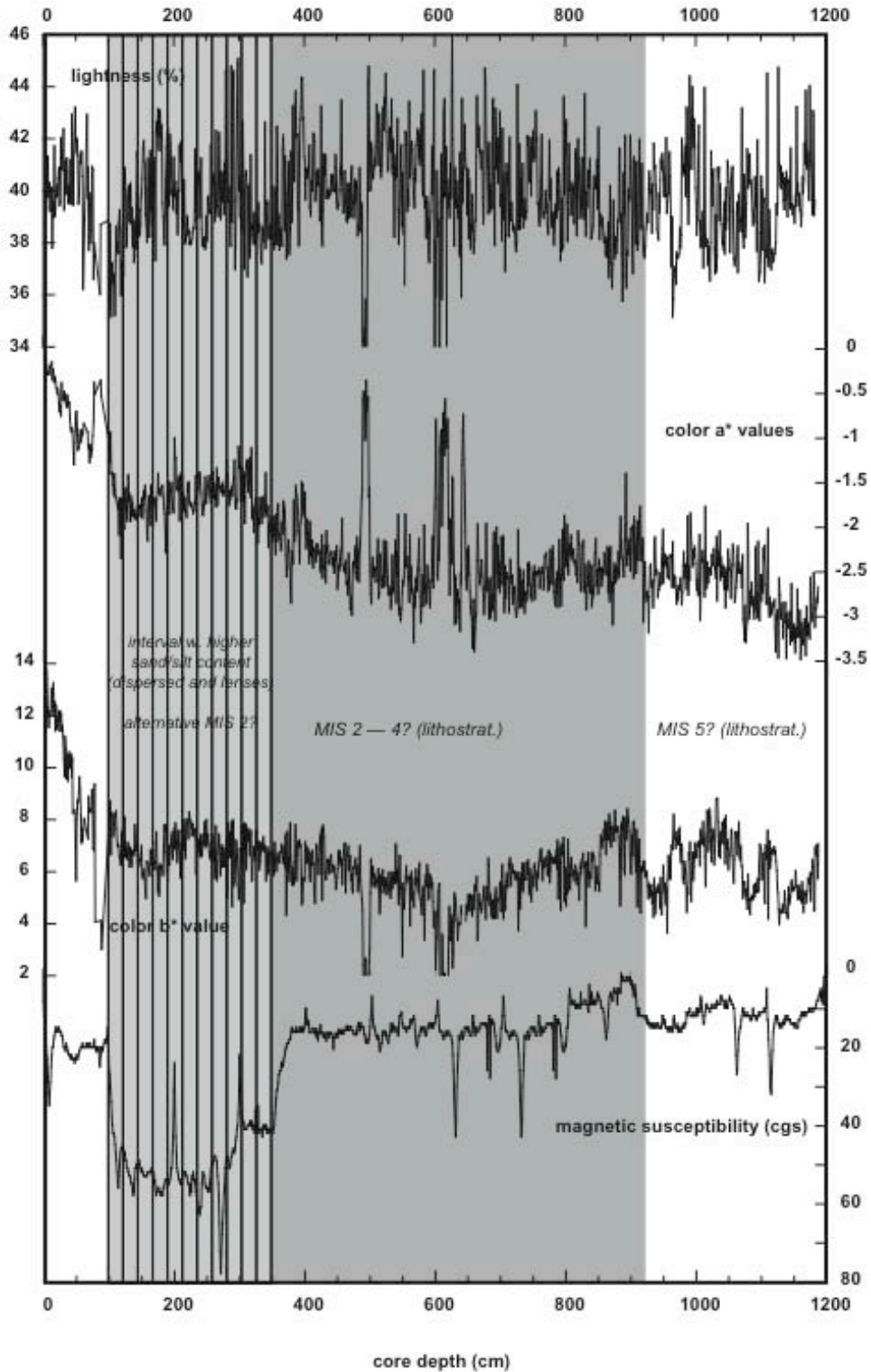
Fig. 10.3: *Piston core SO178-10-6 SL; color scanning and magnetic-susceptibility series. Panels from top to bottom: lightness reflectance (%), color a* (red-green) values, color b* (blue-yellow) values, magnetic-susceptibility record (cgs units, inverted). Vertically hatched and light-gray shading show MIS 2 as supposed by scanning/ logging series; dark-gray shading indicates the MIS 2-4 as proposed by lithostratigraphy.*
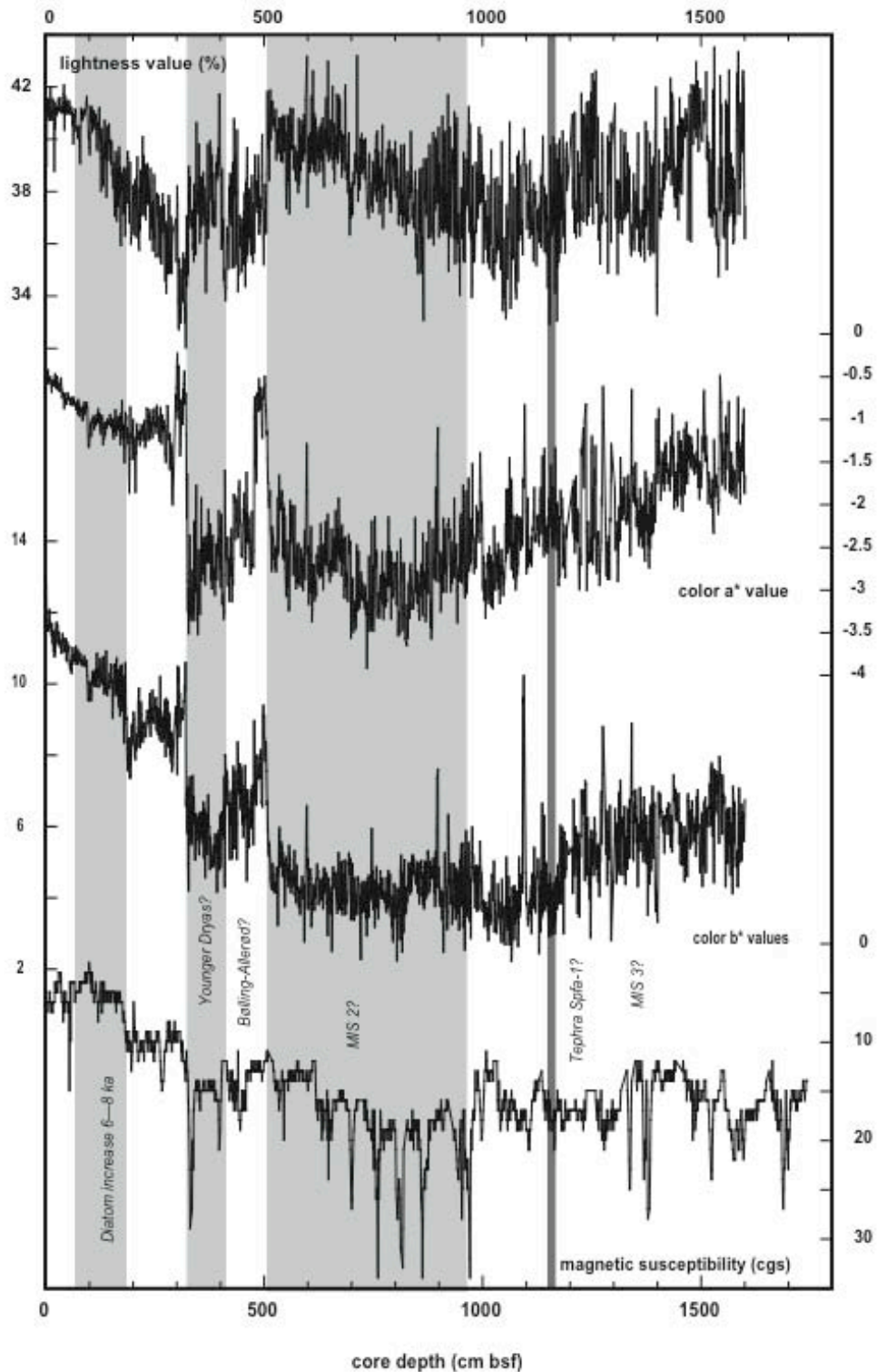
Fig. 10.4: *Piston core SO178-12-3 KL; color scanning and magnetic-susceptibility series. Panels from top to bottom: lightness reflectance (%), color a* (red-green) values, color b* (blue-yellow) values, magnetic-susceptibility record (cgs units, inverted). Lighter gray shading marks (from left to right): the increase of diatom content (6-8 ka), the Younger Dryas-like event, the supposed MIS 2; the darker gray shading denotes the position of presumed tephra layer Spfa-1.*

In general, higher sedimentation rates are characteristic for the two northerly located cores. Diatom ooze sequences are recognized at nearly the same core depths (see Fig. 10.2) and correspond to increases in color b* and lightness values between 90 and 180 cm, placing the upper 2 m in the Middle-Late Holocene. Highly significant carbonate-rich horizons could be identified in smear slides of cores SO178-11-5 KL (420-490 cm, 570-610 cm) and SO178-12-3 (320-330 cm, 450-510 cm). These results agree well with the set of MS and color-scanning values. There, the onset of the Younger Dryas is indicated in all scanning and MS series around 410/420 cm and the corresponding Termination Ib seems to start around 320 cm core depth. A presumptive Bølling-Allerød period is indicated between 420 cm and 510 cm in color a* and b* values (Fig. 10.4). Tephra lenses occur in both cores, at 1,392 cm (SO178-11-5) and at 1,166 cm (SO178-12-3). They may be provisionally identified as tephra *Spfa-1*. Slight shifts in the lithology, MS values and the location of the tephra let us assume a MIS 2-3 boundary around 980 cm sediment depth in core SO178-12-3 KL.

10.3.4 SO178-13-6 KL (713 m water depth, 52°43.881' N, 144°42.647' E)

The sediment of core SO178-13-6 differs from the ones described above, which are more southerly located. At this site, we were likely able to recover a sediment section of predominantly Holocene age. The sequence of clayey diatom ooze/ diatomaceous clay extends down to approximately 1,020 cm. Below, the amount of diatoms gradually decreases down to 1-2% (Fig. 10.1 and Appendix 6). Within these parts of the core, foraminiferal and plant fragments are present as a minor component. Taking evidence from the smear slide analysis, the boundary of Termination Ia and Ib may be set at 1,980 cm and 2,210-2,240 cm core depth, respectively, due to an increase in the amount of both foraminiferal fragments and coccoliths. Using these data, we would infer the end of MIS 2 at about 2,220 cm.

However, the record of magnetic susceptibility (MS) and some alternative features of lithology (small sand lenses and carbonaceous concretions) suggest a different placement of the Termination Ib at a depth of approximately 1,650-1,700 cm. There, we observe a strong gradient towards higher values downcore. The interval between 1,700 cm and 1,820/1,870 cm would then resemble the Younger Dryas period (dark shaded interval, Fig. 10.5) with higher MS values caused by enhanced transport of IRD to the site during this cold period. The section between 1,870 cm and 2,210 cm could represent the analogue to the Bølling–Allerød interval. Future investigations including AMS ^{14}C datings on planktic foraminifera from critical depth intervals will help to resolve this present discrepancies. Nevertheless, we agree on the positioning of Termination Ia around 2,160-2,240 cm core depth based on MS, color scanning and smear slides/ descriptive results. In any case, the complete core seemingly displays a Holocene section of about 20 m thickness.

The very large rate of sedimentation within this site is connected not only with high bioproductivity, but also with the considerable Amur River discharge and the associated delivery of large amounts of fine-fraction terrigenous matter. The high content of organic detritus in the sediments confirms this assertion. Intensive diagenetic conversion took place in the core which is due to an increased content of organic matter. Numerous spots and lenses of hydrotroilite and soft precipitates of cryptocrystalline carbonate aggregates (mainly aragonite) are characteristic for the entire lower part of the core. We also found a glendonite concretion (pseudomorph on ikaite) in the lower part at 2,030 cm depth, indicating that this location likely was an active gas-hydrate/ seep area in the past.

10.3.5 Northeastern part of the Derugin Basin

The isolated isometric depression with water depths of about 1,700 m is located at the north-eastern rim of the Derugin Basin northwards from the Barite Mound area. Core SO178-78-1 KL was deployed within the central, deepest part of this isolated basin. The total core length
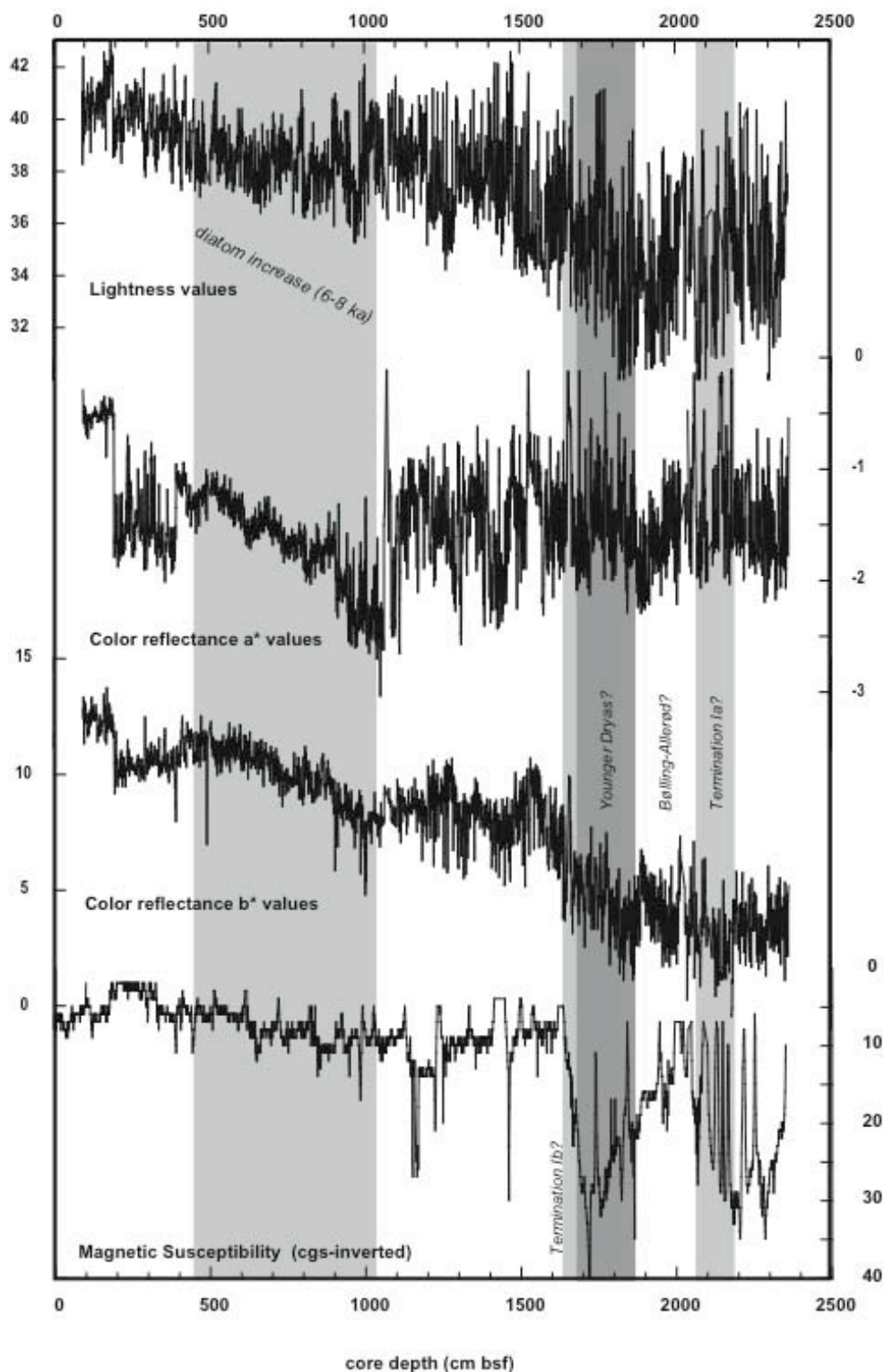
Fig. 10.5: *Piston core SO178-13-5 KL; color scanning and magnetic-susceptibility series. Panels from top to bottom: lightness reflectance (%), color a* (red-green) values, color b* (blue-yellow) values, magnetic-susceptibility record (cgs units, inverted). The light-gray shadings show (from left to the right): the increase of diatom content (6-8 ka), the Terminations Ia and Ib; the darker gray shading indicates the presumed Younger Dryas-like event.*

recovered sums up to 1,825 cm. This core was taken to check the hypothesis that a hydrosulphuric contamination zone existed periodically during the Late Pleistocene within the deeper parts of the Derugin Basin. Support for this assumption first came from hydrotroilitic black sediments in the lower parts of cores LV29-103-2/3 and LV29-104-2/3 that were recovered during cruise LV29 (Biebow et al., 2003). Further shore-based studies of the mineral composition of these sediments let us conclude that they could have formed only within a basin with periodic hydrosulphuric contamination of the near-bottom waters (Derkachev et al., 2003; Nikolaeva et al., 2004). To confirm this supposition and to estimate the scale of the spatial distribution of this event, core SO178-78-1 KL was taken. We recovered well identifiable lithostratigraphic sequences. Based on our lithostratigraphic description, the upper part of the core consists of sediments of Holocene age with a thickness of about 140 cm. Clayey diatom oozes - diatomaceous clay lets us place the Middle to Late Holocene section in the upper 65-70 cm of the core, with a thick oxidized layer (down to 48 cm) and an age of approximately 8-6 kyr. The oxidized horizon is heterogeneous in its color. Above 10 cm core depth, it consists of dark-brown sediments, below grayish lenses occur. Terminations Ia and Ib are attributed to characteristic layers at core depths of 100-105 cm and 122-132 cm, respectively, due to an increased content of foraminifera and coccoliths. These two horizons are divided by a lighter gray layer with mostly terrigenous components. Other lenses of light-gray color occurring within the Holocene part of the section likely consist of Mn-calcite.

The horizon of gray and greenish-gray clayey silt with both rare lenses of authigenic calcite and consolidated diagenetic interlayers occurs below Holocene sediments from 256 cm sediment depth downcore. Below this core depth, the clayey silt changes into a thick (up to 1,150 cm) sequence of homogeneous, highly dispersive clays with a rare occurrence of plant fragments and pyritic sticks (while at some distinct horizons, the amount of pyrite is considerable). This thick clay sequence differs from the other sediments in textural and structural characteristics. It is, however, lithologically similar to black strata as previously described at stations LV29-103 and LV29-104 in the deepest part of the Derugin Basin (Biebow et al., 2003). The sediments display varying colors: brownish-gray clays with a thickness of about 70 cm gradually change into gray and dark-gray clays with a thickness of about 420 cm. Below, this unit is replaced by black clayey sediments (appr. 420 cm thickness) with hydrotroilite streaks and spots, which change to dark-gray clays (approximately 200 cm thickness).

At the base of this sequence, the typical thin-bedded texture of distal turbidites appears. The boundary to the underlying sediments is very sharp with a probable small erosional discordance. The underlying sediments consist of dense and very dense clayey silt and silty clay with occasional sand particles and very rare dropstones. The sediments have a grayish-green color with lenses of olive-green. These lenses have a branchy irregular shape.

Based upon our lithostratigraphic framework, we assume the thick sequence of homogeneous clays to be of Late Pleistocene age, presumably towards the end of the Last Glacial Maximum, when the global sealevel was 100-120 m lower. We assume that within this period, a large portion of the Amur River suspension load was transported rather directly into the Derugin Basin (e.g. Staretsky Trough), where the accumulation of fine sedimentary material - enriched in organic matter - took place in its deepest parts. We presume that the discharge of Amur fresh waters in combination with enhanced sea ice cover may have led to a regionally increased water stratification. A regional halocline may have formed under these conditions, hindering intermediate waters from mixing in isolated parts of the Derugin Basin. The combination of these factors eventually lead to the stagnation of near-bottom waters and to an appearance of conditions with hydrosulphuric contamination features as described above.

11. SAMPLING FOR ISOTOPE ANALYSES OF BIOGENIC SILICA

Andrea Abelmann

Stable isotopes (δ^{30}Si, δ^{18}O, δ^{15}N, δ^{13}C) of biogene silica (BSi) are a new tool successfully used to reconstruct changes in environmental conditions, such as ice volume, surface salinity, nutrient concentration, and primary production. This method significantly contributes to the reconstruction of past ecological and climatic conditions in areas with silicate-rich sediments. It is a suitable method to evaluate the influence of the processes going on in this region on the climate. The Okhotsk Sea is one of the most productive areas of the World Ocean and characterized by high biogenic silica accumulation. It is planned to measure stable isotopes on biogenic silica (radiolarians and diatoms) from plankton and sediment samples in order to precisely describe the structures and properties of water masses in the Okhotsk Sea during the past. The Okhotsk Sea today is characterized by a high mesopelagic zooplankton activity. Comprehensive radiolarian investigations in the water column of the Okhotsk Sea accomplished during KOMEX I and II have shown that the main radiolarian standing stock in the Okhotsk Sea occurs at the mesopelagic depth between 200 and 600 m. Thus, the Okhotsk Sea represents a unique area to obtain information about the isotopic composition of mesopelagic radiolarians. In addition, we collected diatoms from the upper sea surface to compare the mesopelagic information with that of the sea surface.

12.1 Water column sampling

Plankton samples were taken from different water layers on a profile from the southern Sakhalin Slope to its northern end, an area characterized by high productivity. In addition, the water column was sampled in the southern part of the Kashevarov Trough where the productivity is increased. Water samples for isotopic investigations were taken from the same water depth as the plankton samples to correlate the plankton data with the isotope composition of the water from the corresponding layers. At each station on the NS transect along the Sakhalin Slope, we ran the multinet three times to receive a higher amount of siliceous microorganisms. An exception is station SO178-14 where the multinet was run only twice because of bad weather conditions. Generally, we sampled five depth intervals (Fig. 11.1). We took three tows from the mesopelagic layer (600 to 200 m) and one from the dichothermal layer (200 - 50 m) and the upper surface (50 to 0 m) each in combination with a CTD survey at each station. Depth intervals of each station are given in Appendix 7. Samples were split into three fractions (>500 μm, 40 – 500 μm, and <40 μm) and deep-freezed.

We used an opening/closing net (Type MPS 92 B, "Hydrobios" Kiel, Germany) which consists of five nets fixed to a steel frame, each 2.5 m long, with a mesh size of 55 μm. This frame has a 50 x 50 cm large opening and is equipped with a motor and an electronic system for opening and closing the nets as well as a depth-measuring device. Both are connected with the board instrument, which displays the actual depth and which allows to open and to close the nets in specific water depths during heaving or slacking of the net. Each net ends with a sample beaker equipped with a net window of 41 μm mesh size.

The nets were towed vertically at low speed of 0.5 m s^{-1} (slacking) / 0.3 m s^{-1} (heaving) at all stations to avoid clogging of the net. The volume of filtered water was measured with calibrated flowmeters which were installed at the inside of the mouth of each net. Thus, we could record the water passing through each net for each depth interval. The flowmeter measurement allows to quantify the biological record, but also to recognize if the net became clogged in areas of high productivity.
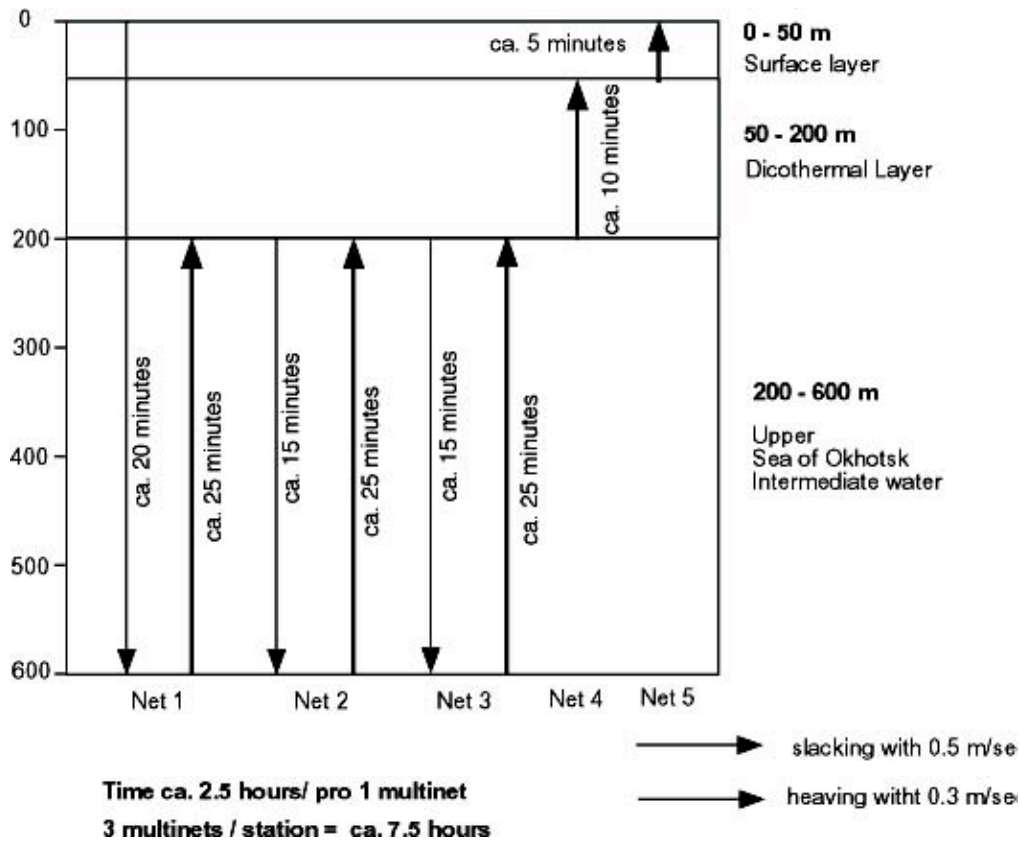
Fig. 11.1: *Schematic presentation of multinet deployment for water column sampling with respect to siliceous plankton.*

The difference between the flowmeter values (the flowmeter rotation values are proportional to the water volume flown through the net) after (F = final value) and before (S = start value) deployment multiplied by the opening diameter of the net frame (0.25 m^2) (A) and the impeller gradient (0.3 m) (P) defines the water volume (V) in m^3 flown through each net (Appendix 7).

$$V\ [m^3] = (F-S) \times P \times A$$
$$= (F-S) \times 0.3 \times 0.25$$
$$= (F-S) \times 0.75$$

11.2 Sediment sampling

For the enlargement of our surface sediment data set which we need as reference for paleoceanographic investigations, surface sediments were taken from various sites with emphasis on the Sakhalin Slope, Derugin Basin, Kashevarov Trough, and the Kurile Basin. The sampling was done with a multicorer (TV-MUC) which provides undisturbed sediment surfaces. For surface sediment investigations, the upper 0-1 cm were sampled. At core stations, 1 cm slices were taken in 1 or 5 cm intervals to document the youngest sediment record which may lack in the record of the gravity and piston cores.

Piston and gravity cores of a length of up to 24 m were taken at the high productive Sakhalin Slope and from the deep Kurile Basin. It is planned to measure BSi stable isotopes on selected cores from the Sakhalin Slope and the deep Kurile Basin to get better knowledge about the past productivity regime, water mass structure and water mass exchange between the North Pacific and the Okhotsk Sea.

12. PETROLOGY AND VOLCANOLOGY

Reinhard Werner, Igor Tararin, and Boris Baranov

12.1 Introduction and objectives

Several volcanic structures in the Okhotsk Sea are located at an anomalous distance from the Kurile Island Arc. Bathymetric mapping and extensive sampling of such volcanoes in the Kurile Basin on former KOMEX cruises (LV27, LV28, GE99, LV29) and subsequent lab analyses of the dredged rocks provided new information on the structure and geodynamic evolution of the Kurile Basin by reconstruction of volcanic, magmatic and tectonic processes and contributions - in cooperation with other KOMEX II working groups - to a model for the evolution of marginal basins (e.g., Baranov et al., 2002a; Tararin et al., 2003).

The dredging program of SO178-KOMEX focussed on the northern slope of the Kurile Basin and its continental rise (Working area I) where bathymetric investigations and geophysical studies, mainly conducted on the most recent KOMEX cruise LV29, proved a very rough basement morphology, thin sediment cover, and indicated the exposure of volcanic (?) edifices (see Chapter 2). Tectonic and magmatic activity in this area may be related to the Sakura Ridge in the central Kurile Basin being interpreted as NNW-striking paleo-spreading ridge (e.g., Baranov et al., 2002b). Detailed mapping using the shipboard SIMRAD EM120 multi-beam echosounding system along with volcanological, mineralogical, geochemical, and geochronological analyses of rocks dredged at volcanic outcrops in this area should constrain

   the paleo-environment of volcanic structures at time of their activity (e.g., subaerial vs. shallow water vs. deep water);

   the age and evolution of the volcanoes (e.g., single or multiple eruption phases);

   the origin and magmatic evolution of the volcanoes and their tectonic setting (situated on continental or oceanic crust; mid-ocean-ridge vs. back-arc vs. arc signatures; etc.).

Combined with geophysical and paleoceanological data, these data should provide further insights into the opening history and evolution of the Kurile Basin.

Apart from the dredging program on the northern slope of the Kurile Basin, several structures in the Kashevarov Trough (Working area IV) should be surveyed and dredged where applicable. The Kashevarov Trough represents a graben system (rift system) which generally elongates in southeastern direction. On seismic lines obtained on former Russian cruises (see Chapter 2), at least one small, less than 100 m high structure appears which resembles a volcanic edifice. Such volcanoes (if existent) could be connected with rifting processes and, therefore, may provide important information on the geodynamic evolution of the Kashevarov Trough. Detailed multi-beam mapping and sampling of these structures aimed at verifying if they are volcanoes and, if so, to constrain their magma sources as well as volcanic and magmatic evolution. Further multi-beam surveys in the Kashevarov Trough were planned in order to constrain the extent of (possible) volcanism in this area and to select additional sites for sampling.

12.2 Methods

Rock sampling was carried out during SO178-KOMEX using rectangular chain bag dredges. Chain bag dredges are similar to large buckets with a chain bag attached to their bottom and steel teeth at their openings which are dragged along the ocean floor by the ship´s winch.

12.2.1 Selection of dredge sites

General station areas were chosen based on bathymetric data and seismic reflection profiles gained on former cruises (see above). The final selection of dredge sites was critically dependent on detailed SIMRAD EM120 surveys carried out at each station before dredging (e.g., Figs. 12.1 - 12.4). Final positioning of the vessel over the dredge sites was done using GPS and the bathymetric data gained on the surveys, and allowing for weather and drift conditions. Dredge tracks at the seamounts were usually located - depending on the morphology of the structures - on steep slopes, at scarps or at small cones on the flanks of the seamounts. This was done (1) to avoid areas of thick sediment cover and (2) to receive rocks as young and accordingly as fresh as possible.

Taking into account the widespread ice-rafted debris in the Okhotsk Sea, detailed analysis of the rocks recovered by dredging was carried out to identify in-situ rock fragments. The criteria used for distinction include but are not restricted to (1) shape of the fragments (angular vs. well-rounded), (2) existence of fresh surfaces formed by tearing away from the bedrock outcrops, and (3) homogeneity of the dredged material.

12.2.2 Shipboard procedure

Once onboard, a selection of the rocks was cleaned and, if necessary, cut using a rock saw. They were then examined with a hand lens and grouped according to their lithologies and degree of marine weathering. The immediate aim was to determine whether in-situ material being suitable for geochemistry and age dating had been recovered. Suitable samples have an unweathered and unaltered groundmass, empty vesicles, glassy rims (ideally), and any phenocrysts are fresh. If suitable in-situ samples were present, the ship moved to the next station. If they were not, then the importance of obtaining samples from the station was weighed against the available time. Additional dredges nearby and at the same station were sometimes possible.

Fresh blocks of representative samples were cut for thin section and microprobe preparation, geochemistry and further processed to remove manganese etc. Each of these sub-samples, together with any remaining bulk sample, was described, labeled, and finally sealed in plastic bags for transportation to IFM-GEOMAR or cooperating institutions. Manganese crusts, biological material, and sediments from the sediment traps installed in the dredges were also sampled for cooperating working groups.

12.2.3 Land-based analyses

Magmatic rocks sampled from the ocean floor will be analyzed with different methods in several geochemical laboratories. The ages of whole rocks and minerals will be determined by $^{40}Ar/^{39}Ar$ laser dating. Major element geochemistry will constrain magma chamber processes within the crust and also yield information on the average depth of melting, temperature and source composition to a first approximation. Further analytical effort will concentrate on methods that constrain deep-seated mantle processes. For example, trace element data help to define the degree of mantle melting and to characterize the chemical composition of the source. Radiogenic isotopic ratios such as $^{87}Sr/^{86}Sr$, $^{143}Nd/^{144}Nd$, $^{206}Pb/^{204}Pb$, $^{207}Pb/^{204}Pb$, and $^{208}Pb/^{204}Pb$ are independent of the melting process and reflect the long-term evolution of a source region and thus serve as tracers to identify mantle and recycled-crust sources. Additionally, morphological studies and volcanological analyses of the dredged rocks will be used to constrain eruption processes, eruption environment and evolution of the volcanoes. Through integration of the various geochemical parameters, the morphological and volcanological data, and the age data, the origin and evolution of the sampled structures can be reconstructed.

12.3 Results

This section gives background information and short summaries of the structures sampled by dredging and/or mapped and summarizes the results of sampling and mapping. Refer to Appendix 1 (SO178-KOMEX station list) for latitude, longitude and depth of dredge sites. Refer to bathymetric maps of the dredge sites generated by the Simrad swath mapping system (Figs. 12.1 - 12.4). All maps presented in this chapter are created by M. Magiulli and M. Grossmann (RF Forschungsschiffahrt GmbH) aboard RV SONNE. Distances between seamounts are given between the seamount tops and are approximate only; dimensions and heights are preliminary and are included only to give a rough idea of seamount dimensions.
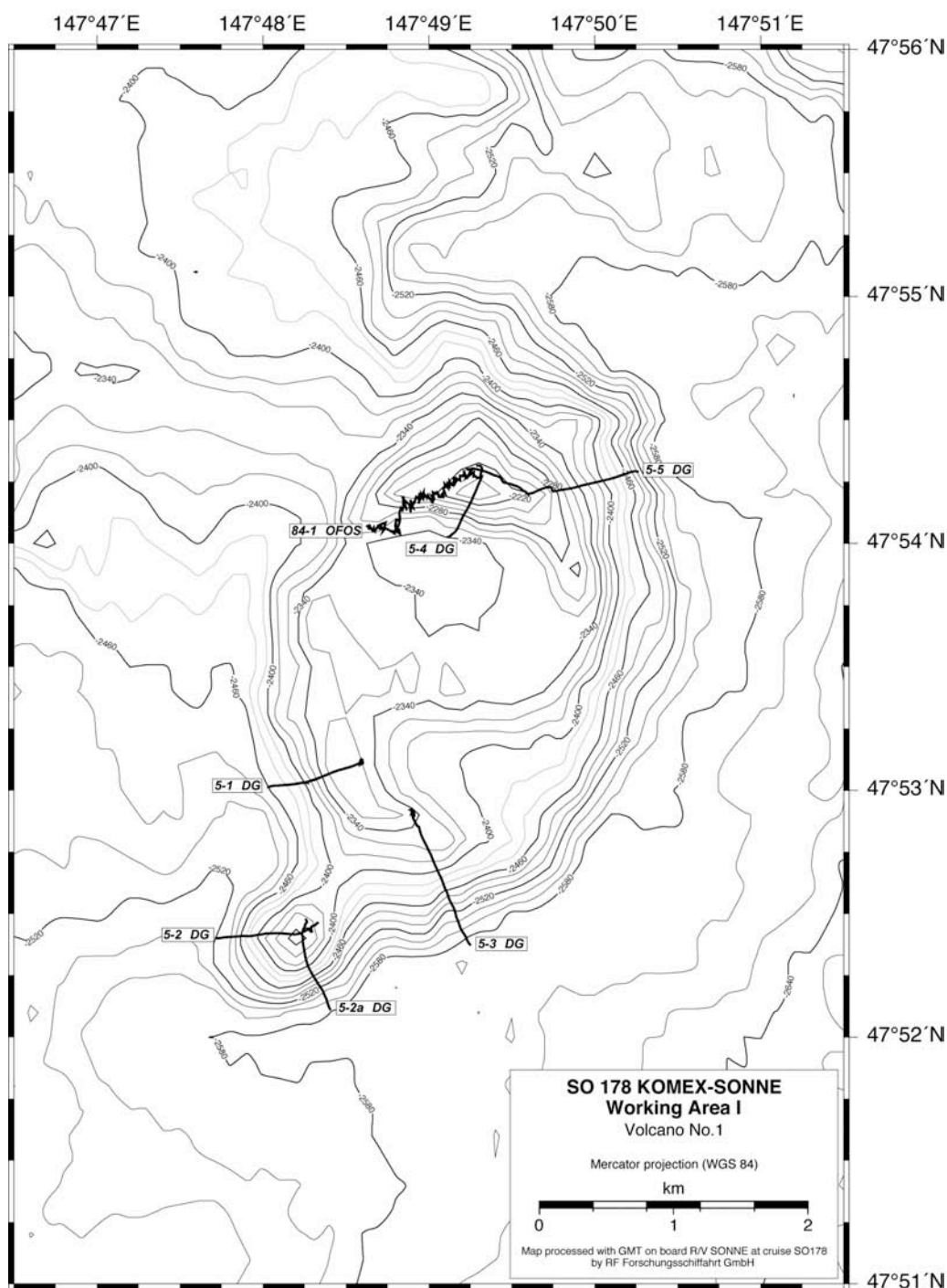

Fig. 12.1: *Bathymetric map of Volcano No. 1 including locations of dredge tracks SO178-5-1 DG to –5 DG and OFOS track SO178-84-1. Contour interval is 20 m.*

12.3.1 Working area I (Northern slope of the Kurile Basin)

Simrad surveys of selected areas on the northern slope of the Kurile Basin revealed four volcanic edifices or small volcanic complexes (see Chapter 2). During SO178-KOMEX, informal working names were assigned to these un-named seamounts ("Volcano No. 1-4", "Sonne Chain"). Dredging of these volcanic structures proved to be rather difficult due to thick sediment cover, encrustation of the volcanic rocks, and lack of steep slopes. Out of the 14 dredges carried out in Working area I, 2 contained igneous rocks (lavas excluding dropstones), 2 volcaniclastic (?) rocks, 7 Mn-Fe oxides, and 12 soft sediments.

Volcano No. 1 is located at ~2,500 m water depth on the lower slope of the Kurile Basin (see Fig. 2.2). It is a ~250 m high, oval-shaped volcanic edifice being ~4.5 x 2.5 km in basal dimensions and elongated in N-S direction (Fig. 12.1). A small conical hill to the southwest represents most likely a satellite cone. The main edifice of the volcano shows some kind of plateau- or crater-like structure on its central part. A prominent top with a steep southern flank marks the northern edge of the volcano, and a deep valley which opens to the east cuts its southern part (Fig. 12.1). This volcanic structure may therefore represent the relics of an old volcanic cone which collapsed due to explosive (?) volcanic activity or tectonic processes. Out of 6 dredge hauls carried out at Volcano No. 1 only one dredge across the steep southern flank of the prominent northern top (SO178-5-4) yielded volcanic rocks. Those comprise heavily altered, fine-grained volcaniclastic rocks covered by up to 4 cm thick manganese crusts. Since mapping and dredging did not provide clear information on the nature and composition of this volcano, OFOS track SO178-84-1 was carried out on the southern flank of the northern top (Fig. 12.1). The OFOS survey revealed a rough morphology and large outcrops of lithified, partly layered volcaniclastic (?) sediments being cut by small canyons on the flank and large sediment blocks (m-scale) at its base. Lavas were not visible along the OFOS track. Taken together, the results of multi-beam mapping, dredging and OFOS survey suggest that the top area of Volcano No. 1 is at least mainly formed of layered, partly collapsed volcaniclastic deposits. This observation leads to the very preliminary working hypothesis that the widespread layered volcaniclastic deposits could indicate explosive hydroclastic eruptions at water depths being much shallower than the present position of Volcano No. 1.

Volcanoes No. 2, 3, and 4, as well as some smaller volcanoes in between, form a 27 km long, SSW-NNE-trending chain (*Sonne Chain*) of volcanic edifices on the upper slope of the Kurile Basin (Fig. 2.2). The Sonne Chain is most likely related to a NNE-SSW-striking fault. A prominent feature of all volcanoes of the Sonne Chain are up to 100 m deep moats around each volcano which may be formed by bottom currents (see Chapter 2). Another common feature of the Sonne Chain volcanoes (and also of Volcano No. 1) seems to be the appearance of small volcanic cones at the southern or southwestern edge of the individual volcanic edifices (see above and below and Figs. 12.1 - 12.3).

Volcano No. 2, located ~33 km north of Volcano No. 1, represents the southernmost volcano of the Sonne Chain and forms a ~300 m high and ~6.5 km long ridge-like structure which strikes similar to the Sonne Chain in NE-SW direction (~45°, Fig. 12.2). At the southwestern end of this ridge a small volcanic cone appears. A steep scarp striking parallel to the axis of Volcano No. 2 cuts the eastern side of the volcano. This scarp proved to be the best position for dredging along the entire Sonne Chain. Two of four dredge hauls carried out at the scarp yielded angular boulders of volcanic rocks. Dredge SO178-7-1 contained up to 25 cm large fragments of porphyritic basalt with a fine-grained or microcrystalline matrix. Phenocrysts (up to 5-7%) are plagioclase (up to 2-3 mm), clinopyroxene, and olivine (up to 0.5 mm). The olivine phenocrysts are completely replaced by iron hydroxides. The groundmass consists

mainly of plagioclase microlites together with variable amounts of olivine, clinopyroxene, Fe-Ti-oxides, and altered glass. All rock fragments are covered by ~2-3 cm thick manganese crusts. The homogeneity of the dredged rocks and their angular shape clearly indicate that they represent in-situ rocks. A very similar, ~23 cm long angular fragment of olivine-clinopyroxene-plagioclase basalt was obtained by dredge SO178-83-1 from the northern part of the scarp. This lava is more intensely altered than the rocks from dredge SO178-7-1. Additionally, the dredges carried out at the scarp of Volcano No. 2 contained manganese crusts, two small pieces of slightly lithified sediments, various dropstones, and a broad variety of biological material dominated by gialospongia and partly living corals. Finally, one dredge (SO178-83-4) on the western flank of the small southwestern satellite cone yielded only manganese crusts and dropstones.
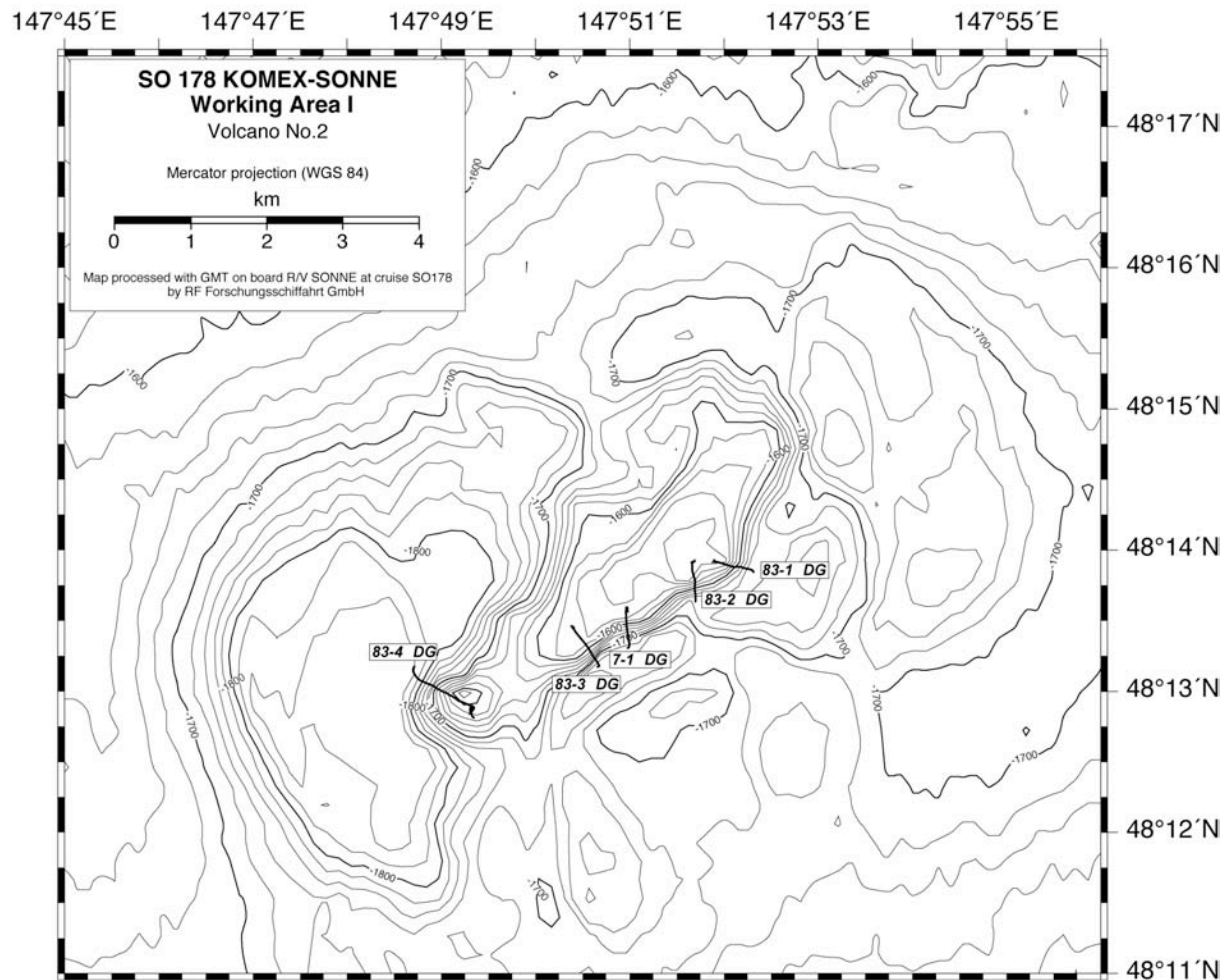
Fig. 12.2: *Bathymetric map of Volcano No. 2 including locations of dredge tracks SO178-7-1 DG and SO178-83-1 DG to –4 DG. Contour interval is 20 m.*

The northern part of the Sonne Chain is formed by a volcanic complex comprising *Volcanoes No. 3 and 4* and several smaller cones (Fig. 12.3). The round, crater-shaped Volcano No 3. is ~ 3 km in diameter. The crater wall rises up to 150 m above the surrounding seafloor. Small, up to 160 m high cones occur on the northeastern edge and to the southwest of Volcano No. 3.
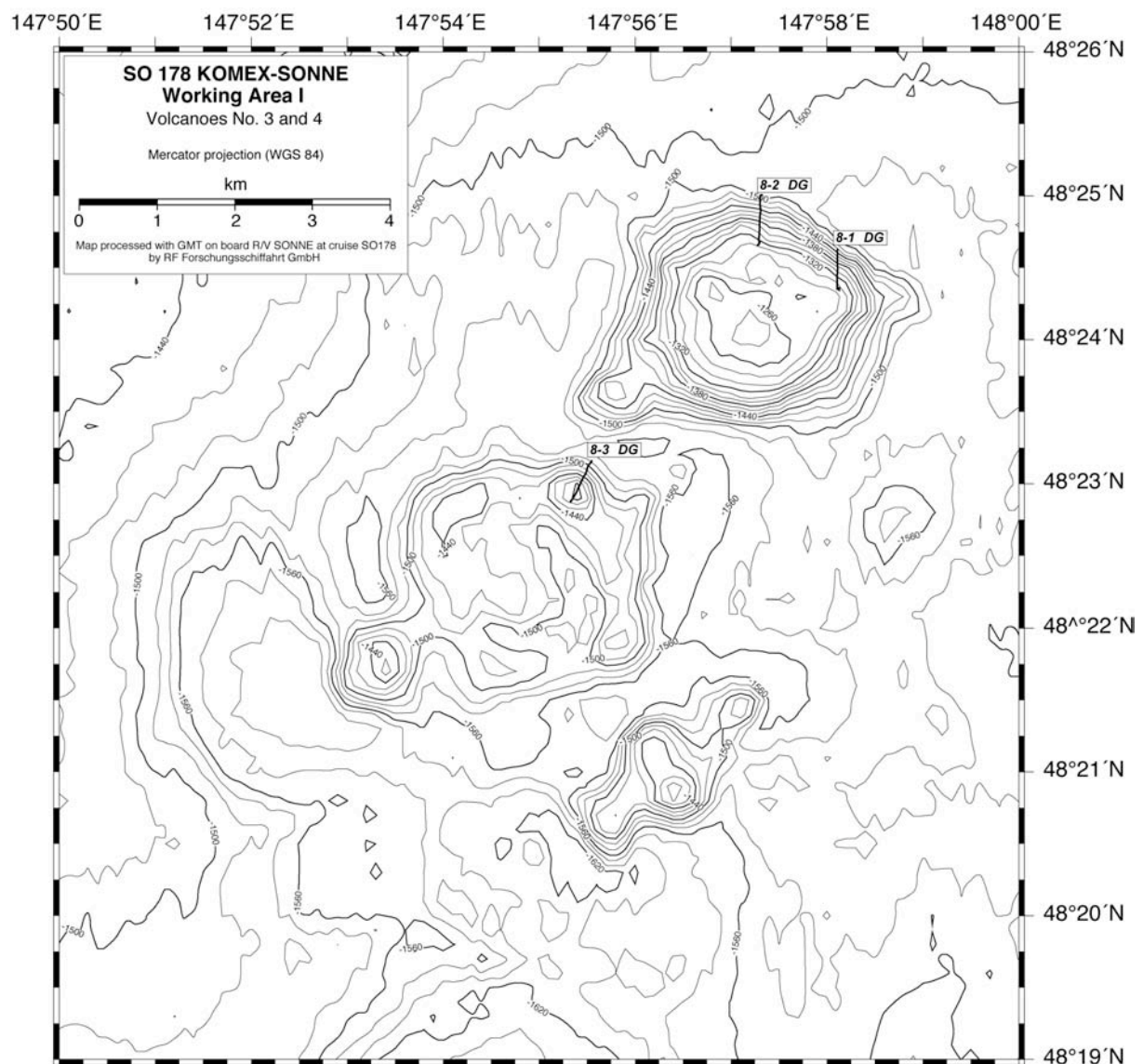
Fig. 12.3: *Bathymetric map of Volcanoes No. 3 and 4 including locations of dredge tracks SO178-8-1 DG to –3 DG. Contour interval is 20 m.*

Dredge SO178-8-3 on the northern flank of the northeastern cone yielded only manganese crusts, dropstones, sediments, gialospongia, and corals. Volcano No. 4 forms a round, flat-topped cone being ~ 3.5 km in diameter and ~300 m high. A small, ~100 m high satellite cone is located to the southwest of Volcano No. 4. Two dredge attempts (SO178-8-1 and –2) were made on the northern flank of Volcano No. 4, but the dredges recovered only manganese crusts, sediments, dropstones, and biological material. Since no other appropriate dredge sites were found in the area of Volcanoes No. 3 and 4, the decision was made to focus further dredge attempts on Volcano No. 2, being the most promising dredge target in the Sonne Chain.

13.3.2 Working area IV (Kashevarov Trough)

Simrad surveys in the Kashevarov Trough focussed on those areas where seismic profiles show needle-shaped structures which resemble volcanic edifices. The multi-beam surveys, however, proved that these seamounts are most likely tilted blocks and that the seismic lines crossed just the narrow edges of the blocks what caused that they look like volcanic edifices
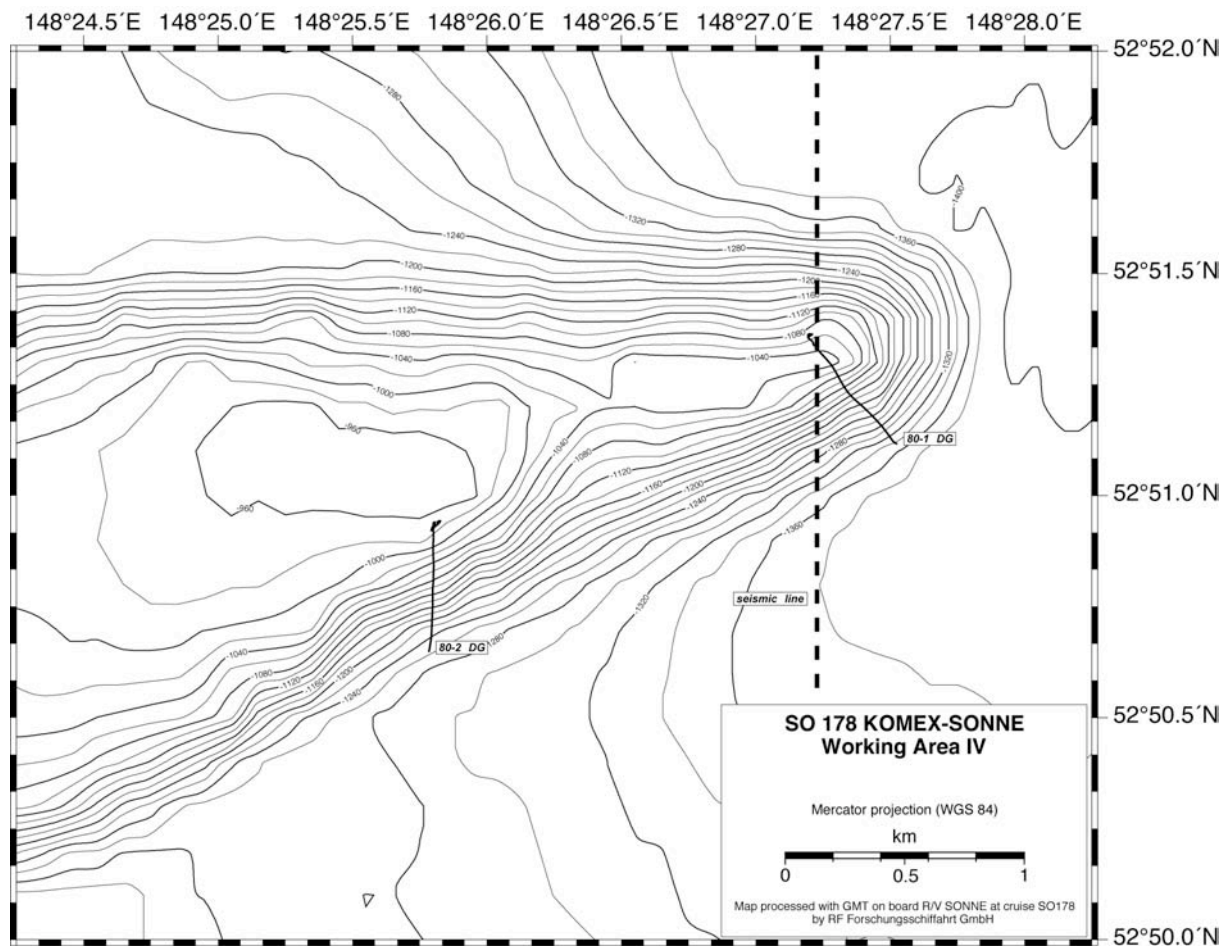
Fig. 12.4: *Bathymetric map of the eastern part of a tilted block in the Kashevarov Trough including locations of dredge tracks SO178-80-1 DG to –2 DG. Contour interval is 20 m. Note the seismic line (dashed line) from a former Russian cruise which crosses the outermost edge of the block causing volcanic-like appearance of this structure in the seismic section (see also Chapter 2).*

in the seismic profiles (Fig. 12.4, see also Chapter 2). Despite considerable Simrad surveys in the Kashevarov Trough, absolutely no structures with a volcanic morphology were found (Fig. 2.6, Chapter 2). To verify the nature of the mapped seamounts, two dredges were carried out on the southern flank of a relatively small block (Fig. 12.4). These dredges (SO178-80-1 and -2) yielded biotite hornfels fragments ranging from 5 to 25 cm in size, tectonic breccias consisting of small (up to 2-3 cm) fragments of biotite hornfels in a fine-grained chlorite-quartz matrix, conglomerates, granodiorites, manganese crusts, corals, gialospongia, and dropstones. Some fragments of biotite hornfels have a broken surface, whereas others are well rounded. The common occurrence of biotite hornfels, being the dominant lithology in the dredges, is consistent with the morphological observations indicating that the seamounts in the Kashervarov Trough are tilted blocks and that volcanic activity most likely did not occur in this area.

13. DEEP-WATER BIOHERMS AND LIVING DEEP-WATER CORALS

Christian Dullo

During cruise SO178-KOMEX, living deep-water scleractinian corals, stylasterid hydro-corals, and isidid gorgonian octocorals were recovered by dredging from the northern margin of the Kurile Basin and from the Kashevarov Trough. The corals, both scleractinians, *Desmophyllum cristagalli*, and octocorals (Isididae, *Keratoisis* sp.) are tied to the boundary of the Okhotsk Sea Intermediate Water (OSIW) where topographically focussed currents concentrate organic particles, maintaining nutrient flux to the heterotrophic organisms. Understanding of the micro- and ultrastructure of isidid gorgonian skeletons which are a potential archive of past paleoceanographic OSIW variations is of utmost importance and will be included into ongoing research at IFM-GEOMAR.

The upslope dredge hauls SO178-7-1 and SO178-8-1 on the volcanic Sonne Chain on the northern Kurile margin (water depths between 1,746 m and 1,278 m) recovered several heavily fragmented living isidid colonies, while the specimens from the Kashevarov Trough derive from shallower sites between 1,346 m and 960 m (So178-80-1 and SO178-80-2, respectively) (Tab. 13.1).

Tab. 13.1: *Localities of coral occurrence recovered by dredging*

Station No. SO178-	Latitude N	Longitude E	Depth (m)	Remarks
7-1 DG	from 48°13.30 to 48°13.56	from 147°50.98 to 147°50.98	1746/ 1548	Recovery: volcanic rocks (in-situ), Mn-crusts, dropstones, corals etc.
8-1 DG	from 48°24.63 to 48°24.34	from 147°58.11 to 147°58.12	1500/ 1278	Recovery: few dropstones, Mn-crust, large sponges, corals
80-1 DG	from 52°51.12 to 52°51.37	from 148°27.53 to 148°27.21	1346/ 1029	Recovery: hornfels; breccias covered by thick manganese crust; corals, sponges; dropstone. hornfels and hornfels breccia - bedrocks?
80-2 DG	from 52°50.65 to 52°50.94	from 148°25.79 to 148°25.81	1266/ 960	Recovery: hornfels; manganese crust; corals; dropstones.

Fragmented skeletal branches of the living isidid colonies are composed of alternating bright calcitic internodes and dark organic nodes (Fig. 13.1) with a concentric horizontal banding in both stages. The surrounding reddish organic coenenchym bearing non-retractile polyps and numerous calcitic sclerites secretes a central skeletal axis which in the form of an endoskeleton supports the soft-bodied part of the octocoral (Fig. 13.1). The original surface of the internodes is well preserved showing a furrowed growth pattern. Root-like calcareous structures served for anchoring the colony in a soft-bottom substratum. On account of the characteristic branching from the internodes and the arrangement of branches in two planes at right angles, the specimen belongs to the genus *Keratoisis* WRIGHT (Family Isididae, Order Holaxonia, Subclass Octocorallia).

Fig. 13.1: *Living Keratoisis after recovery. The coenenchym (white) was largely damaged during dredging giving the colony a clumsy appearance. Note the length of the calcified parts of the branches.*

14. REFERENCES

Baranov, B.V., Werner, R., Hoernle, K.A., Tsoy, I.B, van den Bogaard, P. & Tararin, I.A., 2002a. Evidence for compressionally induced high subsidence rates in the Kurile Basin (Okhotsk Sea). Tectonophysics, 350, 63-97.

Baranov, B., Wong, H.K., Dozorova, K., Karp, B., Luedmann, T. & Karnaukh, V., 2002b. Opening geometry of the Kurile Basin (Sea of Okhotsk) as inferred from structural data. *The Island Arc*, 11 (3), 206-219.

Belousov, V.V. & Udintzev, G.B. (eds.), 1981. Bottom structure of the Okhotsk Sea. Moscow: Science Pub., 251 p.

Biebow, N. & Hütten, E. (eds.), 1999. Cruise Reports: KOMEX I and II: RV Professor Gagarinsky Cruise 22, RV Akademik M.A. Lavrentyev Cruise 28, *GEOMAR Report 82*, 188 pp.

Biebow, N., Kulinich, R., Baranov, B. et al., 2003. Cruise Reports: RV Akademik M.A. Lavrentyev Cruise 29, Leg 1 and Leg 2, *GEOMAR Report 110*.

Biebow, N., Lüdmann, T., Karp, B. & Kulinich, R., 2000. Cruise Reports: KOMEX V and VI: RV Professor Gagarinsky cruise 26, MV Marshal Gelovany cruise 1. GEOMAR Report, 88, 296 pp.

Bohrmann, G., Suess, E., Greinert, J., Teichert, B. & Naehr, T., 2002. Gas hydrate carbonates from Hydrate Rdige, Cascadia Convergent Margin: indicators of near-seafloor clathrate deposits. Fourth Int. Conf. on Gas Hydrates, Yokohama, Japan. 102-107.

Bruevich, S.V., 1944. Determination alkalinity of small volumes of sea water by direct titration. In: Instruction of chemical investigation of sea water. Moscow-Leningrad: Glavsevmorput, 83 pp.

Carpenter, J.H., 1965. The Chesapeake Bay Institute technique for the Winkler dissolved oxygen method. Limnol. Oceanogr., 10, 141-143.

Derkachev, A.N., Bohrmann, G., Greinert, J., Obzhirov, A.I. & Suess, E., 2003. Barite mineralization and sulphide ore formation in the Okhotsk Sea. In: *Metallogeny of paleo- and present oceans. Formation and exploitation of deposits in ophiolitic zones.* Miass, 68-76. (in Russian)

Derkachev, A.N., Obzhirov, A.I., Bohrmann, G., Greinert, J. & Suess, E., 2002. Authigenic mineral formation at sites of cold gas-fluid emanations at the seafloor of the Sea Okhotsk. In: Formation conditions of bottom sediments and related mineral resources in marginal seas. Vladivostok: Dalnauka, 47-60. (in Russian)

Ginsburg, G.D. & Soloviev, V.A., 1994. Submarine gas hydrates. St. Petersburg: VNIIOkeangeologiya, 200 pp. (in Russian)

Gorbarenko, S.A., Chekhovskaya, M.P. & Southon, J.R., 1998. Detailed environmental changes of the Sea of Okhotsk Central part during the last glaciation-Holocene. Oceanology, 38 (2), 277-280 (translated from Okeanologiya, 38 (2), 305-308).

Gorbarenko, SA., Nürnberg, D., Derkachev, A.N., Astakhov, AS., Souton, J.R & Kaiser, A., 2002. Magnetostratigraphy and tephrochronology of the Upper Quaternary sediments in the Okhotsk Sea: implication of terrigenous, volcanogenic and biogenic matter supply. Marine Geology, 183 (1-4), 107-129.

Greinert, J., Bohrmann, G. & Suess, E., 2001. Methane Venting and Gas Hydrate-Related Carbonates at the Hydrate Ridge: Their Classification, Distribution and Origin. In: Paull, C.K. & Dillon, W.P. *Natural Gas Hydrates: Occurence, Distribution, and Detection.* Geopohysical Monograph, 124, 99-113.

Hendy, I.L. & Kennett, J.P., 2003. Tropical forcing of North Pacific intermediate water distribution during Late Quaternary rapid climate change? Quarternary Science Reviews,!22 (5-7), 673-689.

Hendy, I.L., Kennett, J.P., Roark, E.B. & Ingram, B.L., 2002. Apparent synchroneity of submillennial scale climate events between Greenland and Santa Barbara Basin, California from 30-10 ka. Quarternary Science Reviews,!21 (10), 1167-1184.

Holler, P., 1995. Arbeitsmethoden der marinen Geowissenschaften, Stuttgart: Enke.

Ivanenkov, V.N. & Bordovsky, O.K., 1978. The methods of hydrochemical investigation of the ocean. Moscow: Nauka, 271 pp. (in Russian).

Kaiser, A., 2001. Ozeanographie, Produktivität und Meereisverbreitung im Ochotskischen Meer während der letzten ca. 350.000 Jahre. Dissertation, Christian-Albrechts-Universität zu Kiel, 113 S.

Kiefer, T., Sarnthein, M., Erlenkeuser, H., Grootes, P.M. & Roberts, A.P., 2001. North Pacific response to millennial-scale changes in ocean circulation over the last 60 kyr. Paleoceanography, 16 (2), 179-189.

Lucker, T.J., Dickson, A.G. & Keeling, C.D., 2000. Ocean pCO_2 calculated from dissolved inorganic carbon, alkalinity, and equations for K_1 and K_2: validation based on laboratory measurements of CO_2 in gas and seawater at equilibrium. Mar. Chem., 70, 105-119.

Millero, F., 1995. Thermodynamics of the carbon dioxide system in the oceans. Geochim. Cosmochim. Acta, 59, 661-677.

Nikolaeva, N., Derkachev, A., Grigoryeva, T., Mozherovsky, A. & Tishchenko, P., 2004. Indications of a Periodic Existence of a Hydrosulphuric Contamination Zone in the Derugin Basin (Sea of Okhotsk) during the Holocene-Late Pleistocene. Fifth KOMEX Workshop. Vladivostok, May 27-30, 35-36.

Nürnberg, D. & Tiedemann, R., in press. Environmental change in the Sea of Okhotsk over the past 1.1 million years – atmospheric teleconnections to China. *Paleoceanography*.

Obzhirov, A.I., 1993. *Gas and geochemical fields of the benthic layer of seas and oceans*. Moscow: Nauka, 131 pp. (in Russian).

Obzhirov, A.I., Sosnin, V.A., Salyuk., A.N. et al., 2002. *Methane monitoring in the Sea of Okhotsk*. Vladivostok: Dalnauka, 247 pp. (in Russian)

Powers, M.C., 1982. Comparison chart for estimating roundness and sphericity. AGI data sheet 18, American Geological Institute.

Rohling, E.J., Mayewski, P.A. & Challenor, P., 2003. On the timing and mechanism of millennial-scale climate variability during the last glacial cycle. Climate Dynamics, 20 (2-3), 257-267.

Sachs, I.S., Suyehiro, K., Acton, G.D. & Shipboard Scientific Party**,** 2., 2000. Explanatory Notes, In: Proceedings of the Ocean Drilling Programme, Initial reports, 186.

Sahling, H., Galkin, S.V., Salyuk, A., Greinert, J., Foerstel, H., Piepenburg, D. & Suess, E., 2003. Depth-related structure and ecological significance of cold seep communities - A case study from the Sea of Okhostk. *Deep-Sea Research*, I (50), 1391-1409.

Shepard, F.S., 1954. Nomenclature based on Sand-Silt-Clay ratios. Journ. Sed. Petrol., 24, 151-158.

Tararin, I.A., Lelikov, E.P. & Werner, R., 2003. Petrology and geochemistry of the volcanic rocks dredged from the Geophysicist Seamount: evidence for the existence of thinned continental crust. *Gondwana Research*, 6 (4), 757-765.

Tishchenko, P.Ya., Pavlova, G.Yu. & Bychkov, A.S., 1999. Estimation of the biological and thermal effects on partial pressure of carbon dioxide and apparent oxygen utilization in seawater. Proc. 2nd Intern. Symposium CO2 in the Oceans. Tsukuba, 259-266.

Tishchenko, P.Ya., Wong, C.S., Pavlova, G.Yu., Johnson, W.K., Kang, D.-J. & Kim, K.-R., 2001. pH measurements of seawater by means of cell without liquid junction. Oceanology, 41 (6), 849-859.

Tishchenko, P.Ya., Chichkin, R.V., Il'ina, E.M. & Wong, C.S., 2002. pH Measurements in estuary by means of cell without Liquid Junction. Oceanology, 41 (1), 32-41.

Tsunogai, S., Niskimura, M. & Nakaya, S., 1968. Complexometric titration of calcium in the presence of larger amounts of magnesium. Talanta, 15, 385-390.